CARLOS ALBERTO PINHEIRO BAPTISTA

Chemical Approaches to Ubiquitous Computing

Dissertação apresentada para obtenção do
Grau de Doutor em Química,
perfil de Química-Física,
pela Universidade Nova de Lisboa,
Faculdade de Ciências e Tecnologia.

LISBOA
2010

CARLOS ALBERTO PINHEIRO BAPTISTA

Chemical Approaches to Ubiquitous Computing

Supervisor: Prof. António Jorge Parola

Co-supervisor: Prof. Fernando Jorge Pina

Co-supervisor (YDreams): Ivan Franco

Resumo

Nos capítulos 2 e 3 descreve-se o estudo de sistemas cromogénicos em solução, sensíveis a diferentes estímulos. A rede de equilíbrios químicos do 6-hidroxiflavílio foi caracterizada pela formação de uma forma quinoidal da chalcona. A *trans*-6-hidroxichalcona é relativamente estável em soluções ácidas e exibe um processo electroquímico quase-reversível, o que permite introduzir pela primeira vez um estímulo eléctrico nos flavílios. Fotocromismo e electrocromismo permite transitar de um estado incolor a amarelo de soluções de flavílio (capítulo 2). Um sistema supramolecular foi desenvolvido com base em três componentes: Fe(III)/Fe(II), Cristal Violeta Lactona (CVL) e um spiropirano (SPI); este sistema apresenta quatro estados ópticos: incolor, azul, magenta e amarelo. Estes estados estão interconectados e controlados por luz e electricidade. O sistema goza da fina selectividade do complexo Fe(III)/Fe(II) com o CVL e o SPI. A electricidade controla a formação dos complexos corados entre os iões Fe(III)/Fe(II) com o CVL (ionocromismo) e o SPI. A luz opera o processo fotocrómico do composto SPI (Capítulo 3).

Nos capítulos 4, 5 e 6 sistemas cromogénicos electrocrómicos em meio líquido e no estado sólido são descritos. A cor dos filmes electro-polimerizados sobre eléctrodos flexíveis de Azul da Prússia (PB) e de polímeros de complexos de Cu(II), Ni(II) e Pd(II) com ligando *salen* foi caracterizada por colorimetria. A nova família de materiais electrocrómicos com base nos complexos de *salen* apresentou transições de cor entre o verde/amarelo (Pd, Ni) e roxo/amarelo (Cu), e um coeficiente de coloração na ordem de grandeza (150-200cm^2/C) dos valores obtidos com polímeros orgânicos como o PEDOT (Capítulo 4). A performance relativa dos dispositivos electrocrómicos (ECD) em função do meio electrólito foi estudada. Um electrólito polimérico sólido (SPE) e um gel electrólito (GE) foram usados para comparação. Os ECD baseados em SPE mostraram-se inadequados para aplicações como ecrãs, dado o seu longo tempo de transição (na ordem dos minutos). O contrário acontece com ECD baseados em GE, tempos de transição abaixo do segundo foram registados. As diferenças obtidas estão relacionadas com as diferentes condutividades iónicas dos electrólitos testados; SPE (10^{-5}–10^{-6} S/cm) e GE (10^{-2} S/cm) (Capítulo 5).

No âmbito de I&D aplicado em colaboração com a indústria, sistemas electrocrómicos foram explorados para aumentar a funcionalidade do papel, têxtil e quadros brancos. Provas de conceito dos ECD foram produzidos e caracterizados. O maior problema que foi encontrado é a integração invisível de ECD com os substratos (Capítulo 6). Finalmente, um estudo de viabilidade da utilização da impressão por jacto de tinta para construir ECD foi realizada. Tintas electrocrómicas e electrólito curável por UV foram formuladas para a técnica de jacto de tinta. ECD funcionais impressos por jacto de tinta são apresentados (Capítulo 7).

Abstract

In chapters 2 and 3 dual-mode liquid state chromogenic systems are reported. The complex network of chemical reactions of the compound 6-hydroxyflavylium is characterized by the formation of the *p*-quinoidal chalcone. The *trans*-chalcone is metastable in very acidic solutions and exhibits reversible redox reactions, allowing to introduce for the first time in the flavylium network an electrochemical input. Photochromism and electrochromism phenomena operates the system optical states between colourless and yellow (Chapter 2). The supramolecular system obtained by the combination of Fe(III)/Fe(II), Crystal Violet Lactone (CVL) and a spiropyran (SPI) leads to a four optical states system: colourless, blue, magenta and yellow; each independently addressable by light and electrical input. The system profits from fine speciation Fe(III)/Fe(II) complexes with CVL and SPI. Electrical stimulus controls the formation of the coloured adducts between iron ions with CVL (ionochromism) and the merocyanine form of SPI, while light stimulus operates the SPI compound (photochromism) (Chapter 3).

The chapters 4, 5 and 6 are devoted to the study of electrochromic systems and devices in the liquid and solid state. A colorimetric study of electrogenerated Prussian Blue (PB) and electrogenerated polymers based on *salen*-type complexes of Cu(II), Ni(II) and Pd(II) deposited over transparent and flexible electrodes was carried out using the CIELAB colour system. The new family of electrochromic films showed colour transitions between green-yellow (Pd, Ni) and purple-yellow (Cu), with a coloration efficiency in the range of the values reported for the efficient electrochromic organic polymer like PEDOT. PB films showed high optical contrast between colourless and blue colour (Chapter 4). The relative performance of ECD based on solid polymer electrolyte (SPE) and gel electrolyte (GE) was investigated. The ECD based on SPE showed to be inappropriate for displays application due to its long switching times (minutes). In opposite to ECD based SPE, switching times lower than one second was recorded with ECD based on GE. The main differences are attributed to the different ionic conductivity of the electrolytes; SPE (10^{-5}–10^{-6} S/cm), GE (10^{-2} S/cm) (Chapter 5).

In the framework of applied R&D projects in collaboration with Industry, ECD were explored to add functionalities to paper, textile and white boards. Proofs of concept of ECD were produced and characterized. The major difficulty found was to design a seamless ECD and to build electrodes over the different substrates. (Chapter 6). Finally, the feasibility study of the application of ink-jet printing technology as an industrial method to build ECD is reported. Electrochromic ink-jet and UV curable electrolyte ink-jet inks, were formulated. Functional ink-jet printed functional ECD are presented (Chapter 7).

Abbreviature List

A	Absorbance
$A_{\lambda um}$	Absorbance at λnm wavelength
$A_{\lambda nm,n}$	Absorbance at λnm wavelength after n write-erase cycles
α	Electron transfer coefficient
E_{pa}	Anodic peak potential
K^a	Apparent equilibrium constant between AH^+ and A, Cc and B
K'	Apparent equilibrium constant between AH^+ and CB
CRT	Cathode ray tube
E_{pc}	Cathodic peak potential
CIELAB	CIE-*L*a*b**
x, y	CELAB chromaticity coordinates
ΔE^*_{ab}	CIELAB colour difference
*L**	CIELAB coordinate relative to the luminance of the colour
*a**	CIELAB coordinate relative to the redness-greenness of the colour
*b**	CIELAB coordinate relative to the yellow-blueness of the colour
MERO-c	*Cis*-form of the merocyanine form
Cc	*Cis*-chalcone
CE	Coloration efficiency
$\phi(\lambda)$	Colour stimulus function
$\phi(\lambda)$	Colour stimulus function
$x(\lambda), y(\lambda), z(\lambda)$	Colour-matching functions
CIE	Comission international de l'éclairage
CB	Conjugated bases (A, B, Cc and Ct)
CR	Contrast ratio
CP	Coordination polymers
CVL	Crystal violet lactone
I	Current
CMYT	Cyan, magenta and yellow, as well as a transparent state
DPGDA	Dipropyleneglycol diacrylate
λ_d	Dominant wavelength
$\lambda_{c,d}$	Dominant wavelength of the complementary colour
DoD	Drop-on-demand
DSSC	Dye sensitized solar cells
ECD-T	Ecd can be operated in the transmittance
Q	Electrical charge

C	Electrical conductance
E	Electrical potential
ρ	Electrical resistivity
ECD	Electrochromic device
e-	Electron
e	Elementary charge
K_a	Equilibrium constant for the deprotonation of AH^+
$K_{Ct(1)}$	Equilibrium constant for the deprotonation of Ct
$K_{Ct(2)}$	Equilibrium constant for the deprotonation of Ct^-
K_h	Equilibrium constant for the hydration of AH^+
K_i	Equilibrium constant for the isomerization of Cc
K_t	Equilibrium constant for the tautomerization of the B
Λ	Equivalent conductivity
p_c	Excitation purity
AH^+	Flavylium cation
FTO	Fluorine-doped tin oxide
Tg	Glass transition temperature
B	Hemiketal
IP	Impact printing techniques
IJ	Ink-jet printing
IVCT	Inter valence charge transfer
ui	Ionic mobility of the specie i
Ct^-	Ionized trans-chalcone
k_a	Kinetic constant for the direct deprotonation reaction (formation of A)
k_h	Kinetic constant for the direct hydration reaction
k_{-a}	Kinetic constant for the inverse deprotonation reaction (protonation of A)
k_{-h}	Kinetic constant for the inverse hydration reaction (the dehydration of B)
CIELAB	*L*a*b** tristimulus cie colour space
LSE	Liquid state electrolyte
PEO-2	Low molecular weight peo-ppo
MERO	Merocyanine form of the spiropyran
[M(*salen*)]	Metal complex, m with *salen* ligand
poly[M(*salen*)]	Metal complex, m with *salen* ligand polymer
M^+	Metal ion
MV	Methyl viologen
M	Molar

ε	Molar absorption coefficient
χX	Molar fraction of the specie X
NCD	Nanochromic display
NIR	Near infrared region radiation
V^-	Negative voltage
z	Net charge
NIP	Non-impact printing techniques
NMR	Nuclear magnetic resonance spectroscopy
N	Number of charge carriers
k_{obs}	Observed kinetic constant
OTE	Optically transparent electrodes
OLED	Organic light emitting diodes
MERO-oQ	Ortho-quinoidal form of the merocyanine
PANI	poly(acrylonitrile)
FOT group	Photochemistry and supramolecular group
P-ECD	Photoelectrochromic device
PMMA	Poly(methyl methacrylate)
PEDT:PSS	Poly(3,4-ethylenedioxythiophene)-poly(styrenesulfonate)
PEDOT	Poly(ethylene dioxythiophene)
PEO-PPO	Poly(ethylene oxide) and poly(propylene oxide) copolymer
p(TMC)	Poly(trimethylene carbonate)
PVdF	Poly(vinyliden fluoride)
PEO	Polyethylene oxide polymer
PET	Polyethylene terephthalate
PET-ITO	Polyethylene terephthalate films coated with indium tin oxide
ADI	Portuguese innovation agency
V^+	Positive voltage
PB	Prussian blue
PX	Prussian brown
PW	Prussian white
PY	Prussian yellow
PVC	Poly(vinyl chloride)
PVdF	Poly(vinylidene fluoride)
Φi	Quantum yield for a given process i
A	Quinoidal base
R_0	Intensity of reflected light from a non-shiny white card

RGB	Red, green and blue additive colour system
$R_{\lambda nm}$	Reflectance at λnm wavelength
$R_{\lambda nm,n}$	Reflectance at λnm wavelength after n write-erase cycles
$S(\lambda)$	Relative spectral power distribution of the illuminant
τ	Response time
V_{off}	Resting voltage
R_x	Intensity of light reflected diffusely by the coloured state of the ECD
SCE	Saturated calomel electrode
v	Scan rate
Ag/AgCl	Silver/silver chloride reference
SPE	Solid polymer electrolyte
K_{ps}	Solubility constant
κ	Specific electrical conductance or electrical conductivity
$R(\lambda)$	Spectral reflectance factor
$T(\lambda)$	Spectral transmittance factor
SEC	Spectroelectrochemistry
BIPS	Spiroindolinobenzopyran
SPI	Spiropyran
T	Temperature
MERO	Merocyanine form
IJ	Ink-jet printing
ECD-R	Reflectance
ITO	Tin-doped indium oxide
TiO_2-DPGDA	TiO_2 dispersion in dipropyleneglycol diacrylate
TiO_2-W	TiO_2 dispersion in water
C_X	Total concentration of specie X
Ct	*Trans*-chalcone
$T_{\lambda nm}$	Transmittance at lnm wavelength
$T_{\lambda nm,n}$	Transmittance at lnm wavelength after n write-erase cycles
TCO	Transparent conductive oxide
TPM	Triphenylmethane
$x(\lambda)$, $y(\lambda)$, $z(\lambda)$	Tristimulus colour-matching functions
UC	Ubiquitous computing
UV	Ultra-violet radiation
UV-Vis	Ultraviolet-visible spectroscopy
Δ	Variation

vs.	Versus
η	Viscosity
V	Voltage
λ	Wavelength
λ_{max}	Wavelength of maximum emission or absorption

Table of Contents

Chapter 1 ..... **1**

General Introduction

1.1 Motivation 2

1.2 Chromogenic Systems and Applications (Background) 3

1.2.1 Electricity 5

1.2.2 Light 13

1.2.3 Ions 15

1.2.4 Electricity and light or ions and light 16

1.2.5 Temperature, polarity, mechanical pressure and mechanical friction 19

1.3 Industrial Printing Techniques 19

1.4 Outline 21

1.5 Bibliography 23

Chapter 2 ..... **29**

The chemistry of 6-hydroxyflavylium

2.1 Introduction 30

2.1.1 Flavylium compounds 30

2.2 Experimental details 38

2.3 Results and Discussion 41

2.4 Conclusions 53

2.5 Bibliography 55

Chapter 3 ..... **59**

Multiresponsive chromogenic systems operated by light and electrical inputs

3.1 Introduction 60

3.1.1 Leuco Dyes 60

3.2 Experimental details 64

3.3 Results and Discussion 66

3.3.1 Interaction between CVL and iron ions 66
3.3.2 Adding light stimulus: multi-responsive system 75
3.3.3 Two external inputs, Three species, Four Colours 79
3.4 Conclusions 81
3.5 Bibliography 83

Chapter 4 87

Electrocolorimetry of electrochromic materials on flexible ITO electrodes

4.1 Introduction 88
4.1.1 Electrochromic Coordination Polymers 88
4.1.2 Colorimetry 94
4.2 Experimental details 100
4.3 Results and Discussion 102
4.3.1 Prussian blue 102
4.3.2 *Salen*-type complexes of Cu(II), Ni(II) and Pd(II) 106
4.4 Conclusion 115
4.5 Bibliography 117

Chapter 5 123

Non-liquid Electrolytes for Electrochromic Devices

5.1 Introduction 124
5.1.1 Electrolyte systems and application 124
5.2 Gel Electrolytes for ECD applications 130
5.2.1 Experimental Details 130
5.2.2 Results and Discussion 132
5.3 A Solid Polymer Electrolyte for ECD 145
5.3.1 Experimental Details 145
5.3.2 Results and Discussion 149
5.4 General Conclusions 158
5.5 Bibliography 161

Chapter 6 ..... **165**

Paper, textile and white board ECD

6.1 Motivation 166

6.2 Strategy and project execution organization 169

6.3 Results and Discussion 172

6.3.1 Electrochromic layer 172

6.3.2 ECD Assembly with paper-, textile- and white board electrodes 176

6.3.3 ECD characterization 180

6.4 Conclusions 184

6.5 Bibliography 187

Chapter 7 ..... **189**

Feasibility study for an electrochromic display built by ink-jet

7.1 Introduction 190

7.1.1 Ink-jet technique 191

7.2 Strategy and project execution organization 196

7.3 Results and Discussion 197

7.3.1 Printing the Electrochromic Layer 197

7.3.2 Printing the Electrolyte Layer 198

7.3.3 Demonstration of the ink-jet printed electrochromic cells 201

7.4 Conclusion 203

7.5 Bibliography 205

Chapter 8 ..... **209**

List of Publications

8.1 List of Publications 210

Index of Figures

Figure 1.1 – Light interaction with matter; reflectance, scattering, absorption and transmittance 4

Figure 1.2 – Example of an electrochromic device with the "sandwich" like architecture. 6

Figure 1.3 – ECD in transmittance mode (A), and in reflectance mode (B)..... 8

Figure 1.4 – Schematic view of the ECD from Acreo EC technology with a "side-by-side" architecture. 12

Figure 1.5 – ECD architecture employed by NTera where the primary electrode is composed by a chemisorbed viologen derivative on the surface of TiO_2 nanoparticles (coated PET-ITO) (1), a dispersion of light scattering TiO_2 nanoparticles is incorporated in the electrolyte layer (2). 13

Figure 1.6 – T-type photochromic compounds, spiropyrans (A), spirooxazines (B) and chromenes (C) 14

Figure 1.7 – P-type photochromic compounds, fulgides (A) and diarylethenes (B).....14

Figure 1.8 – Acidochromism mechanism of the Methyl Red, the base form is colourless and at a pH = 4.4 the azonium for is red. 15

Figure 1.9 – Dual-mode photochromism and electrochromism of the 1,2-bis(2-methyl-5,2'-dithiophen-3-yl)perfluorocyclopentene, the pale yellow ring-open form (A) is converted both by an electrical potential and by UV light to the coloured ring-closed form (B) 17

Figure 1.10 – The spiropyrans bearing a monoaza-crown shows dual-mode photochromic and ionochromic properties. 17

Figure 1.11 – Example of the operation of a P-ECD by light. Electrons are ejected from the photovoltaic layer (1) and reduction of the electrochromic WO3 layer will cause the darkening of the device. 18

Figure 1.12 – Graphic printing techniques classified by the method ink is transferred to the printing substrate, adapted from ref.[50] 20

Figure 1.13 – Schematic draws of the physical printing plates for Letterpress (A), lithography (B), gravure (C) and screen-printing (D). 20

Figure 2.1 - 2-phenyl-1-benzopyrylium (Flavylium) structure 30

Figure 2.2 – Chemical network of 6-Hydroxiflavylium 31

Figure 2. 3 – Dual-type photochromic system proposed by Pina *et al.*[11] 34

Figure 2.4 – Oxidation mechanism for different polyphenols (Kuromanin[19], Kaempferol[19] and Catechin[20]). ...36

Figure 2.5 – Proposed two electrons, two protons oxidation mechanism of the 3,5-dimethyl-4-hydroxychalcone by Nicole Cotelle *et al.*[21] 37

Figure 2.6 - Spectral variations of 6-hydroxyflavylium perchlorate, $3.5x10^{-5}$M, as a function of pH (acidic region) at the thermal equilibrium. In order to decrease the reaction time, the solutions were kept at 40 °C for 7 hours and left to equilibrate for a day at room temperature. 41

Figure 2.7 - Spectral variations of 6-hydroxyflavylium perchlorate, $3.5x10^{-5}$M, as a function of pH, resulting from a pH jump from 1, measured after 30 seconds. 42

Figure 2.8 - Spectral variations of 6-hydroxyflavylium perchlorate obtained by stopped-flow after 10 ms of a pH jump from 1 to the final pH. 43

Figure 2.9 - Decay trace of a direct pH jump from 1 to 9.65 (left); decay trace of a reverse pH jump from 6.1 to 2.33 (right). The initial solution at pH=6.1 was prepared from a stock solution at pH=1.0, and used immediately, before formation of significant amounts of Ct (pseudo-equilibrium state). The decay of the A form is observed during the direct pH jump, while the formation of the AH^+ form is observed during the reverse pH jump. 44

Figure 2.10 - Kinetics of the zwitterionic base decay followed by stopped flow....44

Figure 2.11 – Proposed kinetic mechanism for the conversion between the form AH^+, A and B, previously described in the literature 45

Figure 2.12 - Observed rate constants upon direct (pH=1 → pH>1, □) and reverse (pH=6.1 → pH<6.1, ■) pH jumps. 47

Figure 2.13 – The *cis-trans* isomerization of 6-hydroxyflavylium perchlorate at pH=6.5 (left) and the Arrhenius plot for the same reaction (right). 48

Figure 2.14 - Rate constant of the *cis*-trans isomerization as a function of pH. 48

Figure 2.15 - Irradiation at 313nm of a freshly prepared solution of 6-hydroxyflavylium perchlorate at pH=6.4. Inset: absorbance changes at 380 nm. 49

Figure 2.16 - Spectral variations occurring upon a titration of the *trans*-2,5-dihydroxychalcone under argon atmosphere, at 25 °C. 50

Figure 2.17 – Cyclic voltammograms of 2.9×10^{-4} M *trans*-2,5-dihydroxychalcone at pH 1, at different scan rates at 21°C (left). The working electrode was a glassy carbon electrode, the reference electrode was a Ag/AgCl electrode and as counter-electrode a platinum wire. The experiments were carried out in hydrochloric acid aqueous solution about pH1.3, containing 1MKCl as supporting electrolyte. Inset: plot of the anodic peak current *vs.* square root of scan rate (*v*), a correlation of 0,99 was found. Comparison of experimental (full line) and simulated (dots line) cyclic voltammograms of $2,9x10^{-4}$M 2,5-dihydroxychalcone at pH 1, run at $0,1Vs^{-1}$ (right). Simulation was made using "GPES4.9 commercial voltammetric simulation package from EcoChemie V.B." with the following parameters: formal potential, E^0 = 0,438V (*vs.* Ag/AgCl) and electron transfer coefficient, α = 0,48. 51

Figure 2.18 - Spectral variations that follow the oxidation (left), and reduction (right) of *trans*-2,5-dihydroxychalcone in a mixture of ethanol (60%) and aqueous 0.2 M HCl (40%). The working electrode was a platinum net electrode, the reference electrode was an Ag/AgCl electrode and as counter-electrode a platinum wire. The supporting electrolyte was 1MKCl. 52

Figure 2.19 – Electrochemical redox mechanism proposed for the *trans*-chalcone form of the 6-hydroxyflavylium....52

Figure 2.20 - Molecular orbital potential energy minima, calculated by semi-empirical method for the 4'-hydroxyflavylium....53

Figure 2.21 – Thermodynamics of the 6-hydroxyflavylium chemical network....53

Figure 3.1 – Ring opening of Crystal Violet Lactone. Left: closed ring Crystal Violet Lactone (CVL); Right: open ring Crystal Violet Lactone (CVOL) 61

Figure 3.2 - (6-NO_2,1'N-CH_2CH_2OH)-BIPS (SPIRO) and ring open merocyanine (MERO) and respective isomers (MERO-c, MERO-t and MERO-oQ). 62
Figure 3.3 - Merocyanine-metal chelate....63
Figure 3.4 – Chelate formation and decolouration chemical equilibrium adapted from ref.20. 63
Figure 3.5 - Absorption spectra of 0.5 mM CVL in the presence of 1 mM Fe(II) (solid line) and 1 mM Fe(III) (dashed line). On the contrary to Fe(II), the oxidized form Fe(III) opens the lactone ring of CVL. 66
Figure 3.8 - Spectroelectrochemical data of 300 μM of CVL in the presence of 1 mM of $FeCl_3$: Chronoabsorptometry followed at the maximum absorbance (631nm) of CVOL (A); Chronoamperometry data (B); Square wave potential program (C); Picture shows the optical transitions of a mixture of 300μM of CVL and 1 mM of $FeCl_3$ between anodic electrolysis (blue colour) and cathodic electrolysis (colourless). 75
Figure 3.10 - Irradiation of the SPI (0.1 mM) in methanol solution and 0.1 M TBAP (left). The same in the presence of Fe(III) in 2-fold excess (0.2 mM) (right). 77
Figure 3.11 - Cyclic voltammograms of Fe(III) (full line) and SPI (dashed line) in ethanol. Electrochemical potential required to operate the Fe(III)/Fe(II) redox process does not affect the SPI species. 78
Figure 3.12 - Operation of the CMYT colour model based on the three component system: SPI (1 mM), CVL (35 μM) and Fe(III) (35 μM); methanol, 0.1 M TBAP. Transition between 1 and 2 is controlled by electricity, transitions between states 2 and 3 and states 3 and 4 are controlled by light. Pictures of the solutions corresponding to the states 1, 2, 3 and 4 from the left to the rigt. 80
Figure 3.13 - Molar absorption spectra of the coloured species involved in the photoelectrochromic system in methanol. MERO (full line); MERO-Fe(III) (dotted line); CVOL-Fe(III) (dashed line). 80

Figure 4.1 - 3D geometry of "soluble" Prussian Blue crystal; full circle: Fe(III), open circle: Fe(II) 90
Figure 4.2 – General strucuture of *salen*-type complexes....92
Figure 4.3 – Proposed polymer strucuture of poly[M(*salen*)][31] 92
Figure 4.4 – Schematic band structure of a dopped semi-conductor. λ1: band-gap; dashed lines: charge carriers (polarons) 94
Figure 4.5 – Visual illusion due to different contrast between the object and the surrounding. At the left side of the image the green strips are actually of the same colour than the blue strips on the right. 95
Figure 4.6 - The *CIE 1931* colour-matching functions (ploted with the data from ref.36)....96
Figure 4.7 – Chromaticity diagram and colorimetric information that can be extracted from it.[40] 99
Figure 4.8 - *In situ* cronocoulometry/cronoabsorptometry data for PB film deposited on PET/ITO in 0.2 M KCl aqueous solution as supporting electrolyte. Left: chronoabsorptometry recorded at 690nm (dashed line), CE (full line). Right: chronoamperometry (full line+full circle), square-wave switching between –0.2 and 0.6V (*vs.* Ag/AgCl), step duration of 40s (full line). 102
Figure 4.9 - CE (dots) calculated from *in situ* chronocoulometry/chronoabsorptometry (see Fig.4.6). Chronoabsorptometry cycles recorded at 690nm (full line). 103

Figure 4.10 - Chromaticity coordinates *xy* obtained by in situ chronocoulomery/chronoabsorptometry for PB films deposited over PET/ITO. Films with 300s (open square), 600s (open circles) and 150s (open triangles) deposition time. Note: all the potentials were measured using Ag/AgCl reference. 105

Figure 4.11 - *Salen*-type complexes of Cu(II), Ni(II) and Pd(II): (A) [M(3-MeOsaltMe)], M=Ni or Cu and (B) [X(3-Me*salen*)], X=Pd. 106

Figure 4.13 - *In situ* cronocoulometry/cronoabsorptometry data for Pd film deposited on PET/ITO in acetonitrile 0.1 M TBAP as supporting electrolyte. Left: Left: chronoabsorptometry recorded at 765nm (full line), CE (dots). Right: chronoamperometry (full line+full circle), square-wave switching between −0.2 and 0,6V (*vs.* Ag/AgCl), step duration of 50s (full line). 108

Figure 4. 14 - *In situ* cronocoulometry/cronoabsorptometry data for Cu film deposited on PET/ITO in acetonitrile 0.1 M TBAP as supporting electrolyte. Left: chronoabsorptometry recorded at 620nm (full line), CE (dots). Right: chronoamperometry (full line+full circle), square-wave switching between −0.15 and 1.4V (*vs.* Ag/AgCl), step duration of 60s (full line). 109

Figure 4. 15 – *In situ* cronocoulometry/cronoabsorptometry data for Ni film deposited on PET/ITO in acetonitrile 0.1 M TBAP as supporting electrolyte. Left: chronoabsorptometry recorded at 576nm (full line), CE (dots). Right: chronoamperometry (full line+full circle), square-wave switching between 0 and 1.3V (*vs.* Ag/AgCl), step duration of 65s (full line). 109

Figure 5.1 – Cation (sphere) transport mechanism in a polymer based electrolyte. Motion coupled to that of the polymer chain (up) and transfer of a cation between chains (bottom). 127

Figure 5.2 – Ionic conductivity (left) and equivalent ionic conductivity (right) of the gel electrolyte at different salt content in M (the chemical concentration was calculated considering stoichiometric chemical quantity of $LiClO_4$ and the volume of acetonitrile in the respective mixture; mol LiClO4 divided by the volume of acetonitrile) at 21ºC. 134

Figure 5.3 – Ionic conductivity (κ) of the clear gel electrolyte as a function of temperature. 135

Figure 5.4 - Electrochemical window for gel polymer electrolyte determined by cyclic voltammetry. A two electrode electrochemical cell was used with the electrolyte film sandwiched in between. The working electrode was a PET-ITO and the counter electrode and reference electrode was used as a one electrode also from PET-ITO; clear gel electrolyte (left) and opaque yellow gel electrolyte (right). 136

Figure 5.5 – ECD-R in a symetric "sandwich-like" architecture. 137

Figure 5.6 – Reflectance spectra of ECD-2 at different percentages of doped PEDOT as a function of the applied electrical potential. Potentials are measure *vs.* PEDOT/ITO electrode. 138

Figure 5.7 – Left: spectroelectrochemical data for the first cycle operated on the ECD-1 (open circle) and the ECD-2 (open square) during the coloration process (+0.4V *vs*. PEDOT/ITO); Right: spectroelectrochemical data for the first cycle operated on ECD-1 (open circle) and ECD-2 (open square) during the bleaching process (-1.5V *vs*. PEDOT/ITO). The insets show a zoom-in for the respective plot, detail on the optical variation during the first second after the electric trigger is shown. 139

Figure 5.8 – The write-erase cycling stability test data from ECD-1. Left: variation of the reflectance of the device during write-erase cycling tests, first cycles (full line) and after 1200 cycles (open circle + full line). Right: square-wave electrical potential used to operate the stability cycling tests of the device (dashed line), and chronoamperometry data during the stability cycles (full line) 140

Figure 5.9 – The write-erase cycling stability test data from ECD-2. Left: variation of the reflectance of the device during write-erase cycling tests, first cycles (full line) and after 1200 cycles (dots). Right: square-wave electrical potential used to operate the stability cycling tests of the device (dashed line), and chronoamperometry data during the initial cycles (full line).....141

Figure 5.10 – Variation of the reflectance *vs.* the charge consumed by the ECD-1 (left) and ECD-2 (right). ...143

Figure 5.11 - Spectroelectrochemical data of the complementar PET/ITO/PB/SPE4/PEDOT/ITO/PET ECD in the coloured state (+1 V *vs.* PEDOT, dashed line) and bleached state (−1.5 V *vs.* PEDOT, continuous line). Inset: Absorbance data at 630nm for the PB/SPE4/PEDOT electrochromic cell as a function of the potential applied. 151

Figure 5.12 - Cyclic voltammogram of the ITO/PB/SPE1/PEDOT/ITO electrochromic cell. The reported cell voltage is that of PB with respect to PEDOT (*vs.* PEDOT).....152

Figure 5.13 - *In situ* chronocoulometry/ chronoabsorptometry data for PET/ITO/PB/SPE1/PEDOT/ITO/PET electrochromic cell during short cycling tests; chronoabsorptometry recorded at 630nm (left), chronoamperometry (right).....153

Figure 5.14 - Full switch in absorbance of the electrochromic cells before (black) and after (grey) 2500 short cycles (write-erase cycling, conditions presented in Table 5.9); the figure in each column accounts for the relative variation of full switch of absorbance at 630nm after 2500 short cycles = ($\Delta A_{2500} \times 100/\Delta A_{initial}$) − 100, see section 1.2.1 ECD parameters. The absorbance at 630nm for the coloured and bleached states for each cell is the values of the top and at the bottom of each column, respectively.....155

Figure 5.16 – The total ΔA at 630nm during the write-erase cycling test of the PET/ITO/PB/SPE5/PEDOT/ITO/PET.....157

Figure 6.1 – Schematic plan of the pipeline of the applied R&D work executed during the IDEIA projects, YInvisible-Papel, YInvisible-Textil and YInvisible-Quadros. 169

Figure 6.2 – Schematic view of the ECD model for the IDEIA projects. 171

Figure 6.3 – Substrate-electrode preparation with an electrical contact. Cupper electrical wires were connected to the TCO layer through conductive silver glue (left, textile-electrode sample). After the silver glue is dried epoxy glue is used to seal and give structure to the contact between electrical wire and the substrate-electrode (right, white board-electrode sample). 172

Figure 6.4 – Prussian Blue film electrochemically deposited over a TCO coated white board (white board electrode). The PB films are highly heterogeneous in all the electrode-substrates tested. 173

Figure 6.5 – Picture of the three electrodes electrochemical cell. Working electrode is the PB modified FORMICA-electrode, counter-electrode is a platinum wire and reference electrode is a SCE electrode. 173

Figure 6.6 –PEDOT:PSS deposited over paper-electrode (left, by spin-coating), textile-electrode (middle, with a brush) and board-electrode (right, by spin-coating). 174
Figure 6.7 – Images of the optical transition of PEDOT:PSS layer deposited over the paper-electrode by electrochemical oxidation (left) and electrochemical reduction(right). See experimental details in Table 6.4. 175
Figure 6.8 – Images of the optical transition of PEDOT:PSS layer deposited over the textile-electrode by electrochemical oxidation (left) and electrochemical reduction (right). See experimental details in Table 6.4. 176
Figure 6.9 – Images of the optical transition of PEDOT:PSS layer deposited over the board-electrode by electrochemical oxidation (left) and electrochemical reduction (right). See experimental details in Table 6.4. 176
Figure 6.10 – Pictures of the bleached (left) and coloured (right) optical transition of an ECD based on PEDOT:PSS modified paper-electrode. Electrochromic device architecture: Paper-electrode/PEDOT:PSS/white opaque electrolyte/PEDOT:PSS/ITO-PET, where the primary electrode is the PET-ITO. 178
Figure 6. 11 - Pictures of the bleached (left) and coloured (right) optical transition of an ECD based on PEDOT:PSS modified paper-electrode. Electrochromic device architecture: Paper-electrode/PEDOT:PSS/white opaque electrolyte/PEDOT:PSS/ITO-PET, where the primary electrode is the paper-electrode. 178
Figure 6.12 - Pictures of the bleached (left) and coloured (right) optical transition of an ECD based on PEDOT:PSS modified textile silicon coated-electrode. Electrochromic device architecture: Textile silicon coated-electrode/PEDOT:PSS/yellow opaque electrolyte/PEDOT:PSS/ITO-PET where the primary electrode is the PET-ITO. 179
Figure 6.13 - Pictures of the bleached (left) and coloured (right) optical transition of an ECD based on PEDOT:PSS coated Flectron N conductive textile. Electrochromic device architecture: Conductive textile-electrode/PEDOT:PSS/white opaque electrolyte/PEDOT:PSS/ITO-PET, where the primary electrode is the PET-ITO. 179
Figure 6.14 – Pictures of the bleached (left) and coloured (right) optical transition of an ECD based on PEDOT:PSS modified white board-electrode. Electrochromic device architecture: White board-electrode/PEDOT:PSS/opaque electrolyte (white)/PEDOT:PSS/ITO-PET. 180
Figure 6.15 – Variation of the total optical contrast of a paper-ECD during write-erase cycling test. 182
Figure 6.16 – Pictures of the proof-of-concept paper-ECD. This device shows an electrochromic map of the Lisbon downtown. The buttons on the bottom of the map will highlight a specific area of interest. The colour contrast is obtained by the electrochemical control of the coloured and bleached states of the PEDOT layer deposited over PET-ITO. The counter electrode is PEDOT coated paper-electrode. The opaque gels electrolytes used were pink (Alfama) and yellow (Bairro Alto). To power the device small flat batteries were integrated in the map. 185

Figure 7. 1 – ECD with a non-patterned electrochromic layer (up) and a patterned electrochromic layer as the primary electrode. Pictures show the bleached and coloured states for both devices at the left and right side, respectively. 190
Figure 7.2 – Schematic view of different ink-jet print-head technologies. Continuous mode technology (A), the drops are deflected by the electric field created between the two plate electrodes at the exit of the nozzle. The deflection of the drops allows to control the position where the ink land. The deflected drops (open circle) are collected back to the ink chamber. The non-deflected drops (full circle) land over the printing substrate. DoD ink-jet technology (B and C). Thermal print-head (B) ejects drops by the rapid vaporization of the ink at the surface of an electrode inside the ink chamber. Piezoelectric print-head in bend-mode (C) expulses a jet of ink by the application of pressure in the ink chamber by the stimulus of the piezoelectric ceramic plate. 192
Figure 7. 3 – Piezoelectric print-head waveform 194
Figure 7.4 – ECD proposed to assemble with the ink-jet printing technique 196
Figure 7.5 - Representative OpticaTM images captured during PEDOT reliability studies 198
Figure 7.6 – Electrolyte consisting in three stacked layers. Clear layer contains polymer, solvent and salt and the white opaque layer contains solvent, salt and TiO_2 nanoparticles. Polymer and TiO_2 suspended particles are not present in the same ink to avoid particle sedimentation (see text). 199
Figure 7.7 – Schematic view of the process to assemble an ECD using ink-jet and lamination techniques. ...202
Figure 7.8 - Ink-jet printed ECD (7 x 7 cm) showing the coloured state (left) and bleached state (right).....202
Figure 7.9 – Schematic representation of the influence of the polymer weight on the ink drop formation. From the left to the right the weight of the polymer dissolved in the ink-jet ink increases. For low molecular weight polymers the drop are easily detached from the ink stream and small drops (satellites) are formed. When the polymer weight is high the drops do not succeed to detach from the ink stream and a "bead-on-a-string" is observed. The drawings are na adaption from the pictures published in ref.10. 203

Index of Tables

Table 1.1 – Colour perceived as a function of the wavelength of radiation 5

Table 1.2 – Chromogenic systems and related characteristics.....19

Table 4.1 - Collected data from *in situ* choronocoulometry/chronoabsorptometry experiments of the PB films deposited on PET/ITO in 0.2 M KCl aqueous solution 104

Table 4.2 – Colorimetric coordinates collected for PB and PW films deposited over.....105

Table 4.3 - Collected data from choronocoulometry/chronoabsorptometry experiments for metal *salen*-type films, after one cycle.....110

Table 4.4 - *In situ* cronocoulometry/cronoabsorptometry of the *salen*-type metal.....111

Table 4.5 - Dominant wavelength (λ_d) for the electrochromic inorganic polymers.....113

Table 5.1 – Ionic conductivity and equivalent conductivity for gel electrolytes with different percentage of $LiClO_4$ salt.....133

Table 5.2 – Ionic conductivity of the clear and opaque gel electrolytes 136

Table 5.3 – Ionic conductivity of the electrolyte layer in ECD*-1 and ECD*-2 137

Table 5.4 – Collected data from spectroelectrochemical experiments for ECD-1, measured before the write-eras cycling test 142

Table 5.5 – Collected data from spectroelectrochemical experiments for ECD-2, measured before the write-eras cycling test 142

Table 5.6 – Performance output of the ECD-1 and ECD-2 144

Table 5.7 - p(TMC)/PEO(X/Y)$_n$$LiClO_4$ electrolytes for application on prototype solid-state electrochromic devices.....150

Table 5.8 - Spectroelectrochemical data for the different electrochromic cells PB/SPE#/PEDOT. 153

Table 5.9 - Short cycling conditions. 154

Table 5. 10 - Coloration efficiency parameters for PB/SPE5/PEDOT before and after cycling test stabilities. 156

Table 6.1 – Raw materials used in each industry, RENOVA, Filobranca and Bi-Silque.....169

Table 6.2 – Electrode substrates used during the IDEIA projects.....171

Table 6.3 – Prussian Blue electrodeposition experimental conditions 172

Table 6.4 – Electrochromism test of the PB layers by cyclic voltammetry, experimental details 174

Table 6.5 - Electrochromism test of the PEDOT:PSS layers by cyclic voltammetry, experimental details.....175

Table 6.6 - Electrochromism test of the PEDOT:PSS layers by chronoamperometry, experimental details ...175

Table 6.7 – Performance of the ECD based on Paper, textile and white board.....180

Table 6.8 – Write-erase cycling test results for the ECD based on paper, textile and white board. 181

Table 6.9 - Collected data from spectroelectrochemical experiments for paper-ECD, befor the write-erase cycles 182

Table 7.1 – General ink-jet ink parameters **195**
Table 7.2 - Formulation of PEDOT-F and respective characteristics **197**
Table 7.3 – PEDOT-F jetting reliability monitored for 100 printing nozzles **198**
Table 7.4- Formulation of the clear and opaque electrolyte ink **200**
Table 7. 5- Formulation of UV-curing electrolyte layer **201**

Preface

The Ph.D. dissertation “Chemical Approaches to Ubiquitous Computing” results from the collaborative work I developed in the last four years as a joint Ph.D. student between the Photochemistry and Supramolecular Chemistry research group (FOT, from FCT-UNL) and YLabs (YDreams Research Division). This Ph.D. work was co-funded by YDreams and Fundação para a Ciência e a Tecnologia through a BDE scholarship (Bolsa de Doutoramento em Empresa). All the scientific work was carried out in the facilities of the FOT Group.

An undefined borderline between fundamental and applied research was the best strategy I could find to meet the challenges proposed by my supervisors A. Jorge Parola and J. Fernando Pina (from academia) and Ivan Franco (from YDreams). As a Ph.D. student, my main objective was to build a knowledge base that would lead to the creation and development of innovative technologies and projects for YDreams.

Back in 2004, YDreams approached the FOT Group with the intent of exploring chemistry-based solutions in the area of invisible tags. The successful collaboration from this first project originated the motivations for my Ph.D. plan. Since that time, chromogenic systems based on photochromic, thermochromic, ionochromic and electrochromic materials have been studied and integrated into real devices. The results pointed out that electrochromism is the most appropriate chemical phenomenon to develop interactive products.

In addition to the results presented in this dissertation, the work developed since that time created scientific knowledge, intellectual property, new ideas and challenges and, most importantly, the motivation to grow and continue. All the know-how created in the field of chromogenic systems and devices is now materialized in the most recent YDreams spin-off – YDreams Interactive Surfaces.

Today, the R&D team in the laboratory from YDreams Interactive Surfaces is working on its first generation of chromogenic products to bring them into the market.

The future of YDreams Interactive Surfaces could not be better described than Prof. António Câmara’s (YDreams CEO) visionary inspiration and thoughts. The text of a futuristic press release written by Prof. António Câmara is partially transcribed below. With this vision, a new R&D and Innovation cluster including some of the most important Portuguese industrial groups have been created – The Invisible Network.

"Invisible Computing makes a splash at CES"

Associated Press, Las Vegas, February 18th, 2013

The booth of Invisible Network (IN), a consortium of leading Portuguese companies and research teams, made a splash at the Consumer Electronics Show in Las Vegas with a new generation of interactive products based on traditional substrates used as screens (cork, paper, plastic, textile, wood, glass, concrete, leather and ceramics) and electrochromic inks (that change color with the use of an electrical current triggered by user interaction).

YDreams Interactive Surfaces, IN leader, used the term "invisible computing" to define the processes of activating and de-activating pre-programmed information layers, displaying animations and performing simple computation operations using electrochromic inks. These inks are deposited onto the different target substrates using ink-jet printing, along with conductive oxides, energy sources, and other electronic, chemical or biological sensors and processors. "Invisible computing" requires less energy, provides imagery with higher resolution and contrast and is faster than conventional computing for trivial visualization processes.

Examples of more than thirty "invisible computing" surfaces and objects displayed at the IN booth included an interactive floor flashing way-finding information, a special edition of Time magazine with interactive graphics, ceramic white boards where calendars and calculators could be activated and de-activated, plastic bottles that incorporate information displays, interactive jeans, tables with interactive games, bottles of wine that offered interactive information and color-changing concrete panels." by Prof. An*tóni*o Câmara, private communication.

I wish to thank my scientific supervisors A. Jorge Parola, J. Fernando Pina and the entire FOT Group not only for the facilities but also for the scientific support during the last four years that still continues. Prof. António Câmara for the opportunity to take part on the development of his visionary concepts. YDreams team in special to Edmundo Nobre and my co-supervisor Ivan Franco for the trust deposited in my work.

Finally, I want to express my debt to the Portuguese State and YDreams for the financial support.

Chapter 1

General Introduction

1.1 Motivation

"The technology required for ubiquitous computing comes in three parts: cheap and low-power computers that include equally convenient displays, a network that ties them all together, and software systems implementing ubiquitous applications." *in* "*The Computer for the 21st Century"* by Mark Weiser.[1]

Mark Weiser's vision of computing and society predicts the so-called third wave of computing - ubiquitous computing (UC). Mark Weiser resumes the relationship between computers and society in three main eras related with technology development and usability. In the first era, one computer was shared by several people – *mainframe era*. In the second era, one computer belongs to one person – *personal computer* era.[2] Finally, the upcoming era will be the UC era, where computers will spread all around us and the computer to person ratio will be much larger than ever before.

Presently we are living in the *personal computing era*, however, the decline in laptop prices, the proliferation of small and mobile devices equipped with strong processors and the dissemination of the internet are preparing our society towards UC. In a not so futuristic scenario, customized computers will integrate our surrounding embedded in the objects of our daily life. Functionalities will be added to common objects, they will turn more interactive and smart. Information will be available without any conscious input from the user; computers will integrate symbiotically our environment and costumes in such a way that they become invisible.

Convenient, cheap and low-power consumption displays are some of the challenges predicted by Mark Weiser to the development of UC. The information can be processed in a completely different physical place from the end-user, the computer can be off-site (for example, weather forecast); however, communication of the results must happen *in loco*. Processing information without an effective communication is useless.

Visual communication is one of the most primitive ways humankind uses to communicate and record information. The oldest evidences of visual communication are from *ca.* 40000 years ago[3] in the form of paintings in caves and still have an enormous presence in our society. Pictograms are still the best way to produce effective communication; a good example is traffic signs. On the other hand, colours by themselves are also able to transmit information or feelings.

UC is strongly dependent on the development of ubiquitous displays. Such displays should harmoniously integrate our surroundings, should be embedded in almost all daily life objects, for example in a cup of coffee, in a pillow, in a sheet of paper, in a chair, in a wall, in a t-shirt. Such applications require flexible, low power consuming, thin and miniaturized devices. State-of-the-art displays are unsuitable for ubiquitous applications; cathode ray tube (CRT)

are bulky size, high weight and energy demanding, plasma technology is also a power consuming technology ant not liable to miniaturization.[4] Companies like Siemens, Fujitsu, Xerox, DuPont, Sony, Siemens and Phillips are investing significant resources in the development of transparent, flexible and energy efficient displays using alternative technologies. The most recent examples are based on the organic light emitting diodes (OLED), electrophoretic suspended particles displays, electro-wetting displays and electrochromic displays.[4] The strategy adopted by such companies is always based on the highly technology demanding matrix of pixels to reach video and image on demand capabilities. However, we believe that this is neither the only nor the most successful way to reach information ubiquity.

At the same time as computers will spread around us, their complexity and multi-function capacity should inversely decrease. It is a waste of resources and energy to use powerful processors to run simple tasks for specific situations. Ubiquitous computing should be shaped for minimal architecture to process customized information. For sure, we do not want our cup of coffee to perform mathematical calculus! The same holds for the displays technology. António Câmara (CEO of YDreams Company) identified a technological gap between static information displays, like an advertisement poster, and state-of-the art displays.

"Chemical Approaches to Ubiquitous Computing" is a Ph.D. project that aims to study and develop low information content displays based on chemical solutions. A brief exposure of the chemical and technology background involved in this work is presented in this chapter; at the end, an outline of the work is presented.

1.2 Chromogenic Systems and Applications (Background)

For a long time chromogenic compounds and materials have been studied and explored in different scientific fields like, analytical chemistry (*e.g.* acid-base titration, complexometric titration), physical chemistry[5], smart materials[6] and even in art.[7] As a general definition chromogenic systems are those which produce (-gen, from Latin *genus* = produce) colour (chromo-, from Greek *khrōma* = colour). IUPAC does not define the term chromogenic and different interpretations can be found in the literature. Nevertheless, in this work the chromogenic term is defined as a compound, material or system that undergoes reversible colour transition between two or more states, triggered by an external stimulus. The optical transition should be in the visible range between two or more differentiable coloured states or between a colourless and a coloured state.

Since Isaac Newton's experiments about optics, colours are known as the elementary components of light. In 1704 Newton's conclusions about light and colour abolished the basic fundamentals that ruled colour knowledge since Aristotle and set a new age for colour science and optics.[8] Light interaction with bulk matter can result in reflection, scattering, absorption and transmission of light (see Fig.1.1). Depending on the light and the nature of the object, several of these phenomena can happen at the same time.

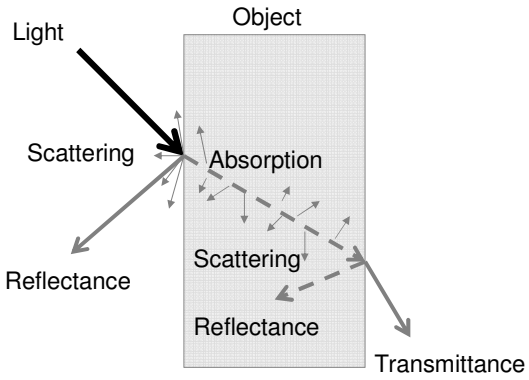

Figure 1.1 – Light interaction with matter; reflectance, scattering, absorption and transmittance

Colour genesis is explained by physical and chemical mechanisms. Kurt Nassau[9] gives a more detailed classification of colour generation based on these two mechanisms: i) vibration and simple excitations of electrons; ii) electronic transitions involving ligand field effects; iii) transitions between molecular orbital; iv) transitions involving energy bands; v) geometrical and physical optics. Physical optics are responsible for the blue sky, rainbows, red sunset, iridescent colours in fauna and for the spectral decomposition of white light by a prism. Geometrical and physical optics deal whit the different interactions between light and bulk material - refraction, scattering and interference.

Chemical colour results from the perfect match in energy between the visible electromagnetic radiation (380 - 780nm) with electrons and their electronic energy levels in chemical species. Electromagnetic wavelengths lower than ultra-violet radiation (UV, <200nm) are too energetic and molecular structures are usually irreversibly destroyed or altered. On the other hand, electromagnetic radiation with wavelengths higher than 780nm up to the near infrared region radiation (NIR) can still interact with several kinds of compounds (strongly conjugated organic molecules, some metal complexes with d-d or f-f transitions); however, we humans are not able to see this interactions.

The colour of the majority of the chromogenic systems arises from the partial absorption of the visible electromagnetic radiation, resulting from the interactions between light (380nm-780nm) and electrons. In Table 1.1, an approximation of the colour perceived based on wavelength of the radiation absorbed by the system is shown.

Table 1.1 – Colour perceived as a function of the wavelength of radiation

Absorbed Wavelength (nm)	Colour of the absorbed light	Observed object colour
400	Violet	Green-yellowish
425	Indigo blue	Yellow
450	Blue	Orange
490	Green-bluish	Red
510	Green	Purple
530	Green-yellowish	Violet
550	Yellow	Indigo blue
590	Orange	Blue
640	Purple	Green bluish
730	Red	Green

The next sections are organized in function of the extend stimulus that leads to colour change and describe the most relevant chromogenic application for each area.

1.2.1 Electricity

Electrochromic materials have the ability to change reversibly its colour properties (coloration/bleaching) when submitted to a determined electric potential. Electrochromism can occur either by an electron-transfer process (redox electrochromism) or as a response to strong enough electric potential (non-redox electrochromism).

Originally, the term electrochromism was attributed to the shift of the UV-Vis bands due to the presence of a strong electric field - Stark effect.[10] The Stark effect is a non-redox electrochromic phenomenon.[11] Nevertheless, the majority of the reported electrochromic systems are redox electrochromism (see Eq.1.1). In the following text, the term electrochromism is always related to the redox electrochromism.

Oxidized form (colour A) + electron(s), e^- → Reduced form (colour B) Eq. 1.1

A great number of chemical systems are reported in the literature using either inorganic compounds such as transition metal oxides and metal hexacyanometallates, organic compounds such as viologens, conducting polymers, metallopolymers and metal phthalocyanines.[12] A particular class of materials show activity only in the NIR region and do not present colour variation upon reduction or oxidation, however, they are still considered as electrochromic materials. Despite the large number of electrochromic materials reported so far, few are those that show relative good performance for applications. The “big player”

electrochromes are: methyl viologen (MV)[13], tungsten oxide (WO_3)[14], Prussian Blue (PB)[15] and the semiconductor polythiophene derivative PEDOT (poly(ethylene dioxythiophene).[16]

Electrochromic Devices

An electrochromic device (ECD) can be regarded as an electrochemical cell where colour changes occur upon electrochemical reactions of two or more redox active electrochromic materials electrically connected by an external circuit and physically separated by an ionic conducting layer (electrolyte layer), see Fig.1.2. The electrochromic material must be in contact with the electrode and with the electrolyte layer to exchange both electrons and ions, respectively. ECD performance is greatly influenced by both the electron exchange and ions exchange kinetics and ultimately controlled by the slowest process. The colouration and bleaching processes are controlled by the amount of the overvoltage and polarity applied at the electrode terminals.

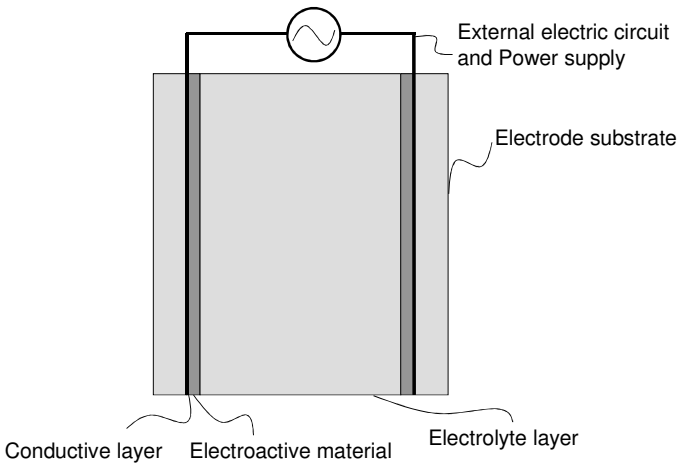

Figure 1.2 – Example of an electrochromic device with the “sandwich” like architecture.

An ECD requires two electroactive materials and at least one of them must be electrochromic. The electrochemical reduction in one of the electrodes is balanced electrically by the electrochemical oxidation at the second electrode. In a second implementation, both electroactive materials can be electrochromic, resulting in either a complementary configuration or a symmetrical configuration.

Complementary ECD shows a synchronised colouration and bleaching response from both electrodes. It is worth to note that bleaching process should not be restricted to the transition from a coloured state to a colourless state, but also a transition to a second coloured state; for example, poly(3-hexylthiophene) presents a transition colour between blue and red. This ECD configuration requires that one of the electrodes present a cathodically colouring process, while the second has an anodically colouring process.

On the other hand, symmetrical configuration results when the same electrochromic material is used at both electrodes. An opaque layer is within the electrolyte layer to mask the colouration process occurring at the second electrode. The symmetric cell presents a non-synchronised colouration and bleaching response from the two electrodes, while one is coloured the other is bleached and vice-versa.

To observe successfully the colour transition of ECD at least one of the electrodes substrate must be optically transparent. The most common electrodes substrates are glass (non-flexible applications) or a plastic film (the most common are the polyethylene terephthalate, PET and polyethylene naphthalate, PEN used for flexible applications) coated with a thin film of a transparent conductive oxide (TCO); tin-doped indium oxide (ITO) or the fluorine-doped tin oxide (FTO). Several substrate-TCO alternatives are commercially available whereas glass-ITO, PET-ITO and FTO-ITO are the most reported in the literature. As defined by Rosseinsky *et al*[11] the electrode where the colour transition is observed should be called the primary electrode and the second the counter-electrode. In this case, the primary electrode must always be optically transparent while the counter-electrode can be either completely transparent or reflective.

The electrolyte layer ensures the electroneutrality of the device cancelling charge accumulation at the surface of the electrodes during the redox process. Different systems can be used from simple salt dissolved in a liquid solvent to inorganic super ionic conductors.[17,18,19,20]

ECD can be operated in the transmittance (ECD-T) or in the reflectance (ECD-R) mode (see Fig.1.3).

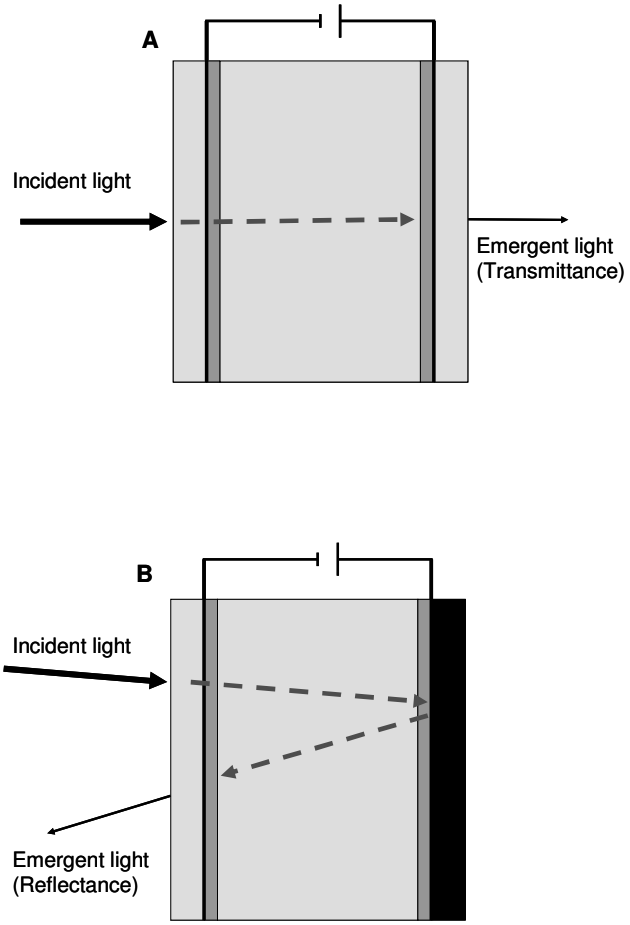

Figure 1.3 – ECD in transmittance mode (A), and in reflectance mode (B)

The ECD-T requires that both the primary and the counter-electrodes are optically transparent. On the other hand, the ECD-R only requires one optically transparent electrode; the other electrode can be made of a thin metallic reflective film, like graphite, gold or platinum alloys. The incorporation of a light scattering layer over the counter-electrode or within the electrolyte layer improves the reflectance characteristics of the ECD-R (see Fig.1.5). A large variety of ECD combinations can be explored depending on the specific application. As an example, ECD-R the reflective layer can take different colour appearance and create new colour combinations with the colours of the electrochromic materials.

Through the text, the nomenclature adopted to describe a specific ECD will be as follows: Electrode-1/Electrochrome-1/Electrolyte/Electrochrome-2/Electrode-2; similar to the one used to define a two-compartment electrochemical cell.

ECD Parameters

The full characterization of an ECD includes determination of parameters such as: contrast ratio (CR), response time (τ), write-erase efficiency, stability towards cycling tests, power consumption and coloration efficiency (CE).[11]

CR is a measure to denote the intensity of colour formed, as seen by eye (see Eq.1.2).

$$\mathrm{CR} = \frac{R_0}{R_x} \qquad \text{Eq. 1.2}$$

Where R_x is the intensity of light reflected diffusely by the coloured state of the device, and R_0 is the intensity of reflected light from a non-shiny white card.[11]

The write-erase efficiency corresponds to the fraction of the originally formed coloration that can be subsequently electro-bleached. For complete reversible electrochromes, the value should be 100%. The write-erase efficiency is however related with the time during which electric potential is applied, slower systems will require longer time to recover completely the initial state. Considering the application requirement the systems may or may not be able to recover completely the original state. Great variability of experimental conditions have been reported to calculate the write-erase efficiency of electrochromic systems, the results reported are not directly comparable.

Power consumption can be calculated for both coloration and bleaching process by Eq.1.3.

$$E = \Delta \mathrm{V} \int_{t_0}^{t_f} I(t)dt \qquad \text{Eq. 1.3}$$

Where ΔV is the amount of electrical potential applied to the ECD and $I(t)$ is the current spent during the cycle.

The stability of the ECD to the number of electrochemical cycles (write-erase cycles or cycling) represents the number of cycles that can be performed before significant extent of degradation has occurred. The maximum colour variation of a specific ECD-R and the ECD-*T* (Full switch), between the bleached and the coloured states, is measured at the beginning of the cycling experiment at a specified wavelength (λ_{nm}): $\Delta\%R_{\lambda nm,0}$, $\Delta\%T_{\lambda nm,0,}$ respectively. A double potential step voltage function is applied to ECD in order to operate a full cycle (*i.e.* a Full switch): write-erase (colouration-bleaching) and *vice versa*. The comparison of the maximum colour variation (100% of Full switch) after the operation of *n* cycles, $\Delta\%R_{\lambda nm,n}$ or $\Delta\%T_{\lambda nm,n}$ with $\Delta\%R_{x,\lambda nm,0}$, $\Delta\%T_{\lambda nm,0,}$ values allows to calculate the loss of colour variation (see Eq. 1.4 for ECD-R, when working in transmittance $\Delta\%R$ is substituted by $\Delta\%T$).

$$\%\ loss\ of\ colour\ variation = 100 - \frac{\Delta\%R_{\lambda nm,n} \times 100}{\Delta\%R_{\lambda nm,0}} \qquad \text{Eq. 1. 4}$$

The CE of the electrochromic system is defined by Reynolds et al.[21] as follows in Eq.1.5 and 1.6, for ECD-T and ECD-R respectively:

$$CE = \frac{\Delta A_{x,\lambda nm,n}}{\Delta Q'} \qquad \text{Eq. 1.5}$$

$$CE = \frac{\%\Delta R_{x,\lambda nm,n}}{\Delta Q'} \qquad \text{Eq. 1.6}$$

where $\Delta\%R_{x,\lambda nm,n}$ and $\Delta\%T_{x,\lambda nm,n}$ is the x percentage of full swithc. *i.e.* the fraction of $\Delta\%R_{\lambda nm,n}$ and $\Delta\%T_{\lambda nm,n}$ respectively, and *Q'* is the amount of charge per unit of active electrochromic area passed during the respective period of time.

Spectroelectrochemistry

Spectroelectrochemistry (SEC) is the most useful characterization procedure for electrochromic materials and devices. SEC combines electrochemistry and spectroscopy techniques. In a specially designed electrochemical cell, a redox active compound is oxidised or reduced. The products of the redox transformation are monitored *in situ* by spectroscopic techniques. In the particular case of chromogenic systems, the UV-Vis spectroscopy is used. In the case of electrochromic films deposited over PET-ITO electrodes, the three electrodes electrochemical cell is mounted in the UV-Vis spectrophotometer cuvette. On the other hand, ECD are directly inserted in the spectrophotometer sample compartment in a perpendicular geometry with the beam of light. The diffuse reflection of the ECD-R is recorded by an integrating sphere.

The electrochromic systems can be controlled both by potentiostatic and potentiodinamic techniques; at the same time, the UV-Vis data is recorded either in absorbance or in reflectance mode. The typical outcome of the SEC experiments is the absorbance (chronoabsorptometry, ΔA or $\Delta\%T$) or reflectance ($\Delta\%R$) evolution of the system. On the other hand, the current evolution of the system gives the chronoamperometry or chronocoulometry data.

Commercial applications

Electrochromic materials have been attracting considerable attention due to their potential applications as controlled optical filter and visual displays. Product applications are self-darkening rear-view mirrors, smart windows, electronic paper and smart labels. Despite the first patent describing the application of an electrochromic effect dates from 1929[22], the number of successful commercial applications of ECD is reduced. Actually, the only known profitable ECD application is the best-selling electrochromic rear-view mirror from Gentex.

Self-darkening rear-view mirror and windows

The auto-dimming rear-view mirrors reduce the inconvenient and sometimes dangerous headlight glare from the vehicles travelling behind, disturbing the driver. Gentex is the company leading the auto-dimming automotive market.[23] The scientist responsible for the invention of the electrochromic rear-view mirror is the chemist Dr. Harlan Byker. Today Dr. Harlan Byker is president and owner of the Pleotint Company (developing thermochromic windows).

The rear-view mirrors from Gentex incorporate a light sensor that detects when headlight glare occurs and triggers the electrical potential of the ECD built in the rear-view. The ECD architecture is based on the reflective mode (ECD-R) and the redox active material are dissolved in the liquid electrolyte layer. The electrical potential promotes the electrochemical colouration of the primary electrode and the colouration of the counter-electrode using a complementary colouring electrochromic material. When the electrical potential is removed, both electroactive materials will diffuse away from the electrodes. The recombination of the oxidised and reduced species will promote the bleaching process chemically. The bleaching time will be controlled by the diffusion of the electrochromic species, however, the process can also be accelerated if an opposite electrical potential (compared to the one used to trigger colouration) is imposed between the electrodes for a short period of time.

A second application of self-coloured ECD has been applied for “smart-windows”.[24] Smart windows were applied in special architectural projects like the switchable glazing applied in the Stadtsparkasse Dresden am Altmarkt in Dresden and also for first class airplane passenger windows in the “Dreamliner” Boeing aircraft.[25] At present, SAGE Electrochromics, Inc. is the only manufacturer selling electrochromic insulating glass units.[26]

Displays

Another interesting application of ECD is in the field of visual displays. The ECD-R is the preferred configuration for display application, because it presents higher CR when compared with ECD-T. As opposed to emissive traditional displays, ECD is a colour subtractive display. The advantages to be a colour subtractive technology are the wide

viewing angle, natural contrast (comparable to pigments used in conventional inks) and power saving technology. Actual ECD display products can be relatively bent without damaging the screen and the thicknesses are around hundreds of nanometres.
It is worth to note that in non specialized literature, electrochromism is often confused with competing technologies for flexible displays such as: electrophoretic technology from E-Ink[27], or the Avesso displays based on acidochromic compounds[28] and electrowetting technology from Liquivista.[29]

PaperDisplay

PaperDisplay's products are based on Acreo's EC technology that uses functional printing inks in conventional printing equipment to achieve low cost visualization displays based on photographic paper.
PaperDisplay presents a colour transition between light-blue and dark-blue corresponding to the neutral and doped states of the organic semiconductor PEDOT. The display is built over photographic paper coated with PEDOT electrochromic material from Agfa - Orgacon. In opposition to "sandwich" like ECD architecture (see Fig.1.2), Acreo EC technology adopts a horizontal architecture where the two electrodes are deposited on the same plane – horizontal architecture (see Fig.1.4).

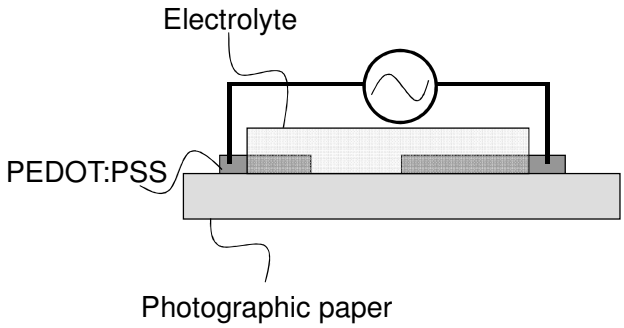

Figure 1.4 – Schematic view of the ECD from Acreo EC technology with a "side-by-side" architecture.

The electrodes 1 and 2 lay down on the same plane, side by side electrically separated but connected by the electrolyte layer. Acreo technology does not require a metallic or semi-metallic electric conductive layer. A special conductive grade of the PEDOT:PSS layer is used as the electrochromic layer and electrode, at the same time.
PaperDisplay announces that their product as a price of 0,005€/cm^2 and they claim to have the capacity for high volume production.[30] Actually, the ECD are roll-to-roll printed by screen-printing method.[31,32]

NTera

NTera developed electrochromic displays with the trademark NanoChromic Display (NCD). The ECD architecture used is based on the "sandwich" like architecture working in a reflective mode (see Fig.1.5).

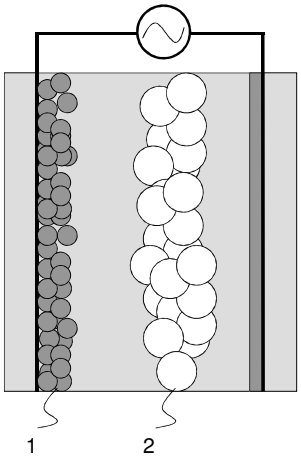

Figure 1.5 – ECD architecture employed by NTera where the primary electrode is composed by a chemisorbed viologen derivative on the surface of TiO_2 nanoparticles (coated PET-ITO) (1), a dispersion of light scattering TiO_2 nanoparticles is incorporated in the electrolyte layer (2).

The electrochromic layer (see Fig. 1.5, **1**) is made with a phosphonated viologen derivative that is adsorbed to titanium dioxide (TiO_2) nanoparticles. This strategy is similar to the one proposed in dye sensitized solar cells (DSSC) by Grätzel.[33] This strategy has the advantages of, i) increase the concentration of electrochromic molecules pre electrode area and ii) avoids diffusion of the electrochrome away from the electrode. The NCD is based on transparent plastic and the semi-metal conductive layer is fluorine-doped tin oxide.[11] The reflective mode was used to improve the CR. The light scattering layer is also composed by TiO_2 nanoparticles within the electrolyte layer.

NCD are also built by printing techniques such as screen-printing, flexography and ink-jet. The NTera company is the only known fabricant commercializing screen-printable inks that allow to build an ECD based on the NanoChromic technology.[34]

1.2.2 Light

Reversible transformation of a molecular system between two forms, A and B, having different absorption spectra, induced in one or both directions by absorption of electromagnetic radiation is the definition of photochromism. The spectral change produced is typically, but not necessarily, of visible colour and is accompanied by differences in other physical properties.[35]

A (colourless) $\underset{\Delta}{\overset{h\nu}{\rightleftharpoons}}$ B (coloured) Eq. 1.7

A (colourless) $\underset{h\nu'}{\overset{h\nu}{\rightleftharpoons}}$ B (coloured) Eq. 1.8

Accordingly to the photochemical backward reaction, systems can be classified in T-type, P-type or both at the same time. Considering a photochemical reactive species, A which is photochemically converted to B, the backward reaction can be controlled either thermally (T-type system, Eq. 1.7) or by light excitation (P-type system, Eq. 1.8) and depending on the activation energy for the backwards reaction (B to A) and on the operation temperature both processes can take place.

Spiropyrans, spirooxazines and chromenes are examples of T-type photochromic systems (see Fig.1.6), while fulgides and diarylethenes are characterized to be P-type photochromic (see Fig.1.7).[36]

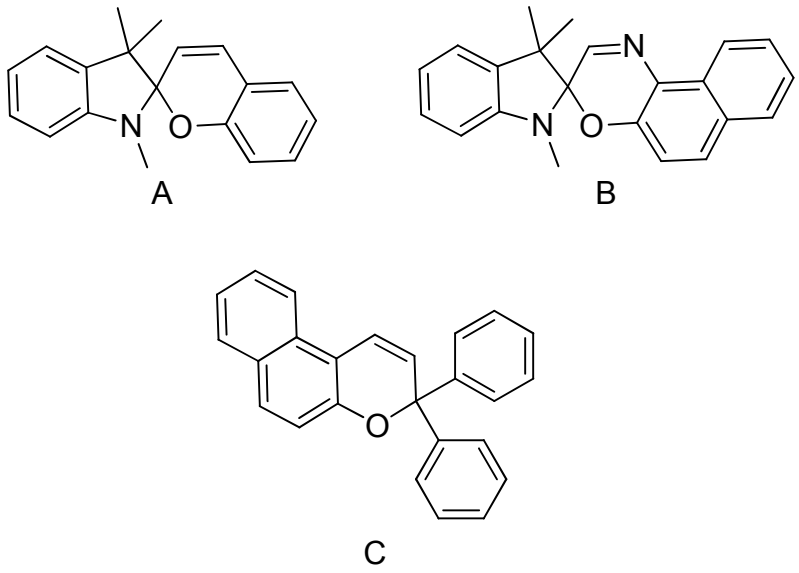

Figure 1.6 – T-type photochromic compounds, spiropyrans (A), spirooxazines (B) and chromenes (C)

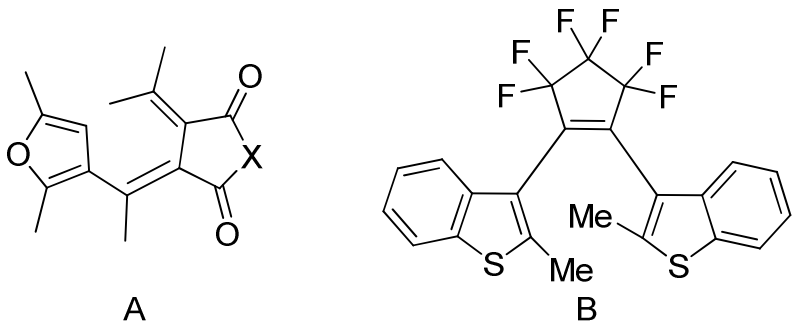

Figure 1.7 – P-type photochromic compounds, fulgides (A) and diarylethenes (B)

Commercial Products

One of the most cited photochromic product is the silver halide photochromic ophthalmic lenses. Launched in 1966 by Corning Inc (Photogray lens).[37] Inorganic based systems have been successfully used in glass lenses. The introduction of plastic in the manufacture of ophthalmic lenses determined the progressive substitution of the silver halide system by spirooxazines and chromene photochromic organic compounds. Organic photochromic lenses were introduced in the market with the commercial name Transitions by PPG Industries and Essilor International.[38]

Commercial photochromic products are also found in printed photochromic logos on T-shirts or other pieces of textile for clothing. Other similar applications have been used on children's toys.[6]

Photochromic dyes under the trade name of Reversacol are available in twenty different colours from Vivimed Labs Europe Ltd.[39] These inks are based on organic photochromic compounds and can be used as a organic dye in inks, paints and incorporated in plastics such as PE, PP, PVC. Photochromic ink formulations are available for printing by gravure, offset, flexographic, pad printing, lithography and screen printing techniques.[40]

1.2.3 Ions

The presence of ionic species such as protons or metal ions can trigger the colour transition of a system; a phenomenon called ionochromism. Ionochromism also includes acidochromic compounds, which show colour transition depending specifically on the presence of H^+ ions. Some authors consider the previous phenomena as distinct; nevertheless, it is acceptable to merge all this phenomena in the ionochromism term.

Classical examples of acidochromic systems are all the pH indicators such as the methyl red (see Fig. 1.8).

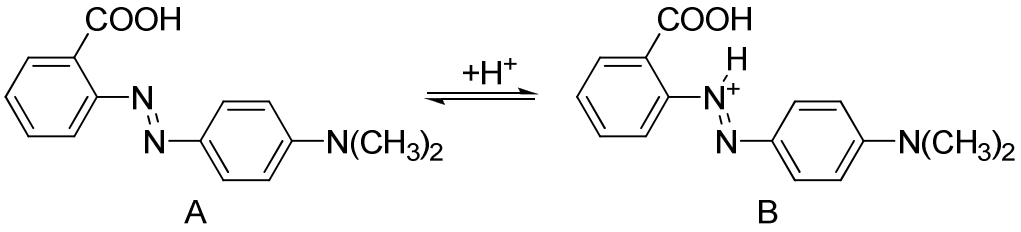

Figure 1.8 – Acidochromism mechanism of the Methyl Red, the base form is colourless and at a pH = 4.4 the azonium for is red.

A large number of ionochromic compounds belong to the family of the *leuco* dyes. The term *leuco*, meaning white, comes from the Greek *Leukos* and is used to characterize the uncoloured state of the (reversibly) reduced state of any kind of dye. Although initially the

term leuco was applied to the reduced form of a dye, the term leuco dye has been used also to describe the colourless form of a dye that may be produced by a non-reductive process, as for example, in the case of intramolecular cyclization, reactions induced by pH change, heat, or light.

Commercial Application

The ionochromism phenomena have been used in analytical chemistry, carbonless copy paper and thermal recording paper. Analytical chemistry techniques explore the colour transition of ionochromic compounds to detect and quantify the presence of hydrogen ions (pH indicators or acid-base titrations) and metal ions in complexometric titrations.[37]

The carbonless copy paper is a handwritten or mechanically typed duplicating process developed to substitute the carbon paper. The simplest carbonless copy paper is composed by two sheets of paper overlaying on top of each other. The top page is undercoated with microencapsulated ionochromic dye known as the colour former, e.g. Crystal Violet Lactone, in a non-volatile solvent. The pressure of the pen causes the microcapsules to break, exposing the dye precursor to a developer that is coated on the top of the lower sheet; usually an acidic material, which can be selected from acidic clays, zinc salicylate and phenolic resins are used as the coating layer. For multiple copies, intermediate sheets are coated on both top (reagent to react with the dye precursor on the sheet above) and bottom (microcapsules of dye precursor to react with the reagent on the sheet below).[41,42]

1.2.4 Electricity and light or ions and light

A higher level of complexity is presented by the chromogenic systems that respond to two different external stimuli. Dual-mode chromogenic systems have been described to be responsive both to electricity (electrochromism) and light (photochromism) and to light and ions (ionochromism). In such a case, electrochromism, photochromism and ionochromism are observed within the same system.

Branda *et al.* reported the dual-mode photochromism and electrochromism of a 1,2-bis(dithienyl)cyclopentene derivative (see Fig. 1.9). The colourless (pale yellow) ring-open form can be converted to the deep-blue coloured ring-closed form, both by UV radiation and oxidative electrochemical reaction.

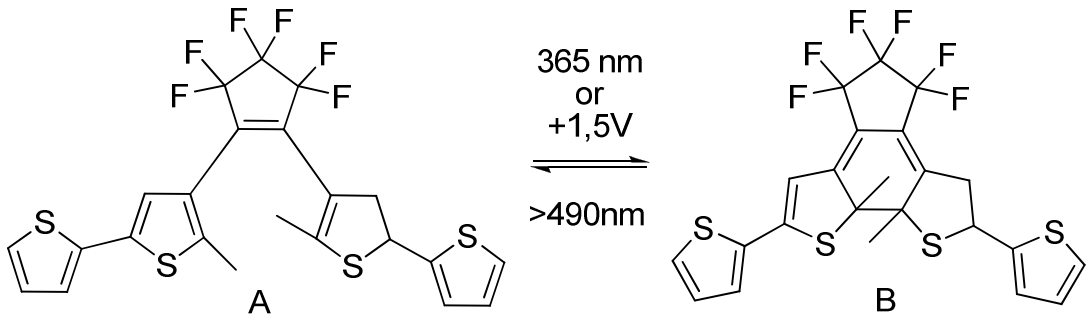

Figure 1.9 – Dual-mode photochromism and electrochromism of the 1,2-bis(2-methyl-5,2'-dithiophen-3-yl)perfluorocyclopentene, the pale yellow ring-open form (A) is converted both by an electrical potential and by UV light to the coloured ring-closed form (B)

The system shows good thermal stability of the coloured form, however, a slight electrochemical degradation during the anodically colouring step is observed. The systems may be reversibly converted to the bleached state by the stimulus of visible light.[43,44] The coloured ring-closed form is thermally stable, however, it may suffer from degradation if overoxidation occurs. The oxometalate compounds (e.g. WO_3) are another class of dual-mode chromogenic systems responsive to both electricity and light.[45]

Dual-mode systems, responsive to light and ions, were also reported (see Fig.1.10). The ring opening of the crown ether-link spirobenzopyran is triggered by metal ions and UV light. The system changes from the colourless closed-ring state to the pink open-ring state. The back-reaction to the bleached state (closed-ring) is operated with visible light irradiation.

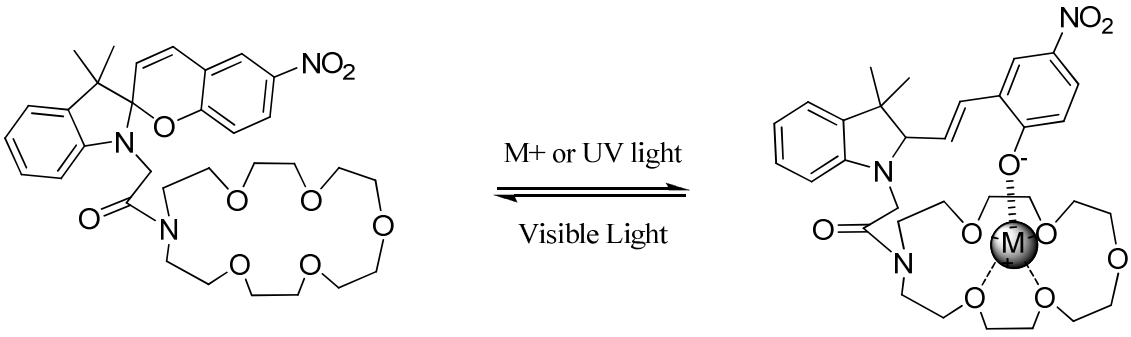

Figure 1.10 – The spiropyrans bearing a monoaza-crown shows dual-mode photochromic and ionochromic properties.

In opposition to the former systems where only one molecule is responsive to two external stimuli, other dual-mode systems can be obtained by the combination of two or more molecules. A photochromic and electrochromic device has been proposed to operate as a photoelectrochromic device (P-ECD).[46,47]

The P-ECD can be assembled using at the primary electrode a layer of electrochromic WO_3 film and at the counter-electrode a layer of the photovoltaic dye doped TiO_2 film. This device

requires that both electrodes are optically transparent to maximise the light absorption from the photoactive dye doped TiO_2 layer. The P-ECD can be envisaged as a DSSC proposed by Gratzel[33], however, the I_2/I_3^- redox relay is substituted by a redox active chromogenic layer. When the device is exposed to sunlight, the photovoltaic layer will produce a sufficient voltage to reduce the WO_3 film to the coloured state. The photoinduced transfer of electrons from the semiconducting TiO_2 layer powers the darkening of the electrochromic layer (see Fig. 1.11). The process is only reverted if light is removed and both electrodes are short-circuited or if an opposite electrical potential is applied to the system to revert the process. Independently the P-ECD can be powered as a normal ECD by an external source of electrical power. The advantages of such dual-mode device is the low-power requirement of the system when sunlight is supplied, the P-ECD darkening can be automatically triggered by light and it can also be operated on demand with electricity.

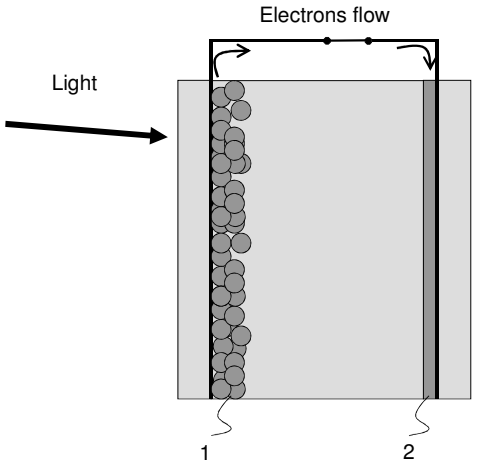

Figure 1.11 – Example of the operation of a P-ECD by light. Electrons are ejected from the photovoltaic layer (1) and reduction of the electrochromic WO_3 layer will cause the darkening of the device.

Commercial Applications

Dual-mode chromogenic systems based on a single molecule or on a combination of two or more molecules have shown great interest from academia, as seen above. They show an increase in complexity when compared with the classical chromogenic systems that allow to reach a multistimulus operated system. Despite the interesting characteristics of dual-mode systems, no commercial application is known as far as we know. The only dual-mode system able to reach the market soon should be the P-ECD.

1.2.5 Temperature, polarity, mechanical pressure and mechanical friction

The chromogenic systems stimulated by electricity, light, ions and combinations thereof described in the previous paragraphs are only a part of the chromogenic systems known. Other systems, like the thermochromism, are of great importance both for academia and for industry. Despite the relevance of the remaining systems, they fall out of the scope of this thesis. In Table 1.2, general information of ot\her chromogenic systems is listed.

Table 1.2 – Chromogenic systems and related characteristics

Phenomena	Stimulus	Commercial applications
Thermochromism	Temperature	Printed thermometers, textile for clothing interactive logos
Solvatochromism	Polarity	Humidity sensors
Piezochromism	Mechanical Pressure	-
Tribocromism	Mechanical friction	-

1.3 Industrial Printing Techniques

At the basis of every application of a chromogenic compound, there is the need for deposition techniques. The laboratory scale technology is useless when it is required to produce one million of devices for a client. High-volume manufacturing requires adequate industrial processes and the scale-up study of the technology is essential. Production of high-tech products, such as flexible displays, are adopting cheaper conventional graphics printing techniques instead of costly microfabrication processes.[48]

The microfabrication techniques are widely used in microelectronics; microchips, thin film transistors, microelectromechanical systems are produced by a subtractive approach were patterning is accomplished with photolithography and etching processes. In opposition to microfabrication, the graphic printing techniques are additive processes and widely available both at the pilot and industrial scale. It has been reported that the cost for printing a square centimetre is 0.00001$ with offset and 3$ with high resolution photolithography.[49]

Graphic printing techniques are divided into impact printing techniques (IP) and non-impact printing techniques (NIP). The image-carrying medium in IP consists on a physical printing plate, while NIP is digitally controlled and the image-carrying medium is bits of information.

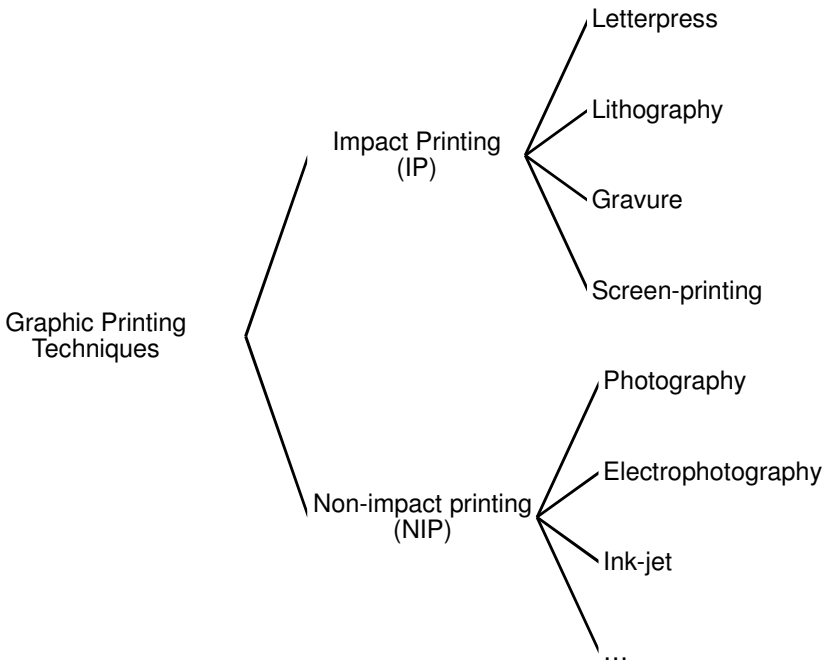

Figure 1.12 – Graphic printing techniques classified by the method ink is transferred to the printing substrate, adapted from ref.50

In IP, the ink is transferred by contact to the printing substrate accordingly to the print image information. Numerous printing techniques and combinations of printing techniques are available. The most representative IP techniques are screen-printing, letterpress, lithography and gravure. In Fig.1.13, the four main IP technologies are compared regarding the image carrier or printing plate.

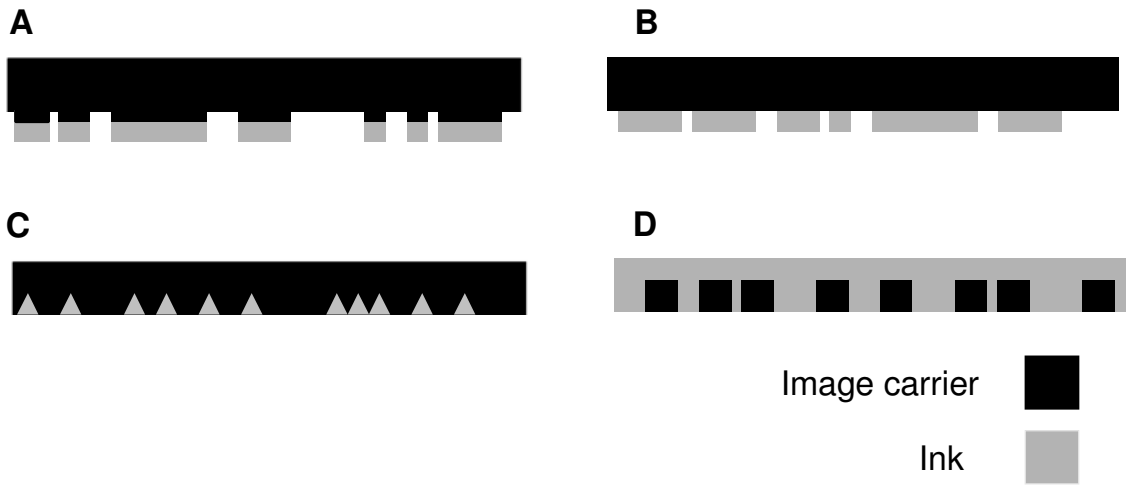

Figure 1.13 – Schematic draws of the physical printing plates for Letterpress (A), lithography (B), gravure (C) and screen-printing (D).

NIP is based on digital image information that allows to produce successive pages with different printed images. The most important techniques in this class is the ink-jet printing (IJ). IJ has completely invaded our life both at work and at home. The technology allows to print high quality photo with a relative low cost. The IJ techniques rely on the controlled ejection of droplets of ink by waves of pressure created in a chamber where the ink is stored (cartridge). The IJ technique has been proposed as a potential technique for printed electronics. Ink-jet technology presents several advantages for the production of high-tech products such as high resolution, low temperature, scalable, customization, low power and low cost. The main disadvantage found in IJ technology is the printing speed (1200 A3 pages per hour) compared to high output printing techniques like offset (15000 A3 pages per hour)[50]; however, the main IJ technology developers like HP and Xaar are working to increase the printing speed.

1.4 Outline

The objective of the present work is to explore new chromogenic system for low information content visual displays. In chapter 2 a derivative of the organic flavylium salt 6-hydroxyflavylium, is explored as a dual-mode electrochromic and photochromic chromogenic system. A more complex chromogenic system was developed in chapter 3. The multicomponent and multistimulus system is composed by the leuco dye Crystal Violet Lactone, a derivative of the spirobenzopyran family and Fe(II)/Fe(III) ions. The system shows a four colour state system controlled by the sequential action of electricity and light. All the work reported in chapters 2 and 3 were done in the liquid phase.

In chapter 4, colorimetric studies were performed to several electrochromic films based on inorganic polymers using spectroelectrochemical techniques. The electrochromes reported are the Prussian Blue and a new class of electrochromic films based on the electropolymerized *salen* based metal complexes. The Prussian Blue polymer is an example of a colourless to coloured state transition while the *salen* based metal complexes polymers present a transition between two coloured states.

In chapter 5, several non-liquid electrolytes were developed to apply in ECD. The results of the optimization of a gel electrolyte medium are presented. A comparative study on the effect of the ionic conductivity of the electrolyte layer and the ECD performances is reported.

The final part of the thesis, chapters 6 and 7, reports on the results obtained from the R&D projects involving several academic and industrial partners. The objective of these projects was to add new functionalities to the conventional products, copy paper (YInvisible-Papel project), textile (YInvisible-Textil project) and white-boards (YInvisible-Quadros project). The strategy adopted was to investigate the development of build-in ECD over non-conventional

substrates. Chapter 6 describes the results obtained by the consortium to obtain ECD based on paper, textile and white-board. The chapter 7 reports on the viability study to build electrochromic devices using pilot scale IJ printing. Finally the chapter 8 the list of publications that are a direct or an indirect result from the present thesis is given.

In each chapter there is an introduction section with detailed introduction about the chromogenic chemical compounds, therefore this information was not included in the General Introduction section.

1.5 Bibliography

1. Weiser, M., The computer for the 21st-century. *Scientific American* 1991, *265* (3), 94-104.
2. Weiser, M.; Brown, J. S. 1996. *The coming age of calm technology* [Online]. Available: http://www.ubiq.com/hypertext/weiser/acmfuture2endnote.htm [Accessed July, 2010 2010].
3. Ayiter, E. *The history of visual communication* [Online]. Available: http://www.citrinitas.com/history_of_viscom/rockandcaves.html [Accessed July 2010 2010].
4. Hilsum, C., Flat-panel electronic displays: a triumph of physics, chemistry and engineering. *Philosophical Transactions of the Royal Society a-Mathematical Physical and Engineering Sciences* 2010, *368* (1914), 1027-1082.
5. Christian, R., Solvents and Solvent Effects in Organic Chemistry. second ed.; VCH: New York, 1990.
6. Ritter, A., Smart materials: in architecture, interior and design. Birkhäuser: Berlin, 2007.
7. Pakhchyan, S., Fashioning technology. O'Reilly: Milan, 2008.
8. Kuehni, R. G., Color: an introduction to practice and principles. 2nd ed.; Wiley-Interscience: New Jersey, 2005.
9. Nassau, K., The physics and chemistry of color. Wiley Interscience: New York, 1983.
10. Platt, J. R., Electrochromism, a possible change of color producible in dyes by an electric field. *Journal of Chemical Physics* 1961, *34* (3), 862-863.
11. Monk, P. M. S.; Mortimer, R. J.; Rosseinsky, D. R., Electrochromism and electrochromic devices. Cambridge University Press: Cambridge, 2007.
12. Mortimer, R. J., Electrochromic materials. *Chemical Society Reviews* 1997, *26* (3), 147-156.
13. Monk, P. M. S., The viologens: physicochemical properties, synthesis and applications of the salts of 4,4'-bipyridine. John Wiley and Sons: Chichester, 1998; pp 239-256
14. Granqvist, C. G., Electrochromic tungsten oxide films: review of progress 1993-1998. *Solar Energy Materials and Solar Cells* 2000, *60* (3), 201-262.
15. Monk, P. M. S.; Mortimer, R. J.; Rosseinsky, D. R., Electrochromism and electrochromic devices. Cambridge University Press: Cambridge, 2007; pp 282-296

16. Kirchmeyer, S.; Reuter, K., Scientific importance, properties and growing applications of poly(3,4-ethylenedioxythiophene). *Journal of Materials Chemistry* 2005, *15* (21), 2077-2088.
17. Wang, Y. M., Recent research progress on polymer electrolytes for dye-sensitized solar cells. *Solar Energy Materials and Solar Cells* 2009, *93* (8), 1167-1175; Thangadurai, V.; Weppner, W., Recent progress in solid oxide and lithium ion conducting electrolytes research. *Ionics* 2006, *12* (1), 81-92.
18. Song, J. Y.; Wang, Y. Y.; Wan, C. C., Review of gel-type polymer electrolytes for lithium-ion batteries. *Journal of Power Sources* 1999, *77* (2), 183-197; Wright, M. R., An Introduction to Aqueous Electrolyte Solutions. Wiley: Chichester, 2007.
19. Wang, P.; Dai, Q.; Zakeeruddin, S. M.; Forsyth, M.; MacFarlane, D. R.; Gratzel, M., Ambient temperature plastic crystal electrolyte for efficient, all-solid-state dye-sensitized solar CeN. *Journal of the American Chemical Society* 2004, *126* (42), 13590-13591.
20. Sekhon, S. S., Conductivity behaviour of polymer gel electrolytes: role of polymer. *Bulletin of Materials Science* 2003, *26* (3), 321-328.
21. Gaupp, C. L.; Welsh, D. M.; Rauh, R. D.; Reynolds, J. R., Composite coloration efficiency measurements of electrochromic polymers based on 3,4-alkylenedioxythiophenes. *Chemistry of Materials* 2002, *14* (9), 3964-3970.
22. Smith, F. H. 1929. United Kingdom patent application UK328,017.
23. *Gentex rear camera display mirror featured on new ford taurus* [Online]. Available: http://www.marketwire.com/press-release/Gentex-Rear-Camera-Display-Mirror-Featured-on-New-Ford-Taurus-NASDAQ-GNTX-1276904.htm [Accessed July 2010 2010].
24. Niklasson, G. A.; Granqvist, C. G., Electrochromics for smart windows: thin films of tungsten oxide and nickel oxide, and devices based on these. *Journal of Materials Chemistry* 2007, *17* (2), 127-156.
25. Lampert, C. M., Chromogenic smart materials. *Materials today* 2004, p 7.
26. Lee, E. S.; Selkowitz, S. E.; Clear, R. D.; DiBartolomeo, D. L.; Klems, J. H.; Fernandes, L. L.; Ward, G. J.; Inkarojrit, V.; Yazdanian, M., A design guide for early-market electrochromic windows. California Energy Commission, PIER. 500-01-023. LBNL-59950.: 2006.
27. Chen, Y.; Au, J.; Kazlas, P.; Ritenour, A.; Gates, H.; McCreary, M., Flexible active-matrix electronic ink display. *Nature* 2003, *423* (6936), 136-136.
28. Vincent, J. B.; Flick, D. W. 2006. *Electrochromic display device*. United States of America patent application US7054050.

29. Shamai, R.; Andelman, D.; Berge, B.; Hayes, R., Water, electricity, and between ... On electrowetting and its applications. *Soft Matter* 2008, *4* (1), 38-45.
30. PaperDisplay [Online]. Available: http://www.paperdisplay.se/ [Accessed July 2010].
31. Hennerdal, L.; Lögdlung, M., Electronic printing paper house. *Aperturen* 2005, *2*.
32. AB, A. *Printing Laboratory* [Online]. Available: http://www.acreo.se/templates/Page____773.aspx [Accessed July 2010].
33. Hagfeldt, A.; Didriksson, B.; Palmqvist, T.; Lindstrom, H.; Sodergren, S.; Rensmo, H.; Lindquist, S. E., Verification of high efficiencies for the gratzel-cell - a 7-percent efficient solar-cell based on dye-sensitized colloidal TiO_2 films. *Solar Energy Materials and Solar Cells* 1994, *31* (4), 481-488.
34. NTERA [Online]. Available : http://www.ntera.com/technology/printing_processes.php [Accessed July 2010].
35. Nic, M.; Jirat, J.; Kosata, B.; Jenkins, A. 2006. IUPAC [Online]. Available: http://goldbook.iupac.org [Accessed July 2010].
36. Dürr, H.; Bouas-Laurent, H., *Photochromism: molecules and systems*. Elsevier: Cornwall, 2003.
37. Bamfield, P., *Chromic phenomena - the technological applications of colour chemistry*. The Royal Society of Chemistry: Cambridge, 2001.
38. Van Gemert, B., The commercialization of plastic photochromic lenses: a tribute to John Crano. *Molecular Crystals and Liquid Crystals* 2000, *344*, 57-62.
39. Vivimed Labs Europe Ltd*: Reversacol photochromic dyes* [Online]. Available: http://www.photochromics.co.uk/index.htm [Accessed July 2010].
40. Solar Active International*: photochromic inks* [Online]. Available: http://www.solaractiveintl.com/index.php [Accessed July 2010].
41. White, M. A., The chemistry behind carbonless copy paper. *Journal of Chemical Education* 1998, *75* (9), 1119-1120.
42. Appleton Papers Inc*.: carbonless paper* [Online]. Available: http://www.encapsys.com/carbon.aspx [Accessed July 2010].
43. Peters, A.; Branda, N., Electrochemically induced ring-closing of photochromic 1,2-dithienylcyclopentenes. *Chemical Communications* 2003, 954-955.
44. Peters, A.; Branda, N. R., Electrochromism in photochromic dithienylcyclopentenes. *Journal of the American Chemical Society* 2003, *125* (12), 3404-3405.
45. Yamase, T., Photo- and electrochromism of polyoxometalates and related materials. *Chemical Reviews* 1998, *98* (1), 307-325.
46. Deb, S. K.; Lee, S. H.; Tracy, C. E.; Pitts, J. R.; Gregg, B. A.; Branz, H. M., Stand-alone photovoltaic-powered electrochromic smart window. *Electrochimica Acta* 2001, *46* (13-14), 2125-2130.

47. Krasovec, U.; Georg, A.; Wittwer, V.; Luther, J.; Topic, M., Performance of a solid-state photoelectrochromic device. *Solar Energy Materials and Solar Cells* 2004, 369-380.
48. *Microfabrication* [Online]. Wikipedia. Available: http://en.wikipedia.org/wiki/Microfabrication#Microfabrication_processes [Accessed July 2010].
49. Arias, A. C.; MacKenzie, J. D.; McCulloch, I.; Rivnay, J.; Salleo, A., Materials and applications for large area electronics: solution-based approaches. *Chemical Reviews* 2010, *110* (1), 3-24.
50. Kipphan, H., *Handbook of print media: technologies and production methods*. Springer: Heidelberg, 2001.

Chapter 2

The chemistry of 6-hydroxyflavylium: A Multiswitchable System operated by Proton, Electron and Photon inputs

2.1 Introduction

The investigation of molecules that can exist in two or more forms (multistate), interconvertible by an external input[1-2] is of fundamental importance. In particular, systems capable of responding to a given combination of multiple stimuli can be envisaged to process multiple information. Multistimuli and multistate systems match the predictions of the UC (see section 1.1).[3] Besides the chromogenic molecules other systems can show multiple states, for example the flavylium molecules. Flavylium compounds are a paradigmatic example of multistate and multistimulus systems, and in particular cases, it shows photochromism as well.

In this chapter, the 6-hydroxyflavylium is studied towards its possible application as a chromogenic system. The entire chemical network was elucidated by spectroscopic techniques in different time scales. Another particular characteristic of the introduction of the hydroxyl group in the position 6 is the possibility to operate electrochemically the *p*-quinone/*p*-hydroquinone chalcone.

2.1.1 Flavylium compounds

Anthocyanins and anthocyanidins are ubiquitous natural pigments of flowers and fruits responsible for the colours ranging from blue to red. Both classes of molecules have the same chemical skeleton described in Fig. 2.1 constituted by the 2-phenyl-1-benzopyrylium ring system, the so-called flavylium. The intense study devoted to anthocyanins and anthocyanidins is due to their practical application as colorants not only in the antiquity[4], but also for industrial modern applications.[5]

In 1902 Bülow and Wagner reported for the first time the synthesis of a flavylium salt.[6] State-of-the-art flavylium syntheses have developed along different approaches, leading to synthetic flavylium salts containing a variety of substitutes in the aromatic ring, e.g., hydroxyl, alkoxy, amino, N-alkyl and N, N – dialkylamino, carboxy, halogens, nitro and cyano.

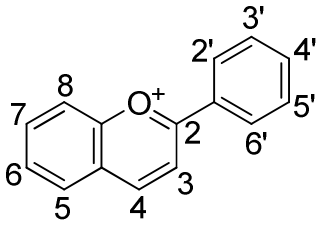

Figure 2.1 - 2-phenyl-1-benzopyrylium (Flavylium) structure.

Chemical network

Flavylium compounds are paradigms of multistate compounds.[7,8,9,10] The main species arising in aqueous solution from the common 2-phenyl- 1-benzopyrylium core are shown in Fig. 2.2 for the particular case of 6-hydroxyflavylium.

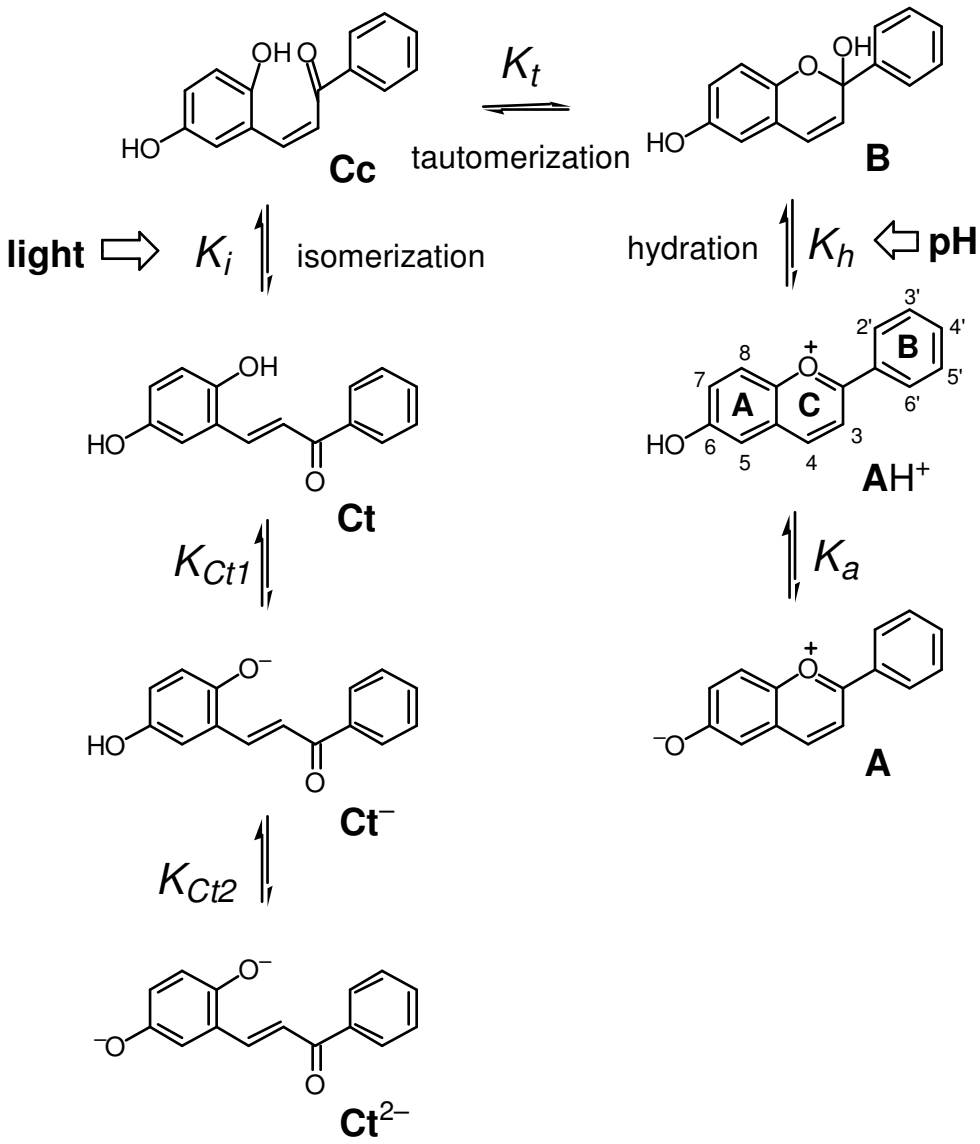

Figure 2.2 – Chemical network of 6-Hydroxiflavylium.

In acidic and neutral solutions, 6-hydroxyflavylium presents five states, interconvertible by pH modifications and light: the flavylium cation, AH^+; the hemiketal species, B, obtained by hydration in position 2 of the AH^+; the *cis*-2-hydroxychalcone, Cc, formed from the hemiketal B through a tautomeric process (ring opening) and the *trans*-2-hydroxychalcone, Ct, obtained from Cc via a *cis–trans* isomerization reaction.

Flavylium Thermodynamics

The network of chemical equilibria in acid medium reported in Fig. 2.2 can be accounted for by the following set of equilibriums:

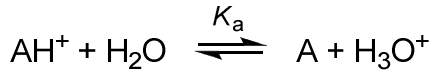

Eq. 2.1

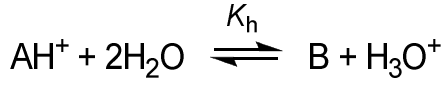

Eq. 2.2

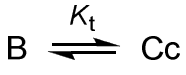

Eq. 2.3

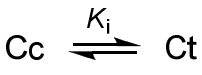

Eq. 2.4

Eq. 2.1–2.4 can be substituted by single acid–base equilibrium, as shown by Eq. 2.5:

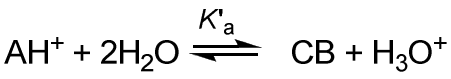

Eq. 2.5

Where

$$[CB] = [A] + [B] + [Cc] + [Ct]$$ Eq. 2.6

$$K'_a = K_a + K_h + K_h K_t + K_h K_t K_i$$ Eq. 2.7

In the cases where an activation barrier exists for the interconversion of *cis*- to *trans*-chalcone, a pseudo-equilibrium can also be defined:

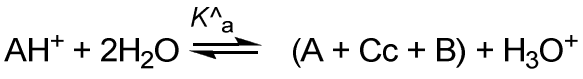

Eq. 2.8

where

$$K^\wedge_a = K_a + K_h + K_h K_t$$ Eq. 2.9

In both, equilibrium and pseudo-equilibrium, the stable species at more acidic pH values is the AH^+ form; with increasing pH, AH^+ is substituted by the "neutral forms", A + B + Cc + Ct and A + B + Cc respectively.

It is worth mentioning that not only K_a, but also the relative concentration of the "neutral species" is dramatically dependent on the functional groups present in the 2-phenyl-1-benzopyrylium core. In particular, our group has reported[11] that a hydroxyl group in position 4' or 7, respectively, increases or decreases the *cis–trans* isomerisation barrier. The effect of the substituent is also observed in the kinetics of the network depicted in Fig. 2.2. The rate of the hydration reaction is strongly pH dependent and typically occurs in the second or sub-second timescale. The hemiketal ring can open, leading to the *cis*-chalcone, Cc; this reaction occurs also in the subsecond timescale and is slightly dependent on the pH. Finally, the *trans*-chalcone, Ct, is obtained from its *cis*-isomer, in a timescale that ranges from several minutes to days.[11] If the *cis–trans* process is slow enough, a pseudo-equilibrium state involving the AH^+, B and Cc species can be defined. With time, the pseudo-equilibrium, *K*^a will evolve to the final thermodynamic equilibrium, *K*'a. At alkaline pH values, when phenolic groups are present, all species can deprotonate. Fig. 2.2, the base A results from deprotonation of the flavylium cation and the *trans*-chalcone deprotonates to give Ct^- and Ct^{2-}. The hemiketal B and the *cis*-chalcone Cc can also deprotonate. While hydroxyl groups in positions 5, 7, 2' or 4' of the AH^+ give rise to the formation of quinoidal bases A by simple deprotonation; the hydroxyl groups in positions 6, 8 or 3' originate a zwitterion that cannot delocalize to a quinoidal system (see Fig. 2.2, A form).

Flavylium Salt Photochromism

Within the chemical network found in flavylium salts the *cis-trans* chalcone isomerisation is generally photo-reactive. The colourless Ct species can be converted into Cc by a photoisomerization reaction. As described by the thermodynamic of the flavylium chemical network[12] the pH of the solution will influence the photo-isomerisation product. In acidic media the thermodynamically more stable specie is AH^+, thus Ct is mainly converted to flavylium cation, defining a photochromic system. At more neutral pH the predominant species will be Cc and B, and a photostationary state is reached, depending on the light absorbed by each species and on the quantum yields.

Photochemical quantum yield can be simply defined as the ratio between the number of molecules undergoing a particular photochemical reaction and the number of photons absorbed by photoreactive system (Eq. 2.10):

$$\Phi = \frac{number\ of\ molecules\ of\ product\ formed}{number\ of\ photon\ absorbed\ by\ the\ reagent} \qquad \text{Eq. 2.10}$$

Depending on the flavylium derivative, different quantum yields can be found and more important to define the system is the ratio found for the quantum yield for the Cc to Ct reaction and the backward process. It has been reported a quantum yield ratio between direct and backward reactions lower than 1. Explanation has been rationalized based on the energy potential of the excited state.[13]

Optical memories and molecular logic system

In 1956, Yehuda Hirshberg introduced the idea that photochromic systems could be used as models for optic memories. The method described follows the bottom-up approach to improve memory density thus increasing the data storage capacity per unit of area. The advantage to use chemistry to build such operating units is based on the advantages of molecular level miniaturization capacity.

To build an optical memory it is essential to have two photochemically interconvertible and stables species. In addition, the speed of this conversion must be as fast as possible. As proposed by several authors photochromic systems are the preferred chemical system to meet the described requirements.

As it is essential to reach bistability to obtain useful optical memories the T- and P-type photochromic systems (see section 1.2.2) are not suitable. In the T-type system one of the memory states will revert thermally loosing the state definition (and consequently the stored information). In the P-type system the light used to read the memory state would cause the conversion of the photochromic state thus loosing also state definition.

Pina *et al* has proposed dual-type system based on the flavylium chemical network to avoid the destructive reading or thermal destruction of the defined optical memory. The strategy requires a system that responds to two stimuli: (i) one used to write the information (Y) and (ii) another to lock the written state (Z, see Fig. 2.3). The Z state corresponds to a more stable written state that is thermally and photochemically stable. This state is used to read the memory content (Z). A reverse stimulus is applied to unlock the written state and the system can be erased to the original state (X).

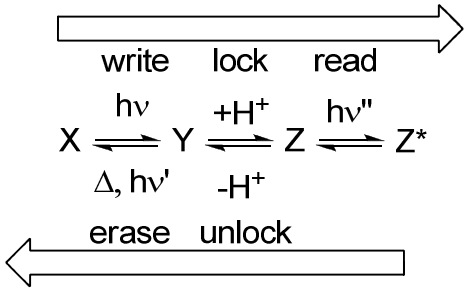

Figure 2.3 – Dual-type photochromic system proposed by Pina *et al.*[11]

Exploring further the concept of molecular computing units, Pina and co-workers have explored the multistate properties of the chemical flavylium network to design molecular logical operators. Based on the photochromic bistables Ct and Cc species, more complex input-output relationship systems have been used to perform AND, OR logic operations.[14]

Electrochemical behaviour of flavylium systems

Natural flavylium salts constitute an interesting class of compounds due to their organoleptic properties, such as colour (anthocyanins or curcumin, for example), astringency (tannins), bitterness (flavanols) or taste[15], and more recently their benefits to human health were recognised as they can reduce the risk of chronic disease and, in general, they have a positive effect on health.[16] They have been reported to help the prevention against severe diseases like cancer.[17] Many of these probiotic properties have been attributed to the antioxidant power of natural compunds.[18]

Antioxidant activity has been related to their redox potentials found by electrochemical techniques. Although synthetic flavylium have been used as models for their natural counterparts for chemical network reactions, only few electrochemical data has been published.

Polyphenols electrochemistry

The antioxidant properties of natural polyphenol compounds are attributed to the oxidation of hydroxyl groups. The general redox mechanism proposed for polyphenols bearing reactive structural groups such as chatechol, pyrogallol or *para* diol is a two-electron, two-proton reversible process (see Fig. 2.4) coupled to an homogeneous chemical reaction.

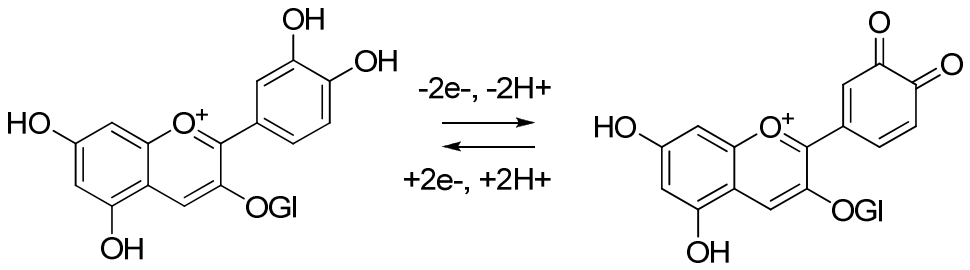

Kuromanin

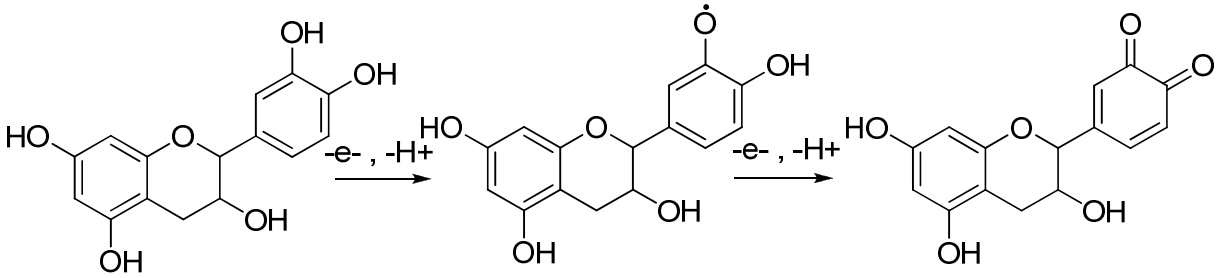

Catechin

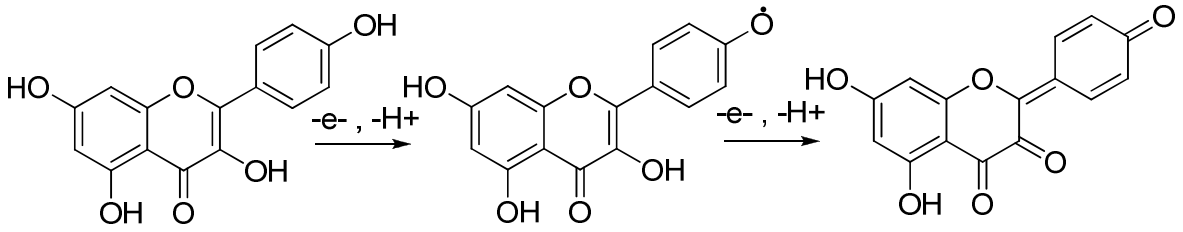

Kaempferol

Figure 2.4 – Oxidation mechanism for different polyphenols (Kuromanin[19], Kaempferol[19] and Catechin[20]).

The homogeneous chemical reaction is attributed to the radical dimerization of the phenoxyl radicals formed with the first electron extraction.

It has been reported almost none or weak effects on the ionisation of OH groups from ring A or B when the opposite ring groups are or are not ionised[20], the same has been reported for the chalcones species.[21] Hence, ionisations of OH groups of ring A are independent and distinguishable from those of ring B.[20] Although hydroxyl groups can occur in both rings A and B, the redox mechanism in anthocyanins is correlated with hydroxyls in ring B.[22]

Chalcones species can be obtained either by the flavylium network reactions or by direct organic synthesis. A serie of synthetic hydroxychalcones have been studied towards their electrochemical activity in dimethyl sulfoxide by Nicole Cotelle *et all.*[21] Also, a comparative study has been done with smaller polyphenols like caffeic acid, coumaric acid and ferulic acid which present the same basic chemical structure but different hydroxyl substituents.[23]
It was found that chalcone without any OH group (1,3-diphenyl-propenone) has no electrochemical reactivity. In the other case hydroxychalcones bearing one hydroxyl group in ring A and none in ring B is oxidised to the phenoxyl radical (see Fig. 2.5 - A and -B), which goes through a second oxidation to the phenoxonium cation (see Fig. 2.5 - C). Then the phenoxonium cation can be reduced again.

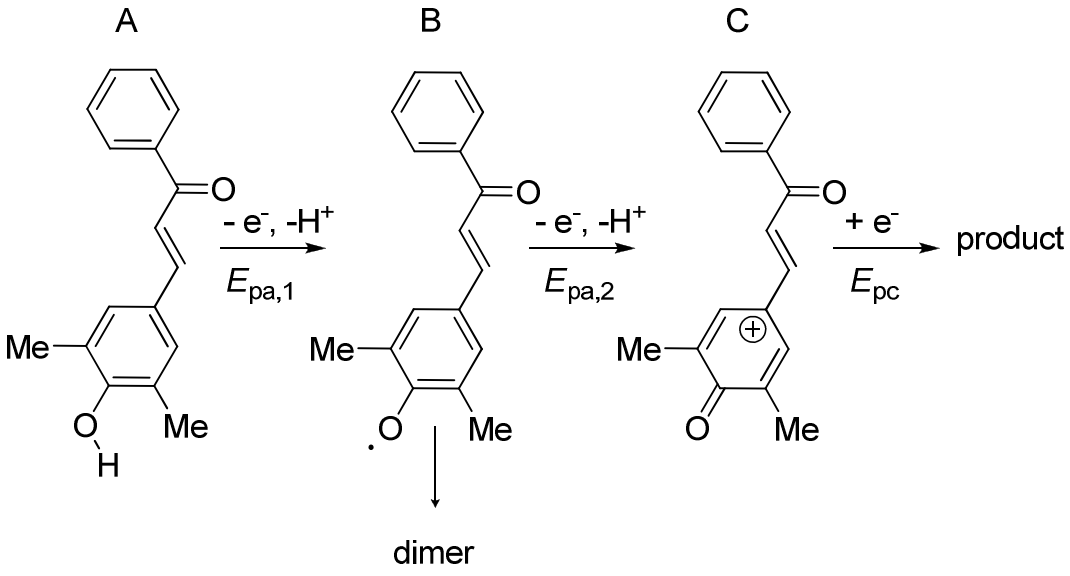

Figure 2.5 – Proposed two electrons, two protons oxidation mechanism of the 3,5-dimethyl-4-hydroxychalcone by Nicole Cotelle *et al.*[21]

The species with one hydroxyl group in ring B and none in ring A shows a two electron in one wave oxidation at more anodic potentials than hydroxychalcones bearing OH group in ring A. Finally, hydroxychalcones bearing OH groups in both rings show a voltammogram that is the sum of the individual voltammograms of the cases one and two. Small influence is detected between OH groups between ring A and ring B.

2.2 Experimental details

Synthesis

All reagents and solvents used were of analytical grade. ^{1}H NMR spectra were run on a Bruker AMX400 operating at 400 MHz; field desorption MS spectra were run on a Micromass GCT; elemental analysis were obtained on a Thermofinnigan Flash EA 1112 Series.

6-hydroxyflavylium perchlorate was prepared from condensation of acetophenone (1.16 ml, 10 mmol) and 2,5-dihydroxybenzaldehyde (1.38 g, 10 mmol), on the basis of a method originally described by Robinson[24] and later explored by Michaelis and Wizinger.[25] The reagents were dissolved in acetic acid (8 ml) and dried gaseous hydrogen chloride produced *in situ* was bubbled for 3 h. Addition of 20 ml of 20 % perchloric acid led to the precipitation of a yellow-brown solid that was filtered, washed with cold glacial acetic acid, ether and vacuum dried; 1.72 g (48 %). The solid may be recrystallized from acetic acid and perchloric acid. Elemental analysis: exp. (calc. for $C_{15}H_{11}ClO_6.2H_2O$) %C 49.95 (50.22), %H 3.77 (4.21). FD-MS: *m/z* 223.08 (100%, $[M–ClO_4^–]^+$, M=$C_{15}H_{11}ClO_6$, calc. 223.08). ^{1}H NMR (400 MHz, D_2O/DCl, pD<1,[26] 300 K, flavylium cation, AH^+): δ 7.50 (s, 1H, H5), 7.68 (dd, 2H, H3'+H5', $^3J_{H3'H5'-H4'}$=$^3J_{H3'H5'-H2'H6'}$=7.7 Hz), 7.79-7.83 (m, 2H, H4'+H7), 8.18 (d, 1H, H8, $^3J_{H8-H7}$=9.3 Hz), 8.40 (d, 2H, H2'+H6', $^3J_{H2'H6'-H3'H5'}$=7.7 Hz), 8.58 (d, 1H, H3, $^3J_{H3-H4}$=8.9 Hz), 9.22 (d, 1H, H4, $^3J_{H4-H3}$=8.9 Hz); (400 MHz, D_2O/NaOD, pD>12, 300 K, di-ionized *trans*-chalcone, $Ct^{2–}$): δ 7.50-7.65 (m, 2H, H7+H8), 7.15 (s, 1H, H5), 7.53 (dd, 2H, H3'+H5', $^3J_{H3'H5'-H4'}$=$^3J_{H3'H5'-H2'H6'}$=7.9 Hz), 7.61 (d, 1H, H3, $^3J_{H3-H4}$=15.4 Hz), 7.65 (t, 1H, H4', $^3J_{H4'-H3'H5'}$=7.9 Hz), 7.93 (d, 1H, H4, $^3J_{H4-H3}$=15.4 Hz), 7.96 (d, 2H, H2'+H6', $^3J_{H2'H6'-H3'H5'}$=7.7 Hz).

Trans-2,5-dihydroxychalcone was prepared according with the method described by Robinson *et al*.[27] Potassium hydroxide (1.5 g, 6.7 mmol) dissolved in the minimal amount of water was added to a solution of 2,5-dihydroxybenzaldehyde (0.69g, 5 mmol) and acetophenone (0.58ml, 5 mmol) in ethanol (5 ml). The mixture became red-brown. After stirring overnight, the mixture was neutralized with acetic acid (1.8 ml) to obtain the neutral *trans*-chalcone, leading to the precipitation of brown oil. After decantation, the oil was dissolved in dichloromethane and acetone, dried over $MgSO_4$, filtered, concentrated and purified by flash chromatography (silica-gel 230-400 mesh), eluting with dichloromethane:acetone 90:10. Pure *trans*-chalcone was obtained as a dark yellow powder (yield < 20 %). FD-MS: *m/z* 240.05 (100%, M^+, M=$C_{15}H_{12}O_3$; calc. 240.08). ^{1}H NMR (400 MHz, CD_3CN, 300 K, *trans*-chalcone, Ct): δ 6.73-6.81 (m, 2H, H7+H8), 7.14 (s, 1H, H5), 7.53 (dd, 2H, H3'+H5', $^3J_{H3'H5'-H4'}$=$^3J_{H3'H5'-H2'H6'}$=7.7 Hz), 7.61 (t, 1H, H4', $^3J_{H4'-H3'H5'}$=7.7 Hz), 7.65 (d, 1H, H3, $^3J_{H3-H4}$=15.8 Hz), 7.95 (d, 1H, H4, $^3J_{H4-H3}$=15.8 Hz), 8.02 (d, 2H, H2'+H6', $^3J_{H2'H6'-H3'H5'}$=7.7 Hz).

General

All chemicals were of analytical grade. All experiments were carried out in aqueous solutions. The pH was adjusted by addition of HCl and NaOH to buffered solutions, and was measured in a Radiometer-Copenhagen PHM240 MeterLab potentiometer.

pH Jumps

pH Jumps were done by adding a certain volume of a stock solution of the flavylium salt in 0.1 M HCl to a 10 cm^3 flask containing an equivalent amount of NaOH to neutralize the HCl, and 1 cm^3 of 0.1 M universal buffer of Theorell and Stenhagen[28] at the desired final pH, followed by addition of water to the final volume. Reverse pH jumps involved a second pH jump to a lower pH value, by addition of HCl.

Optical spectroscopic measurements

UV-Vis absorption spectra were recorded using a Shimadzu UV2501-PC spectrophotometer. Spectrophotometric pH titration data were fitted using the Solver facility of Microsoft Excel. Determined pK_a values have a mean error of ±0.1. Light excitation was carried out using a medium-pressure mercury arc lamp, and the excitation bands were isolated with interference filters (Oriel). The flash photolysis experiments were performed as previously described.[29] The stopped-flow experiments were collected in a SFM-300 spectrophotometer, controlled by a MPS-60 unit (Bio- Logic) and the data were collected using a TIDAS diode array (J & M), with wavelength range between 300 and 1100nm, all connected to a computer. The standard cuvette has an observation path length of 1 cm. For these experiments the dead time of each shot was previously determined to be 5.6 ms with a flow rate of 8 $mL.s^{-1}$.

Electrochemical experiments

Linear cyclic voltammetry measurements were conducted in a conventional three-electrode cell under argon atmosphere at 21ºC performed using a computer controlled potentiostat AUTOLAB (Eco-Chemie). The working electrode was a glassy carbon disk (BAS) polished with 0.05 μm alumina (Metkron) before each run. The auxiliary electrode was a platinum wire. The reference electrode was an Ag/AgCl (BAS). The experiments were carried out in hydrochloric acid aqueous solution about pH 1.3, containing 1M KCl as supporting electrolyte. Solutions were initially deaerated with an argon stream for 20min.

Spectroelectrochemistry

Electrolysis was performed using a platinum net as a working electrode, a reference electrode (saturated calomel electrode, ref. 921 from Radiometer Analytical) and a platinum wire counter-electrode was immersed in the electrolyte solution. Absorbance spectra of bulk

electrolysed solution were accomplished taking samples from the electrolysis cell. The solution was looped between the electrolysis cell and the spectrophotometric cell. All solutions were deaereted under an argon stream - initially for 20 minutes and during the whole electrolysis.

Semi-empirical calculations

Ground and first singlet excited heats of formation were obtained from single point calculations (AM1-RHF-CI, 99 single excited configurations) on geometries.

2.3 Results and Discussion

6-Hydroxyflavylium perchlorate

The spectral variations occurring in aqueous solutions of the compound 6-hydroxyflavylium as a function of pH, at the thermal equilibrium, are reported in Fig. 2.6.

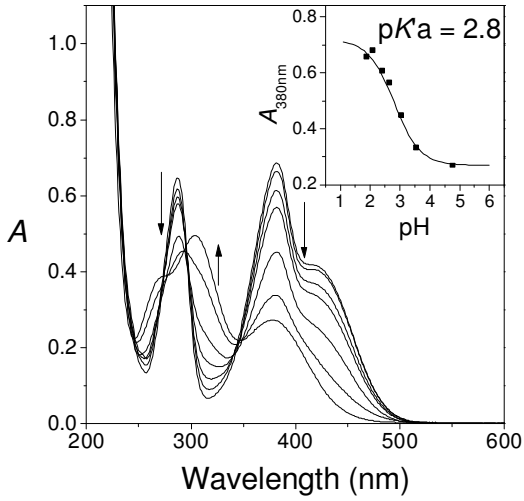

Figure 2.6 - Spectral variations of 6-hydroxyflavylium perchlorate, 3.5×10^{-5}M, as a function of pH (acidic region) at the thermal equilibrium. In order to decrease the reaction time, the solutions were kept at 40 ºC for 7 hours and left to equilibrate for a day at room temperature.

At very acidic pH values the yellow flavylium cation is the stable species. Increasing pH gives rise to the disappearance of this species with concomitant formation of the "neutral species" absorption bands. The identification of the *trans*-chalcone Ct as the "neutral species" was made by ^{1}H NMR, on the basis of the coupling constant of 15.8 Hz between proton 3 and 4. This was further confirmed by performing the synthesis of this species through another method, see experimental details (section 2.2). In both samples, there is a coincidence between the absorption and the ^{1}H NMR spectra. As shown by Eq. 2.5, 2.6 and 2.7 the system behaves as single acid–base equilibrium, and therefore the respective apparent constant, *K*'a, can be calculated by a standard fitting procedure, as shown in the inset of Fig. 2.6.

$$K'_a = 10^{-2,8}$$

In Fig. 2.7, the spectral variations occurring 30s after a pH jump from 1 to the final pH are shown.

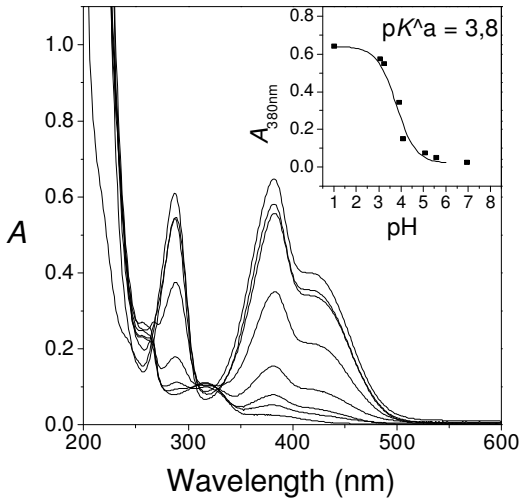

Figure 2.7 - Spectral variations of 6-hydroxyflavylium perchlorate, 3.5×10^{-5}M, as a function of pH, resulting from a pH jump from 1, measured after 30 seconds.

The spectral changes *vs.* pH reported in Fig. 2.7 describe the system at the pseudo-equilibrium and are clearly different from those reported in Fig. 2.6. Moreover, when the pH jump is carried out at pH > 5, an orange-red colour is immediately formed that fades in less than 1 s (see Fig. 2.8). These results show that the pseudo-equilibrium, characterized by the presence of B and Cc species, is preceded by a very fast process (formation and disappearance of base A), and followed by a very slow one that leads to the final equilibrium characterized by the presence of Ct. According to Eq. 2.8, the data reported in Fig. 2.7 can be fitted as a single acid–base equilibrium, which allows to calculate the pseudo-equilibrium apparent constant, *K*^a, as shown in the inset of the Fig. 2.7.

$$K\text{^a} = 10^{-3,8}$$

Comparison of Fig. 2.7 with Fig. 2.6 shows that in the latter an absorption band around 315nm can be observed (Ct) which is not still formed in the pseudo-equilibrium of Fig. 2.7. This result indicates that there is a barrier for the *cis–trans* isomerization, in other words, only in Fig. 2.6 the *trans*-chalcone appears. Important to note that the base A can only be observed as a transient species immediately after pH jumps to neutral and basic pH values; it remains neither at the equilibrium nor at the pseudo-equilibrium. In order to follow the disappearance of the zwitterionic base A, stopped-flow experiments were carried out. The results are reported in Fig. 2.8, where the absorption spectra were taken 10 ms after a pH jump from 1 to the final represented pH.

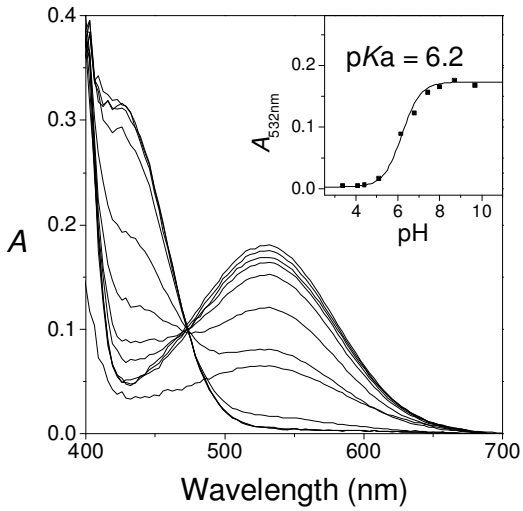

Figure 2.8 - Spectral variations of 6-hydroxyflavylium perchlorate obtained by stopped-flow after 10 ms of a pH jump from 1 to the final pH.

The formation of the base can be clearly observed, and the pK_a of the flavylium cation, Eq. 2.1, can be obtained by fitting the data (see inset of Fig. 2.8).

$$K_a = 10^{-6,2}$$

The decay of the base A is reported in Fig. 2.9-left, and the respective changes in absorption spectra are also presented in Fig. 2.10. This trace was obtained upon a pH jump from solutions equilibrated at pH = 1 to pH = 9.65. The decay follows a first order kinetic process with a rate constant equal to 1.3 s^{-1}. A series of similar pH jumps starting from pH = 1 to higher pH values was carried out, and the respective rate constant represented as a function of pH, see Fig. 2.12 (open squares).

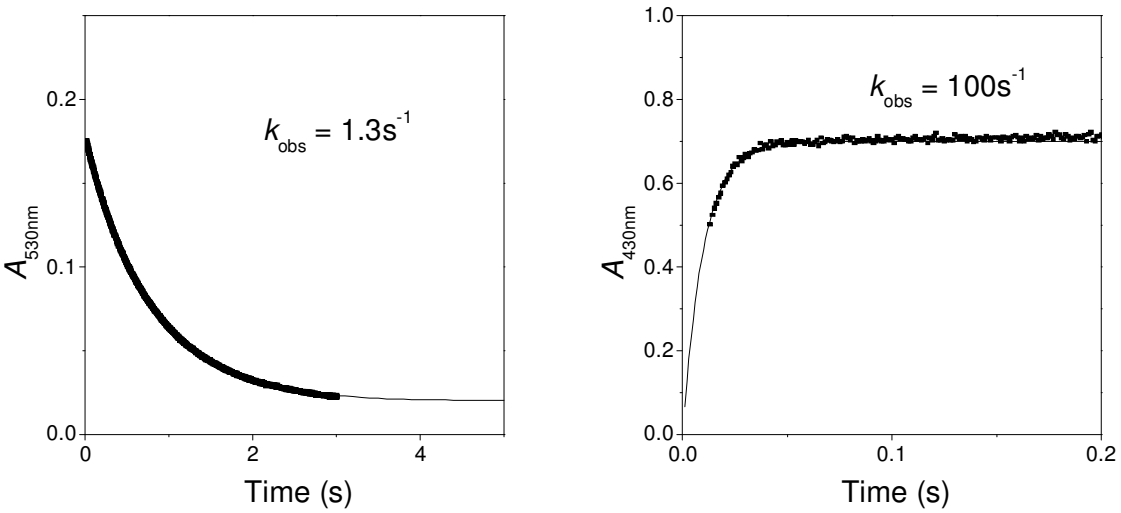

Figure 2.9 - Decay trace of a direct pH jump from 1 to 9.65 (left); decay trace of a reverse pH jump from 6.1 to 2.33 (right). The initial solution at pH=6.1 was prepared from a stock solution at pH=1.0, and used immediately, before formation of significant amounts of Ct (pseudo-equilibrium state). The decay of the A form is observed during the direct pH jump, while the formation of the AH^+ form is observed during the reverse pH jump.

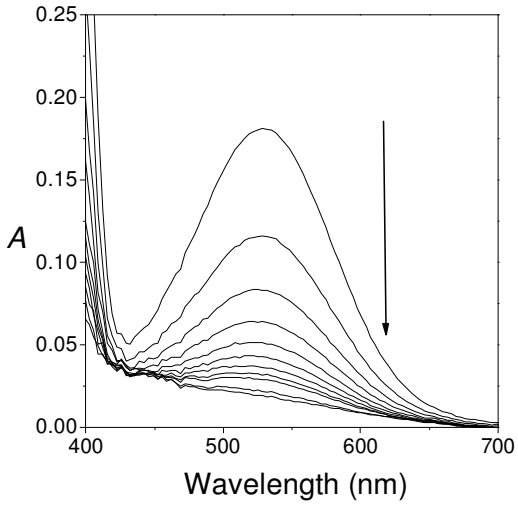

Figure 2.10 - Kinetics of the zwitterionic base decay followed by stopped flow

The stopped-flow data show that the lifetime of the zwitterionic base is extremely short compared with other flavylium compounds bearing hydroxyl substituents capable of forming quinoidal bases; for example, in the case of the compound 7,4' - dihydroxyflavylium, the quinoidal base at pH *ca.* 7–8 is stable for hours.[30] In such compounds, the (quinoidal) base exhibits a relatively long lifetime at pH values near the neutrality because it constitutes a

kinetic product. In the case of anthocyanins in moderately acidic media, Dubois and Brouillard have shown in a seminal paper[9] that mechanism III in Fig. 2.11 is the operating one.

Mechanism I

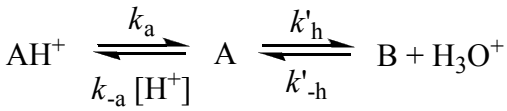

Mechanism II

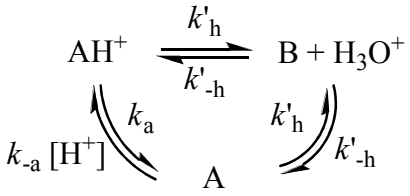

Mechanism III

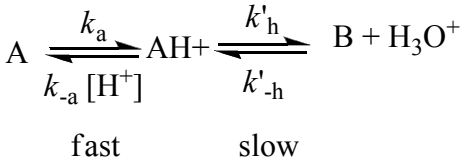

Figure 2.11 – Proposed kinetic mechanism for the conversion between the form AH^+, A and B, previously described in the literature.

This model was also proved to account for the chemical behaviour of many synthetic flavylium networks.[8,9,10,11,12,31,32,33] One immediate consequence of mechanism III is the possibility of formation of base A as a kinetic product. Once A is formed, the system can go forward to B (and Cc) only through the hydration reaction of AH^+. However, the rate of the hydration process is proportional to the concentration of AH^+ (see Eq. 2.11):

$$\frac{-d[AH^+]}{dt} = k'_h [AH^+] - k'_{-h} [H_3O^+] \times [B] \qquad \text{Eq. 2.11}$$

If the pH is higher than the pK_a of the system, the pseudo-equilibrium is shifted to the species A, and the kinetic process becomes slower. On the other hand, the base A can be directly attacked by OH^-,[34] but near the neutrality, A reacts slowly since OH^- is present in very low concentrations. The quinoidal base starts to react faster only at more basic pH values, where OH^- is available at higher concentrations for nucleophilic attack. On the contrary, the

zwitterionic base of the present compound is very reactive even at neutral and moderately basic solutions, essentially because the nucleophilic attack by water is facilitated by the maintenance of the positive charge in the zwitterionic form, relatively to the neutral quinoidal base. In order to get more insight on this network, solutions at pH 6 were freshly prepared from the stock at pH = 1.0, and reverse pH jumps back to acid were immediately carried out, Fig. 2.9-right and Fig. 2.12 (black squares). This procedure allows the formation of the pseudo-equilibrium at this pH value (essentially B and Cc are present), and permits the study of the kinetics of flavylium formation from these species. The traces are also compatible with a fast first order kinetic process. This procedure was extended to different final pH values; see black squares in Fig. 2.12. The observed rate constants, obtained by the direct and reverse pH jumps, are plotted together in Fig. 2.12. The fitting of the experimental points can be done considering that the rate determining step of the kinetics followed by stopped-flow is the hydration reaction. Eq. 2.12 can account for the process and fitting with k_h = 0.09 s^{-1} and k_{-h} = 900 M^{-1} s^{-1} can be obtained, allowing to calculate K_h (see Eq. 2.13):

$$k_{obs} = k_h + k_{-h}[H^+] = 0{,}09 + 900[H^+] \qquad \text{Eq. 2.12}$$

$$K_h = \frac{k_h}{k_{-h}} = 10^{-4} M^{-1} \qquad \text{Eq. 2.13}$$

It is interesting to note that up to pH *ca.*5 the species A is not formed at a large extent (p*K*a = 6.2), and by consequence the forward process should take place through the flavylium hydration to give B. On the other hand, for pH values higher than *ca.* 6, the base A is formed but does not give rise to a kinetic product, as reported for other synthetic flavylium salts and anthocyanins.[11] The zwitterionic base A reacts in less than 3 s in a large pH range, from pH 6 to 10. Moreover, up to pH = 10, the reaction of the base A with OH^- (hydroxylation), observed in other flavylium salts bearing hydroxyl substituents,[34] is negligible, because water is very efficient on the hydration process of this zwitterionic base and, being the solvent, it is in large excess relatively to hydroxide concentration at moderately basic pH values. On the other hand, the hydration reaction seems to be also the rate determining step of the reverse pH jumps. In fact, after the dead time of the stopped- flow apparatus, the absorption of the flavylium cation at 430nm increases according to a single first order kinetic process. The fitting of both sets of data obtained by direct and reverse pH jumps according to Eq. 2.12 indicates that hydration is in fact the rate determining step whenever the Ct form is not involved. The *cis–trans* isomerization is a very slow process that is only completed in a time scale of several hours. In conclusion, the chemical behaviour of the present flavylium

compound suggests a mechanistic change from mechanism III at more acidic pH values to mechanism I in Fig. 2.11 at moderately basic pH values. For example, when a pH jump from 1 to pH = 9.65 takes place, A is "immediately" formed, Fig. 2.8. According to Eq. 2.12, the hydration of AH^+ would occur with a rate constant of $0.09 \times 3.5 \times 10^{-4} = 3.2 \times 10^{-5}\ s^{-1}$, where the last term is the mole fraction of the flavylium cation. This value is much slower than the real disappearance rate of A ($1{,}3 s^{-1}$, see Fig. 2.9-left) showing that at this pH value the hydration reaction is negligible. Moreover, in this pH range, the hydration should take place by water attack, because the alternative attack by OH^- would lead to pH dependence in the basic region which is not observed in Fig. 2.12.

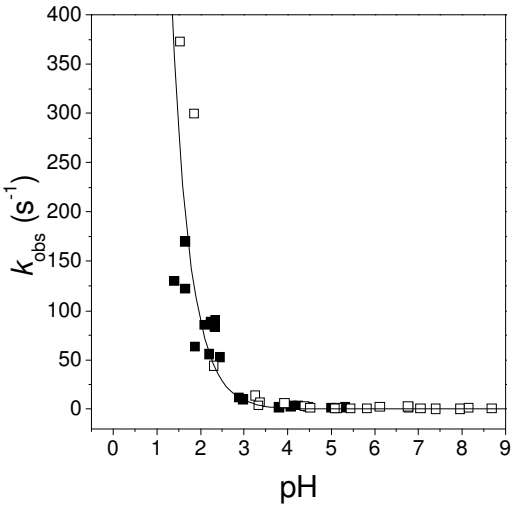

Figure 2.12 - Observed rate constants upon direct (pH=1 → pH>1, □) and reverse (pH=6.1 → pH<6.1, ■) pH jumps.

In Fig. 2.7, the absorption spectra at the end of the stopped-flow measurements are presented. The observed spectra correspond to the absorption of the species occurring at the pseudo-equilibrium, B and Cc. The final spectra, corresponding to the Ct species, are obtained through a slow process that takes several days at room temperature (see Fig. 2.6). The kinetics of conversion from the pseudo to the final equilibrium, *i.e.*, the kinetics of the *cis–trans* isomerization, follows a first order kinetic process, as shown in Fig. 2.13-left. The activation energy of the *cis–trans* isomerization was obtained from the dependence of the rate constant with the temperature through an Arrhenius plot, Fig. 2.13-right. At room temperature, the *cis–trans* isomerization is not dependent on pH, as shown in Fig. 2.14.

Using the data from the pseudo and final equilibrium, respectively Fig. 2.7 and 2.6, as well as the data from the stopped flow measurements, the four equilibrium rate constants can be calculated by means of the four independent equations above obtained, Eq. 2.7, Eq. 2.9, Eq. 2.12 and K_a:

$K_a = 10^{-6.2}$

$K_h = 10^{-4}\ M^{-1}$

$K_t = .57$

$K_i = 25$

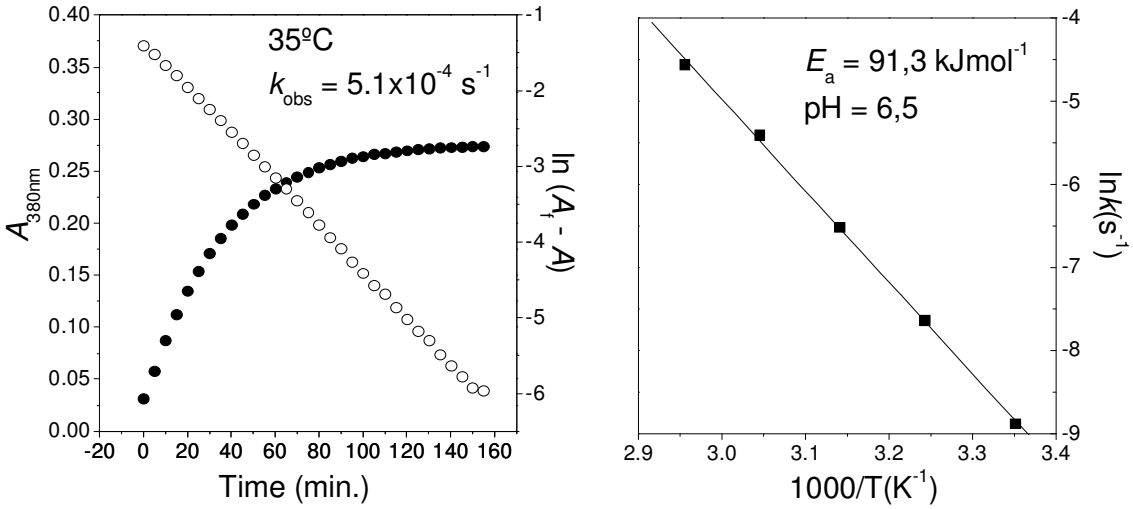

Figure 2.13 – The *cis-trans* isomerization of 6-hydroxyflavylium perchlorate at pH=6.5 (left) and the Arrhenius plot for the same reaction (right).

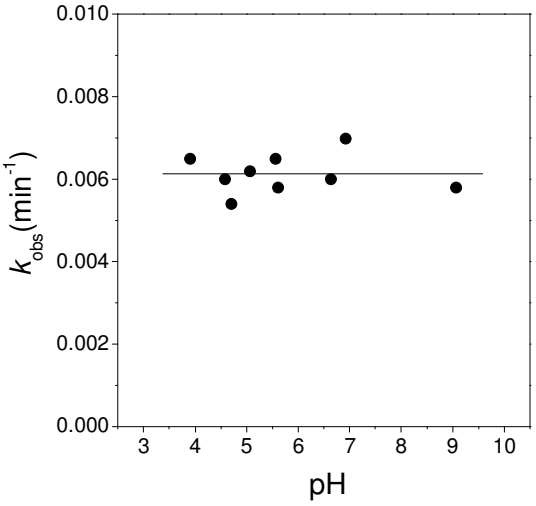

Figure 2.14 - Rate constant of the *cis*-trans isomerization as a function of pH.

As previously reported[8,11,12] the knowledge of the equilibrium constants permits the calculation of the mole fraction distribution of the several species as a function of pH, both at the equilibrium as well as at the pseudo-equilibrium. For example, at pH=6, 65% of B and 35% of Cc are present at the pseudo-equilibrium, evolving to a mixture containing 90% of Ct, 6% of B and 4% of Cc at the final equilibrium.

Photochemistry

The Ct species does not exhibit any significant photochemistry, and the respective solutions decompose slowly after prolonged irradiation. In contrast with the Ct photochemical behaviour, the Cc species that is present at the pseudo-equilibrium leads, by irradiation at 313nm, to the Ct with a high quantum yield of Φ=0.52, Fig.2.15.

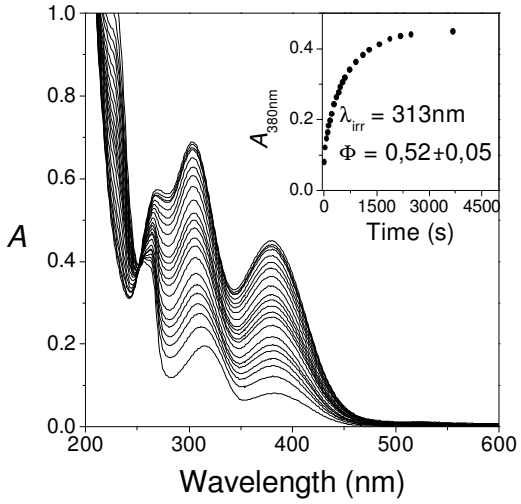

Figure 2.15 - Irradiation at 313nm of a freshly prepared solution of 6-hydroxyflavylium perchlorate at pH=6.4. Inset: absorbance changes at 380nm.

***Trans*-2,5-dihydroxychalcone**

In order to check the nature of the Ct species obtained in neutral or moderately basic solution upon equilibration, the synthesis of the *trans*-2,5-hydroxychalcone was carried out. As mentioned above, the absorption spectrum of the Ct species obtained by direct synthesis is the same of that recorded in samples of Ct formed by the network of the flavylium salt. Due to the existence of a *cis–trans* kinetic barrier, the Ct can be obtained in a metastable state at very acidic pH values. As reported for other p-hydroquinones[35,36] this chalcone is hardly stable at highly basic pH values, even after argon bubbling, leading to fast formation of decomposition products. The nature of these products was not investigated, but they do not give back Ct (or AH^+) upon acidification to pH = 1.0. In spite of its reactivity in basic media,

determination of the first acidity constant of the Ct species could be carried out, Eq. 2.14, Fig. 2.16.

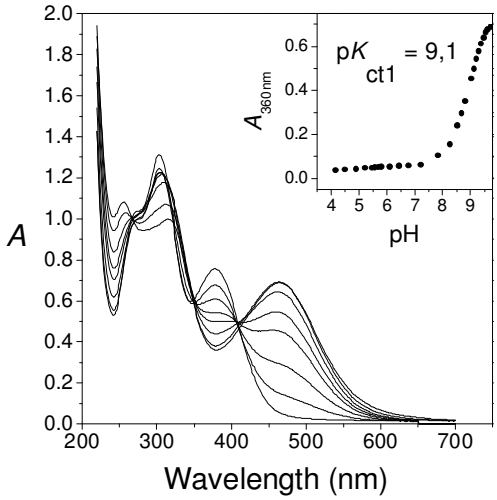

Figure 2.16 - Spectral variations occurring upon a titration of the *trans*-2,5-dihydroxychalcone under argon atmosphere, at 25 °C.

$$Ct + H_2O \overset{K_{Ct1}}{\rightleftharpoons} Ct^- + H_3O^+ \qquad \text{Eq. 2.14}$$

$K_{ct1} = 10^{-9,1}$

Spectroelectrochemistry of the quinoidal chalcone

Synthetic flavylium salts, as well as anthocyanins, can be involved in several electrochemical processes, but usually no reversible electrochemistry is observed on flavylium species[37] nor on chalcones.[38] In 2009 M.M.C. dos Santos *et al* reported for the first time the reversible two-electron two-proton process coupled to a irreversible chemical step of the 4-methyl-7,8-dihydroxyflavylium salt.[22]

In the case of the 6-hydroxyflavylium, the quinone/hydroquinone character of the respective chalcones shows a quasi-reversible voltammogram, as reported in Fig. 2.17-left. Cyclic voltammograms of Ct at pH = 1 were recorded at different potential scan rates, showing a quasi-reversible system with a separation between the positive and the negative peaks (ΔEp) of 0.11V (*vs.* Ag/AgCl). Linear variation of the peak current with the square root of the scan rate shows that process is diffusion control rather than charge transfer kinetics.[39] The cyclic voltammogram of Ct at pH = 1 run at $0.1Vs^{-1}$ was simulated by employing a quasi-reversible redox reaction as mechanistic model. The simulation was reasonable, yielding an electron *trans*fer coefficient (α) of 0.48 (see Fig.2.17-right).

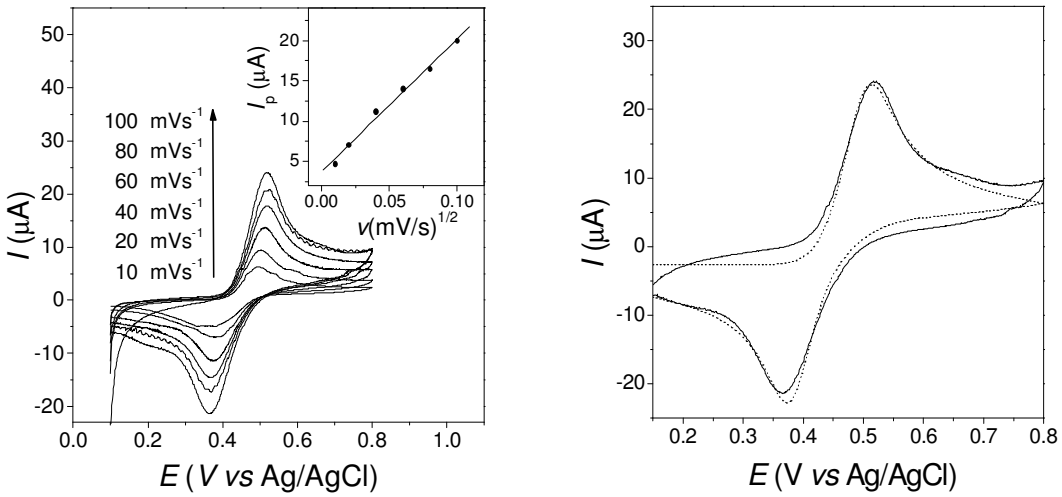

Figure 2.17 – Cyclic voltammograms of 2.9×10^{-4} M *trans*-2,5-dihydroxychalcone at pH 1, at different scan rates at 21°C (left). The working electrode was a glassy carbon electrode, the reference electrode was a Ag/AgCl electrode and as counter-electrode a platinum wire. The experiments were carried out in hydrochloric acid aqueous solution about pH1.3, containing 1MKCl as supporting electrolyte. Inset: plot of the anodic peak current *vs.* square root of scan rate (v), a correlation of 0,99 was found. Comparison of experimental (full line) and simulated (dots line) cyclic voltammograms of $2{,}9\text{x}10^{-4}$M 2,5-dihydroxychalcone at pH 1, run at $0{,}1\text{Vs}^{-1}$ (right). Simulation was made using "GPES4.9 commercial voltammetric simulation package from EcoChemie V.B." with the following parameters: formal potential, E^0 = 0,438V (*vs.* Ag/AgCl) and electron transfer coefficient, α = 0,48.

Cyclic voltammograms were also obtained at other pH values. In basic media (pH = 11.3), the voltammograms obtained on freshly prepared solutions show a voltammetric wave shifted to lower potentials, whose intensity rapidly disappears. These results can be interpreted considering that after the pH jump, the ionized chalcone species is formed and reacts chemically, leading to decomposition products (not investigated) and losing its p-quinone/p-hydroquinone character.

Electrolysis of the Ct species in aqueous solutions at pH=1 was monitored by UV-Vis spectrophotometry. Due to the adsorption of the oxidation product to the glassy carbon (or platinum) electrode when water is used as solvent, the experiments were repeated in ethanol–water mixtures, see Fig. 2.18.

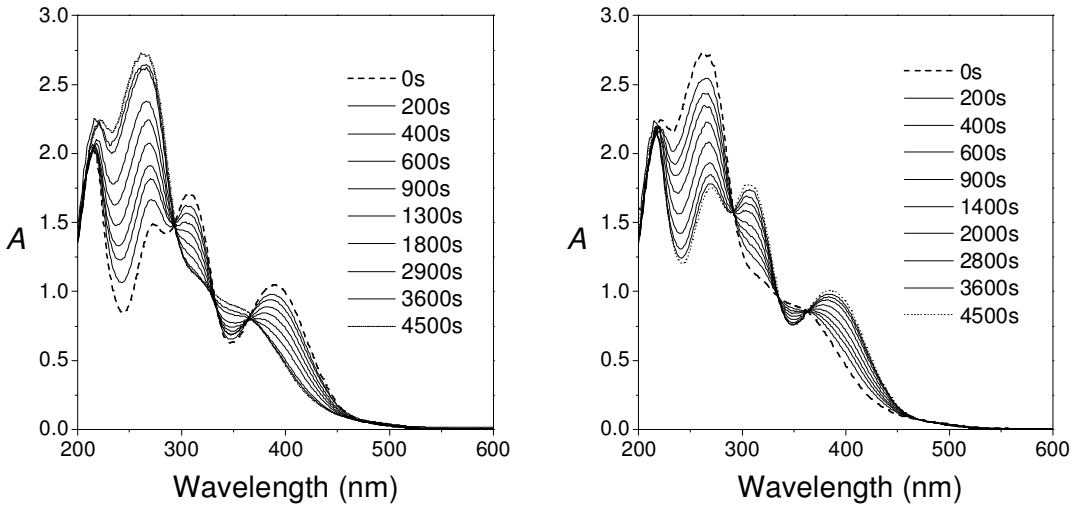

Figure 2.18 - Spectral variations that follow the oxidation (left), and reduction (right) of *trans*-2,5-dihydroxychalcone in a mixture of ethanol (60%) and aqueous 0.2 M HCl (40%). The working electrode was a platinum net electrode, the reference electrode was an Ag/AgCl electrode and as counter-electrode a platinum wire. The supporting electrolyte was 1MKCl.

As shown in Fig. 2.18, the oxidation of Ct leads to a chemical species that can be reversibly reduced back to Ct; this species is the p-quinone oxidized chalcone, Ct_{ox}, represented in Fig. 2.19.[35,36] In spite of the observation of isosbestic points, the redox process is not fully reversible and some side products are formed, in particular at the end of the oxidation process, where the isosbestic points are no longer maintained.

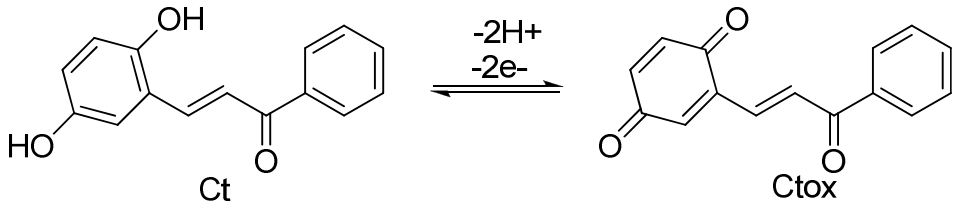

Figure 2.19 – Electrochemical redox mechanism proposed for the *trans*-chalcone form of the 6-hydroxyflavylium

2.4 Conclusions

The substitution of the flavylium compound in position 6 by a hydroxyl group can be compared with the same substitution in positions 4' and 7; like 4'-hydroxyflavylium and unlike 7-hydroxyflavylium, there is a kinetic barrier for the *cis–trans* isomerization. Molecular orbital calculations using semi-empirical methods predict that the potential energy minima of the excited states of 2,5-dihydroxychalcones follow the same trend of the ground states, explaining why the photochemical reaction occurs from the *cis* to the *trans* and not vice versa, see Fig. 2.20.

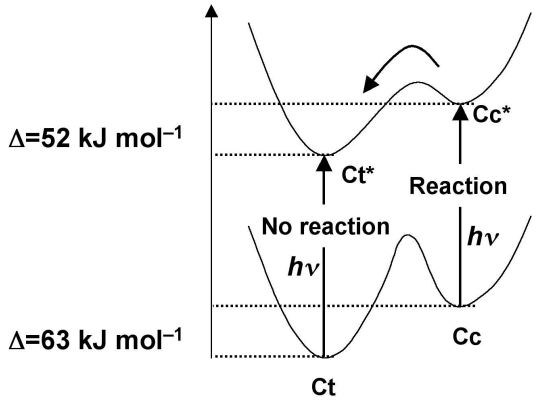

Figure 2.20 - Molecular orbital potential energy minima, calculated by semi-empirical method for the 4'-hydroxyflavylium

Following a procedure previously reported[11], it is possible to draw an energy level diagram of the different species constituting the network, see Fig. 2.21.

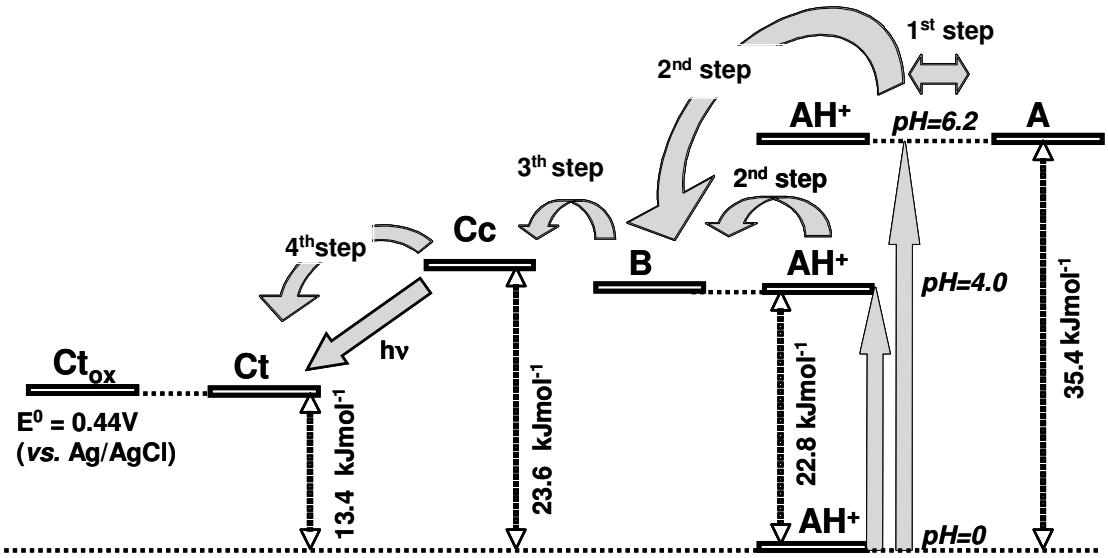

Figure 2.21 – Thermodynamics of the 6-hydroxyflavylium chemical network.

At very acidic pH values, the AH^+ species is the dominant form; raising the pH up to 4–5 leads directly to B and Cc, because the pH is not high enough to form the base A. Only when the pH is higher than 5 can the base be formed, but it reacts immediately towards B and Cc, due to its zwitterionic nature. The *cis–trans* isomerization process is the slowest one, allowing the establishment of pseudo-equilibrium. In spite of its not complete electrochemical reversibility, the 6-hydroxyflavylium compound serves to illustrate the possibility of using electrochemistry as a new input to reach a state of the network.

System presented in this chapter is not suitable as an optical memory due to its photochemical properties. Optical memories based on the dual-type photochromic system should be able to operate efficiently the *cis-trans* isomerization in both directions (*cis*→*trans* and *trans*→*cis*) photochemically.

The spectroscopic studies of the several species of the flavylium salt controlled by light and electricity did not show interesting colour transition. The *cis-trans* photoisomerization of the chalcone form present a colour variation between the colourless (*cis*-chalcone) and light yellow (*trans*-chalcone). On the other hand the *p*-quinone/*p*-hydroquinone chalcone system lead also to a poor colour transition between colourless and light yellow. The colour characteristics of the stable species of the chemical network of the 6-hydroxyflvaylium are not adequate for chromogenic purposes.

2.5 Bibliography

1. Niemz, A.; Rotello, V. M., From enzyme to molecular device. Exploring the interdependence of redox and molecular recognition. *Accounts of Chemical Research* 1999, *32* (1), 44-52.
2. Lederman, H.; Macdonald, J.; Stefanovic, D.; Stojanovic, M. N., Deoxyribozyme-based three-input logic gates and construction of a molecular full adder. *Biochemistry* 2006, *45* (4), 1194-1199.
3. Weiser, M., The computer for the 21st-century. *Scientific American* 1991, *265* (3), 94-104.
4. Bechtold, T.; Mussak, R., *Handbook of Natural Colorants*. John Wiley & Sons: Wiltshire, 2009.
5. Jiang, L. H.; Shoji, T.; Kanda, T.; Morimitsu, Y.; Kubota, K. Novel anthocyanin compound used as colorant in foodstuffs, beverages and pharmaceuticals. WO2007055105-A1; JP2007544090-X, WO2007055105-A1 18 May 2007 C09B-061/00 200745, 2007.
6. Hill, D. W., The synthesis and structure of benzopyrylium (chromylium) salts. *Chemical Reviews* 1936, *19* (1), 27-54.
7. Feringa, B. L., *Molecular Switches*. Wiley-VCH: Weinheim, 2001.
8. Figueiredo, P.; Lima, J. C.; Santos, H.; Wigand, M. C.; Brouillard, R.; Macanita, A. L.; Pina, F., Photochromism of the synthetic 4',7-dihydroxyflavylium chloride. *Journal of the American Chemical Society* 1994, *116* (4), 1249-1254.
9. Brouillard, R.; Dubois, J. E., Mechanism of structural transformations of anthocyanins in acidic media. *Journal of the American Chemical Society* 1977, *99* (5), 1359-1364.
10. McClelland, R. A.; Gedge, S., Hydration of the flavylium ion. *Journal of the American Chemical Society* 1980, *102* (18), 5838-5848.
11. Maestri, M.; Pina, F.; Balzani, V., Multistate/multifunctional molecular-level systems-photochromic flavylium compunds. In *Molecular switches*, Feringa, L. B., Ed. Wiley-VCH: Weinheim, 2001; pp 309-334.
12. Pina, F.; Maestri, M.; Balzani, V., Photochromic flavylium compounds as multistate/multifunction molecular-level systems. *Chemical Communications* 1999, (2), 107-114.
13. Roque, A.; Lima, J. C.; Parola, A. J.; Pina, F., Substitution and solvent effects in the chalcones isomerization barrier of flavylium photochromic systems. *Photochemical & Photobiological Sciences* 2007, *6* (4), 381-385.

14. Pina, F.; Roque, A.; Melo, M. J.; Maestri, I.; Belladelli, L.; Balzani, V., Multislate/multifunctional molecular-level systems: light and pH switching between the various forms of a synthetic flavylium salt. *Chemistry-a European Journal* 1998, *4* (7), 1184-1191.
15. Valls, J.; Millan, S.; Marti, M. P.; Borras, E.; Arola, L., Advanced separation methods of food anthocyanins, isoflavones and flavanols. *Journal of Chromatography A* 2009, *1216* (43), 7143-7172.
16. Scalbert, A.; Manach, C.; Morand, C.; Remesy, C.; Jimenez, L., Dietary polyphenols and the prevention of diseases. *Critical Reviews in Food Science and Nutrition* 2005, *45* (4), 287-306.
17. Nichenametla, S. N.; Taruscio, T. G.; Barney, D. L.; Exon, J. H., A review of the effects and mechanisms of polyphenolics in cancer. *Critical Reviews in Food Science and Nutrition* 2006, *46* (2), 161-183.
18. Dudonne, S.; Vitrac, X.; Coutiere, P.; Woillez, M.; Merillon, J. M., Comparative study of antioxidant properties and total phenolic content of 30 plant extracts of industrial interest using DPPH, ABTS, FRAP, SOD, and ORAC assays. *Journal of Agricultural and Food Chemistry* 2009, *57* (5), 1768-1774.
19. Jorgensen, L. V.; Cornett, C.; Justesen, U.; Skibsted, L. H.; Dragsted, L. O., Two-electron electrochemical oxidation of quercetin and kaempferol changes only the flavonoid C-ring. *Free Radical Research* 1998, *29* (4), 339-350.
20. Janeiro, P.; Brett, A. M. O., Catechin electrochemical oxidation mechanisms. *Analytica Chimica Acta* 2004, *518* (1-2), 109-115.
21. Cotelle, N.; Hapiot, P.; Pinson, J.; Rolando, C.; Vezin, H., Polyphenols deriving from chalcones: investigations of redox activities. *Journal of Physical Chemistry B* 2005, *109* (49), 23720-23729.
22. Moncada, M. C.; de Mesquita, M. F.; dos Santos, M. M. C., Electrochemical oxidation of the synthetic anthocyanin analogue 4-methyl-7,8-dihydroxyflavylium salt. *Journal of Electroanalytical Chemistry* 2009, *636* (1-2), 60-67.
23. Hapiot, P.; Neudeck, A.; Pinson, J.; Fulcrand, H.; Neta, P.; Rolando, C., Oxidation of caffeic acid and related hydroxycinnamic acids. *Journal of Electroanalytical Chemistry* 1996, *405* (1-2), 169-176.
24. Pratt, D. D.; Robinson, R., A synthesis of pyrylium salts of anthocyanidin type. *Journal of the Chemical Society* 1922, *121*, 1577-1585.
25. Michaelidis, C.; Wizinger, R., Beitrag zur kenntnis der 2-aryl-benzopyryliumsalze. *Helvetica Chimica Acta* 1951, *34* (6), 1761-1770.
26. Glasoe, P. K.; Long, F. A., Use of glass electrodes to measure acidities in deuterium oxide. *Journal of Physical Chemistry* 1960, *64* (1), 188-190.

27. Robinson, R.; Crabtrfe, H. G.; Das, C. K.; Lawson, W.; Lunt, R. W.; Roberts, B. H.; Williams, P. N., Some derivatives of benzopyrylium. *Journal of the Chemical Society* 1924, *125*, 207-214.
28. Küster, F. W.; Thiel, A., *Tabelle per le analisi chimiche e chimico-fisiche*. 12th ed.; Hoepli: Milano, 1982.
29. Maestri, M.; Ballardini, R.; Pina, F.; Melo, M. J., An easy and inexpensive flash spectroscopy experiment. *Journal of Chemical Education* 1997, *74* (11), 1314-1316.
30. Pina, F.; Melo, M. J.; Parola, A. J.; Maestri, M.; Balzani, V., pH-controlled photochromism of hydroxyflavylium ions. *Chemistry-a European Journal* 1998, *4* (10), 2001-2007.
31. McClelland, R. A.; McGall, G. H., Hydration of the flavylium ion .2. the 4'-hydroxyflavylium ion. *Journal of Organic Chemistry* 1982, *47* (19), 3730-3736.
32. Brouillard, R., Flavonoids and the flower colour. In *The flavonoids, advances in research*, Harborne, J. B., Ed. Chapman and Hall: London, 1988; pp 525-538.
33. Brouillard, R., Chemical structure of anthocyanins. In *Anthocyanins as food colors*, Markakis, P., Ed. Academic Press: New York, 1982; pp 1-40.
34. Moncada, M. C.; Parola, A. J.; Lodeiro, C.; Pina, F.; Maestri, M.; Balzani, V., Multistate/multifunctional behaviour of 4'-hydroxy-6-nitroflavylium: a write-lock/read/unlock/enable-erase/erase cycle driven by light and pH stimulation. *Chemistry-a European Journal* 2004, *10* (6), 1519-1526.
35. Bishop, C. A.; Tong, L. K. J., Equilibria of substituted semiquinones at high pH. *Journal of the American Chemical Society* 1965, *87* (3), 501-505.
36. Patai, S., *The chemistry of the quinoid compounds*. John Wiley & Sons: London, 1974; p 942.
37. Hicks, L. D.; Fry, A. J.; Kurzweil, V. C., Ab initio computation of electron affinities of substituted benzalacetophenones (chalcones): a new approach to substituent effects in organic electrochemistry. *Electrochimica Acta* 2004, *50* (4), 1039-1047.
38. da Silva, P. F.; Lima, J. C.; Quina, F. H.; Macanita, A. L., Excited-state electron transfer in anthocyanins and related flavylium salts. *Journal of Physical Chemistry A* 2004, *108* (46), 10133-10140.
39. Bard, A. J.; Faulkner, L. R., *Electrochemical methods - fundamentals and applications*. 2nd ed.; Wiley: New York, 2001.

Chapter 3

Multiresponsive chromogenic systems operated by light and electrical inputs

3.1 Introduction

The chromogenic systems are usually based on one stimulus - one output or in the case of dual-mode systems several stimulus – one output (see section 1.2). Many practical applications, however, require systems with different output responses. As an example, image production requires chromogenic systems with multiple outputs able to compose several colours. A system possessing three coloured states, cyan, magenta and yellow, as well as a transparent state (CMYT), all of them independently addressable, might be useful for image production. However, this is not an easy task to achieve, since multiresponsive systems usually require a high degree of complexity.

Recent investigation made in our group with crystal violet lactone found that the two iron cations Fe(III) and Fe(II) display very different affinities towards CVL ring opening; (i) Fe(III) leads to a ring opening, and therefore development of blue colour in solvents like methanol, and (ii) Fe(II) possessing a much lower affinity towards CVL ring opening allows thermal conversion of the CVOL (blue coloured state) to CVL (colourless state). Addition to the system of a photochromic molecule introduces two more optical states (yellow and magenta) to the system.

We show that the conjugate action of electrons and light input in a three-component system, crystal violet lactone (CVL), spiropyran (SPI) and a developer Fe(III)/Fe(II), leads to the selective appearance of colourless, blue, yellow and magenta that can be composed to obtain the four components of the CMYT colour model.

3.1.1 Leuco Dyes

Leuco dyes belongs a class of molecules that are able to switch between a coloured state and a leuco state, by the mean of an external action (see section 1.2.3). Leuco dyes are of great importance for many commercial applications. The most relevant one is in the textile industry – vat dyes, but other applications have been explored such as carbonless copy paper, thermosensitive recording paper and thermochromic materials.

Crystal Violet Lactone – Ionochromism

Crystal Violet Lactone (3,3-bis-(4-dimethylaminophenyl)-6-dimethylaminophthalide; CVL; see Fig. 3.1)[1,2,3] is the lactone form of the crystal violet dye. CVL has been used for a long time in carbonless copy paper[4], irreversible thermal printing[5], and as a thermochromic system in several applications.[6]

In 1945 The National Cash Register Company applied for a patent published in 1947, describing the synthesis of CVL.[7] They claimed that CVL has the unique characteristic of

being colourless under normal conditions, while it changes to an intense blue colour upon being placed in adsorption contact with highly polar substances such as clay, silicon dioxide and magnesium carbonate. Its use for carbonless paper was patented.

In fact CVL presents with a closed-ring lactone form in low-polarity and non-acidic media. In the presence of a so-called developer, however, the lactone ring opens and a coloured state develop. In its leuco state (ring-closed form, see Fig. 3.1) the dye is colourless and presents a π–π^* transition with λ_{max} at 280nm.[5]

In the presence of weak acids or electron acceptors CVL is converted to the triphenylmethane (TPM) form (open-ring form, see Fig. 3.1), with increased conjugation and lower energy π–π^* transition, λmax at 620nm (depending on the solvent media) giving rise to strongly coloured state.

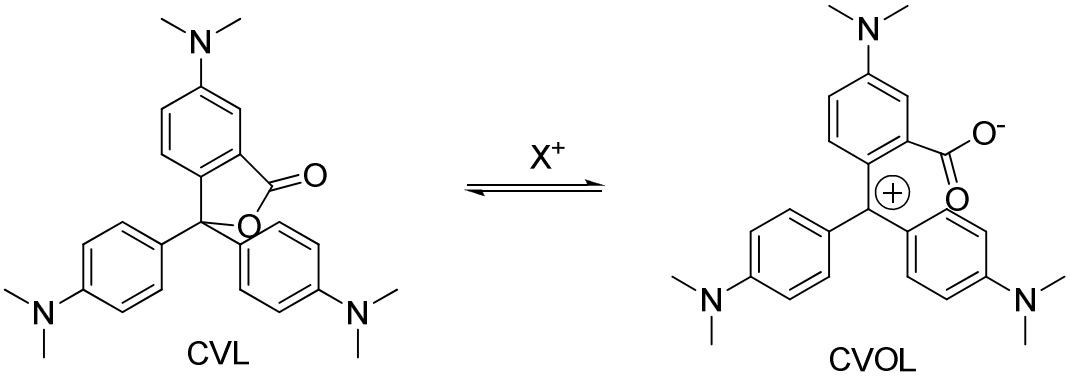

Figure 3.1 – Ring opening of Crystal Violet Lactone. Left: closed ring Crystal Violet Lactone (CVL); Right: open ring Crystal Violet Lactone (CVOL)

The ring opening can also be triggered by the presence of some metals halides such as Ca^{2+}, Mg^{2+},[7] Ni^{2+},[8] forming the CVOL coloured state. The ability of CVL to complex such metals allows building an ionochromic system, *i.e.*, a system that change colour upon the presence of ions.

Spiropyran – Photochromism

Spiropyrans are a widely studied class of compounds which exhibit photochromism (see section 1.2.2).[9] They consist structurally of a pyran derivative linked by a common spiro carbon atom with another heterocyclic ring. The most well known spiropyran is the spiroindolinobenzopyran (BIPS).[1] In Fig. 3.2 the different species of the (6-NO_2,1'N-CH_2CH_2OH)-BIPS derivative is represented.

Photochemistry of spiropyrans, especially of 6-NO_2-substituted, is well documented.[1,9,10,11,12,13,14,15] Upon UV irradiation of the spiro form the photochemical

heterolytic cleavage of the carbon–oxygen bond yields the ring-opened coloured forms, often called the 'merocyanine' form (MERO), which can be either cis-(MERO-c) or trans-(MERO-t), or the *ortho*-quinoidal form represented by (MERO-oQ)[9,14] (see Fig. 3.2). The *cis*-merocyanine isomer is formed as a short-lived intermediate as described by H. Gorner.[14]

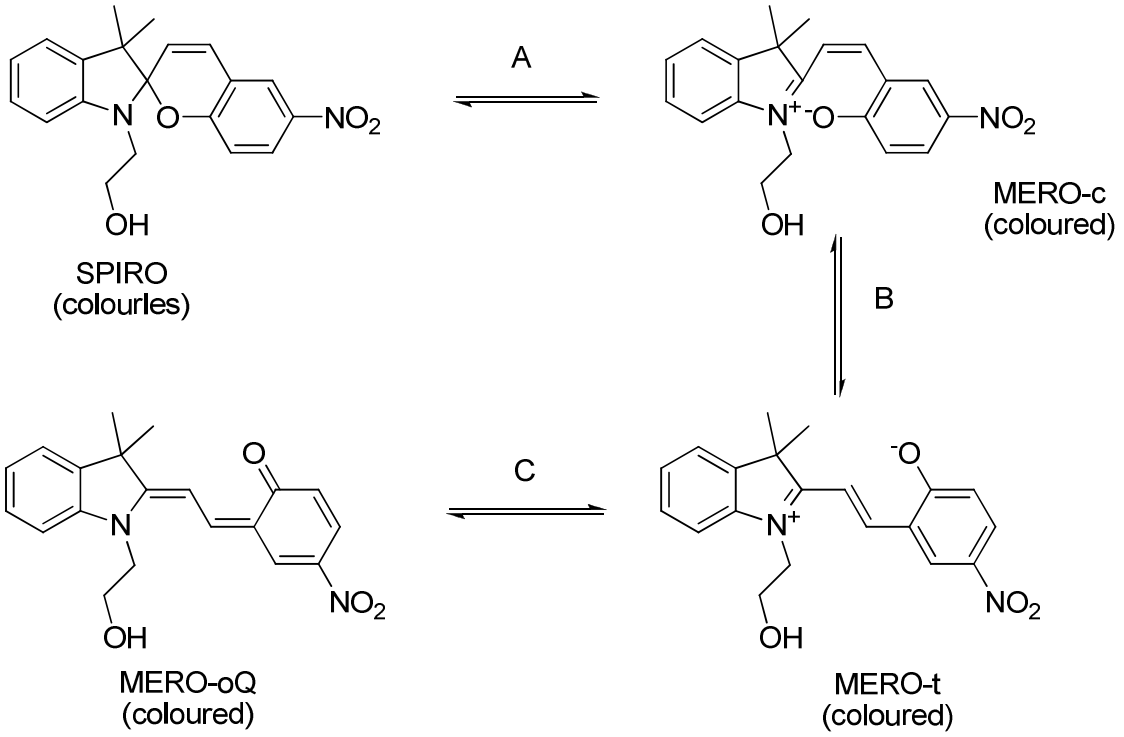

Figure 3.2 - (6-NO_2,1'N-CH_2CH_2OH)-BIPS (SPIRO) and ring open merocyanine (MERO) and respective isomers (MERO-c, MERO-t and MERO-oQ).

The general behaviour of spiropyrans is the enhancement of colouration upon UV irradiation. After removal of light, the colour of the spiropyran returns to its original value within a time which depends essentially on temperature.[10]

Although spiropyrans are efficient photochromic molecules they show a low fatigue resistance.[8,11] In the attempt to increase the stability of the photochromic system ions were add to the spiropyran solutions.

Complexes of the merocyanine form of spiropyrans possessing a co-ordinating group[16] (like the 6-NO-8-OMe-BIPSs) with certain d- and f-elements (see Fig. 3.3) was reported in solution.[17,18] It has been also reported merocyanine chelates with several metal ions like Cu(II)[17,16,19,20] Fe(II)[17], Ca(II)[16], Pb(II)[16], Ni(II)[16,20], Zn(II)[19,20], Nd(III), Mg(II), Mn(II), Co(II), Cd(II), Pb(II), Y(III), Pr(III), Eu(III), Tb(III), La(III).[18]

Merocyanine-metal chelates show a spectral blue shift (towards higher energies) compared to the original spectra of the merocyanine form (c.a. of 100nm blue shift have been reported).[19]

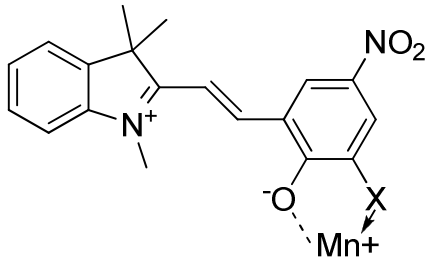

Figure 3.3 - Merocyanine-metal chelate

Kinetic studies of the chelation between 6-NO_2-8-Ome-1'N-CH_3-BIPS and Cu(II) shows a two coupled reactions: (i) formation of the merocyanine form and (ii) substitution of the solvent coordinated at the metal ion by the ligand. Thermally activated ring opening (i) is the slowest process, but when the ring opening is induced photochemically the rate limiting process is the thermal ligand substitution (ii).[18, 19]

The decolouration process (closed-ring form) may occur via the chelate or via the uncomplexated merocyanine form. In the first case the chelate dissociates (release of the metal ion) and this is followed by the formation of the spiropyran (see Fig. 3.4, process K3). In the second case, the free form of the merocyanine thermally recovers to spiropyran form (see Fig. 3.4, process K1) pushing the complex equilibria towards dissociation.[20]

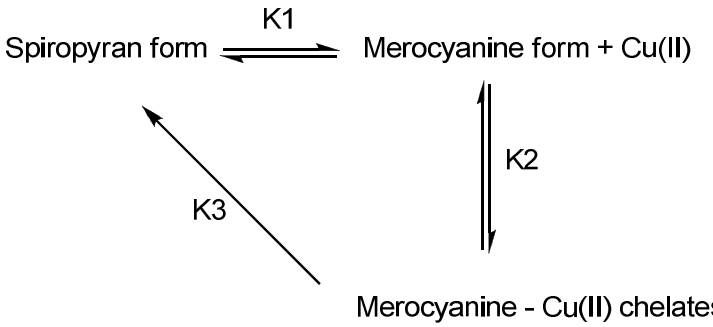

Figure 3.4 – Chelate formation and decolouration chemical equilibrium adapted from ref.20.

3.2 Experimental details

Synthesis

N-(2-Hydroxyethyl)-3',3'-dimethyl-6-nitro-spiro[2H-1-benzopyran-2,2'-indoline] (SPI) was synthesized as described elsewhere.[21] Crystal violet lactone (Aldrich, 97%), iron(III) chloride hexahydrate (Aldrich), iron(II) sulphate heptahydrate (Merck, 99.5%), anhydrous iron(III) chloride (Riedel, 98%) and tetrabutylammonium perchlorate (TBAP, Fluka) were certified analytical grade and used without further purification. Absolute ethanol (Panreac, 99.5%), methanol (Aldrich, 99.9%) and all other solvents were purchased from Sigma-Aldrich, were of HPLC grade and used without further purification.

Optical spectroscopic measurements

Absorption spectra were recorded on a Shimadzu UV-2501-PC spectrometer. A standard cuvette holder and cuvettes with an optical path length of 1 cm were used.

Electrochemical measurements

Cyclic voltammetry was performed in a conventional three-electrode cell under an argon atmosphere at 21°C using a potentiostat–galvanostat Model 20 Autolab from Eco Chemie BV (Utrecht, The Netherlands). The collection of data was controlled by GPES version 4.9 Eco Chemie BV software. The working electrode was a vitreous carbon microelectrode, the auxiliary electrode was a platinum wire and the reference electrode was Ag/AgCl (RE-5B from BAS). All solutions were initially saturated with argon (during 20 min.) and kept under argon atmosphere.

Spectroelectrochemistry

Electrolysis was performed using a two electrochemical half-cell configuration. The first half-cell was composed of the chromogenic solution, with a platinum net as a working electrode and a reference electrode (saturated calomel electrode, ref. 921 from Radiometer Analytical). In the second half-cell, a counter-electrode was immersed in the electrolyte solution. Both cells were ionically connected by a liquid electrolyte diaphragm using Vycor® glass rods to avoid solution migration between the half-cells. Absorbance spectra of bulk electrolysed solution were accomplished using a spectrophotometric flow-through absorbance cell (175.050-QS from Hellma). Chromogenic solution was pumped from the electrolysis cell through the flow-through absorbance cell using a peristaltic pump. The solution was looped between the electrolysis cell and the spectrophotometric cell under an argon atmosphere during cathodic and anodic electrolysis. All solutions were initially saturated with argon (during 20 min.) and kept under argon atmosphere.

Photochemistry

Photochemical reactions were performed using monochromatic radiation. An irradiation setup built from a Spex Lamp Housing containing a 450W Xenon lamp was focused in a monochromator (Jobin Yvon Horiba, model H10 UV) with 5nm slits. Sample volumes of 3 to 8 ml were used. All solutions were initially deaerated for 20 minutes under an argon stream (Concerning the photochemistry of CVL alone, no spectral changes were observed upon irradiation. However, in the presence of Fe(III), a slow degradation of CVL under UV light takes place, but the reaction is strongly minimized in the absence of oxygen).

Mass spectrometry

MALDI-TOF-MS analyses were performed with the positive reflector mode. The apparatus used is a Voyager-DE™ PRO Biospectrometry Workstation model (Applied Biosytems) and data were analysed with Voyager V5.1 software.

3.3 Results and Discussion

3.3.1 Interaction between CVL and iron ions

Spectroscopic Studies

First experiments were carried out using $FeCl_3.(H_2O)_6$ and $FeSO_4{\cdot}(H_2O)_7$ as possible colour developers of CVL in ethanol. It turned out that blue colour appears in CVL solutions as soon as Fe(III) is present in solution, but addition of Fe(II) does not lead to any colour change (see Fig. 3.5). The presence of Fe(III) gives rise to an absorption spectrum similar to those obtained for the parent molecule crystal violet in glycerol.[22] This behaviour was not only observed in ethanol, but also in the n-alcohol series from methanol to 1-decanol and also in polar solvents such as propylene carbonate and even in ionic liquids such as 1-Butyl-3-methylimidazolium hexafluorophosphate.

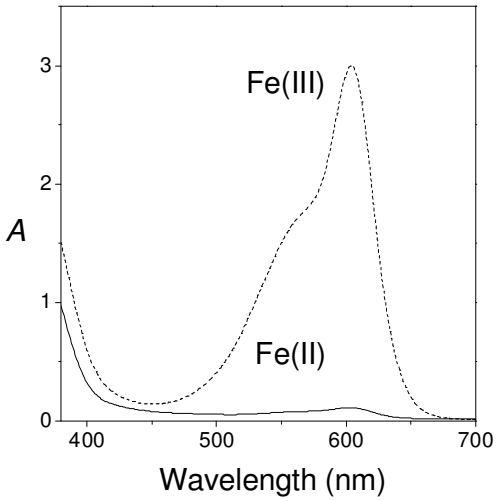

Figure 3.5 - Absorption spectra of 0.5 mM CVL in the presence of 1 mM Fe(II) (solid line) and 1 mM Fe(III) (dashed line). On the contrary to Fe(II), the oxidized form Fe(III) opens the lactone ring of CVL.

Anhydrous $FeCl_3$ was used afterwards in order to avoid possible ferric hydroxide precipitates and a titration in methanol was performed. Fig.3.6 shows the absorption spectra at different composition fractions of both CVL and $FeCl_3$. As expected, the absorption spectra of the CVL opened species (CVOL) increase its intensity when the concentration of both solutes is comparable.

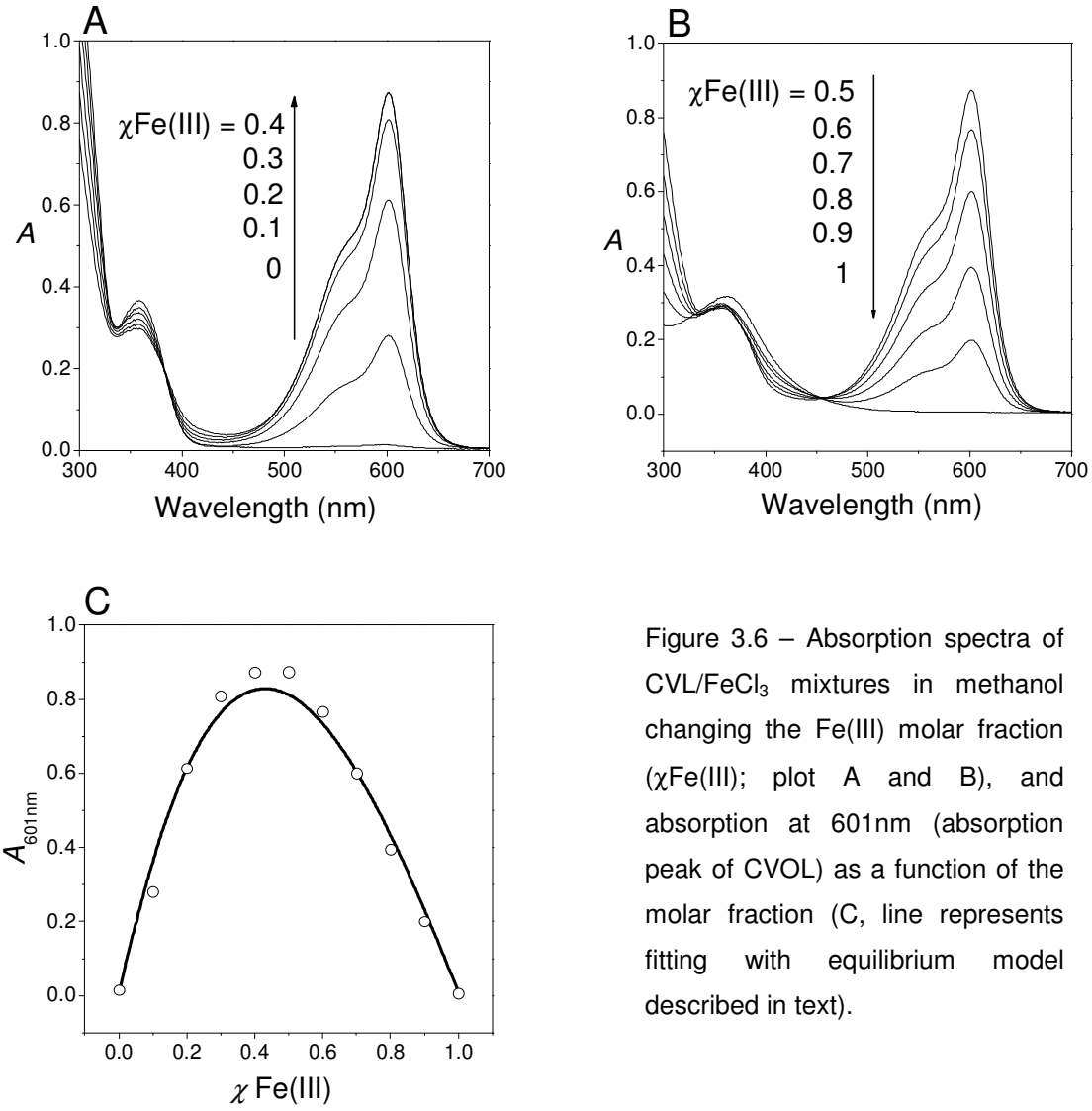

Figure 3.6 – Absorption spectra of CVL/$FeCl_3$ mixtures in methanol changing the Fe(III) molar fraction (χFe(III); plot A and B), and absorption at 601nm (absorption peak of CVOL) as a function of the molar fraction (C, line represents fitting with equilibrium model described in text).

Job's plot analysis of the complex between CVL and Fe(III) is presented in Fig. 3.6-C. Result is not conclusive about possible stoichiometries of the complexes. The association constants are not high, since there is not a sharp plot as usually observed when a strong complex is formed. Also, taking into account the CVL concentrations used ([CVL] = 150μM) and the crystal violet extinction coefficient, even when the absorption spectrum reaches its maximum value at 601nm, only about 5% of CVL is converted into CVOL (A_{601nm} = 0,9, [CVOL] = 7,5μM). High extinction coefficients are normal for chromogenic dyes. It has been assigned to CVOL in acidified acetonitrile an extinction coefficient of 1,1x10^5 $mol^{-1}cm^{-1}$ at 586nm.[5] We determined almost the same value 1,2x10^5 $mol^{-1}cm^{-1}$ at 601nm using the Job's Plot data.

MALDI-TOF-MS experiments of CVL in methanol in a concentration of 1 mg/ml and no matrix added (see Mass Spectra 3.1 in pg.64) show the presence of several species. A strong peak at 415.2 m/z (peak 1 in Mass Spectra 3.1) is found, which is attributed to $CVL^{+\bullet}$.

Fragmentation peaks are also found at 371.2 (peak 2 in Mass Spectra 3.1) and 327.2 m/z (peak 3 in Mass Spectra 3.1), attributed to the loss of dimethylamine groups by CVL. Solutions with stoichiometry of 1:1 of CVL/$FeCl_3$ (see Mass Spectra 3.2, in pg.65) showed the same peaks, but showed also additional peaks, namely at 541.1 m/z attributed to CVOL-$FeCl_2^+$ (peak 1 in Mass Spectra 3.2), 506.1 m/z attributed to CVOL-$FeCl^{+\bullet}$ (peak 2 in Mass Spectra 3.2), and 829.4 m/z attributed to a photogenerated dimer CVL_2^+ (peak 3 in Mass Spectra 3.2), among others.

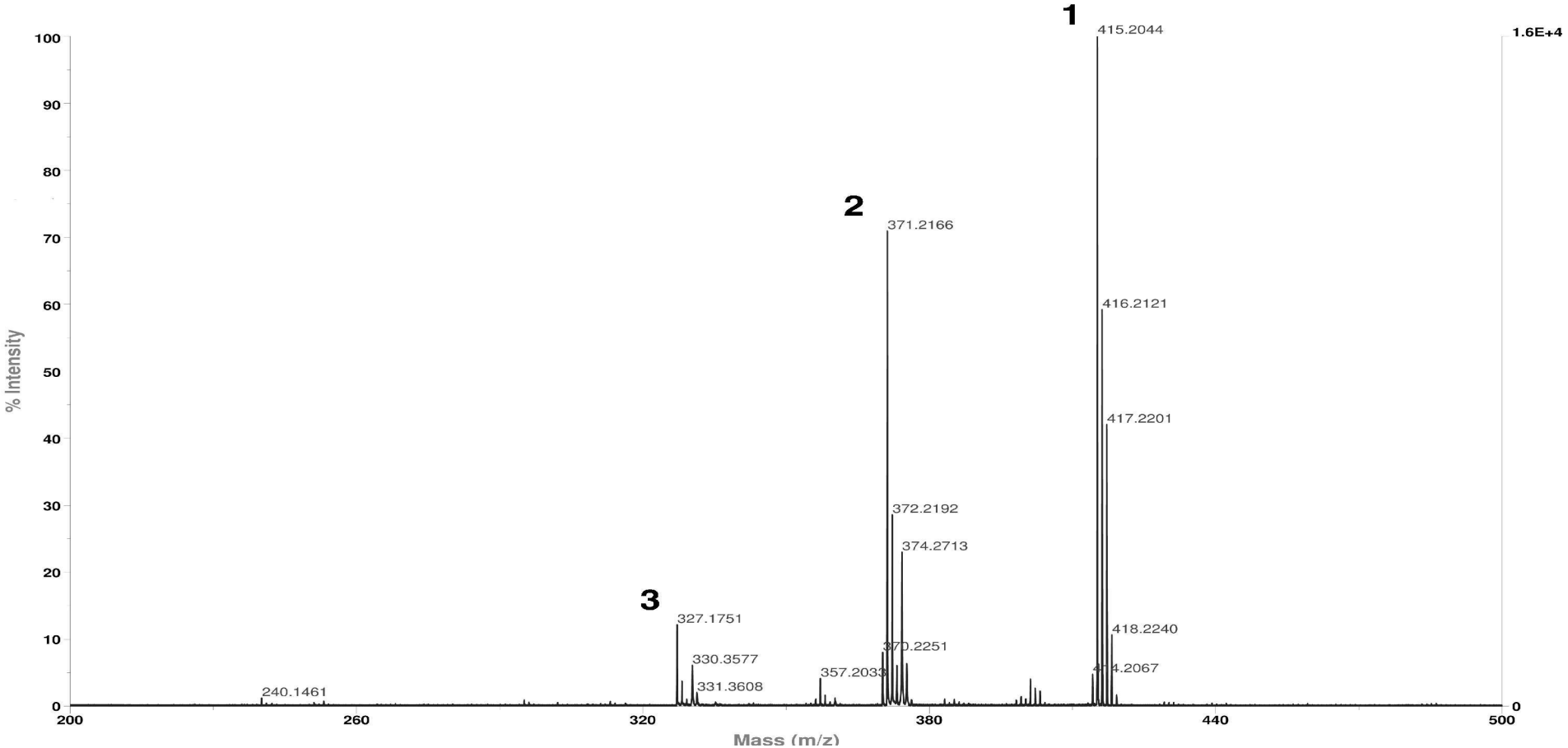

Mass Spectra 3.1 - MALDI-TOF-MS analysis of CVL in methanol in a concentration of 2,9mM. Experimental details: no matrix was added and positive reflector mode was used. The apparatus used is a Voyager-DE™ PRO Biospectrometry Workstation model (Applied Biosytems) and data were analysed with Voyager V5.1 software.

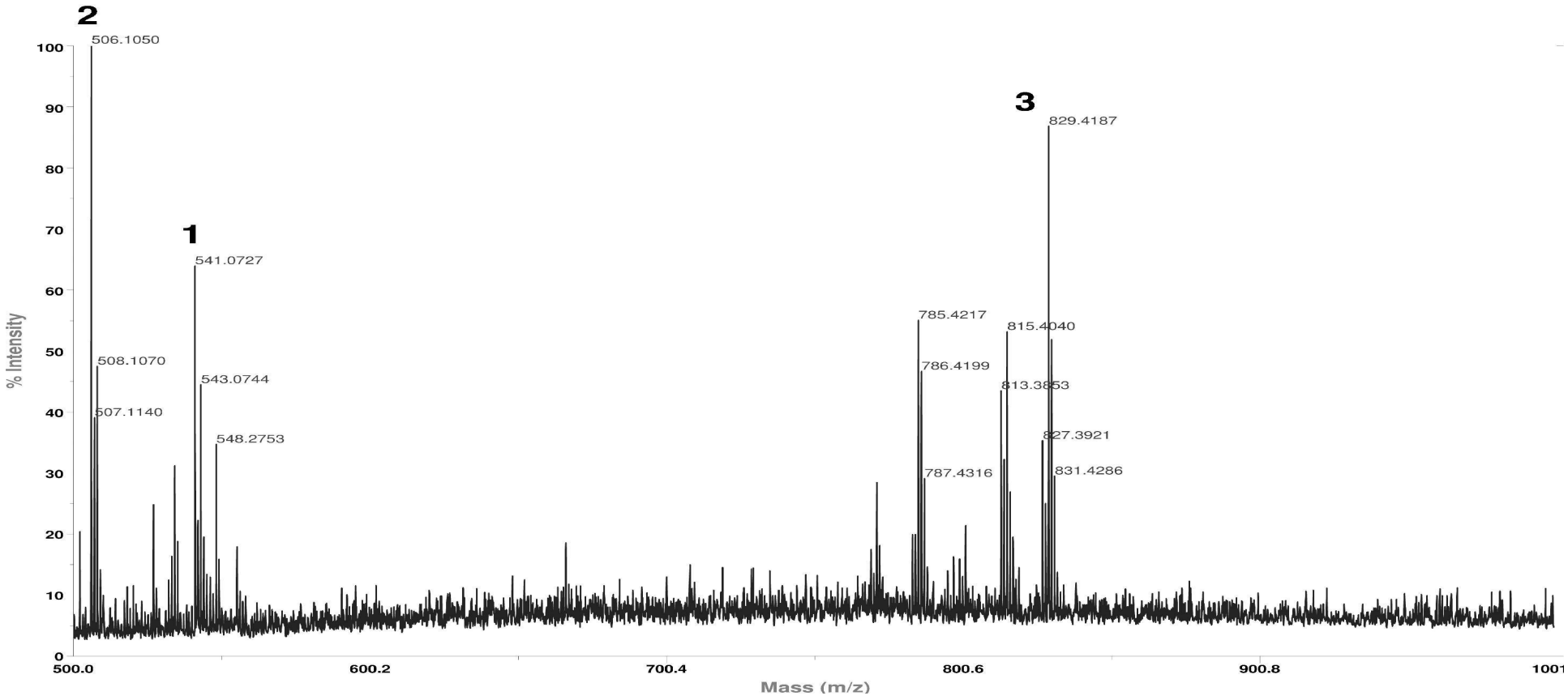

Mass Spectra 3.2 – MALDI-TOF-MS analysis of a mixture of equimolar concentration (2,45mM) of CVL and Fe(III) in methanol. Experimental details: no matrix was added and positive reflector mode was used. The apparatus used is a Voyager-DE™ PRO Biospectrometry Workstation model (Applied Biosytems) and data were analysed with Voyager V5.1 software.

These experiments show that the coloured species appear probably due to an exchange between Cl^- and CVL in the coordination sphere of Fe(III). Therefore one can write the following equilibria to describe approximately the system, neglecting the possible presence of CVOL-$FeCl^+$ species:

$$CVL \overset{K_L}{\rightleftharpoons} CVOL \qquad \text{Eq.3.1}$$

$$FeCl_3 \overset{K_{diss}}{\rightleftharpoons} FeCl_2^+ + Cl^- \qquad \text{Eq.3.2}$$

$$CVL + FeCl_2^+ \overset{K_{comp}}{\rightleftharpoons} CVOL - FeCl_2^+ \qquad \text{Eq.3.3}$$

From a mass balance, the following equations may be written:

$$C_{CVL} = [CVL]\left(1 + K_L + K_{comp}K_{diss}\frac{[FeCl_3]}{[Cl^-]}\right) \qquad \text{Eq. 3.4}$$

$$C_{FeCl_3} = [FeCl_3]\left(1 + \frac{K_{diss}}{[Cl^-]} + K_{comp}K_{diss}\frac{[CVL]}{[Cl^-]}\right) \qquad \text{Eq.3.5}$$

$$[Cl^-] = \sqrt{K_{diss}[FeCl_3] + K_{comp}K_{diss}[CVL][FeCl_3]} \qquad \text{Eq. 3.6}$$

$$[CVOL] + [CVOL - FeCl_2^+] = K_L[CVL] + K_{comp}K_{diss}\frac{[CVL][FeCl_3]}{[Cl^-]} \qquad \text{Eq. 3.7}$$

Where C_{CVL} and C_{FeCl3} are the total concentrations of CVL and $FeCl_3$, respectively. Eq.3.4, 3.5 and 3.6 cannot be solved analytically in an explicit way. Therefore a numerical analysis was performed in order to fit the observed change in the absorption at 601nm (the peak of the coloured species CVOL and CVOL-$FeCl_2^+$) with two adjustable variables (K_{diss} and K_{comp}), since the extinction coefficient of all species and K_L are known or could be obtained independently. Fitting the model into the experimental data, allowed the following solutions to be obtained:

$K_{diss} = 1\times10^{-4}$ M

$K_{comp} = 2.2\times10^{3}$ M^{-1}

Fig. 3.6-C shows the fitting to the experimental data. Slight deviations from experimental results are observed, nevertheless, accordance with MALDI-TOF-MS results is achieved: only 1:1 stoichiometries for the complexes are observed.

Other ions were studied, but no other metal was found to present the same reversible ionochromic effect controllable by an electrical stimulus, as shown by the redox pair Fe(III)/Fe(II).

Spectroelectrochemistry in Methanol

The fact that the strong colour differences are displayed when using either Fe(III) or Fe(II) prompted the study of this system in order to check the use of an electrical stimulus to operate reversibly the ionochromism presented the CVL. The electrochemical stability of CVL was measured performing a cyclic voltammetry (see Fig.3.7).

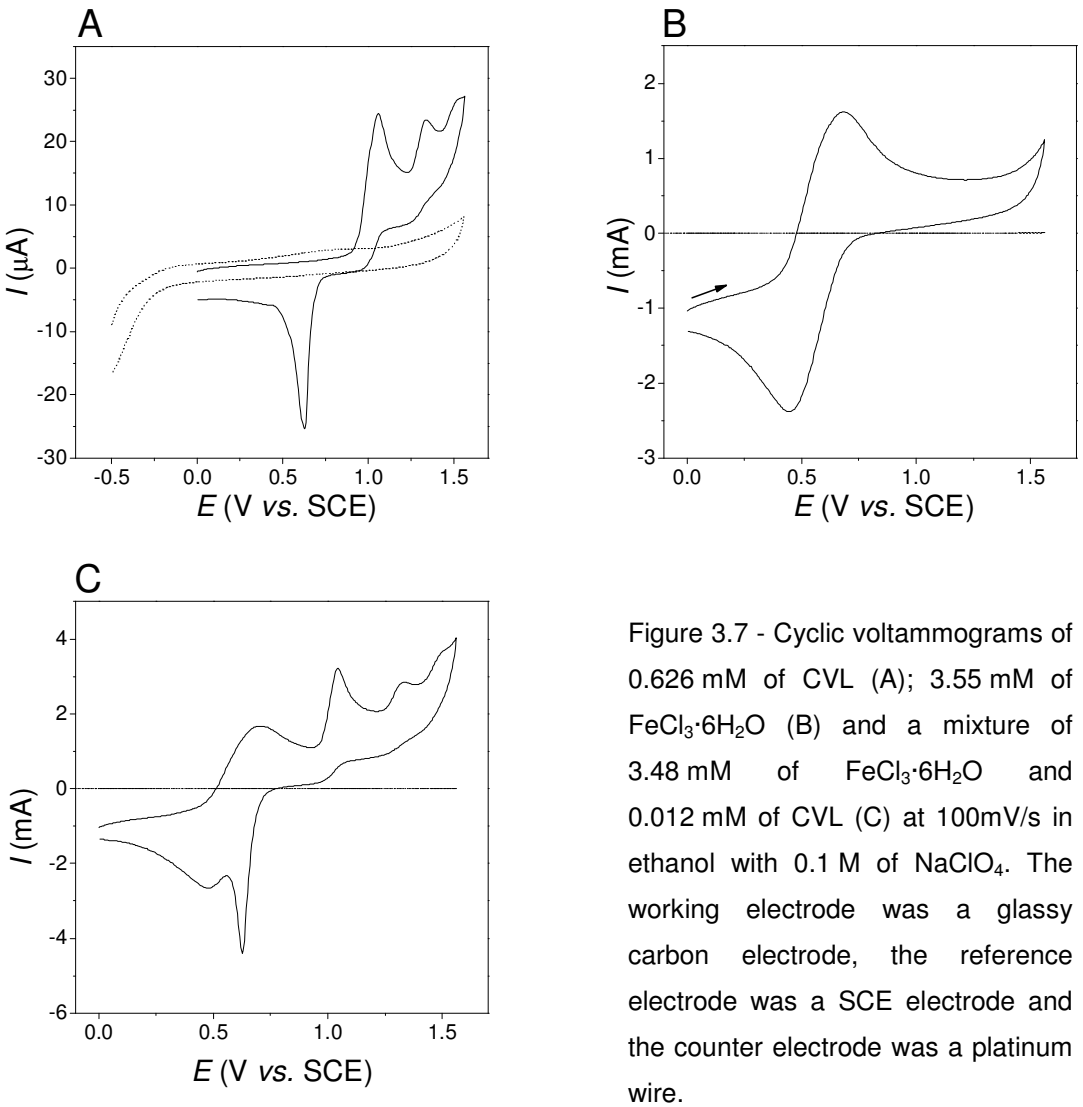

Figure 3.7 - Cyclic voltammograms of 0.626 mM of CVL (A); 3.55 mM of $FeCl_3 \cdot 6H_2O$ (B) and a mixture of 3.48 mM of $FeCl_3 \cdot 6H_2O$ and 0.012 mM of CVL (C) at 100mV/s in ethanol with 0.1 M of $NaClO_4$. The working electrode was a glassy carbon electrode, the reference electrode was a SCE electrode and the counter electrode was a platinum wire.

Fig.3.7-A shows the cyclic voltammogram of CVL, (A) $FeCl_3$ and (B) a mixture of both components. CVL voltammogram presents two anodic peaks around 1,05 and 1,35V (*vs.* SCE), which are attributed to the formation of radical cation and dication of the dimethylaniline moiety.[23] This attribution is confirmed with spectroelectrochemistry measurements which show an absorption band appearing at about 450nm (results not shown), in accordance with published spectra of N,N-dimethylaniline radical cation.[24,25] The cathodic peaks of CVL are related to electrochemical products resulting from reactions with the solvent and with CVL radical cation (in the case of N,N-dimethylaniline, it can proceed

into a polymerization reaction).[23] The Fe(III)/Fe(II) couple in the absence of CVL was also studied in methanol. In this case, as expected, an anodic peak appears at 0.6 V (*vs.* SCE) that we assign to the well known oxidation of Fe(II) to Fe(III), the most stable species in solution at moderate pH. The cathodic peak occurs at 0.4V (*vs.* SCE) were reduction of Fe(III) occurs. Voltammograms obtained shows a quasi-reversible electrochemical behaviour. The ΔE_p is 244mV, far from the 59mV[26] obtained for completely reversible redox (one electron process) voltammogram, as discussed previously in the literature.[27,28] On the other hand cyclic voltammetry, of a solution of Fe(III), performed at different scan rate showed a direct correlation between current peak and the square root of the scan rate, indicating that the system is controlled by diffusion. Finally, the voltammograms of the CVL and Fe(III) obtained for the mixture (see Fig.3.7-C) are almost the same (no significant shift of the peak potentials were observed) as the ones obtained for the pure compounds (se Fig.3.7 – A and B). Therefore it follows that one can selectively perform electrochemical reactions on the Fe(III)/Fe(II) without affecting CVL by judicious selection of electric potentials.

The most interesting feature is observed when a complete electrochemical reduction of Fe(III) to Fe(II) in the presence of CVL is performed. The cathodic electrolysis leads to a complete conversion to Fe(II) without reducing CVL (Fig.3.8-A), and the blue colour disappears completely. Afterwards a 0.55 V (*vs.* SCE) potential can be applied in order to re-oxidize Fe(II) back to Fe(III), and indeed the blue colour could be recovered. The cycle was repeated 10 times without showing any significant degradation of the sample, and therefore this system reveals to be indirectly electrochromic as well.

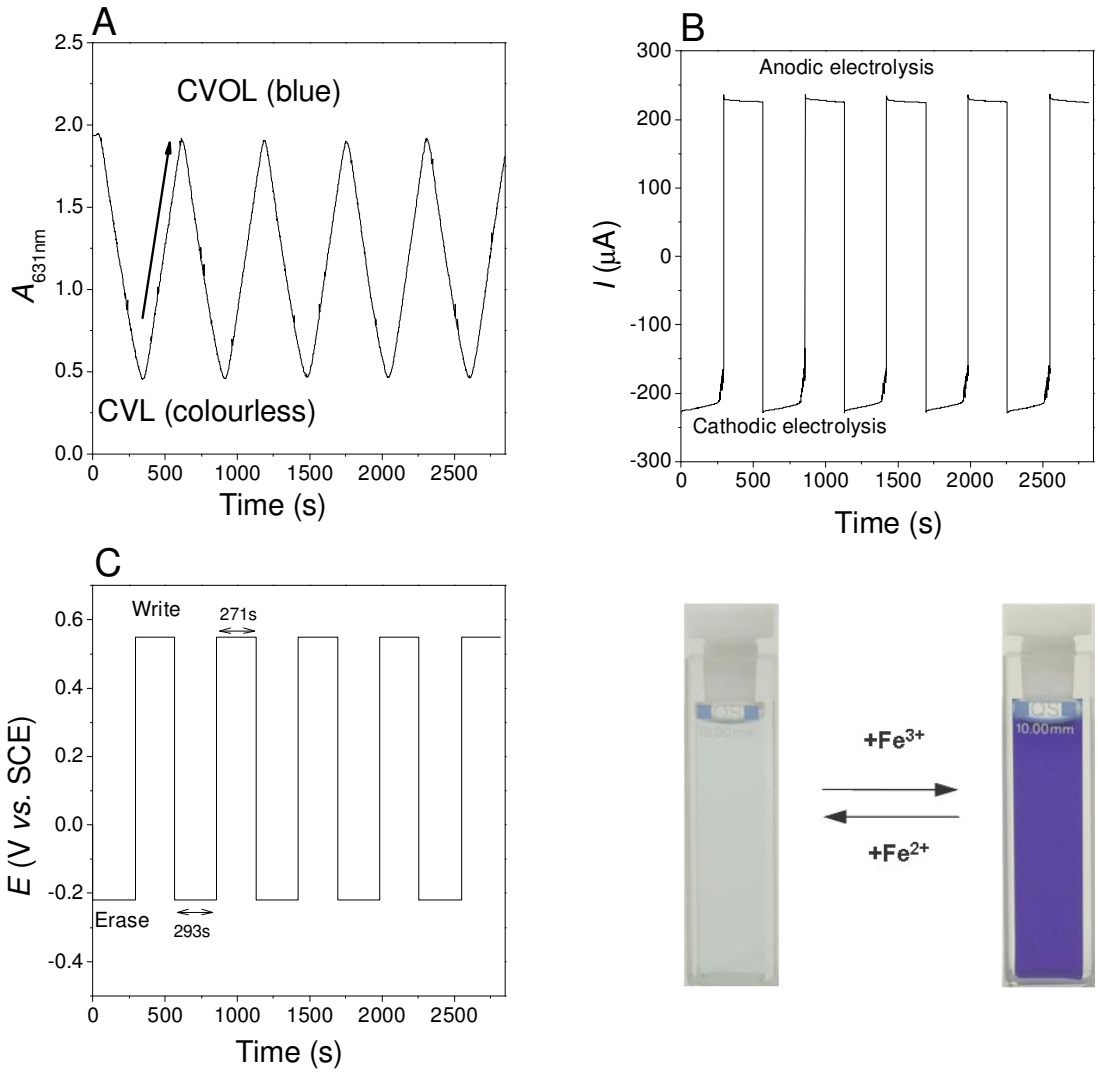

Figure 3.8 - Spectroelectrochemical data of 300 µM of CVL in the presence of 1 mM of $FeCl_3$: Chronoabsorptometry followed at the maximum absorbance (631nm) of CVOL (A); Chronoamperometry data (B); Square wave potential program (C); Picture shows the optical transitions of a mixture of 300µM of CVL and 1 mM of $FeCl_3$ between anodic electrolysis (blue colour) and cathodic electrolysis (colourless).

The process described here is not exclusive of CVL. In fact preliminary results with the Malachite Green Lactone also showed up the same phenomenon, giving different colours, promising the possibility of a fine-tuning of the desirable colour.

3.3.2 Adding light stimulus: multi-responsive system

CVL and iron ions interact as shown in Eq. 3.3. CVL solubilised in methanol is converted into the open form (CVLO) upon adding Fe(III), giving rise to an absorption spectrum (blue colour) similar to the one obtained for the parent molecule crystal violet. On the contrary,

Fe(II) is unable to open the lactone of CVL (see Fig.3.5). Taking profit from this behaviour, the mixture can be switch reversibly from blue to colourless by the action of an electrical input. The addition of a photochromic element (SPI) allows the increase from two possible optical states (colourless ↔ blue) to four (colourless ↔ blue ↔ yellow ↔ magenta, see Fig. 3.12), *i.e.*, a multistimulus system operated with electricity and light.

Interaction between SPI and iron ions

At thermal equilibrium in methanol, the SPI and the MERO are the major and minor species, respectively (Fig. 3.2 and Fig.3.9-A for χFe(III) = 0).

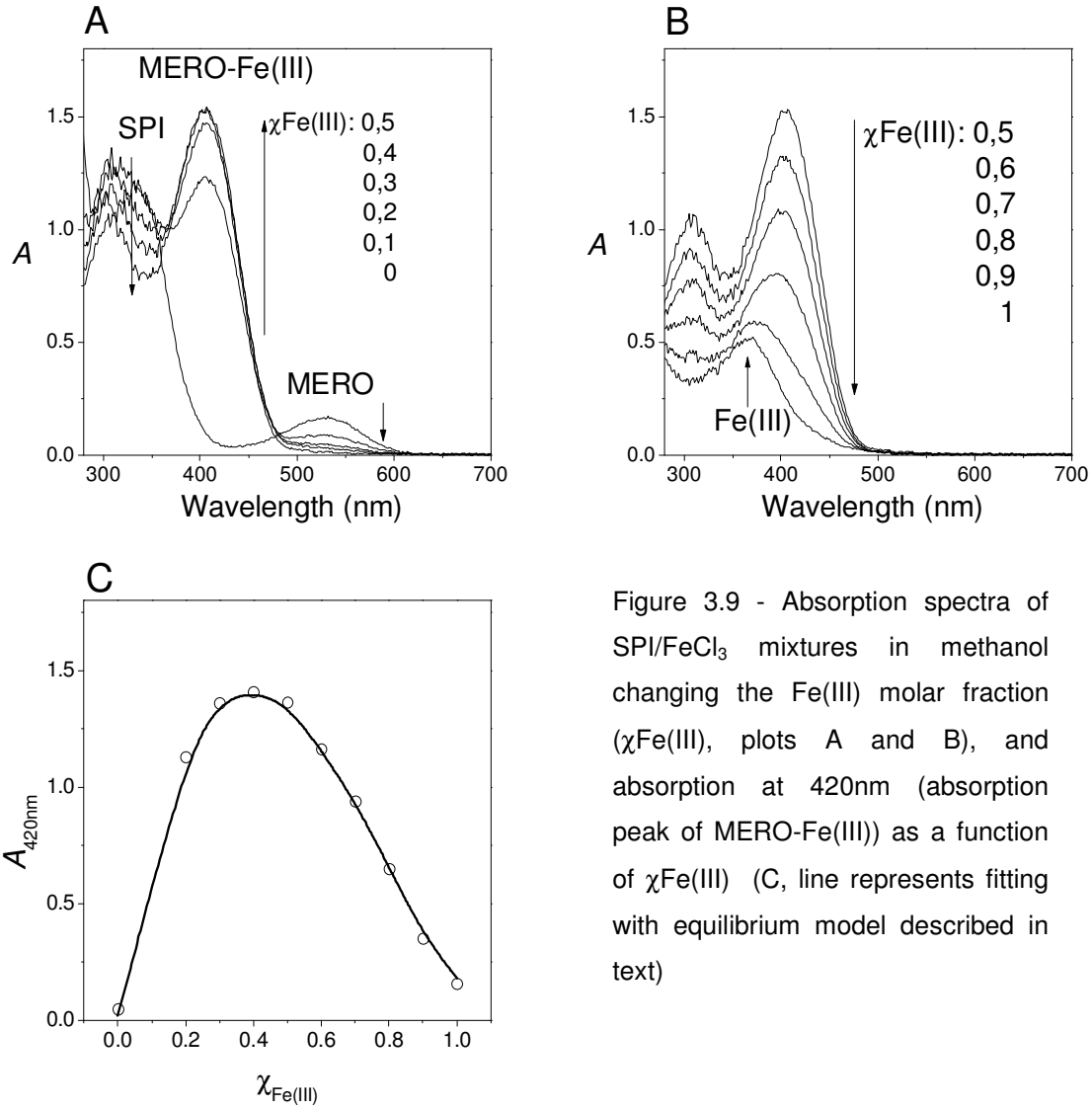

Figure 3.9 - Absorption spectra of SPI/$FeCl_3$ mixtures in methanol changing the Fe(III) molar fraction (χFe(III), plots A and B), and absorption at 420nm (absorption peak of MERO-Fe(III)) as a function of χFe(III) (C, line represents fitting with equilibrium model described in text)

The spiropyran compound used in this work exhibits the usual photochromic properties of its family, switching between colourless (SPI) and pink (MERO) by the action of UV light (Fig. 3.2, mechanism A; Eq. 3.8, Fig.3.10-left).

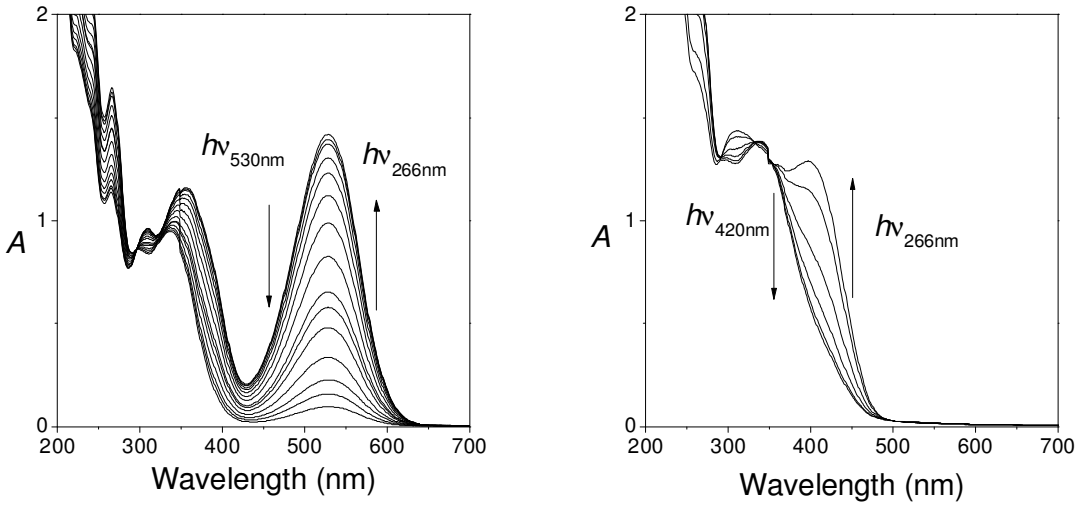

Figure 3.10 - Irradiation of the SPI (0.1 mM) in methanol solution and 0.1 M TBAP (left). The same in the presence of Fe(III) in 2-fold excess (0.2 mM) (right).

One interesting feature of this compound is its interaction with Fe(III) ions (Eq. 3.9).[29] The addition of Fe(III) to an equilibrated solution of the compound shifts the equilibrium towards a MERO-Fe(III) complex form, giving rise to a yellow adduct (420nm, see Fig.3.10-B). The adduct is also photoactive, and it can be converted to the SPI form upon irradiation at 420nm with the concomitant releasing of the metal ion (Eq. 3.9 and Fig. 3.10-right).

An analogous behaviour is also observed for the interaction of Fe(II) with the MERO species. In this case, a smaller shift to 496nm appears, but this state was not used in the present cycle because it is not fully.

MALDI-TOF-MS experiments were not conclusive about the possible complexes formed between iron ions and MERO. However, the interactions between SPI and Fe(III) were fairly described with the set of three equilibria: Eq.3.8, Eq.3.9 and Eq.3.10.

$$\mathrm{SPI} \overset{K_{spiro}}{\rightleftharpoons} \mathrm{MERO} \qquad \text{Eq. 3.8}$$

$$\mathrm{MERO + Fe(III)} \overset{K_{MERO\text{-}Fe}}{\rightleftharpoons} \mathrm{MERO - Fe(III)} \qquad \text{Eq. 3.9}$$

$$\mathrm{MERO - Fe(III) + MERO} \overset{K_{MERO2\text{-}Fe}}{\rightleftharpoons} \mathrm{MERO_2 - Fe(III)} \qquad \text{Eq. 3.10}$$

From a mass balance, the following equations may be written:

$$C_{\text{MERO}} = [\text{MERO}][1 + K_{\text{SPI}} + K_{\text{MERO-Fe}}[\text{Fe(III)}]] + 2K_{\text{MERO-Fe}}K_{\text{MERO2-Fe}}[\text{Fe}][\text{MERO}] \quad \text{Eq.3.11}$$

$$C_{\text{Fe}} = [\text{MERO}][1 + K_{\text{SPI}} + K_{\text{MERO-Fe}}[\text{Fe(III)}]] + 2K_{\text{MERO-Fe}}K_{\text{MERO2-Fe}}[\text{Fe}][\text{MERO}]^2 \quad \text{Eq.3.12}$$

Fitting this set of equations into the experimental data (results shown in Fig.3.9-C), the following solutions were obtained:

$K_{\text{SPI}} = 42.6$
$K_{\text{MERO-Fe}} = 5.9\times10^{5}\ \text{M}^{-1}$
$K_{\text{MERO2-Fe}} = 1.52\times10^{6}\ \text{M}^{-1}$

The SPI alone exhibits redox properties[30], but none of the SPI and MERO species are oxidized in the range of potentials used in this work to operate the Fe(III)/Fe(II) developer: [-0,2V; 0,8V] (*vs.* SCE).

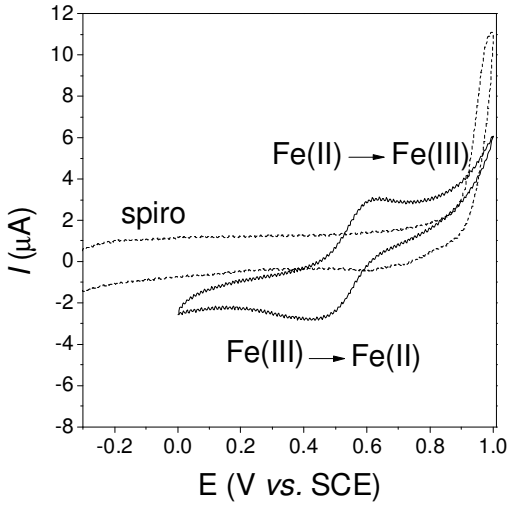

Figure 3.11 - Cyclic voltammograms of Fe(III) (full line) and SPI (dashed line) in ethanol. Electrochemical potential required to operate the Fe(III)/Fe(II) redox process does not affect the SPI species.

In Fig.3.11 the cyclic voltammetry of iron ions and SPI shows that their redox potentials are different. The reduction of both species (SPI and MERO) is possible, but at a lower potential than the one used to operate the developer. On this basis, the electrochemistry of the mixture of SPI and iron ions can be operated by changing the oxidation state of the metal

without significantly interfering with the electrochemistry of the SPI/MERO component, similar to what happens with the system iron ions and CVL.

3.3.3 Two external inputs, Three species, Four Colours

When equimolar concentrations of CVL and Fe(II) (0.035 mM) and a 25-fold excess of SPI are mixed (in a total volume of 10 ml) under visible light and electric stimulus (cathodic, –0.1V *vs.* SCE), the solution is colourless (Fig. 3.12, state **1**). Under these conditions, no coloured complexes are formed, the predominant species being the leuco CVL form, Fe(II) and SPI. Blue colour (Fig.3.12, state **2**) is reached by re-oxidation of the metal at +0.7V for 20min. The formation of Fe(III) opens the CVL form to yield the CVOL–Fe(III) complex, as shown previously in Fig. 3.5. Yellow (Fig.3.12, state **3**) is obtained upon controlled irradiation of state 2 with UV light for about 2 min. The SPI form opens to give the MERO coloured species, which competes more efficiently than CVLO for the Fe(III) ion (note that: log $K_{\text{MERO–Fe(III)}}$ = 5.8, log $K_{\text{MERO2–Fe}}$ = 6.2; log $K_{\text{CVLO–Fe(III)}}$ = 3.0 at 21°C in MeOH), decreasing substantially the blue colour and forming the yellow MERO–Fe(III) complex. When all the Fe(III) has been sequestered by the MERO species (SPI is in excess), further irradiation for about 15 min converts the remaining SPI form into the red MERO species, giving rise to state 4.(Fig.3.12, state **4**). It is worth noting that the system can reverse back from state 4 to state 3 by selective irradiation at 530nm (3 min.) of the MERO species (Eq. 3.8). In the same way, irradiation of the MERO–Fe(III) complex at 420nm (2 min) permits a change back from state 3 to state 2. In this case, the released Fe(III) (Eq. 3.9 and Eq.3.10) becomes available to open the CVL to give back the blue colour state 2 (Eq. 3.1). Finally, the system can return to state 1 by cathodic electrolysis (9 min) of Fe(III) ions to Fe(II) ions. From this point onwards, the cycle can be repeated.

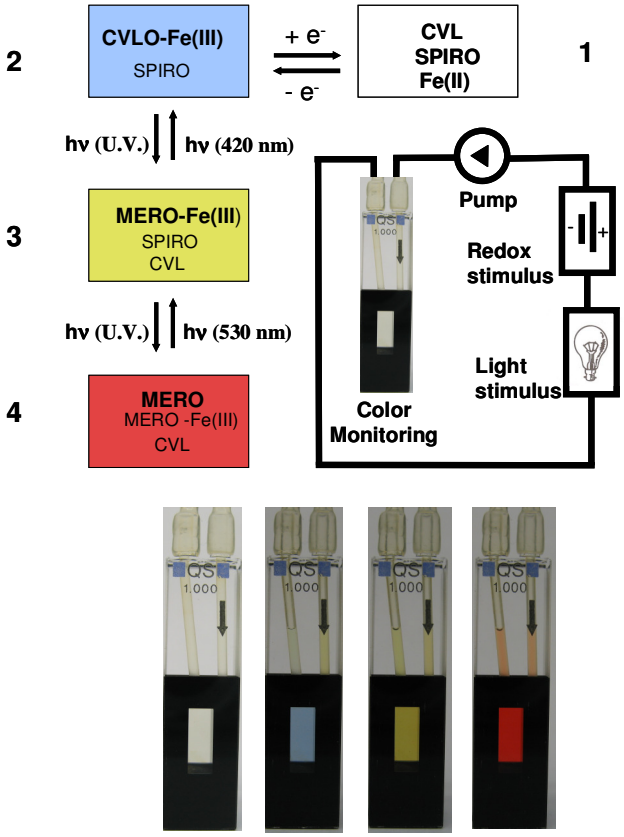

Figure 3.12 - Operation of the CMYT colour model based on the three component system: SPI (1 mM), CVL (35 µM) and Fe(III) (35 µM); methanol, 0.1 M TBAP. Transition between 1 and 2 is controlled by electricity, transitions between states 2 and 3 and states 3 and 4 are controlled by light. Pictures of the solutions corresponding to the states 1, 2, 3 and 4 from the left to the rigt.

In Fig.3.13 the spectra of the three coloured species are depicted (molar absorptivities obtained by fitting Job's Plot experiments).

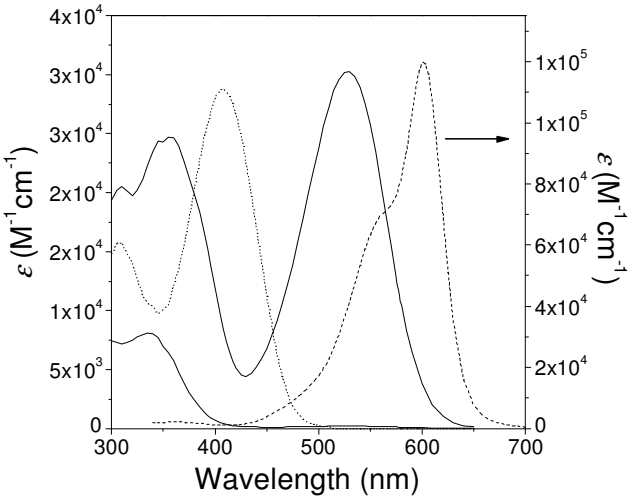

Figure 3.13 - Molar absorption spectra of the coloured species involved in the photoelectrochromic system in methanol. MERO (full line); MERO-Fe(III) (dotted line); CVOL-Fe(III) (dashed line).

3.4 Conclusions

The spectroelectrochemistry results show that the present ionochromic system is operated by electricity due to the different affinities between the CVL and the Fe(III)/Fe(II) ions. The system can be regarded as an indirect electrochromism. If the oxidation is carried out at a slightly higher potential, however, radical CVL species can appear. Indeed, anodic electrolysis carried out with 0.60V leaded to the appearance of a band with a peak at 450nm that compromised the stability of the electrochromic system. While this system does not depend strongly of the reduction potential, a fine tuning of the oxidation potential was necessary in order to ensure the electrochemical stability of CVL. Profit is also taken from the complexes of Fe(III)/Fe(II) with CVL and SPI. Redox stimuli operate the metal ion, leading to different coloured complexes with CVL (blue) and the coloured MERO (yellow) species (electro-ionochromism), while light stimuli operate the SPI component (pink). Finally a colourless state (T state) is reached when we have the following species combination: Fe(II), CVL and SPI. The present system arises within the framework of supramolecular chemistry, where the assembly of different molecules can result in properties not present in the individual components.

Although, no useful and immediate application of the present system can be envisaged (due to the operation in the liquid state), the chemical equilibria described and optical outputs obtained will set the fundamentals to develop CMYT systems into the solid state.

3.5 Bibliography

1. Muthyala, R., *Chemistry and applications of leuco dyes*. Plenum Press: New York, 1997.
2. Noack, A.; Schroder, A.; Hartmann, H., Synthesis and spectral characterization of a new class of heterocyclic analogues of Crystal Violet dyes. *Angewandte Chemie-International Edition* 2001, *40* (16), 3008-3011.
3. Nair, V.; Thomas, S.; Mathew, S. C.; Abhilash, K. G., Recent advances in the chemistry of triaryl- and triheteroarylmethanes. *Tetrahedron* 2006, *62* (29), 6731-6747.
4. White, M. A., The chemistry behind carbonless copy paper. *Journal of Chemical Education* 1998, *75* (9), 1119-1120.
5. MacLaren, D. C.; White, M. A., Dye-developer interactions in the crystal violet lactone-lauryl gallate binary system: implications for thermochromism. *Journal of Materials Chemistry* 2003, *13* (7), 1695-1700.
6. *Crystal violet lactone* [Online]. Available: http://en.wikipedia.org/wiki/Crystal_violet_lactone [Accessed April 2010].
7. Clyde, S. A. 1947. *3,3-bis-(4-dimethylamino phenyl)-6-dimethylamino phthalide*. United States of America patent application US2417897.
8. Zhu, C. F.; Wu, A. B., Studies on the synthesis and thermochromic properties of crystal violet lactone and its reversible thermochromic complexes. *Thermochimica Acta* 2005, *425* (1-2), 7-12.
9. Bamfield, P., *Chromic phenomena - the technological applications of colour chemistry*. The Royal Society of Chemistry: Cambridge, 2001.
10. Flannery, J. B., Photo- and thermochromic transients from substituted 1',3',3'-trimethylindolinobenzospiropyrans. *Journal of the American Chemical Society* 1968, *90* (21), 5660-5671.
11. Sakuragi, M.; Aoki, K.; Tamaki, T.; Ichimura, K., The role of triplet-state of nitrospiropyran in their photochromic reaction. *Bulletin of the Chemical Society of Japan* 1990, *63* (1), 74-79.
12. Pimienta, V.; Lavabre, D.; Levy, G.; Samat, A.; Guglielmetti, R.; Micheau, J. C., Kinetic analysis of photochromic systems under continuous irradiation. Application to spiropyrans. *Journal of Physical Chemistry* 1996, *100* (11), 4485-4490.
13. Chibisov, A. K.; Gorner, H., Photoprocesses in spiropyran-derived merocyanines. *Journal of Physical Chemistry A* 1997, *101* (24), 4305-4312.

14. Gorner, H., Photochemical ring opening in nitrospiropyrans: triplet pathway and the role of singlet molecular oxygen. *Chemical Physics Letters* 1998, *282* (5-6), 381-390.
15. Zhu, L. Y.; Zhu, M. Q.; Hurst, J. K.; Li, A. D. Q., Light-controlled molecular switches modulate nanocrystal fluorescence. *Journal of the American Chemical Society* 2005, *127* (25), 8968-8970.
16. Tamaki, T.; Ichimura, K., Photochromic chelating spironaphthoxazines. *Journal of the Chemical Society-Chemical Communications* 1989, (19), 1477-1479.
17. Phillips, J. P.; Mueller, A.; Przystal, F., Photochromic chelating agents. *Journal of the American Chemical Society* 1965, *87* (17), 4020.
18. Chibisov, A. K.; Gorner, H., Complexes of spiropyran-derived merocyanines with metal ions: relaxation kinetics, photochemistry and solvent effects. *Chemical Physics* 1998, *237* (3), 425-442.
19. Zhou, J. W.; Li, Y. T.; Tang, Y. W.; Song, X. Q., UV-Vis spectroscopic study of the solvatochromism and chelating reaction of a benzothiazoline merocyanine in mixed-solvents. *Journal of Solution Chemistry* 1995, *24* (9), 925-933.
20. Zhou, J. W.; Li, Y. T.; Song, X. Q., Investigation of the chelation of a photochromic spiropyran with Cu(II). *Journal of Photochemistry and Photobiology a-Chemistry* 1995, *87* (1), 37-42.
21. Raymo, F. M.; Giordani, S., Signal processing at the molecular level. *Journal of the American Chemical Society* 2001, *123* (19), 4651-4652.
22. Du, H.; Fuh, R. C. A.; Li, J. Z.; Corkan, L. A.; Lindsey, J. S., PhotochemCAD: A computer-aided design and research tool in photochemistry. *Photochemistry and Photobiology* 1998, *68* (2), 141-142.
23. Ocon, P.; Herrasti, P., Electrosynthesis and properties of N,N-dimethylaniline. *Journal of Materials Science* 1991, *26* (23), 6487-6490.
24. Malinauskas, A.; Holze, R., An in situ UV-Vis spectroelectrochemical investigation of the initial stages in the electrooxidation of selected ring- and nitrogen-alkylsubstituted anilines. *Electrochimica Acta* 1999, *44* (15), 2613-2623.
25. Karpiuk, J., Dual fluorescence from two polar excited states in one molecule. Structurally additive photophysics of crystal violet lactone. *Journal of Physical Chemistry A* 2004, *108* (51), 11183-11195.
26. Bard, A. J.; Faulkner, L. R., *Electrochemical methods - fundamentals and applications*. 2nd ed.; Wiley: New York, 2001.
27. Ugo, P.; Moretto, L. M.; Rudello, D.; Birriel, E.; Chevalet, J., Trace iron determination by cyclic and multiple square-wave voltammetry at nafion coated electrodes. Application to pore-water analysis. *Electroanalysis* 2001, *13* (8-9), 661-668.

28. Torres, L. M.; Gil, A. F.; Galicia, L.; Gonzalez, I., Understanding the difference between inner- and outer-sphere mechanisms - An electrochemical experiment. *Journal of Chemical Education* 1996, *73* (8), 808-810.
29. Wojtyk, J. T. C.; Kazmaier, P. M.; Buncel, E., Effects of metal ion complexation on the spiropyran-merocyanine interconversion: development of a thermally stable photo-switch. *Chemical Communications* 1998, (16), 1703-1704.
30. Zhi, J. F.; Baba, R.; Hashimoto, K.; Fujishima, A., Photoelectrochromic properties of a spirobenzopyran derivative. *Journal of Photochemistry and Photobiology a-Chemistry* 1995, *92* (1-2), 91-97.

Chapter 4

Electrocolorimetry of electrochromic materials on flexible ITO electrodes

4.1 Introduction

As already discussed in Chapter 1 electrochromism is one of the most promising technologies to develop low content information displays. The scientific and technological achievements in the field of transparent electronics[1,2], functional materials and printed batteries will overcome the limitations reached by conventional ones like CRT, LED and LCD displays (see Chapter 1).

In this chapter we report the deposition of an unexplored family of electrochromic coordination polymer films based on *salen*-type complexes on commercial flexible polyethylene terephthalate films coated with indium tin oxide (PET-ITO electrodes) and the deposition of the well-known electrochromic material PB for comparative purposes. Taking profit of the synthetic versatility of the *salen* ligand, which allows the change of either the metal centre (M=Ni, Cu, Pd), or the substituents in the diimine bridge and/or substituents in the aldehyde moiety[3,4,5], the following monomers were used to carry this study. Colour and CE were determined by colorimetry and tandem chronocoulometry/chronoabsorptometry techniques.

4.1.1 Electrochromic Coordination Polymers

Coordination polymers (CP) are a class of polymers that contains metal ions linked convalently by coordinated ligands into an infinite array. The final array can take the form of a 1D, 2D or 3D net.[6] Diferent properties of CP were studied such as - magnetism, porosity, non-linear optical activity, chiral networks, reactive networks, heterogeneous catalysis, chromogenics and multifuncional materials.[6] Potential applications are found for gas storage, ion and guest exchange, molecular switches, molecular data storage and optical displays.

Several redox-active CP present interesting optical transitions through oxidation (anodic coloration) and/or reduction (cathodic coloration).[7,8] Solid state electrochromic characterization must proceed *via* a chemically modified electrode. Electrochromic films can be formed on an electrode surface from solutions of either the polymer or the monomer. Methods that start with dissolved polymer include: cast or dip coating, spin coating, electrodeposition, and covalent attachment via functional groups. Starting with the monomer, one can produce films by thermal, electrochemical, plasma, or photochemical polymerization.[9]

Prussian Blue films

In 1704 Diesbach (a Berlin colourmaker) was preparing a red lake pigment based on potash and iron sulphate, when accidentaly he obtained an intense blue pigment. The contamination present in the potash used by Diesbach produced the highly valuable Prussian Blue pigment.

The three main blue pigments used in this time were the Ultramarine produced from the very expensive lapis lazuli mineral; smalt, a cobalt blue glass which presents a weak covering power; and indigo extracted from a native Indian plant very susceptible to fading.[10] Prussian Blue arrived as a winner substitute due to its great coloring power and good stability towards colour fading and soon became commercially available. Diesbach obtained with this failed synthesis not only a valuable blue pigment, which had several social and historical consequences, but he became also the first man to synthetise a coordination polymer.[6]

Prussian Blue (PB) is a polynuclear transition-metal hexacyanometallates able to form coordinating polymer. The general formula of transition-metal hexacyanometallates is $M'_m[M''(CN)_6]_n$ where M' and M'' are transition metals with different oxidation numbers and *m* and *n* are integral numbers.

Chemical synthesis of PB is performed by the mixture of $[Fe^{III}(CN)_6]^{3-}$ or $[Fe^{II}(CN)_6]^{2-}$ and Fe(II) or Fe(III), respectively. When a solution of $[Fe^{III}(CN)_6]^{3-}$ is poured into a flask containing Fe(II) solution an espectacular blue pigment is instantaneously precipitated. Addition of an excess of $[FeIII(CN)_6]^{3-}$ will capp PB nanoparticles and make them dispersible in water (100mg/ml).[11]

PB films can also be obtained by reductive electrochemical polymerization (electropolymerization) of the brown/red adduct obtained from an equimolar solution of ferric ferricyanide and Fe(III) ions (see Eq. 4.1). Potentiodinamic[12] or potentiostatic[13] techniques can be used.

$$Fe(III) + [Fe(III)(CN)_6]^{3-} \longrightarrow Fe(III)[Fe(III)(CN)_6] \qquad \text{Eq. 4.1}$$

The exact composition of PB solid is extremely preparation-sensitive. Two different crystal composition were identified; “insoluble” PB, see Eq. 4.2 and and “soluble” PB, Eq. 4.3. Although, their designation are “insoluble” and “soluble”, both forms are highly insoluble in water ($K_{ps}=10^{-40}$).[14]

$$Fe(III)(Fe(III)[Fe(II)(CN)_6])_3 \qquad \text{Eq. 4. 2}$$

$$KFe(III)[Fe(II)(CN)_6] \qquad \text{Eq. 4. 3}$$

The net charge of the PB complex is neutralized by positive counter-ions: a) Fe(III) in “insoluble” PB and K^+ in “soluble” PB. X-Ray powder diffraction for “soluble” PB indicates a face-centered cubic lattice, where Fe(II) coordinates octahedrally with the carbon atom of the cyanide ligands and Fe(III) coordinates octahedrally with the nitrogen atoms of the cyanide

ligands (see Fig.4.1).[15] On the other hand, “insoluble” PB presents a primitive cubic lattice where one quarter of the Fe(II) sites are vacant, and there are no interstitial ions. Both crystals, “insoluble” and “soluble” PB, are pure crystaline forms and the most probable situation is to obtain a polycrystaline compound due to the rapid growth of the crystals during synthesis, just like in electrochemical polymerization.[14]

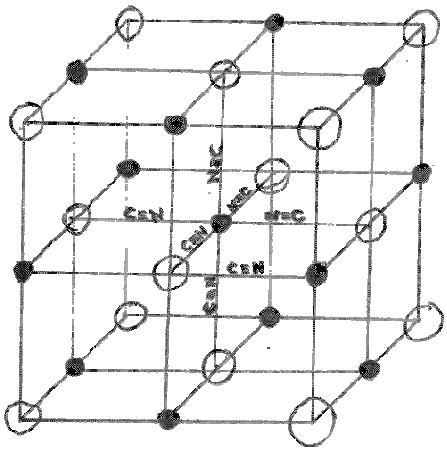

Figure 4.1 - 3D geometry of “soluble” Prussian Blue crystal; full circle: Fe(III), open circle: Fe(II)

The cathodic electropolymerization of PB results at the surface of inert electrodes results in a uniform blue film – PB modified electrode. It is still not clear which PB crystal form (“insoluble” or “soluble”) predominates in the films. Mortimer et al. observed variation of the cyclic voltammograms of the PB films between the first scan and the subsequent scans. It is also observed a variation of the electronic spectra between the as prepared PB film and after some voltammetric cycles.[16] Based on this observations it is claimed that PB is electropolymerized as “insoluble” PB and when submitted to cyclic voltammetry it is fully or partially converted to “soluble” PB.[14] Other authors believe that electropolymerized PB films are in any circunstance “insoluble” PB form.[17] Through the text we will consider that the electrochemical response of PB modified electrodes is mainly due to “soluble” PB crystals.

Electrochemistry of PB films deposited over a platinum electrode was first studied in 1978 by Neff.[18] Neff observed two redox processes of the PB modified electrode, one on the anodic side of the voltammogram and a second on the cathodic side. He also reports optical transitions of the deposited PB film. PB film is bright blue at 0.6V (*vs.* SCE), whereas on the cathodic side (0.0 V *vs.* SCE) it was colourless. At a potential of *ca.* 1V (*vs.* SCE), the film became green. He also stated that these colours can be switched back and forth rapidly by changing the potential.

$$KFe(III)[Fe(II)(CN)_6] + K^+ + e^- \rightleftharpoons K_2Fe(II)[Fe(II)(CN)_6] \quad \text{Eq. 4.4}$$

Blue Colourless

$$KFe(III)[Fe(II)(CN)_6] - K^+ - e^- \rightleftharpoons Fe(III)[Fe(III)(CN)_6] \quad \text{Eq. 4.5}$$

Blue Yellow

The electronic spectra of the PY films shows a maximum of absorbance at 425nm that corresponds to the maximum of absorbance of the complex $[Fe^{III}(CN)_6]^{3-}$ in solution.[14]

Reversible electrochemical switching between the different PB redox states (PB, PY and PW) allows to display three different optical states: blue, yellow and uncoloured (see Eq. 4.4 and 4.5).

Efficient electrochromism found in PB films has lead its application for electrochromic devices (ECD). In 1982 a seven segmented electrochromic display was reported using PB.[19] A Nafion membrane was used as the electrolyte and the PB film support, layered between two glass transparent electrodes. A more exoctic architecture was reported by Carpenter et al. They assemble an ECD using PB has the electrochromic layer and the electrolyte.[20] This was based on the fact that the highly porous PB films conduct efficiently K^+ ions. Here again a film of PB was layered between two transparent glass electrodes. More conventional structures have been studied using a complementar electrochromic material relative to PB – tungsten trioxide (WO3).[21] Since WO_3 and PB are cathodically and anodically coloured respectively, they can be used to build complementar ECD. PB and WO3 films are deposited over optically transparent electrodes (OTE's) and separated by an electrolyte layer. In such devices the colours of both electrochromic materials are summed, since while one is reduced the other is oxidized. Other complementar materials have been used as counter-electrode for PB layer, one of the well known is the poly(ethylenedioxitiophene) (PEDOT). PEDOT presents also a cathodic colouration that allows using it in a single device with PB.[22] Other aproaches have combined PB with conducting polymers.[23] Poly(aniline) was used as a co-electrochromic layer with PB enhancing the colour density of devices using WO_3 as complementar electrochromic layer.[24]

Other hexacyanometallates have been synthetised using different metals such as Ni, Co; however, their electrochromic properties are far from those found for the PB.[14]

Polymer films based on *salen*-type complexes

Late transition metal complexes (M=Ni, Cu, Pd and Pt) with *salen*-type ligands -[M(*salen*)] - can form CP by oxidative polymerization at the electrode surfaces. General structure of the *salen*-type ligand is a bis(salicylaldimine) which complexes with metal through O and N coordinating atoms (see Fig. 4.2)

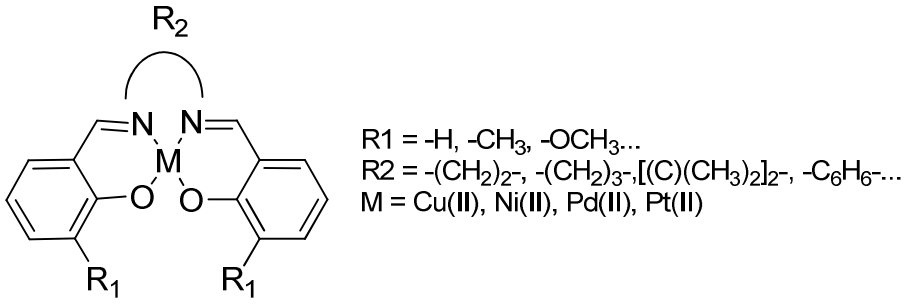

Figure 4.2 – General strucuture of *salen*-type complexes.

Electrochemistry of [M(*salen*)] compounds is strongly influenced by the donor strenght of the solvent. It has been experimentally observed that [Ni(*salen*)] is reversibly oxidized in strong donor solvents[25], however, in the presence of acetonitrile the oxidation of the Ni complex results in a polymerization reaction.

In weak or moderatly donor solvents like acetone, methylene chloride and propylene carbonate oxidation of [M(*salen*)] leds to its polymerization forming a film over the electrode surface.[25, 26] Two different mechanisms concerning the electropolymerization are proposed in the literature[25,26,27]: metal-based[26] and ligand-based.[27] During the last ten years experimental data from coulometry, FTIR and EPR of [M(*salen*)] polymers indicates that the most probable polymerization mechanism is ligand-based.[3,4,28,29]

Despite the controversy related to the oxidation center responsible for the polymerization of [M(*salen*)], it is concensual that the polymer is formed by phenyl-phenyl linkage of the ligand (see Fig. 4.3); based on the carbon-carbon coupling mechanism of phenols either in *ortho* or *para* position.[3,4,28,29]

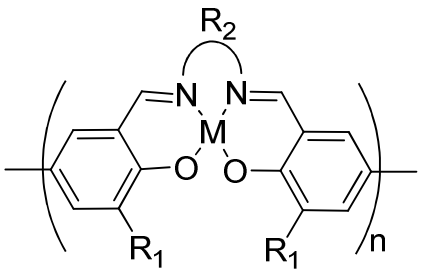

Figure 4.3 – Proposed polymer strucuture of poly[M(*salen*)][31]

Monomer solutions of [M(*salen*)] are potentiodinamically cycled within an electrochemical window where oxidative polymerization of the monomer occurs. During the first voltammetric cycles, film thickness increases linearly until it reaches a maximum. The maximum thickness is accompanied by a maximum of the peak current obtained on the cyclic voltammetry and afterwards it starts to decrease. Maximum film thickness is limited by the density of the resultant film packing over the surface of the electrode and redox-active sites accessibility. Electrochemical behaviour resulting from such films ranges from a thin-film with a charge transfer regime to a diffusional controled regime. Both situations can be obtained and are related with the number of electropolymerization cycles performed.[3]

Cyclic voltammetry of several poly[M(*salen*)] films have shown a one electron reversible reduction of the metal complex in the polymer Ni(II)/Ni(I)[27] and a second pocess at higher potencials associated with ligand based oxidation.[4] It has been found that the nature of the metal complex influences the potential at which the ligand based redox process occurs. Polymers based on Pd(II) show lower potentials for oxidation than the homologous polymers based on metals of the first transition serie, Ni(II) and Cu(II).[4]

Poly[M(*salen*)] modified electrodes were shown to exhibit polyphenylene-like properties (ligand based electrochemical responses), with the transition metal cations acting as a bridge between the phenyl rings. The proposed electronic structure of the poly[M(*salen*)] is analogous to that of a *p*-type semi-conducting organic polymer.[3, 4, 28, 29, 30, 32, 33]

Spectroelectrochemical studies on poly[M(*salen*)], M=Ni(II)[33] Cu(II)[3] and Pd(II)[4] show interesting electrochromic behaviour at the surface of the electrode. Electronic spectra of the poly[M(*salen*)] show significant changes from the reduced (undoped) to the oxidized (doped) state. General UV-Vis spectra of the poly[M(*salen*)] present several bands that are also present in the respective monomer UV-Vis spectra: d-d transition, intraligand transition and charge transfer. Polymer bands can suffer significant shift within the UV-Vis spectra compared to their monomer counterpart, due to high monomer condensation. New bands are also found within the polymer spectra when it is fully oxidized. The new electronic transition found in the polymer lay within the visible range (380-780nm). Electronic transition dependence with redox states of the poly[M(*salen*)] have been interpreted based on the polaronic model, see Fig. 4.4.

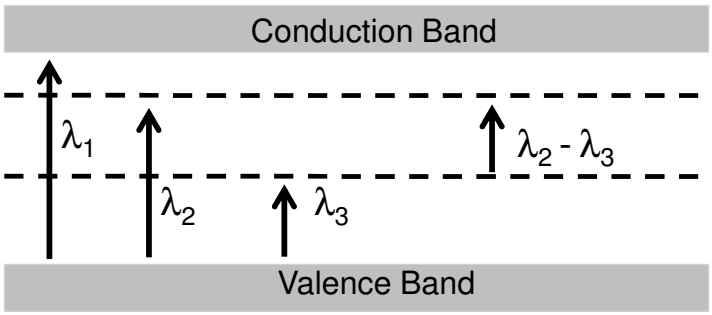

Figure 4.4 – Schematic band structure of a dopped semi-conductor. λ1: band-gap; dashed lines: charge carriers (polarons)

The oxidized state of the poly[M(*salen*)] presents a larger absorption through the visible region of the spectrum when compared to the absorption spectra of the reduced state. The dopping of the poly[M(*salen*)] with charge carriers (*p*-type semiconductor) allows three new electronic transitions (λ_2, λ_3 and λ_2-λ_3, see Fig.4.4) to occur, enhancing the absorption bands within the visible range of the spectrum. Reversible dopping/undopping state of the poly[M(*salen*)] allows to operate successfully the film as an electrochromic material.

4.1.2 Colorimetry

Colour is a very subjective and environment-dependent property, influenced by object, light source spectral properties, level of illumination, background lightness and psychological/physiological factors.[34] Colour sense results from the mental interpretation of the signals send by the optical nerves when stimulated by reflected, transmitted or emitted light from an object. The eye captures the light similarly to a photographic camera, an ingenious lens is composed by the cornea, iris, lens, aqueous and vitreous Humor and the photoreceptors (cones and rods) act as the light sensor.

The light excites the photoreceptors cells situated in the retina. A *cis-trans* photoisomerization of retinal molecule (present in the photoreceptors) triggers a cascade of electrical stimulus through a complex network of neuronal cells until the signal reaches the optical nerve. Finally, the cortex receives the information which is translated to our consciousness of colour.

Besides the biological factors, colour we perceive is also influenced by ambience factors. The most relevant ones are: the light source of illumination (illuminant), the background colour, the size of the object, the angle between the source of light and the object, and the angle between the observer and the object.

The spectral light of the illuminant will vary depending on the source; e.g. the sun, incandescent lamp, fluorescent lamp, etc…; each kind of lamp has a unique spectrum of emitted electromagnetic radiation. Background and ambience surrounding the object

influence how we perceive its colour. In Fig.4.5 the perceived blue coloured strips observed on the right of the figure and the apparently green strips on the left were printed with the same ink composition. This phenomenon reflects the influence of the colour background and the perceived colour stimulus of the object.

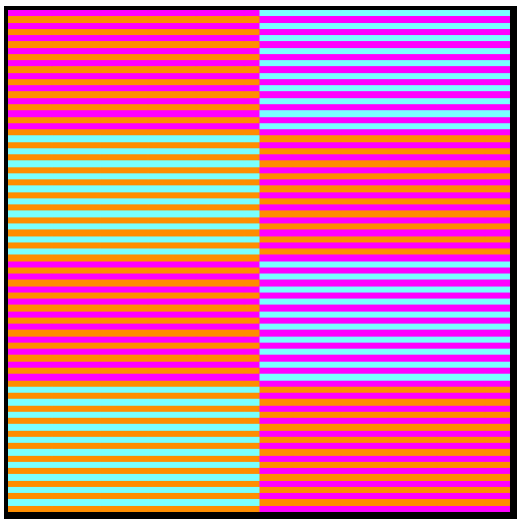

Figure 4.5 – Visual illusion due to different contrast between the object and the surrounding. At the left side of the image the green strips are actually of the same colour than the blue strips on the right.

Several authors have reported human capacity to distinguish from one hundred thousand to ten million different colours.[35] The large palette of colours we can distinguish surpass our capacity to create an objective and simple nomenclature. Since Newton studies on optics, geometric colour order systems have been proposed.[36]

With the development and accessibility of spectrophotometric techniques within the academia and industry, colour scientists were seeking to develop electronic colour measurements able to predict the human colour perception – colorimetry.

Colorimetry can be defined as a science devoted to the colour measurement/characterization, trying to obtain the most reliable colours coordinates.

Starting in 1931, much of this work has been done under the direction of the "Commission Internationale de l'Éclairage" (CIE), an international clearinghouse for colour research at universities and research laboratories – CIE colorimetry.[37]

All the models derived from CIE colorimetry are based on the CIE-*XYZ* colour-matching system. *X, Y* and *Z* are a set of virtual primary colours (related to real set of primary colours - RGB)[38] defined by the *CIE 1931* colour-matching functions - $x(\lambda)$, $y(\lambda)$ and $z(\lambda)$ respectively (see Fig.4.6).

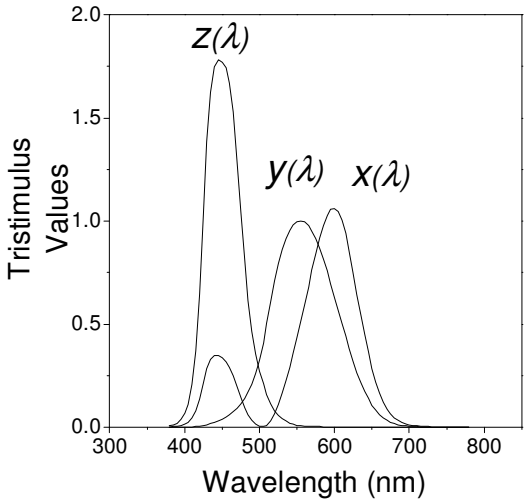

Figure 4.6 - The *CIE 1931* colour-matching functions (ploted with the data from ref.36)

The CIE 1931 colour-matching functions were obtained experimentally based on the colour-matching data obtained by W. D. Wright and J. Guild experiments.[39] These experiments consisted on the visual colour-matching of a monochromatic light with the mixture of another set of three monochromatic lights (R, G and B), experiments were performed with several standard observers and for several colours.

The CIE-XYZ tristimulus values can be calculated as described in Eqs.4.6, 4.7 and 4.8,

$$X = k \int_{380nm}^{780nm} \phi(\lambda) \cdot x(\lambda) d\lambda \qquad \text{Eq. 4.6}$$

$$Y = k \int_{380nm}^{780nm} \phi(\lambda) \cdot y(\lambda) d\lambda \qquad \text{Eq. 4.7}$$

$$Z = k \int_{380nm}^{780nm} \phi(\lambda) \cdot z(\lambda) d\lambda \qquad \text{Eq. 4.8}$$

where $\phi(\lambda)$ is the the colour stimulus function of the light seen by the observer, k is a constant and $x(\lambda)$, $y(\lambda)$ and $z(\lambda)$ are the colour-matching functions.[38]

The colour stimulus function, $\phi(\lambda)$, defines the spectral distribution of the light observed from the coloured object. Considering non-self-luminous objects (defined in colorimetry as secondary sources of light, *i.e.* objects that need to be illuminated) will reflect or transmit light coming from standard source of light (illuminant). The resultant product between the spectral

reflectance factor, *R*(λ), or the spectral transmitance factor, *T*(λ) with the relative spectral power distribution of the illuminat S(λ) defines $\phi(\lambda)$, Eqs. 4.9 and 4.10.

$$\phi_R(\lambda) = R(\lambda)S(\lambda) \qquad \text{Eq. 4.9}$$

$$\phi_T(\lambda) = T(\lambda)S(\lambda) \qquad \text{Eq. 4.10}$$

The *k* value is an experimental calibrating factor (see Eq.4.11).[38]

$$k = \frac{100}{\int_{380nm}^{780nm} S(\lambda) \cdot y(\lambda) d\lambda} \qquad \text{Eq. 4.11}$$

The colour-matching functions $x(\lambda)$, $y(\lambda)$ and $z(\lambda)$ derived from W. D. Wright and J. Guild data defined the standard CIE 1931 colorimetric observer. Later in 1964 CIE defined a new standard observer to improve colorimetric calculations when larger colour stimulus is used. A new set of colour-matching functions - $x_{10}(\lambda)$, $y_{10}(\lambda)$, $z_{10}(\lambda)$ - where calculated based on new studies on colour-match functions using a 10º angle observer. The CIE 1931 standard colorimetric observer was based on experiments where a 2º angle observer was used. The angle of vision of the observer will determine the colour perception of the object.[38]

To reproduce conveniently the colour perception, the $S(\lambda)$ is a critical factor as we can see in Eq. 4.9 and 4.10. To be able to reproduce a colour stimulus we need to use standard sources of irradiation with a determined spectral power distribution – illuminant. For this reason in 1931 the CIE defined three standard illuminants: *A*, *B* and *C*.

The *A* illuminant was designed in a manner to resemble to an average incandescent light, illuminant *B* is similar to direct sunlight and the illuminant *C* emulates an average daylight. Later in 1964 the CIE defined a new illuminant, the *D65*; in contrast to the precedent illuminants the power spectra of this illuminant is also defined in the UV region and is equal to a specific period of the day which was considered as the most representative spectral distribution of sunlight.[38]

Any colour stimulus can be fully described with the tristimulus values. But, for several reasons it is not necessary to have absolute information of the tristimulus values, and so a chromaticity *x, y, z* system can be derived from the tristimulus values *X, Y* and *Z*, see Eqs. 4.9, 4.10 and 4.11.[38]

$$x = \frac{X}{X + Y + Z}$$ Eq. 4.12

$$y = \frac{Y}{X + Y + Z}$$ Eq. 4.13

$$z = \frac{Z}{X + Y + Z}$$ Eq. 4.14

From these values a chromaticity diagram can be plotted based on *x, y* coordinates (see Fig.4.7). These values allow us to compare two colours and determine if they match. A chromaticity diagram was found to be useful in industry to control colour reproductions and to obtain useful information in a simple and direct manner.

Within the chromaticity diagram (see Fig.4.7), we can define the coordinates of the visible monochromatic light (horseshoe-shaped line) called the spectral locus. The non-spectral (purples) is within the line that connects the point of 380nm and 780nm.[40] The region enclosed by the horseshoe-shaped line and the non-spectral colour line lays the colour locus which contains all the colours. The point W within this locus is known as the white point, and its location is dependent on the light source used in either reflection or transmission experiments. The location of an object coulour on the xy diagram allows to determine the dominant wavelenght of the colour $\lambda_{d.}$ The λ_d of a colour gives the closest hue found in monochromatic light wich best describes the sample colour. Consider a colour stimulus P, the hue of that sample (see Fig.4.7) is determined by drawing a straight line through the W point and the P point to the spectral locus.The intercection of the drawn line and the spectral locus give the λ_d for the colour stimulus P. For points lying along the purple line (see point S in Fig. 4.7), a straight line containing the point and the W point, and the purple line is reflected back through the white point to the spectral locus, yielding the dominant wavelength of the complementary color ($\lambda_{c,d}$).[40]

Chromaticity diagram is not suitable to determine wether two xy coordinates colours are or are not distinguishable to a standard observer. It means that the same geometric distance between two colours in the chromaticity diagram will not represent the same apparent colour variation in all the colour locus area.[38]

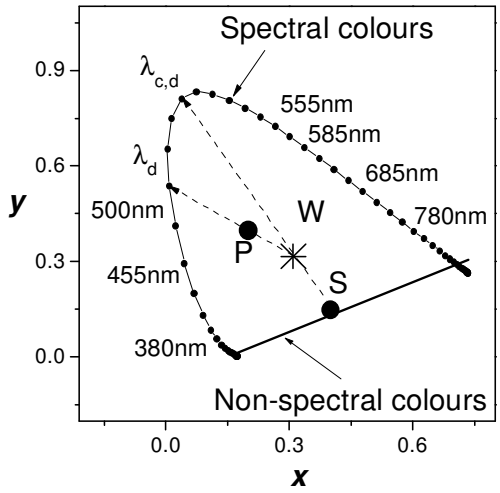

Figure 4.7 – Chromaticity diagram and colorimetric information that can be extracted from it.[40]

In order to obtain a uniform colour space, the CIE stablished in 1976 the CIE-*L*a*b** (CIELAB) colour system. The CIELAB coordinates are based on the tri-stimulus colour matching defined by the CIE-*XYZ*. A non-linear transform of the *X, Y* and *Z* values follows, resulting in opponent-type coordinates (mathematical equations can be consulted in refs. 38,41) *L**, *a** and *b**.

The parameter *L** is correlated with the luminance of the stimulus which can be understood as the lightness (larger values of *L** means lighter colour). The parameter *a** is correlated with the redness-greenness of the colour (positive *a** values points in the direction of red colour and negative values in the direction of green colour). Finally *b** parameter is correlated with yellow-blueness of the colour (positive *b** values points in the direction of yellow and negative in the direction of blue colour).[34,38]

Euclidean distances in CIELAB color space can be used to represent approximately the perceived magnitude of color differences between object color stimuli of the same size and shape, viewed in identical conditions. In Eq. 4.15 CIELAB color difference is calculated, ΔE^*_{ab}. The minimum value of ΔE^*_{ab} which represents two distinguishable colours is a matter of controversy. If the system were perfect than one unit of , ΔE^*_{ab} should represent two distinguishable colours, however, this is not true. We will consider through our text that , $\Delta E^*_{ab} > 6$ will be perceived as different colour.

$$\Delta E^*_{ab} = \sqrt{\left[(\Delta L^*)^2 + (\Delta a^*)^2 + (\Delta b^*)^2\right]} \qquad \text{Eq. 4.15}$$

4.2 Experimental details

General

Iron(III) chloride hexahydrate ($FeCl_3 \cdot 6H_2O$, Merck), potassium hexacyanoferrate (III) ($K_3[Fe(CN)_6]$, Fluka), potassium chloride (KCl, Pronalab) and tetrabutylammonium perchlorate (TBAP, Fluka) were certified p. a. grade and used without further purification. Acetonitrile (Riedel, p. a. grade) was dried following a procedure reported in literature[42]: pre-drying over CaH_2 during 2 days, followed by reflux and distillation.

The compounds 2-hydroxy-3-methylbenzaldehyde, ethylenediamine and palladium acetate were purchased from Aldrich and were used as received, except ethylenediamine, which was distilled prior to use.

Prussian blue film preparation

PB films were electrogenerated on flexible electrodes of polyethylene terephthalate films coated with indium tin oxide (PET/ITO, Aldrich with a resistivity of 60Ω/sq and a useful area between 3 and 4 cm^2 (0.9×4 cm^2)). The electrochemical polymerizations were performed in a 1 cm path quartz cuvette. A three-electrode holder was constructed to fit in the electrochemical cell. An aqueous solution of 5 mM $K_3[Fe(CN)_6]$, 5 mM $FeCl_3 \cdot 6H_2O$ and 0.2 M KCl was used as PB polymerization solution. Electropolymerization was conducted under a constant applied voltage of 0.55 V (*vs.* Ag/AgCl), during 300 s. After deposition, the electrode was gently rinsed with distilled water.

Salen-type complexes of Cu(II), Ni(II) and Pd(II) film preparation

The complexes *N,N'*-2,3-dimethylbutane-2,3-dyil-bis-(3-methoxysalicylideneiminate) metal(II), M=Ni or Cu ([Ni(3-MeOsaltMe)] or [Cu(3-MeOsaltMe)]) were prepared as described elsewhere.[32] The complex *N,N'*-bis(3-methylsalicylideneiminate)Pd(II), [Pd(3-Me*salen*)], was synthesized by refluxing an acetonitrile solution containing stoichiometric amounts of palladium(II) acetate and the ligand H_2(3-Me*salen*), prepared previously by standard procedures[43]; the complex was recrystalized from dichloromethane.

[M(*salen*)], M=Ni, Cu and Pd complexes were electropolymerized by potential cycling at a scan rate 0.02 V/s, using a flexible PET/ITO (Aldrich with a resistivity of 60 Ω/sq and useful area between 3 and 4 cm^2 (0.9×4 cm^2)) electrodes as working electrode in a 1 cm path quartz cuvette. The potential range used in film polymerization depends on the metal complex: for the nickel complex was 0.0–1.3 V, for the copper complex was −0.15 to 1.4 V and for the Pd complex was −0.1 to 1.2 V (*vs.* Ag/AgCl).

Electrochemical measurements

Electrochemical polymerization and choronocoulometry/chronoabsorptometry were performed with a conventional three-electrode cell using a computer-controlled computerized potentiostat-galvanostat model 20 Autolab, from Eco-Chemie Inc. The collection of data was controlled by the GPES Version 4.9 Eco Chemie B.V. Software (Utrecht, The Netherlands). The working electrodes were constructed as described above, auxiliary electrode was a platinum wire and the reference electrode was an Ag/AgCl (BAS). Electrochemical measurements of PB films were performed in a 0.2 M KCl aqueous solution and for *salen*-type complexes were performed in 0.1 M TBAP salt in freshly dried/distilled acetonitrile.

Spectroscopic/colorimetric measurements

UV/Vis absorbance spectra and chronoabsorptometry were recorded in a Shimadzu UV2501-PC spectrophotometer at 1nm resolution. Colorimetric "titrations" were performed in a total transmittance geometry configuration (CIE illuminating/viewing standards)[34] using an integrating sphere installed in the sample compartment of the spectrophotometer. The illuminant used is the C. Transmittance spectra were recorded after each potential had been applied for 50–60 s. Colorimetric data were calculated with the UVPC optional colour analysis software v2.72 version from Shimadzu Scientific Instruments Inc. All spectroscopic measurements of the electrochromic films were done *in situ* in a 1 cm path quartz cuvette with a 1 cm^2 square top aperture and a designed adapter to allow potentiostatic.

4.3 Results and Discussion

4.3.1 Prussian blue

The spectroelectrochemical and colorimetric study of the PB films deposited over ITO coated glass were by Mortimer and Reynolds.[44] However, spectroelectrochemical studies of PB deposited on transparent flexible electrodes were never reported. In Fig.4.8 shows the choronocoulometry/chronoabsorptometry study for the PB/PW transition for films deposited on flexible PET/ITO electrodes.

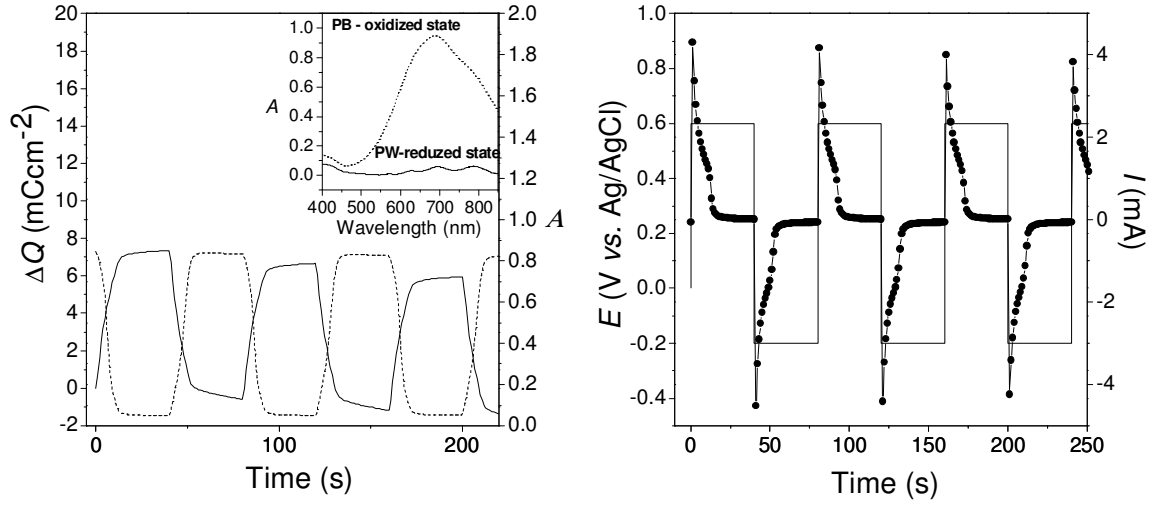

Figure 4.8 - *In situ* cronocoulometry/cronoabsorptometry data for PB film deposited on PET/ITO in 0.2 M KCl aqueous solution as supporting electrolyte. Left: chronoabsorptometry recorded at 690nm (dashed line), CE (full line). Right: chronoamperometry (full line+full circle), square-wave switching between –0.2 and 0.6V (*vs.* Ag/AgCl), step duration of 40s (full line).

The chronocoulometry/chronoabsorptometry shows for the same sample a larger amount of charge *per* unit area ($\Delta Q'$) for the reduction (PB→PW) process than for the oxidation (PW→PB) over time per unit electrode area). Differences in the CE values for the reduction and the oxidation process are also found (see Fig.4.9).

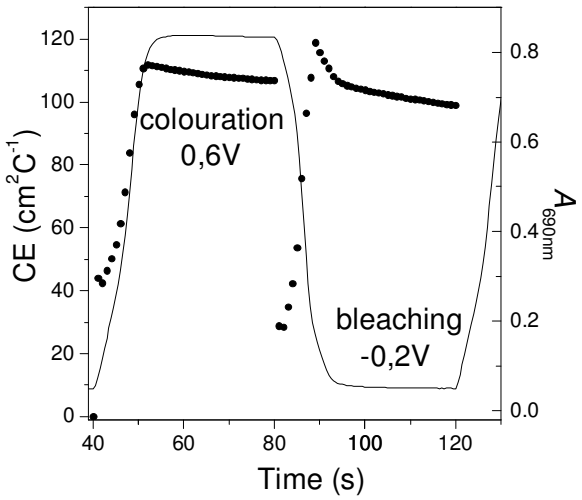

Figure 4.9 - CE (dots) calculated from *in situ* chronocoulometry/chronoabsorptometry (see Fig.4.8). Chronoabsorptometry cycles recorded at 690nm (full line).

The PB films deposited on flexible PET/ITO electrodes show a relative stability over a range of at least five write-erase cycles (9 steps of 40 s each one, the last cycle have only one step, see Table 4.1). The evolution of CE along one step potential, shown in Fig.4.9 increases until its maximum; then reaches a plateau. In Table 4.1, CE values along the *in situ* choronocoulometry/chronoabsorptometry experiment at a specific percentage of full switch (%Full switch, see section 1.2.1 – ECD parameters) are reported.

Table 4.1 - Collected data from *in situ* choronocoulometry/chronoabsorptometry experiments of the PB films deposited on PET/ITO in 0.2 M KCl aqueous solution

Cycle nº	Redox transition*	% Full switch**	Δ%T	ΔA	ΔQ' (mC/cm^2)	CE (cm^2/C)	Time (s)
1	PW/PB	85	63.76	0.543	5.65	96	9
		96	71.8	0.707	6.38	111	11
		98	73.38	0.748	6.69	112	12
		99	74.19	0.770	6.9	112	13
	PB/PW	86	64.16	0.729	6.45	113	11
		95	71.19	0.767	7.08	108	13
		98	73.47	0.778	7.41	105	17
		99	74.16	0.781	7.60	103	23
2	PW/PB	99	74.32	0.780	7.09	110	20
	PB/PW	98	73.19	0.770	7.45	103	20
3	PW/PB	99	73.74	0.770	6.99	110	20
	PB/PW	97	72.59	0.761	7.32	104	20
4	PW/PB	98	73.13	0.760	6.86	111	20
	PB/PW	96	71.79	0.751	7.19	104	20
5	PW/PB	96	72.19	0.749	6.71	112	20

*Applied potentials: PW/PB = 0.6 V (*vs.* Ag/AgCl) and PB/PW = –0.2 V (*vs.* Ag/AgCl).

**% full switch calculated with T_{max} (89.35%) and T_{min} (14.49%) obtained during the first step of the first cycle. T_{max} and T_{min} were determined with the A_{max} and A_{min} values obtained by chronoabsorptometry, respectively.

While the colour efficiency maintains approximately the same value, the calculated percentage of full switch for both PW/PB and PB/PW at the same time step (20 s) decreases with the number of cycles. Different CE and switching times are observed for the PB/PW and PW/PB process, performed during the *in situ* chronocoulometry/chronoabsorptometry experiment (see Fig.4.8 and Fig.4.9). Comparing results from Table 4.1 with those described by Mortimer and Reynolds[44], concerning PB deposited on glass/ITO electrodes (non-flexible electrodes), several differences are found. The CE obtained in flexible electrodes is 25% inferior and the time expended to obtain the same % of full switching almost doubles when compared to PB deposited over a glass ITO electrode. Moreover, the Δ%T obtained for the same % of full switching are 11–13% greater, indicating a large amount of PB deposited. This could explain the lower rate of colour variation and the lower CE values.

The CIELAB coordinates observed for the PB and PW films deposited over flexible PET/ITO are comparable with those obtained with PB deposited over glass ITO-coated electrodes,

however, the ΔE^*_{ab} is greater than 6 for the coloured state and visual differences should be espected between the two films (see Table 4.2).

Table 4.2 – Colorimetric coordinates collected for PB and PW films deposited over the same period of time (300s at 0.5V *vs.* Ag/AgCl) on PET/ITO electrodes (a) and glass ITO coated electrodes (b).

Film redox state	*L**	*a**	*b**	*x*	*y*	ΔE^*_{ab}
PB(a)	64	-18	-36	0.203	0.250	12***
PB(b)**	73	-26	-33	0.255	0.340	
PW(a)	100	0	6	0.323	0.341	6****
PW(b)**	97	0	1	0.359	0.386	

**data from ref.47

***CIELAB value difference between PB(a) and PB(b)

****CIELAB value difference between PW(a) and PW(b)

In Fig. 4.10 the evolution of *xy* coordinates for the PB/PW optical transition is shown for the films deposited over PET-ITO electrodes with different deposition time. The PB state is the most influenced by the film thickness, while the perceived transparency for the PW state is identical for all the films. In contrast to other electrochromic materials such as PEDOT, where the film thickness results in a loss of the transparency of the bleached state.

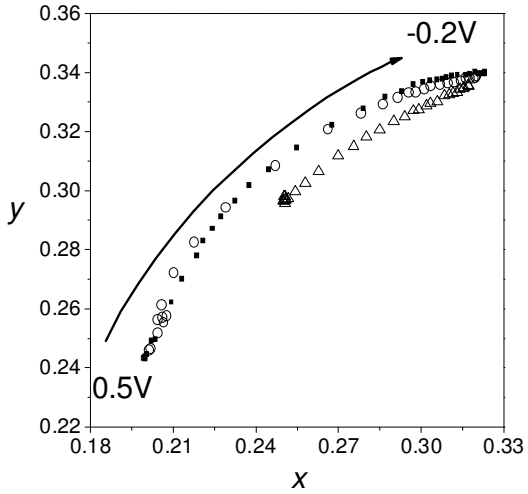

Figure 4.10 - Chromaticity coordinates *xy* obtained by in situ chronocoulomery/chronoabsorptometry for PB films deposited over PET/ITO. Films with 300s (open square), 600s (open circles) and 150s (open triangles) deposition time. Note: all the potentials were measured using Ag/AgCl reference.

4.3.2 *Salen*-type complexes of Cu(II), Ni(II) and Pd(II)

Previously, optical variations for the [Ni(3-MeOsaltMe)] and [Cu(3-MeOsaltMe)] at their different redox states (oxidized state - coloured and reduced state - bleached) were reported.[29] A comparative study with the different metal complexes: [Ni(3-MeOsaltMe)] (**Ni**), [Cu(3-MeOsaltMe)] (**Cu**) and [Pd(3-Me*salen*)] (**Pd**) (see Fig. 4.11) are presented in this chapter.

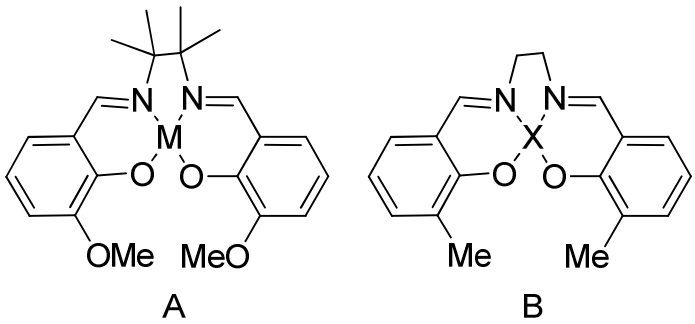

Figure 4.11 - *Salen*-type complexes of Cu(II), Ni(II) and Pd(II): (A) [M(3-MeOsaltMe)], M=Ni or Cu and (B) [X(3-Me*salen*)], X=Pd.

The polymers of the **Ni**, **Cu** and **Pd** complexes were obtained by potential cycling with increasing number of cycles (2–10). In Fig. 4.12, their full visible absorbance spectra in the coloured (oxidized, dopped) and bleached (reduced, neutral) states recorded under potentiostatic control are depicted.

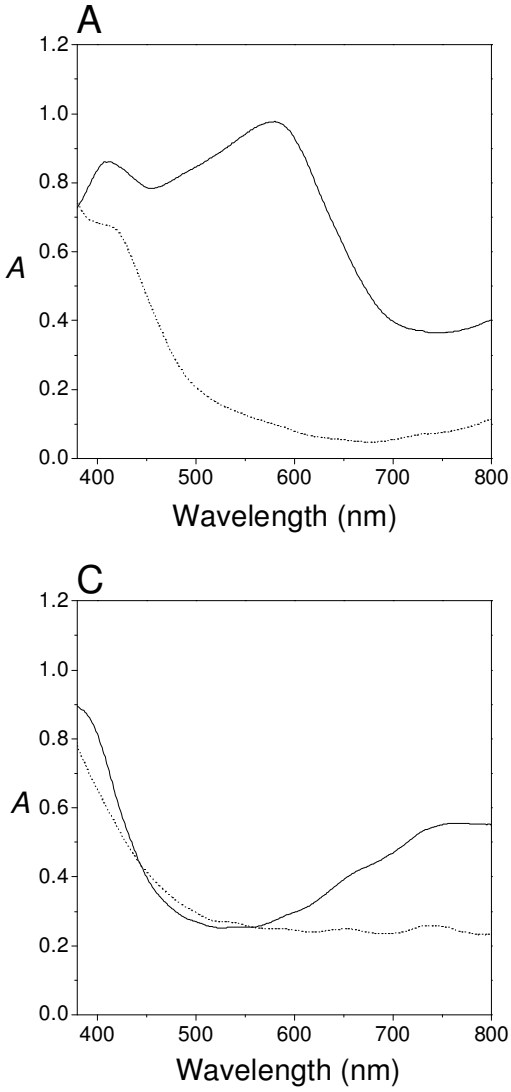

Figure 4.12 - Absorbance spectra recorded *in situ* for the different *salen*-based metal electrochromic films deposited on PET/ITO electrode in acetonitrile containing 0.1 M TBAP as supporting electrolyte. (A) **Ni**, 4 deposition cycles; full line: oxidized state 1.3 V; dashed line: reduced state –0.1 V. (B) **Cu**, 2 deposition cycles; full line: oxidized state 1.4 V; dashed line: reduced state –0.15 V. (C) **Pd**, 2 deposition cycles; full line: oxidized state 1.3 V; dashed line: reduced state 0 V. Note: all the potentials were measured using Ag/AgCl reference electrode.

Coloration efficiency

Using the same methods described for the PB films, the CE values were calculated for the **Ni**, **Cu** and **Pd** modified electrodes with two electropolymerization cycles. In Figs.4.13, 4.14 and 4.15 spectroelectrochemistry data of the cycling between the oxidized and reduzed states for **Pd, Cu** and **Ni** modified electrode is shown.

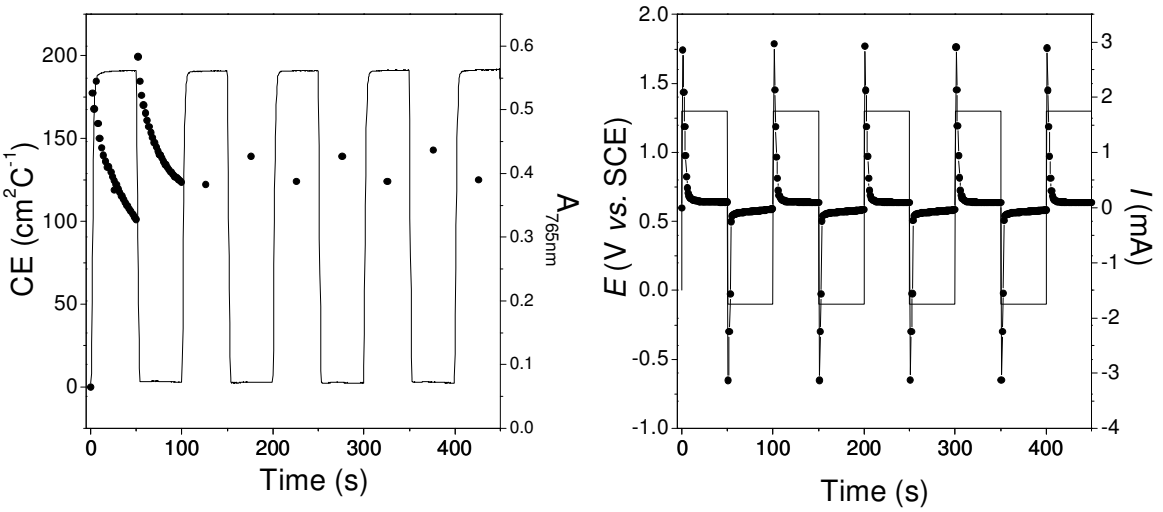

Figure 4.13 - *In situ* cronocoulometry/cronoabsorptometry data for **Pd** film deposited on PET/ITO in acetonitrile 0.1 M TBAP as supporting electrolyte. Left: chronoabsorptometry recorded at 765nm (full line), CE (dots). Right: chronoamperometry (full line+full circle), square-wave switching between –0.1 and 1.3V (*vs.* Ag/AgCl), step duration of 50s (full line).

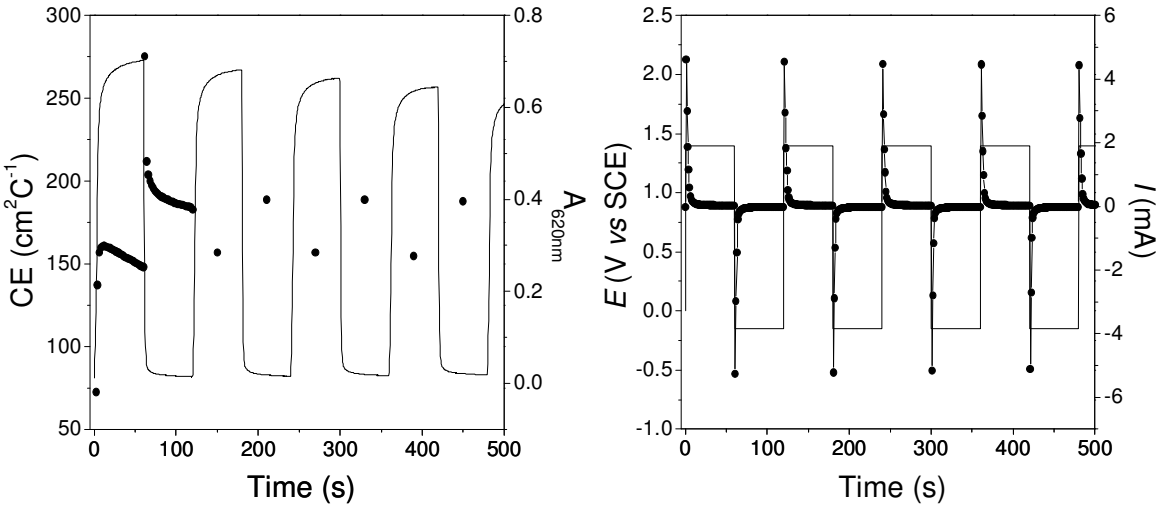

Figure 4.14 - *In situ* cronocoulometry/cronoabsorptometry data for **Cu** film deposited on PET/ITO in acetonitrile 0.1 M TBAP as supporting electrolyte. Left: chronoabsorptometry recorded at 620nm (full line), CE (dots). Right: chronoamperometry (full line+full circle), square-wave switching between –0.15 and 1.4V (*vs.* Ag/AgCl), step duration of 60s (full line).

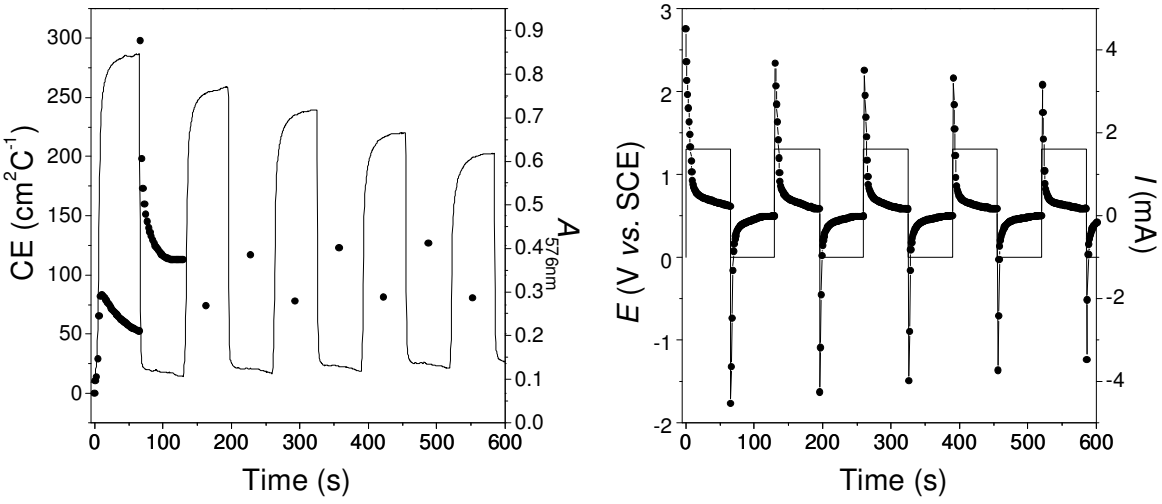

Figure 4.15 – *In situ* cronocoulometry/cronoabsorptometry data for **Ni** film deposited on PET/ITO in acetonitrile 0.1 M TBAP as supporting electrolyte. Left: chronoabsorptometry recorded at 576nm (full line), CE (dots). Right: chronoamperometry (full line+full circle), square-wave switching between -0.1 and 1.3V (*vs.* Ag/AgCl), step duration of 65s (full line).

In Fig. 4.13-left CE data shows a maximum immediately after the potential pulse and decreases all along the pulse period for both the oxidation process (anodic coloration) and the reduction process (cathodic bleaching). The values of CE calculated at half height of the

pulse of each step are constant relatively to the values obtained in the first cycle. This behaviour is followed for all the *salen*-type complexes tested (See Figs. 4.14 and 4.15).
Table 4.3 summarizes the data obtained from the cronocoulometry/cronoabsorptometry results for the first cycle of the three coordination polymer tested.

Table 4.3 - Collected data from choronocoulometry/chronoabsorptometry experiments for metal *salen*-type films, after one cycle

Complex	Redox transition	% Full switch	Δ%*T*	Δ*A*	Δ*Q'* (mC/cm^2)	CE (cm^2/C)	Switch time (s)
Pd	Coloration	66	38.24	0.260	1.46	177	2
		93	53.69	0.434	2.59	168	4
		98	56.64	0.477	2.59	184	6
	Bleaching	51	29.25	0.315	1.58	199	2
		99	56.89	0.488	2.64	185	4
Cu	Coloration	92	71.06	0.571	3.63	157	6
		96	74.09	0.624	3.88	161	10
		98	75.75	0.657	4.10	160	18
	Bleaching	93	71.74	0.664	3.13	212	4
		95	73.46	0.672	3.29	204	6
		98	75.85	0.683	3.58	191	22
Ni	Coloration	90	60.01	0.591	7.21	82	9
		94	62.56	0.646	7.77	83	11
		98	65.09	0.711	9.27	77	19
	Bleaching	90	60.16	0.718	4.14	173	6
		95	63.09	0.735	6.5	113	52
		96	63.93	0.739	6.55	113	65

Colorimetric analysis

Table 4.4 reports the CIELAB coordinates corresponding to tandem cronocoulometry/cronoabsorptometry experiments for each metal *salen*-type complex.

Table 4.4 - *In situ* cronocoulometry/cronoabsorptometry of the *salen*-type metal complexes deposited on PET/ITO flexible electrode in acetonitrile 0.1 M TBAP.

E (V *vs.* Ag/AgCl)	Pd			Cu			Ni		
	*L**	*a**	*b**	*L**	*a**	*b**	*L**	*a**	*b**
1.4	–	–	–	35	10	–18	–	–	–
1.3	60	-24	16	–	–	–	50	9	-10
1.2	67	-29	24	51	11	1	51	8	-8
1.15	73	-33	33	52	10	3	52	8	-7
1	75	-33	37	61	7	12	55	6	-5
0.9	78	-33	42	73	0	22	62	-1	7
0.85	79	-33	44	74	-1	22	75	-6	21
0.8	80	-33	45	76	-2	23	84	-9	31
0.75	81	-32	46	77	-3	22	86	-9	34
0.65	83	-30	47	80	-5	22	89	-9	36
0.55	85	-27	48	83	-6	23	91	-9	36
0.45	87	-23	48	85	-6	23	92	-8	35
0.4	89	-21	48	85	-5	23	93	-8	34
0.30	92	-17	48	85	-5	23	93	-7	34
0.25	94	-14	48	–	–	–	–	–	–
0.20	96	-13	46	86	-5	23	–	–	–
0.15	98	-12	44	–	–	–	94	-7	33
0	99	-12	41	86	-5	23	94	-7	33
–0.1	100	-12	41	–	–	–	–	–	–
–0.15	–	–	–	87	-4	23	–	–	–

Films deposited with 5 cycles.

Based on the colorimetric data of Table 4.4 a chromaticity diagram for each polymer with different number of cycles of deposition can be drawn (see Fig.4.16).

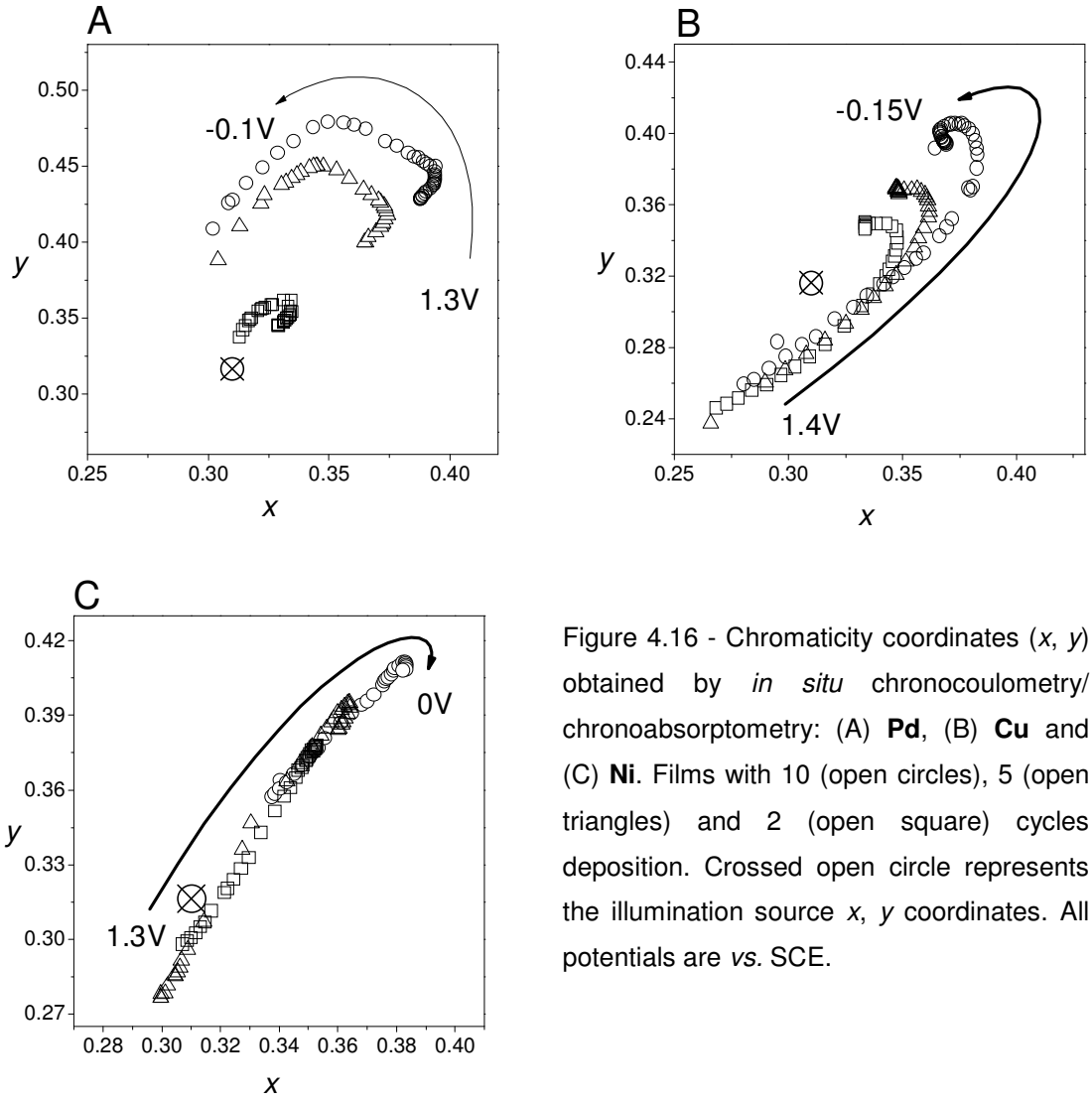

Figure 4.16 - Chromaticity coordinates (*x*, *y*) obtained by *in situ* chronocoulometry/ chronoabsorptometry: (A) **Pd**, (B) **Cu** and (C) **Ni**. Films with 10 (open circles), 5 (open triangles) and 2 (open square) cycles deposition. Crossed open circle represents the illumination source *x*, *y* coordinates. All potentials are *vs.* SCE.

The evolution of *xy* coordinates along the potential shows a very peculiar curvature when compared with those obtained with PB both in PET/ITO (see Fig. 4.10) and glass/ITO electrodes.[44] The colour changes spread over a larger *xy* region, indicating more saturated colour on alternating between undoped and doped state. The modified electrodes with 10 deposition cycles have larger *xy* values than those obtained with 5 and 2 deposition cycles, showing a more saturated colour approximating the spectral locus coordinates. From the plot in Fig. 4.16 and the spectrum locus it is possible to calculate the λ_d that correlates with the visual aspects of hue and chroma of perceived colour.[34] The λ_d calculated for the electrodes with 10 deposition cycles are presented in Table 4.5.

Table 4.5 - Dominant wavelength (λ_d) for the electrochromic inorganic polymers films upon 10 deposition cycles on PET/ITO in 0.1 M TBAP in acetonitrile.

Complex	Redox state	λ_d (nm)	Colour description
Pd	Ox	545	Green
	Red	570–575	Yellow
Cu	Ox	455–460	Violet
	Red	570–575	Yellow
Ni	Ox	560[a]	Violet
	Red	570–575	Yellow

[a] Value refers to complementary-dominant wavelength (λ_c).

The Cu and Ni electrochromic films present the larger variation of λ_d among the three samples. The coloured state of the nickel film presents a non-spectral colour closest to the mauve colour, curiously the first industrial artificial dye (by William Henry Perkin in 1856).
The variation of relative luminance (*L**) at electrochemically controlled redox applied potential is presented in Fig. 4.17. The luminance values show intervals of a great variation over a narrow potential range corresponding to pseudo potential of reduction of the inorganic polymer. Working in transmittance, the CIELAB coordinate *L** stands for perceived transparency, indicating greater levels of transparency for the Cu complex films.

The new family of electrochromic inorganic polymers shows good values of CE in comparission to other inorganic materials like WO_3 (40 and 50 cm^2/C)[45] or IrO_2 (15–18 cm^2/C)[45] and PB. Compared with organic conducting polymers, which have shown the highest CE results[45], the *salen*-type metal complexes inorganic polymer films studied here, lay between the performance of PEDOT and PProDOT.[45]

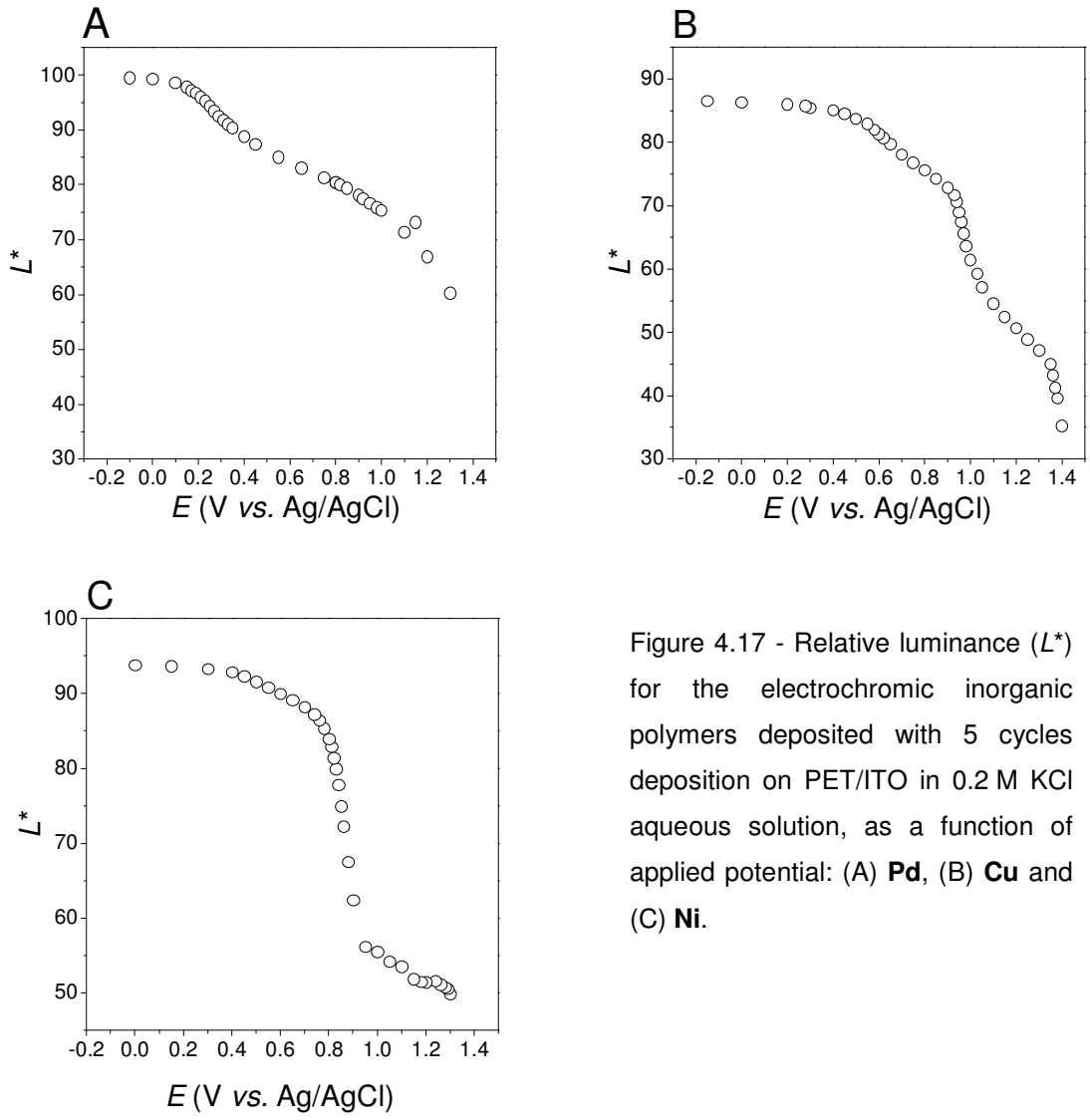

Figure 4.17 - Relative luminance (*L**) for the electrochromic inorganic polymers deposited with 5 cycles deposition on PET/ITO in 0.2 M KCl aqueous solution, as a function of applied potential: (A) **Pd**, (B) **Cu** and (C) **Ni**.

4.4 Conclusion

PB films were successfully deposited over flexible electrodes. The film stability and the performance are, however, inferior relatively to those deposited over glass ITO-coated electrodes.[44] *Salen*-type metal complex polymers were also successfully deposited as films over flexible PET/ITO electrodes and fully characterized. CE results can be compared with those for conducting organic polymers. Colorimetry of the electrochromic *salen*-type complexes revealed colour states between yellow, green and purple as dominant chroma.

The chronocoulometry/chronoabsorptometry study of electrochromic materials deposited over flexible electrodes permits the evaluation of their potentialities for special purposes like flexible displays. To construct a wide electrochromic material database, the information about colour and CE characteristics conserning the electrochromic materials must be basic and uniform. Such database could predict colour gamut of combinations of different electrochromic materials within electrochromic displays.

4.5 Bibliography

1. Minami, T., Transparent conducting oxide semiconductors for transparent electrodes. *Semiconductor Science and Technology* 2005, *20* (4), S35-S44.
2. Fortunato, E.; Barquinha, P.; Pimentel, A.; Goncalves, A.; Marques, A.; Pereira, L.; Martins, R., Recent advances in ZnO transparent thin film transistors. *Thin Solid Films* 2005, *487* (1-2), 205-211.
3. Martins, M.; Boas, M. V.; de Castro, B.; Hillman, A. R.; Freire, C., Spectroelectrochemical characterisation of copper *salen*-based polymer-modified electrodes. *Electrochimica Acta* 2005, *51* (2), 304-314.
4. Fonseca, J.; Tedim, J.; Biernacki, K.; Magalhães, A. L.; Gurman, S. J.; Freire, C.; Hillman, A. R., Structural and electrochemical characterisation of [Pd(*salen*)]-type conducting polymer films. *Electrochim. Acta* 2010.
5. Tedim, J.; Goncalves, F.; Pereira, M. F. R.; Figueiredo, J. L.; Moura, C.; Freire, C.; Hillman, A. R., Preparation and characterization of poly Ni(*salen*)(crown receptor) /multi-walled carbon nanotube composite films. *Electrochimica Acta* 2008, *53* (23), 6722-6731.
6. Batten, S. R.; Neville, S. M.; Turner, D. R., Coordination polymers design, analysis and application. The Royal Society of Chemistry: Cambridge, 2009.
7. Mortimer, R. J.; Dyer, A. L.; Reynolds, J. R., Electrochromic organic and polymeric materials for display applications. *Displays* 2006, *27* (1), 2-18.
8. Higuchi, M.; Akasaka, Y.; Ikeda, T.; Hayashi, A.; Kurth, D. G., Electrochromic Solid-State Devices Using Organic-Metallic Hybrid Polymers. *Journal of Inorganic and Organometallic Polymers and Materials* 2009, *19* (1), 74-78.
9. Bard, A. J.; Faulkner, L. R., *Electrochemical methods - fundamentals and applications*. 2nd ed.; Wiley: New York, 2001.
10. Ware, M., Cyanotype. In *The history, science and art of photographic printing in Prussian Blue*, Science Museum: London, 1999; pp 21-37.
11. Gotoh, A.; Uchida, H.; Ishizaki, M.; Satoh, T.; Kaga, S.; Okamoto, S.; Ohta, M.; Sakamoto, M.; Kawamoto, T.; Tanaka, H.; Tokumoto, M.; Hara, S.; Shiozaki, H.; Yamada, M.; Miyake, M.; Kurihara, M., Simple synthesis of three primary colour nanoparticle inks of Prussian Blue and its analogues. *Nanotechnology* 2007, *18* (34), 6.
12. Goncalves, R. M. C.; Kellawi, H.; Rosseinsky, D. R., Electron-transfer processes and electrodeposition involving the iron hexacyanoferrates studies voltammetrically. *Journal of the Chemical Society-Dalton Transactions* 1983, (5), 991-994.

13. Garcia-Jareno, J. J.; Benito, D.; Navarro-Laboulais, J.; Vicente, F., Electrochemical behavior of electrodeposited Prussian Blue films on ITO electrodes - An attractive laboratory experience. *Journal of Chemical Education* 1998, *75* (7), 881-884.
14. Monk, P. M. S.; Mortimer, R. J.; Rosseinsky, D. R., Electrochromism and electrochromic devices. Cambridge University Press: Cambridge, 2007.
15. Itaya, K.; Uchida, I.; Neff, V. D., Electrochemistry of polynuclear transition-metal cyanides - Prussian Blue and its analogs. *Accounts of Chemical Research* 1986, *19* (6), 162-168.
16. Mortimer, R. J.; Rosseinsky, D. R., Iron hexacyanoferrate films - spectroelectrochemical distinction and electrodeposition sequence of soluble (K^+-containing) and insoluble (K^+-free) Prussian Blue, and composition changes in polyelectrochromic switching. *Journal of the Chemical Society-Dalton Transactions* 1984, (9), 2059-2061.
17. Itaya, K.; Uchida, I., Nature of intervalence charge-transfer bands in Prussian Blues. *Inorganic Chemistry* 1986, *25* (3), 389-392.
18. Neff, V. D., Electrochemical oxidation and reduction of thin-films of Prussian Blue. *Journal of the Electrochemical Society* 1978, *125* (6), 886-887.
19. Itaya, K.; Shibayama, K.; Akahoshi, H.; Toshima, S., Prussian-Blue-modified electrodes - an application for a stable electrochromic display device. *Journal of Applied Physics* 1982, *53* (1), 804-805.
20. Carpenter, M. K.; Conell, R. S., A single-film electrochromic device. *Journal of the Electrochemical Society* 1990, *137* (8), 2464-2467.
21. Chen, L. C.; Ho, K. C., Design equations for complementary electrochromic devices: application to the tungsten oxide-Prussian Blue system. *Electrochimica Acta* 2001, *46* (13-14), 2151-2158.
22. Deepa, M.; Awadhia, A.; Bhandari, S.; Agrawal, S. L., Electrochromic performance of a poly(3,4-ethylenedioxythiophene) - Prussian Blue device encompassing a free standing proton electrolyte film. *Electrochimica Acta* 2008, *53* (24), 7266-7275.
23. DeLongchamp, D. M.; Hammond, P. T., Multiple-color electrochromism from layer-by-layer-assembled polyaniline/Prussian Blue nanocomposite thin films. *Chemistry of Materials* 2004, *16* (23), 4799-4805.
24. Jelle, B. P.; Hagen, G., Performance of an electrochromic window based on polyaniline, Prussian Blue and tungsten oxide. *Solar Energy Materials and Solar Cells* 1999, *58* (3), 277-286.
25. Goldsby, K. A.; Blaho, J. K.; Hoferkamp, L. A., Oxidation of nickel(II) bis(salicylaldimine) complexes - solvent control of the ultimate redox site. *Polyhedron* 1989, *8* (1), 113-115.

26. Hoferkamp, L. A.; Goldsby, K. A., Surface-modified electrodes based on nickel(II) and copper(II) bis(salicylaldimine) complexes. *Chemistry of Materials* 1989, *1* (3), 348-352.
27. Dahm, C. E.; Peters, D. G., Catalytic reduction of iodoethane and 2-iodopropane at carbon electrodes coated with anodically polymerized films of Nickel(II) *salen*. *Analytical Chemistry* 1994, *66* (19), 3117-3123.
28. VilasBoas, M.; Freire, C.; deCastro, B.; Christensen, P. A.; Hillman, A. R., New insights into the structure and properties of electroactive polymer films derived from Ni(*salen*). *Inorganic Chemistry* 1997, *36* (22), 4919-4929.
29. Vilas-Boas, M.; Santos, I. C.; Henderson, M. J.; Freire, C.; Hillman, A. R.; Vieil, E., Electrochemical behavior of a new precursor for the design of poly Ni(*salen*) -based modified electrodes. *Langmuir* 2003, *19* (18), 7460-7468.
30. Jiang, J. A.; Leung, A. C. W.; MacLachlan, M. J., Synthesis and characterization of an oligomeric conjugated metal-containing poly(p-phenylenevinylene) analogue. *Dalton Transactions* **2010,** *39* (28), 6503-6508.
31. Abd-El-Aziz, A. S.; Manners, I., *Metal-containing p-conjugated polymers*. Wiley-Interscience: New Jersey, 2007.
32. Vilas-Boas, M.; Freire, C.; de Castro, B.; Hillman, A. R., Electrochemical characterization of a novel *salen*-type modified electrode. *Journal of Physical Chemistry B* 1998, *102* (43), 8533-8540.
33. Vilas-Boas, M.; Freire, C.; de Castro, B.; Christensen, P. A.; Hillman, A. R., Spectroelectrochemical characterisation of poly Ni(saltMe)-modified electrodes. *Chemistry-a European Journal* 2001, *7* (1), 139-150.
34. Berns, R. S.; Billmeyer; Saltzman's, Principles of color technology. John Wiley & Sons Inc.: New York, 2000.
35. Leong, J. 2006. *Number of colors distinguishable by the human eye* [Online]. Available: http://hypertextbook.com/facts/2006/JenniferLeong.shtml [Accessed May 2010].
36. Kuehni, R. G., Color: an introduction to practice and principles. 2nd ed.; Wiley-Interscience: New Jersey, 2005.
37. MacEvoy, B. 2002. *Color models & color wheels* [Online]. handprint media. Available: http://personales.upv.es/gbenet/teoria%20del%20color/water_color/color6.html#munsell [Accessed May 2010].
38. Schanda, J., Colorimetry. Wiley-Interscience: New Jersey, 2007; pp 25-76.
39. Broadbent, A. D., A critical review of the development of the CIE1931 RGB color-matching functions. *Color Research and Application* 2004, *29* (4), 267-272.

40. Thompson, B. C.; Schottland, P.; Zong, K. W.; Reynolds, J. R., In situ colorimetric analysis of electrochromic polymers and devices. *Chemistry of Materials* 2000, *12* (6), 1563-1571.
41. Kuehni, R. G., Color: an introduction to practice and principles. 2nd ed.; Wiley-Interscience: New Jersey, 2005.
42. Perrin, D. D.; Armarego, W. L. F., Purification of laboratory chemicals. Pergamon Press: New York, 1988.
43. Holm, R. H.; Everett, G. W.; Chakravorty, A., Metal complexes of schiff bases and ß-ketoamines. *Progress in Inorganic Chemistry* 1966, *7*, 83-204.
44. Mortimer, R. J.; Reynolds, J. R., In situ colorimetric and composite coloration efficiency measurements for electrochromic Prussian Blue. *Journal of Materials Chemistry* 2005, *15* (22), 2226-2233.
45. Gaupp, C. L.; Welsh, D. M.; Rauh, R. D.; Reynolds, J. R., Composite coloration efficiency measurements of electrochromic polymers based on 3,4-alkylenedioxythiophenes. *Chemistry of Materials* 2002, *14* (9), 3964-3970.

Chapter 5

Non-liquid Electrolytes for Electrochromic Devices

5.1 Introduction

Electrolytes are one of the most challenging components in the development of reliable solid-state electrochemical devices. The electrolyte system serves as an ion storage layer that exchanges charged species in the electrode–electrolyte interface and through the electrolyte layer during the redox process. Electrolytes are of extreme importance to the correct function of electrochemical cells, and in particular for ECD.

The correct operation of an ECD implies the injection of electrons in one electrode and extraction of equivalent amount of electrons from the second one. The continuous flow of electrons (current) will charge the electrodes and create a polarization through the cell; consequently the current flow is blocked otherwise the electroneutrality law would be infringed. To avoid polarization the charge accumulated over the electrodes surface must be electrically balanced by the electrolyte medium ions – charge carriers.

The present chapter reports on the spectroelectrochemical studies and write-erase cycling tests of ECD using two different kinds of polymer electrolyte – solid polymer electrolyte (SPE) and gel electrolyte. The SPE used is a blend of poly(ethylene oxide) and poly(trimethylene carbonate) (p(TMC)/PEO). The SPE films were supplied by M. M. Silva from Centro de Química of Univ. do Minho in the framework of a scientific collaboration. M. M. Silva was responsible for the film preparations and characterization of the thermal behaviour, ionic conductivity and electrochemical stability. The gel electrolyte is based on polyethylene oxide (PEO). Both systems were doped with lithium perchlorate salt.

5.1.1 Electrolyte systems and application

The electrolyte layer must be placed between and in direct contact with the modified electrodes. The electrolyte system consists of a salt dissolved or contained in a matrix. The salt is responsible for the introduction of positive and negative charge carriers and the matrix as the medium where they can move between the polarized electrodes. The movement of charged particles between the electrodes will reduce electrode polarization by charge neutralization.

The accumulation of negative charges can be neutralized by an equivalent accumulation of positive charges within the vicinity of the electrode surface. On the other hand, a negative charged electrode can be neutralized by the depletion of equivalent charge of negative ions from its surface. The same holds for positively charged electrodes. Both mechanisms can happen at the same time.

Ionic conductivity background

The ability of a system to support current flow generated by motion of charged particles when an electric field exists within the system is called the conductivity[1], or specific conductance, κ (Scm^{-1}).[2] Conductivity is defined as the inverse of resistivity, ρ (ohm.cm), see Eq.5.1.

$$\kappa = \frac{1}{\rho} \qquad \text{Eq. 5.1}$$

The conductivity is related with the conductance (*C*) of a specific electrolyte system, and is dependent on the dimensions of the electrolyte. In Eq. 5.2 the conductance is defined,

$$C = \kappa \times \frac{A}{l} \qquad \text{Eq. 5.2}$$

where A is the cross section area of an electrolyte column between two electrodes and *l* the length of the column.

Conductance can also be expressed as a function of resistivity; Eq. 5.3 can be obtained from Eq. 5.2 and Eq. 5.1.

$$C = \frac{1}{\rho} \times \frac{A}{l} \qquad \text{Eq. 5.3}$$

A useful derived function from specific conductivity is the equivalent conductivity, Λ ($S.cm^2.equiv.^{-1}$), see Eq. 5.4,

$$\Lambda = \frac{1000\kappa}{c_{eq}} \qquad \text{Eq. 5.4}$$

where c_{eq} is the concentration of equivalents per dm^3 of positive or negative ions of the respective salt.

The ionic conductivity of an electrolyte system is proportional to the product of the total quantity of charge carriers (*N*) available by their ionic mobility (u_i), see Eq. 5.5,

$$\kappa = N u_i |ze| \qquad \text{Eq. 5.5}$$

where ze is the charge of each ion. Based on previous equations we can predict that for ideal situations the bulk conductance of an electrolyte will increase when both *N* and u_i increase

too. Electrolytes with larger amount of salt will increase ionic conductivity, considering ideal conditions. On the other hand the mobility can be tuned with viscosity (η) of the microenvironment of the charge carriers, see Eq. 5.6.

$$u_i = \frac{|ze|}{6\pi r\eta} \qquad \text{Eq. 5.6}$$

where r is the radius of the mobile ion.

Electrolyte systems

Many different kinds of electrolytes have been developed including liquid, gel, polymer, solid and hybrid electrolytes. The main trends in the field of electrochromic cells are based on gel electrolytes[3,4] and ionic liquids immobilized in organic polymers.[5]

In early works on ECD the electrolyte medium was based on liquid state electrolyte (LSE), for example Deb's works in 1973[6] or the best-selling "self-darkening electrochromic rear-view mirror" developed by the Gentex Corporation.[7] Liquid electrolytes present high ionic conductivities on the order of 10^{-1} Scm^{-1} for salt concentration around 1M.[8] Electrolytes with high ionic conductivity allow to develop ECD's with short switching times. Practical devices with switching times of less than 1s, were already fabricated in the 70's.[9]

In spite of their high ionic conductivities that convey LSE as supporting electrolytes in most electrochemical applications, they present several drawbacks towards real applications. LSE are not suitable for large scale applications due to their lack of structural stability for flexible devices, leakage[9,10] and homogeneity problems during the coloration process[11]; in some cases liquid electrolyte can even react with the electroactive materials.[12]

In 1973, P. V. Wright reported on the ionic conductivity from a "solvent-free" poly(ethylene oxide)-salt system. Later, in 1978, M. B. Armand highlighted the potential applications of such SPE, specifically for energy storage applications. Since then, both academia and industry have contributed to polymer electrolyte development.[9]

In contrast to LSE, SPE's can be easily formed into thin films and avoid leaking problems. Moreover SPE's show several advantages towards ECD applications such as[12]:

- Improved safety to mechanic attack of the devices (shock, vibration and mechanical deformation);
- Enhanced endurance to varying electrode volume during redox cycling;
- Polymer layer can act as an electrode spacer;
- Confer structural stability to the entire device;
- Can act as a binder between electrodes;

- Polymer films can adopt any geometrical shape.

Elimination of the LSE layer should facilitate the manufacture to highly automated processes, adapting existing industrial technology for thin film processing. For this reason SPE's[13,14] have been used as components for commercial applications such as rechargeable lithium batteries[15], fuel cells[16] and electrochromic devices.[17]

SPE's are obtained by the dissolution of a salt in a ion-coordinating macromolecule (polymer host), free of any low weight solvent or additives.[18] Here the polymer host acts as a solid solvent where the salt is dissociated. Extended salt dissociation is obtained when the polymer host has good electron donor groups such as ether oxygen like in poly(ethylene oxide) (PEO).

The ionic conduction mechanism of this class of polymer electrolytes is intimately associated with the local segmental motions of the polymer (see Fig.5.1).[12] The transport of ions through local relaxation processes in the polymer chain can be compared with those in liquid state.[9]

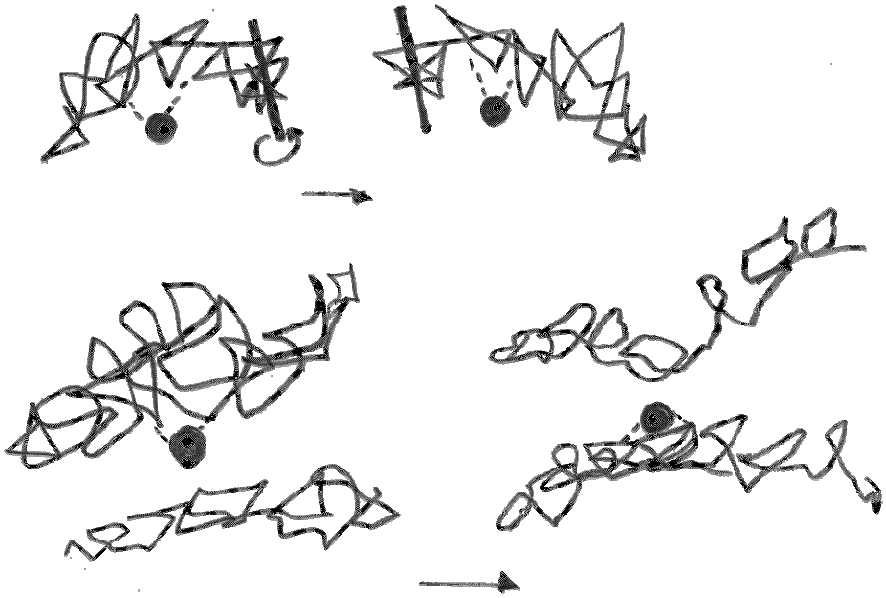

Figure 5.1 – Cation (sphere) transport mechanism in a polymer based electrolyte. Motion coupled to that of the polymer chain (up) and transfer of a cation between chains (bottom).

A low boiling-point temperature solvent may be used to mix the polymer host and the salt, being slowly evaporated after casting the mixture. In order to obtain a freestanding membrane, cast films can be further dried using simultaneously temperature and low pressure conditions.

Representative classes of polymer host studied for SPE's are: PEO, poly(acrylonitrile) (PAN), poly(methyl methacrylate) (PMMA), poly(vinyl chloride) (PVC) and poly(vinylidene fluoride) (PVdF).[9] Although the broad range of polymers studied as polymer hosts for SPE's none have shown any considerable advantage over PEO, the most widely studied host polymer for

SPE applications. PEO continues to be the best choice for "dry", solvent-free lithium ion containing SPE's.

Polyethylene oxide based polymer electrolyte systems

A wide variety of polymer electrolytes based on the ethylene oxide repeating unit have been synthesized and characterized. The resulting macromolecules include linear and branched polymers, block co-polymers and plasticized polymers with morphologies that almost cover the entire range between amorphous and crystalline states. [11,19,20,21]

PEO exhibits good coordinating properties towards the salt cation resulting in a high content salt dissociation. However, PEO is highly crystalline (for high molecular-weight) showing poor ionic conductivity at room temperature.[12] In general, SPE's show several technological advantages but present poor ionic conductivity values at room temperature, 10^{-8} to 10^{-4}Scm^{-1}.[12,22,23] Application of this kind of electrolytes is not suitable for applications such as ECD.

To increase ionic conductivity of SPE's several strategies were pursued: introduction of a plasticizer, promoting cross-linking, branched and block copolymers derivatives of PEO and blends with other polymers.[9] All these modifications have the main goal to lower the glass transition temperature (Tg) of the polymer host and to increase the amorphous phase in order to improve room temperature ionic conductivity.

Addition of large quantities of plasticizer (*e.g.* ethylene oxide, propylene oxide) and/or solvent (*e.g.* Acetonitrile, alcohols, benzene, chloroform, cyclohexanone, esters, DMF) increases effectively the ionic conductivity of the polymer based electrolyte. Such strategy leads to the formation of a gel showing an effective increase of room temperature ionic conductivity, between 10^{-3} to 10^{-2} Scm^{-1}.[3,12,23,24,25]

Gel electrolytes are a ternary mixture of polymer, salt and a large content of liquid solvent or plasticizer, around 40 to 60% (w/w).[26] The fact that the gel is a solid permeated by a solvent means that it can be thought of as a combination of a solid and a liquid.[27] Gel electrolytes share properties of SPE and LSE, such as the cohesive forces of polymers and the ionic conductivity properties similar to liquid electrolytes.

The development and optimization of electrolyte systems for ECD's requires very specific conditions. The electrolyte must have a high transparency to maximize chromatic contrast in the case of see-through displays, an adequate room temperature conductivity (>10^{-4} Scm^{-1})[3] to permit rapid colour switch, mechanical flexibility to form an appropriate electrode/electrolyte interface and low thermal expansion or volatile components so that the device may operate over a relative wide range of temperatures. Although novel electrolyte systems with improved electrochemical performance continue to be developed, it is worth to note that since 1987 the International Symposium on Polymer Electrolytes took place every

two years. This year the 12th edition will be held in Padova;[28] it seems likely that the preparation of electrolytes for application in any given device will involve optimization of electrochemical and physical parameters for the specific requirements of the device.

5.2 Gel Electrolytes for ECD applications

5.2.1 Experimental Details

General

Poly(3,4-ethylenedioxythiophene)-poly(styrenesulfonate) (PEDOT, 1.3 wt.% dispersion in H_2O, conductive grade—Aldrich) certified *p.a.* grade and used without further purification. Lithium perchlorate (Aldrich, 99.99%) was supplied as a pure, dry solid, packed under nitrogen and was used as received.

Gel electrolyte preparation

Homogeneous solutions of a polyethylene oxide and polypropylene oxide co-polymer (PEO-PPO) and lithium perchlorate in a polar solvent were prepared by stirring known masses of polymer components and lithium salt. An homogeneous viscous solution is obtained. Opaque gel electrolytes were produced by incorporation of pigments. The following pigments were tested: yellow chrome ($PbCrO_4$), titanium dioxide (TiO_2) and Natural Red 9; the yellow and white pigments and the red dye were first suspended in a polar solvent prior to the addition of PEO-PPO polymer. Gel electrolyte films were obtained by casting small volumes of the mixture.

PEDOT films

PEDOT films were spin-coated on the flexible electrodes of polyethylene terephthalate (PET) films coated with indium tin oxide (PET/ITO, Aldrich with a resistivity of 60 Ω/sq and a useful area is *ca.* 4 cm^2). Spin conditions were set as follows: 2000 rpm for 30 s. The spin-coated film was dried at 50 °C during 2 h.

Electrochromic cell assembly

Electrochromic cells were assembled in a sandwich-like structure. Gel electrolyte was casted over PET/ITO/PEDOT modified electrodes forming a sticky gel film. The second modified PET/ITO/PEDOT electrode is then placed over the gel film. Finally the edges of the cell were sealed with normal adhesive tape. Useful area of ECD is *ca.* 4cm^2.

Conductivity

Ionic conductivity of gel electrolyte was measured using a Metrohm 644 Conductometer (ref.1.644.0010) and an Immersion Type Cell (ref. 6.0901.110). The cell constant ($0.78cm^{-1}$) was determined using an electrolyte standard solution (KCl, 1 mM). The sample temperature was controlled.

Electrochemical measurements

Electrochemical measurements were performed using a computer controlled Autolab potentiostat–galvanostat Model 20 (Eco-Chemie). Evaluation of the electrochemical stability window of gel electrolyte was carried out using a two-electrode cell configuration: PET/ITO/Gel Electrolyte Layer/ITO/PET. The cell was assembled as described above (see 5.2.1.4) except that the electrodes were not modified with electrochromic material.

Spectroelectrochemical measurements

UV/Vis reflectance spectra and transient reflectance were recorded in a Shimadzu UV2501-PC using an integrating sphere installed in the sample compartment of the spectrophotometer. Spectra were run with 5nm resolution. Transient reflectance spectra obtained during potentiostatic titration of ECD were recorded after each potential had been applied for 50–60 s. All spectroscopic measurements of the electrochromic cells were carried out *in situ* with the electrochromic cells positioned perpendicular to the light beam of the spectrophotometer. The cells were connected to the potentiostat apparatus by means of electrical wires and flat contacts.

5.2.2 Results and Discussion

Formulation of the gel electrolyte

In order to obtain gel electrolytes with viscosities adequate for ECD assembly, several polymer:solvent (w/w) ratios were used to prepare gels. It was found that polymer:solvent 30:70 (w/w) led to viscous solution that was fluid enough to be easily casted over the electrodes. It was also found that in less than one hour a powerful sticky gel film was formed. These characteristics facilitated the assembly of the ECD presenting a good adhesion between the electrodes.

The final viscosity of the fluid obtained was around 400cP at room temperature.

Development of a fast switching and high optical contrast ECD is mainly dependent on the bulk conductance of the electrolyte layer. It is desirable to have a high ionic mobility and a high number of charge carriers. Addition of salt on the electrolyte medium will increase the ionic conductivity. The last statement is true until ion pairing occurs between cations and anions and the number of effective charge carriers will decrease. The study of the variation of bulk conductivity for different salt concentrations was performed. In Table 5.1 gel electrolytes with different salt contents tested are listed.

Table 5.1 – Ionic conductivity and equivalent conductivity for gel electrolytes with different percentage of $LiClO_4$ salt.

%$LiClO_4$ (w/w)	[Li] (M)*	κ (S/cm)	Λ ($Scm^{-2}equiv.$)	%$LiClO_4$ (w/w)	[Li] (M)	κ (S/cm)	Λ ($Scm^{-2}equiv.$)
0.0012	1.2E-04	2.7E-05	2.2E-01	1.26	0.13	4.0E-03	3.0E-02
0.0037	3.8E-04	3.2E-05	8.3E-02	1.72	0.18	5.7E-03	3.1E-02
0.0099	1.0E-03	6.4E-05	6.2E-02	1.79	0.19	5.5E-03	2.9E-02
0.04	4.2E-03	1.4E-04	3.3E-02	2.39	0.25	9.0E-03	3.5E-02
0.06	6.2E-03	2.4E-04	3.8E-02	2.91	0.31	9.4E-03	3.0E-02
0.09	9.4E-03	2.9E-04	3.1E-02	3.29	0.35	1.1E-02	3.1E-02
0.11	1.1E-02	3.6E-04	3.1E-02	3.54	0.38	1.2E-02	3.1E-02
0.12	1.2E-02	3.9E-04	3.1E-02	3.7	0.4	1.2E-02	3.0E-02
0.36	3.8E-02	1.2E-03	3.1E-02	3.77	0.41	1.3E-02	3.1E-02
0.44	4.6E-02	2.0E-03	4.3E-02	3.76	0.41	1.3E-02	3.1E-02
0.59	6.2E-02	1.8E-03	2.9E-02	3.79	0.41	1.3E-02	3.1E-02
0.79	8.3E-02	3.6E-03	4.4E-02	4.82	0.53	1.3E-02	2.5E-02
1.03	1.1E-01	3.0E-03	2.8E-02	5.39	0.59	1.3E-02	2.3E-02

*the chemical concentration of Li^+ was calculated considering stoichiometric chemical quantity of $LiClO_4$ and the volume of solvent in the respective mixture; mol LiClO4 divided by the volume of solvent

In Fig. 5.2-left the dependence of κ with salt content shows two distinct regimes. For low and medium range concentrations of salt a linear increase of the ionic conductivity is observed. Addition of salt will increase *N* by dissociation of $LiClO_4$. This behaviour is observed until a concentration of *ca.* 0,41M salt. This behaviour is predicted in Eq. 5.5, were κ is proportional to *N*.

At higher salt concentrations (>0,41M) conductivity reaches a plateau (see ionic conductivity for 0,53 and 0,59M of $LiClO_4$, Table 5.1 and Fig. 5.2-left) . At high salt concentration ion pairing may occur between the cation and anion of the salt. The ion pair can present either zero net charge (if $z_+ = z_-$) or a resulting charge (if $z_+ \neq z_-$). In both cases the number of available charge carriers will be smaller than it would be expected in terms of the salt stoichiometric concentration and the assumption of complete dissociation. Consequently the equivalent conductivity will decrease. [30]

Another approach to evaluate the effective increase in conductivity with the addition of salt is to calculate the molar conductivity (Λ, see Eq. 5.4). It is interesting to observe that Λ shows a maximum for the lower salt concentration measured ($1{,}2 \times 10^{-4}$M of $LiClO_4$) and decreases abruptly with further addition of salt. At $9{,}4 \times 10^{-4}$M of $LiClO_4$, Λ reaches a plateau. At higher salt concentrations (>0,41M of $LiClO_4$) Λ starts to decrease again, see Fig.5.2-right.

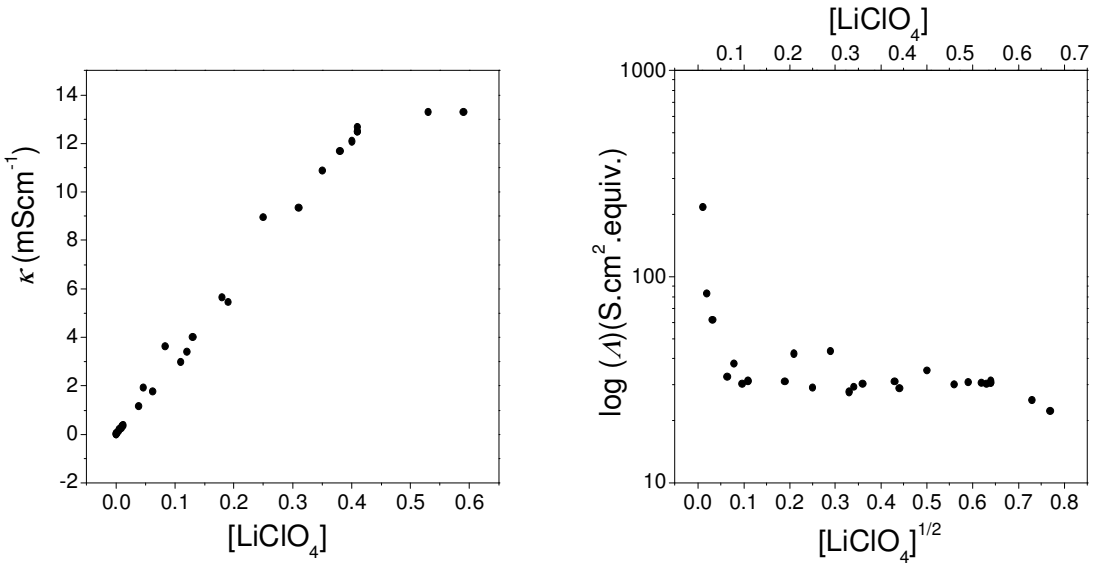

Figure 5.2 – Ionic conductivity (left) and equivalent ionic conductivity (right) of the gel electrolyte at different salt content in M (the chemical concentration was calculated considering stoichiometric chemical quantity of $LiClO_4$ and the volume of solvent in the respective mixture; mol $LiClO_4$ divided by the volume of solvent) at 21ºC.

Observation of the behaviour of Λ is comparable to that observed for weak electrolytes.[2] In weak electrolytes the salt is not completely dissociated and thus the number of charge carriers available is not equal to stoichiometric salt concentration. In this case a relationship between the theoretical molar conductivity Λ_T and the observed molar conductivity Λ_{Obs} is expressed as follows in Eq.5.7

$$\Lambda_{Obs} = \alpha\Lambda_T \qquad \text{Eq. 5.7}$$

where α is the degree of dissociation of the salt.

The ion pairing phenomenon and incomplete salt dissociation can explain the decrease of the molar conductivity observed in the gel electrolyte. Based on the results, it was decided to use as standard clear gel electrolyte composed by solvent:PEO-PPO:salt equal to 70:26:4 (w/w) ratios.

Temperature

For the standard clear gel electrolyte a temperature study was performed (see Fig.5.3):

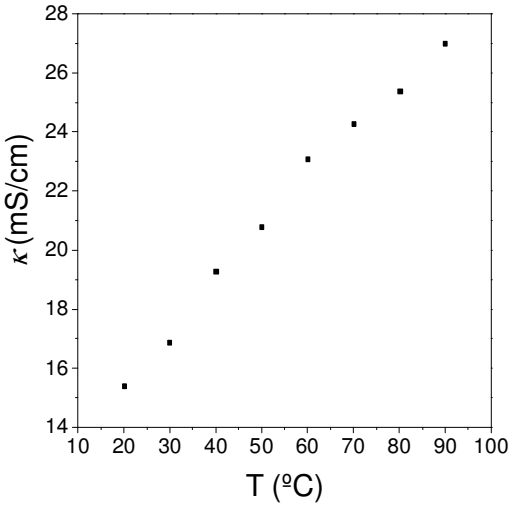

Figure 5.3 – Ionic conductivity (κ) of the clear gel electrolyte as a function of temperature.

Although room temperature will be the desired range of temperature for ECD applications, it was interesting to observe the linear relationship between the ionic conductivity with the temperature. Value of κ obtained at 90ºC almost doubled compared to the obtained at 20ºC. A possible explanation of the phenomena is the increase of the ions mobility due to the decrease of the bulk viscosity of the gel (see Eq.5.6).

Pigments

As described in section 1.2.1 ECD-R and symmetric cell configuration requires (both electrodes are coated with the same electrochromic material) a light scattering layer. In our configuration we decided to introduce pigments in the electrolyte layer to allow us to build a symmetrical ECD-R with the organic electrochromic polymer PEDOT.

Several synthetic and natural pigments were incorporated in the clear gel electrolyte to form an opaque gel. Yellow chrome, TiO_2 and Natural Red 9 (a mixture of Alizarin and Purpurin) were used to prepare an opaque yellow, white and pink gel electrolyte layer. A stable suspension was obtained upon addition of the pigment in the clear gel electrolyte mixture – opaque gel electrolyte. The introduction of a small percentage of the pigment or dye resulted in a small increase of the ionic conductivity when compared to the clear gel electrolyte, see Table 5.2.

Table 5.2 – Ionic conductivity of the clear and opaque gel electrolytes

Gel Electrolyte	Pigment	κ (S.cm^{-1})
Clear	-	1.25x10^{-2}
Opaque yellow	Yellow Chrome	1.66x10^{-2}
Opaque white	TiO2	1.73x10^{-2}
Opaque pink	Natural Red 9	1.93x10^{-2}

Electrochemical stability

Electrochemical stability of the clear and opaque gel electrolyte was investigated by cyclic voltammetry.

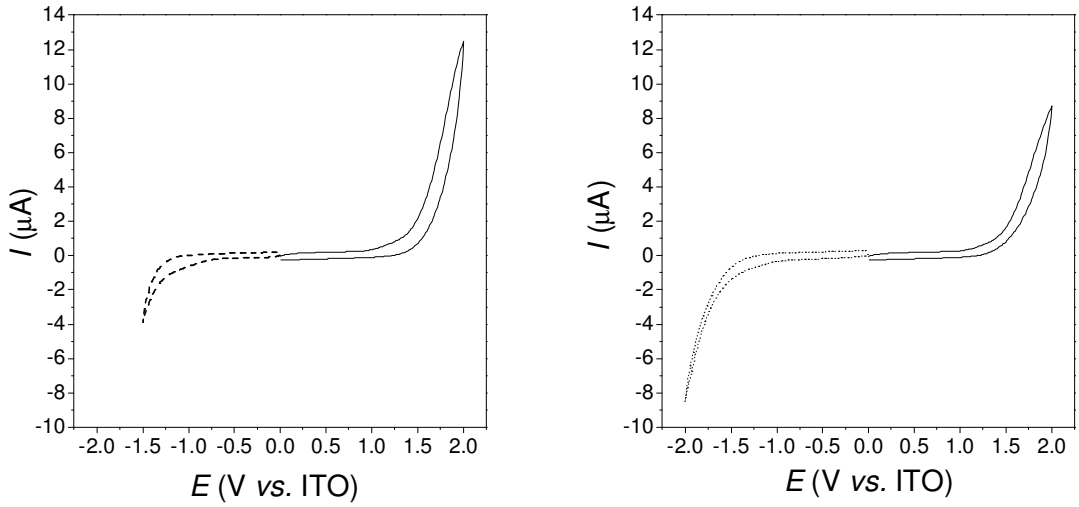

Figure 5.4 - Electrochemical window for gel polymer electrolyte determined by cyclic voltammetry. A two electrode electrochemical cell was used with the electrolyte film sandwiched in between. The working electrode was a PET-ITO and the counter electrode and reference electrode was used as a one electrode also from PET-ITO; clear gel electrolyte (left) and opaque yellow gel electrolyte (right).

In Fig. 5.4-left and –right the cyclic voltammograms show a safe range of electric potential between -1.5 to 1.5V (*vs.* ITO) for the clear and opaque gel polymer electrolyte.

Gel electrolyte as ionic conductor layer in ECD

Several publications devoted to the development of electrochromic devices are mainly focused in the individual components: electrochromic layer and electrolyte systems both SPE, LSE and gel electrolytes. Some authors are only interested on the ECD performances such as coloration efficiency and electrochromic device stability. However, few works have focused in the effect of how the ionic conductivity of the electrolyte will influence the ECD output in terms of optical contrast, switching time and cycling stability.

Here we report on the effect of ECD devices based on a symmetric configuration PET/ITO/PEDOT/opaque gel electrolyte/PEDOT/ITO/PET, where PEDOT is the electrochromic layer and the opaque gel electrolyte the ionic conducting layer. Two opaque gel electrolytes with different ionic conductivities were used to assemble the ECD; ECD-1 and ECD-2. The different ionic conductivities were obtained mixing different quantities of salt in the gel electrolyte mixture, see Fig. 5.5 and Table 5.3.

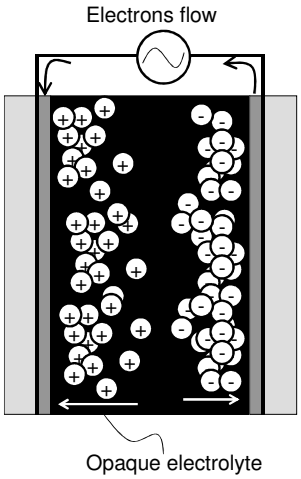

Figure 5.5 – ECD-R in a symetric "sandwich-like" architecture.

Table 5.3 – Ionic conductivity of the electrolyte layer in ECD*-1 and ECD*-2

ECD designation	Eelectrolyte layer κ(S.cm^{-1})	Salt content %w/w
ECD-1	1.95x10^{-3}	0.43
ECD-2	1.25x10^{-2}	3.7

* PET/ITO/PEDOT/opaque gel electrolyte/PEDOT/ITO/PET

In Fig. 5.6, the reflectance spectra of the symmetric ECD-R based on PEDOT is represented at different applied electrical potentials – potentiostatic titration.

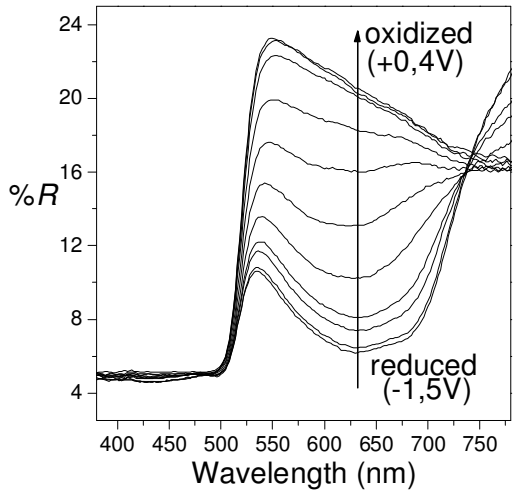

Figure 5.6 – Reflectance spectra of ECD-2 at different percentages of doped PEDOT as a function of the applied electrical potential. Potentials are measure *vs.* PEDOT/ITO electrode.

ECD-1 shows a maximum variation of reflectance at *ca.* 630nm, being a typical value for the PEDOT material. Complete coloration of the ECD is reached at *ca.* -1,5V (*vs.* PEDOT) and full bleaching at +0,4V (*vs.* PEDOT). These values were used to operate both ECD (ECD-1 and ECD-2) in the following tests.

To evaluate how the ionic conductivity of the electrolyte layer affects the performance of the ECD write-erase cycles were performed. A square wave potential between -1.5V and +0.4V (*vs.* PEDOT) was used to cycle the ECD between the coloured and bleached optical states, respectively.

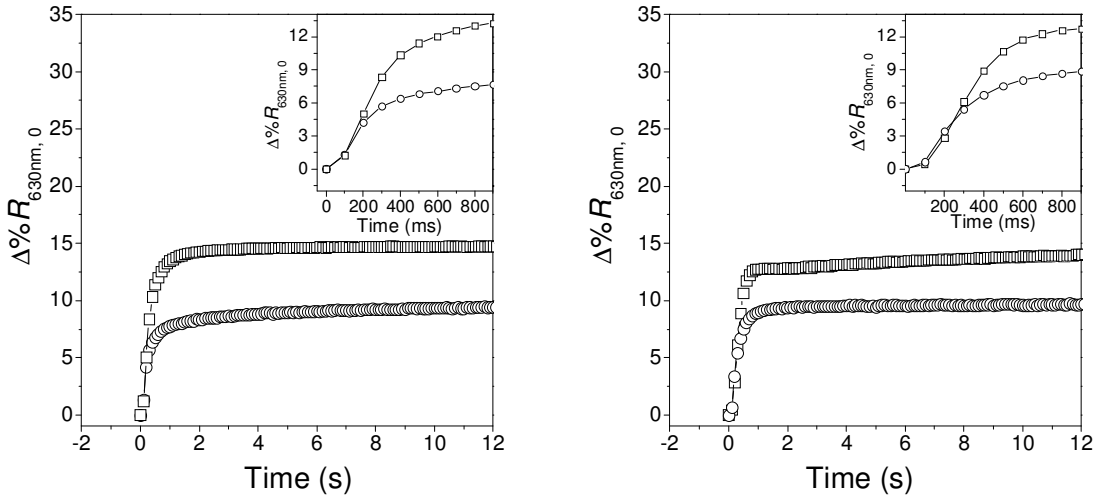

Figure 5.7 – Left: spectroelectrochemical data for the first cycle operated on the ECD-1 (open circle) and the ECD-2 (open square) during the coloration process (-1.5V *vs*. PEDOT/ITO); Right: spectroelectrochemical data for the first cycle operated on ECD-1 (open circle) and ECD-2 (open square) during the bleaching process (+0.4V *vs*. PEDOT/ITO). The insets show a zoom-in for the respective plot, detail on the optical variation during the first second after the electric trigger is shown.

In Fig. 5.7-left and Fig. 5.7-right the reflectance variation ($\Delta\%R_{630nm}$) observed for the first write-erase cycle for the ECD-1 and the ECD-2 is shown.

Spectroscopic data presented in Fig.5.7 show that ECD-1 presents a lower optical variation for the full switch when compared with the data of ECD-2. This result is a direct consequence of the different electrolytes used in both ECD's.

Complete oxidation or reduction of the electrochromic layer will result in the largest possible optical contrast for a specific ECD. As described in Eq. 5.8, PEDOT:PSS reduction (colouration, neutral state) and oxidation (bleaching, dopped state) is accompanied by the movement of ions in the electrolyte/electrochromic film interface.

$$\text{PEDOT:PSS} + e^- + M^+ \rightleftharpoons \text{PEDOT:PSS-M} \qquad \text{Eq. 5.8}$$

To perform complete electrolysis of the PEDOT layers a determined amount of electrical charge must be readily compensated by an equivalent amount of ionic charge (see Eq.5.8). ECD-1 shows an optical transition 35% lower than that found in ECD-2; however, both ECD's were assembled with the same electrochromic area and thickness layer. The optical transition of ECD-1 seems to be limited by the salt content within the electrolyte layer.

The switch time between both optical states observed for ECD-1 and ECD-2 are identical. Inset of Fig. 5.7-left and Fig. 5.7-right shows the optical evolution after the electrical voltage

trigger (Time = 0s) and the following 1s. The behaviour observed indicates that the ionic mobility for both electrolytes used in ECD-1 and ECD-2 were not affected by the electrolyte salt content.

Further write-erase cycles were performed within the range of electric potential to perform full colour transition (see Fig. 5.8 and Fig. 5.9).

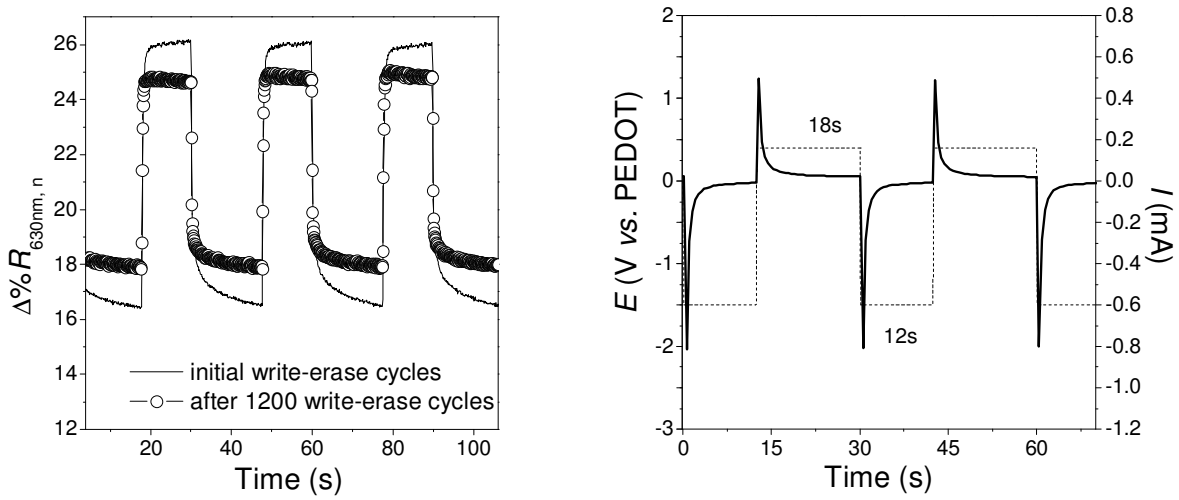

Figure 5.8 – The write-erase cycling stability test data from ECD-1. Left: variation of the reflectance of the device during write-erase cycling tests, first cycles (full line) and after 1200 cycles (open circle + full line). Right: square-wave electrical potential used to operate the stability cycling tests of the device (dashed line), and chronoamperometry data during the stability cycles (full line)

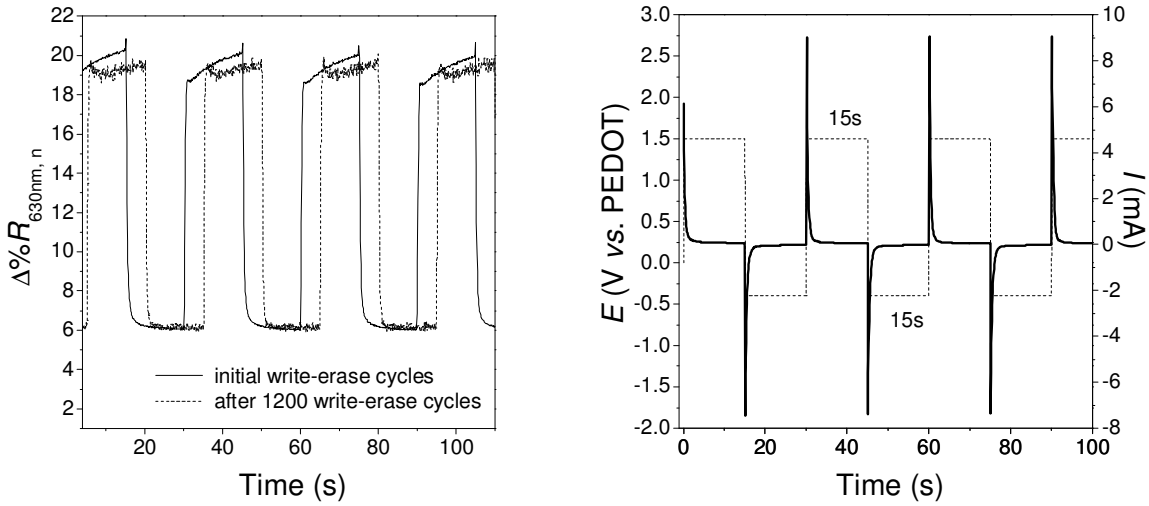

Figure 5.9 – The write-erase cycling stability test data from ECD-2. Left: variation of the reflectance of the device during write-erase cycling tests, first cycles (full line) and after 1200 cycles (dots). Right: square-wave electrical potential used to operate the stability cycling tests of the device (dashed line), and chronoamperometry data during the initial cycles (full line).

Fig. 5.8 and Fig. 5.9 show the reflectance data for the first and after 1200 cycles for the ECD-1 and ECD-2, respectively. The ECD-1 present a decrease of the total reflectance variation after the 1200 operated cycles, while ECD-2 presents almost the same reflectance variation after 1200 cycles as for the first cycle. ECD-1 and ECD-2 show also differences for the chronoamperometric data (Figs.5.8-right and 5.9-right). ECD-2 presents a current peak that occurs during the first moments of the potential transition that is one order of magnitude greater than the peak of current obtained with ECD-1. In Table 5.4 and 5.5 data from spectroelectrochemistry study of both cells is resumed.

Table 5.4 – Collected data from spectroelectrochemical experiments for ECD-1, measured before the write-eras cycling test

Optical transition	Time (s)	%full switch	$\%\Delta R_{630nm,0}$	$\Delta Q'$ (Ccm^{-2})	CE ($C^{-1}cm^2$)	$\%R$
bleaching	0	0	0	0	0	16.4
	1	92.3	9.0	1.2E-04	7.6E+04	25.4
	1.5	95.7	9.3	1.5E-04	6.4E+04	25.7
	4.5	98.9	9.6	1.9E-04	5.0E+04	26.0
	7	99.1	9.6	2.0E-04	4.7E+04	26.1
	11	99.7	9.7	2.2E-04	4.5E+04	26.1
	12	100.0	9.7	2.2E-04	4.5E+04	26.1
colouration	0	0	0	0	0	26.1
	1	80.5	7.8	7.3E-05	1.1E+05	18.4
	3	90.1	8.7	1.2E-04	7.1E+04	17.5
	7	95.1	9.2	1.6E-04	5.6E+04	17.0
	14.5	99.0	9.5	2.1E-04	4.5E+04	16.6
	17	99.9	9.6	2.3E-04	4.2E+04	16.5
	17.6	100	9.6	2.3E-04	4.2E+04	16.5

Table 5.5 – Collected data from spectroelectrochemical experiments for ECD-2, measured before the write-eras cycling test

Optical transition	Time (s)	%full switch	$\%\Delta R$	$\Delta Q'$ (Ccm^{-2})	CE ($C^{-1}cm^2$)	$\%R$
bleaching	0	0	0	0	0	6.1
	1	90.1	12.8	7.5E-04	1.7E+04	18.9
	6.1	94.9	13.5	9.2E-04	1.5E+04	19.6
	12.1	99.0	14.0	9.6E-04	1.5E+04	20.1
	14.3	99.9	14.2	9.8E-04	1.5E+04	20.3
	14.4	100.0	14.2	9.8E-04	1.5E+04	20.3
colouration	0	0.0	0.0	0	0	20.9
	1	91.0	13.5	8.4E-04	1.6E+04	7.4
	1.5	94.9	14.0	9.0E-04	1.6E+04	6.8
	5.3	99.0	14.7	1.0E-03	1.4E+04	6.2
	14.1	99.9	14.8	1.2E-03	1.3E+04	6.1
	14.2	100.1	14.8	1.2E-03	1.3E+04	6.0

The reflectance data analysed for both ECD's during the first cycle (see, Fig. 5.7) shows that the ECD-2 has a higher contrast then the observed for the ECD-1. In contrast to colour contrast, CE values obtained for ECD-1 are in average 70% higher than those found for ECD-2. It could be hypothesised that ECD-2 current is consumed in parasitic reactions to the electrochromic switching, and this would be traduced in a lower stability of the colour contrast during the write-erase cycles. However, ECD-2 shows an improved stability (see Fig. 5.9) towards write-erase cycling compared to ECD-1 that shows 17% loss after 1200 cycles (see Fig.5.8); opposed to ECD-2 that shows less than 1% loss.

To understand why ECD-2 requires more charge per unit of colour contrast the reflectance variation during colouration and bleaching *vs.* the charge consumed per unit of electrode area ($\Delta Q'$) is plotted in Fig.5.10. Both ECD's present a linear behaviour for at least 80% of the full switch. After this point a plateau is reached and the charged consume is not effective for colour variation, from this point forward the CE value usually decrease. This behaviour was also observed for other electrochromic systems (see section 4.3.1 and 4.3.2).

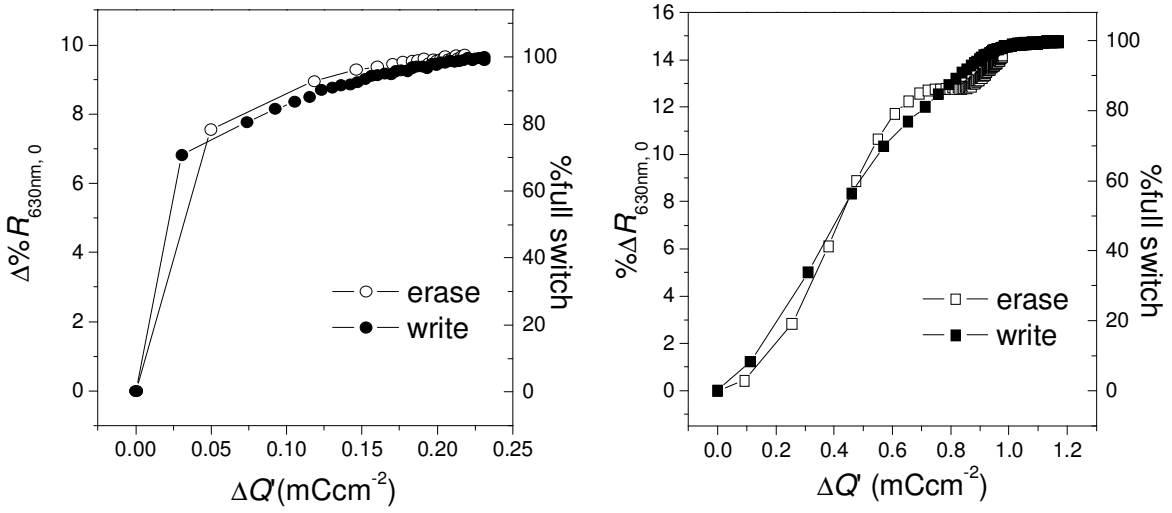

Figure 5.10 – Variation of the reflectance *vs.* the charge consumed by the ECD-1 (left) and ECD-2 (right).

Inspection of Fig.5.10-right in the first instants after the redox switch (colouration and bleaching) the reflectance shows a delayed response towards the charge consumed and after this point the evolution becomes linear until full electrolysis of the electrochromic layer is reached. For ECD-1 (see Fig.5.10-left) this phenomenon is not observed, within the limitation of the experimental technique (sampling rate of 100ms for the reflectance and charge data was used). A possible explanation is that a non-Faradic current is being originated during the first moments after the ECD is switched. This phenomenon is only observable for ECD-2 that has the higher salt content in the electrolyte layer. Processes like double layer formation of

the ions along the surface of the electrode may be the reason for the lag-phase optical response. The electrical double-layer is absolutely analogue to an electrical capacitor, which has a specific charge capacity.

The consumption of charge through innocuous non-faradic processes seems to explain both the low CE for the ECD-2 and its high stability towards the write-erase cycles. On the other hand, the pronounced degradation found for ECD-1 could consequently be explained as the result of deficient charge compensation of the polarized electrodes. The continuous operation of the device will create electrostatic repulsion between the polarized electrode and the electrochromic layer, promoting leaching of the electrochromic layer from the electrode.

Based on the data obtained from the spectroelectrochemical experiments with both ECD the energy required to power the write process (colouration) and the maximum CR were calculated, see Table 5.6.

Table 5.6 – Performance output of the ECD-1 and ECD-2

	Energy consumption (mJ/cm^2)	CR
ECD-1	0.4	6.1
ECD-2	1.8	16.7

5.3 A Solid Polymer Electrolyte for ECD

5.3.1 Experimental Details

General

Iron (III) chloride hexahydrate ($FeCl_3 \cdot 6H_2O$, Merck), potassium hexacyanoferrate (III) ($K_3[Fe(CN)_6]$, Fluka), potassium chloride (KCl, Pronalab), poly(3,4-ethylenedioxythiophene)-poly(styrenesulfonate) (PEDOT, 1.3 wt.% dispersion in H_2O, conductive grade—Aldrich) and tetrabutylammonium perchlorate (TBAP, Fluka) were certified p. a. grade and used without further purification. Acetonitrile (Riedel, p. a. grade) was dried following a procedure reported in literature[29]: pre-drying over CaH_2 during 2 days, followed by reflux and distillation.

High molar mass p(TMC) (3×10^5 g mol^{-1}), prepared by catalyzed bulk polymerization and characterized by gel permeation chromatography, was provided by Shell Chemicals, Houston, TX, USA. This polymer, obtained as a transparent amorphous elastomer, was dried before use at 70 ℃, with argon/vacuum purge cycles, for a period of about 7 days. PEO, with molar mass of approximately 10^6, was obtained from Aldrich and dried at 50℃, also with argon/vacuum purge cycles, for 7 days. No further purification of either of the polymeric components was carried out. Lithium perchlorate (Aldrich, 99.99%) was supplied as a pure, dry solid, packed under nitrogen and was used as received.

SPE film preparation

Homogeneous solutions of PEO, p(TMC) and lithium perchlorate in acetonitrile (Aldrich, anhydrous 99.99%) were prepared by stirring known masses of polymer components and lithium salt for a period of at least 48 h within a dry argon-filled preparative glove box. A combined mass of polymer and salt component of about 0.7 g was dissolved in a volume of approximately 8mL of acetonitrile. The resulting homogeneous viscous solutions were combined, stirred and decanted into glass rings seated on Teflon plates and the solvent was removed slowly in an isolated chamber within the preparative glove box. The atmosphere of this chamber was recirculated through a column of molecular sieves to effect a slow evaporation of the casting solvent and form free-standing films of about 150μm thickness. These electrolyte films were subjected to a final drying procedure in which the temperature was raised from 30 ℃ to 60 ℃ over a period of 3 days. During this period the tube oven was periodically evacuated and purged with dry argon. All manipulations of salt, electrolyte sample preparations and measurements were carried out within high-integrity, dry argon-filled glove boxes.

In this study an SPE formulation with a host matrix composed of 95 wt.% p(TMC) and 5 wt.% PEO was represented as p(TMC)/PEO(95/5). An electrolyte with lithium salt content such that the combined ratio of oxygen and carbonate coordinating sites to lithium cations was *n*,

was identified as p(TMC)/PEO(95/5)$_n$ $LiClO_4$. This designation follows the conventional use of the subscript *n* as an indication of the salt content in polymer electrolytes.

Prussian blue films

PB films were electrogenerated on flexible electrodes of polyethylene terephthalate (PET) films coated with indium tin oxide (PET/ITO, Aldrich with a resistivity of 60 Ω/sq and a useful area between 3 and 4 cm^2). The electrochemical polymerizations were performed in a conventional three-electrode electrochemical cell. An aqueous solution of 5 mM $K_3[Fe(CN)]_6$, 5 mM $FeCl_3 \cdot 6H_2O$ and 0.2 M KCl was used as PB polymerization solution. Electropolymerization was conducted under a constant applied voltage of 0.55 V (*vs.* Ag/AgCl), during *ca.* 30 s. After deposition, the electrode was gently rinsed with distilled water.

PEDOT films

PEDOT films were spin-coated on the flexible PET/ITO electrode substrate at 2000 rpm for 30 s. The spin-coated film was dried at 50 °C during 2 h.

Electrochromic cell assembly

Electrochromic cells were assembled in a sandwich-like structure. The SPE film was located between the PET/ITO/PB and PEDOT/ITO/PET modified electrodes. To improve the contact between the layers of the assembly pressure was applied to the cell overnight using a spring-loaded support. After this period the edges of the cell were sealed with normal adhesive tape. This structure was subsequently referred to the PB/SPE#/PEDOT assembly, where # represents a serial cardinal number used to identify the different electrolyte compositions used in the formulation of the SPE.

DSC and TGA measurements

Polymer electrolyte sections were removed from dry films and subjected to thermal analysis under a flowing argon atmosphere between –60 and 350 °C and at a heating rate of 5 °C min^{-1} using a Mettler DSC 821e. All samples were presented for analysis in 40 µL aluminium cans with perforated lids to permit the release and removal of decomposition products.

Samples for thermogravimetric studies were prepared in a similar manner, transferred to open platinum crucibles and analyzed using a Rheometric Scientific TG 1000 thermobalance operating under a flowing argon atmosphere. A heating rate of 10 °C min^{-1} was used to analyze all the electrolyte samples.

Conductivity

Total ionic conductivities of electrolyte samples were determined using a constant volume support with gold blocking electrodes, located within a Buchi TO 50 oven. The sample temperature was evaluated by means of a type K thermocouple placed close to the electrolyte film and impedance measurements were carried out at frequencies between 65 kHz and 500 mHz with a Solartron 1250 frequency response analyzer and 1286 electrochemical interface, over a temperature range of 20–90 ℃. Measurements of conductivity were effected during heating cycles. The reproducibility of recorded conductivities was demonstrated by comparing the results obtained for a sample subjected to two heating–cooling–heating cycles. This procedure confirmed the correct operation of the support and the mechanical stability of the samples.

Electrochemical measurements

Electrochemical polymerization was performed with a conventional three-electrode cell using a computer controlled Autolab potentiostat–galvanostat Model 20 (Eco-Chemie). The modified working electrodes were constructed as described above (see PB and PEDOT film), the auxiliary electrode was a platinum wire and the reference was an Ag/AgCl electrode (BAS). Electrochemical measurements of PB films were performed in a 0.2 M KCl aqueous solution and PEDOT in 0.1 M TBAP in acetonitrile.

The evaluation of the electrochemical stability window of the electrolyte compositions was carried out under an argon atmosphere using a two-electrode cell configuration. The preparation of a 25 µm diameter gold microelectrode surface, by polishing with a moist cloth and 0.05 µm alumina powder (Buehler), was completed outside the drybox. The microelectrode was then washed with THF (Aldrich, 99.9% inhibitor-free), dried with a hot-air blower and transferred to the drybox. The cell was assembled by locating a clean lithium disk counter electrode (cut from Aldrich, 99.9%, 19 mm diameter, 0.75-mm thick) on a stainless steel current collector and centring a sample of electrolyte on the electrode surface. A small volume (2 µL) of THF was placed on the microelectrode surface. The microelectrode was then located on the electrolyte surface and supported firmly by means of a clamp. The use of THF to soften the electrolyte was necessary to achieve a reproducible microelectrode/electrolyte interfacial contact. An Autolab PGSTAT-12 (Eco-Chemie) was used to record voltammograms at a scan rate of 100 mV/s. Measurements were performed at room temperature, within a Faraday cage.

Spectroelectrochemical measurements

UV/Vis absorbance spectra and chronoabsorptometry were recorded in a Shimadzu UV2501-PC spectrophotometer at 1nm resolution. All spectroscopic measurements of the electrochromic cells (PB/SPE#/PEDOT) were carried out *in situ* with the electrochromic cells positioned perpendicular to the light beam of the spectrophotometer. Cells were connected to the potentiostat apparatus by means of electrical wires and flat contacts.

5.3.2 Results and Discussion

In order to assess the improvement that might be accessible as a result of the substitution of the liquid electrolyte or gel electrolyte, electrochromic devices were assembled using a solid polymer electrolyte as the ion-conducting layer. Electrolytes based on interpenetrating p(TMC)/PEO blends doped with lithium perchlorate were prepared by co-deposition from acetonitrile. Thermal and ionic conductivity as well as the electrochemical stability data of the SPE films were supplied by M. M. Silva, however, the results will be resumed in the next paragraph because it is relevant information for the study.

p(TMC)/PEO blend general properties

In order to obtain PEO-based materials containing a high percentage of stable amorphous phases, with a low Tg and high ionic conductivity, a pTMC matrix was incorporated into the PEO structure.

It was observed that the p(TMC)/PEO(X/Y)$_n$ $LiClO_4$ electrolyte series is presented as a completely amorphous material. Any PEO crystals are observable in any of the samples evaluated, confirming that the samples are entirely amorphous. The introduction of a polymer matrix, chemically compatible with PEO, has the effect of inhibiting the crystallization and leads to the formation of amorphous materials.

The incorporation of the pTMC component into the PEO matrix improves the mechanical performance of the polymer blends. Electrolytes prepared with high pTMC concentration were very transparent and flexible, well-adapted as functional components in optical devices.

A single T_g was registered in all electrolyte samples, confirming miscibility of the system components. In the three polymer mixtures (85/15, 90/10 and 95/5) the value of T_g increases with the guest salt concentration. This observation is consistent with the chain-stiffening effect *i.e.* an increase in salt concentration would be expected to cause an increase in the intensity of salt–polymer segment interaction.

Thermogravimetric studies of these polymer blends confirmed that the onset of the thermal degradation of samples is lower than that of pure component polymers. Although, thermal degradation of the electrolyte formulations takes place with a gradual onset it is found a minimum thermal stability of about 200 ± 10 ºC for the three p(TMC)/PEO electrolytes composition used in this study. This temperature is more than adequate for applications in electrochromic devices.

In these $LiClO_4$-doped, blend-based systems higher conductivities are generally observed for compositions with higher wt.% of PEO. This may suggest that lithium ions form more labile complexes with PEO host segments than with the pTMC component, thus increasing the ionic conduction in the PEO phase. A marked improvement is seen in the

p(TMC)/PEO(X/Y)$_5$LiClO$_4$ compositions, which present higher conductivities than the reference PEO$_5$LiClO$_4$ composition.

Although electrolytes with greater p(TMC) content do not show as high ionic conductivity they have better mechanical and optical properties, an aspect of critical importance in the present application.

The electrochemical stability of the p(TMC)/PEO(95/5)$_{10}$LiClO$_4$ electrolyte was evaluated by microelectrode cyclic voltammetry over the potential range from –2.0 to 7.0 V *vs.* Li/Li$^+$.

The overall stability of the electrolytes is good with no electrochemical oxidation occurring at potentials less than 5 V *vs.* Li/Li$^+$. At the anodic potentials it was found electroactive safe at least until a potential of -2V versus Li/Li$^+$. This result confirms the applicability of this electrolyte composition in commercial electrochemical devices.

In table 5.7 the major characteristics of the p(TMC)/PEO electrolytes chosen to test as ionic conductor layer in electrochromic devices in this study are presented.

Table 5.7 - p(TMC)/PEO(X/Y)$_n$LiClO$_4$ electrolytes for application on prototype solid-state electrochromic devices.

p(TMC)/PEO(X/Y)$_n$LiClO$_4$ (Designation)	κ(Scm^{-1})	Tg (ºC)
p(TMC)/PEO(95/5)$_{12}$LiClO$_4$ (SPE1)	1.6x10^{-8}	-10
p(TMC)/PEO(95/5)$_{15}$LiClO$_4$ (SPE2)	7.9x10^{-9}	-11,5
p(TMC)/PEO(90/10)$_{12}$LiClO$_4$ (SPE3)	5.6x10^{-9}	-13
p(TMC)/PEO(90/10)$_{15}$LiClO$_4$ (SPE4)	1.8x10^{-8}	-17
p(TMC)/PEO(85/15)$_{12}$LiClO$_4$ (SPE5)	1.5x10^{-10}	-16
p(TMC)/PEO(85/15)$_{15}$LiClO$_4$ (SPE6)	2.4x10^{-11}	-17

Spectroelectrochemistry data

Complementary electrochromic devices based on PB and PEDOT have been proposed as display elements capable of long-term cycle stability and high performance.[31] In this study, we use a PB/SPE#/PEDOT electrochromic cell configuration to explore the characteristics of a batch of SPE samples (Table 5.7). These electrolytes were chosen on the basis of their high optical transparency and excellent mechanical properties.Electrochromic device potential limits were chosen to be –1.5 V (*vs.* PEDOT) and +1 V (*vs.* PEDOT) in order to effect the transition between the bleached state (light blue) and the coloured state (deep blue), respectively. Absorption spectra of the entire PEDOT/SPE#/PB cell show a maximum wavelength of absorption at *ca.* 630nm. The PEDOT layer presents a maximum absorption wavelength at 600nm[31], and PB at 700nm[32], in the coloured state. Fig.5.11 illustrates the UV-Vis spectra corresponding to the coloured and bleached states of the electrochromic cell PEDOT/SPE4/PB and is representative of all the studied cells. Comparing absorption

spectra of the entire cell to those published in previous papers[31] we can identify the bands corresponding to both reduced PEDOT (predominant) and oxidized PB at the potential used (+1 V *vs.* PEDOT).

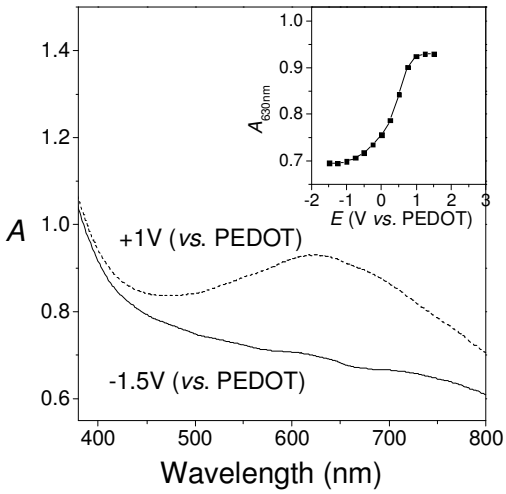

Figure 5.11 - Spectroelectrochemical data of the complementar PET/ITO/PB/SPE4/PEDOT/ITO/PET ECD in the coloured state (+1 V *vs.* PEDOT, dashed line) and bleached state (–1.5 V *vs.* PEDOT, full line). Inset: Absorbance data at 630nm for the PB/SPE4/PEDOT electrochromic cell as a function of the potential applied.

The potential limits were determined by a potentiostatic titration (inset Fig.5.11) in which the absorbance at 630nm was recorded for different potentials applied to the electrochromic cell. All the cells studied showed colour transitions between light and dark blue. In Fig.5.12 cyclic voltammetry of the ECD shows a very broad/unresolved signal. Two oxidation peaks and two reduction peaks should appear in the voltammogram since the cyclic voltammetry results of the ECD are a simple combination of the voltammogram of PEDOT and PB.[33] Although, only one oxidation peak and two reduction peaks are distinguishable from Fig.5.12.

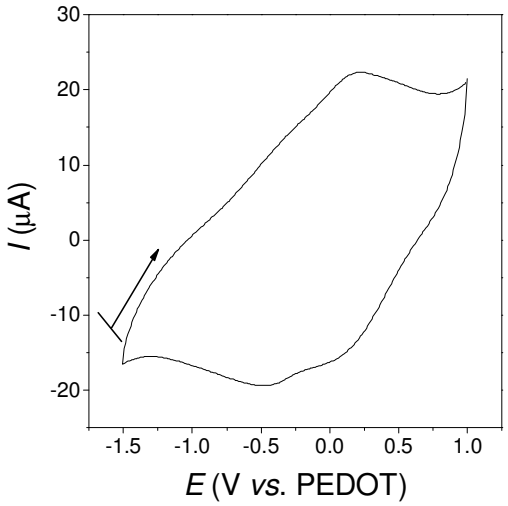

Figure 5.12 - Cyclic voltammogram of the ITO/PB/SPE1/PEDOT/ITO electrochromic cell. The reported cell voltage is that of PB with respect to PEDOT (*vs.* PEDOT).

In situ chronocoulometry/chronoabsorptometry data (Fig.5.13) show the behaviour of the current flow through the electrochromic cell during the switching steps. A decay of the device current is observed after switching (Fig.5.13-right). Considering that the exchange of one electron is followed by the exchange (insertion or extraction) of one ion between the electrochromic surface and the electrolyte, we can explain this current decay by the existence of an ion diffusion limit (assuming that the kinetics involving ion transfer are much slower than those of the corresponding electron transfer) or exhaustion either of labile ions to be exchanged or of redox centres on the electrochromic surface. The time needed for full colour switch between coloured–bleached states is rather long in these cells (*e.g.*, a cycle corresponding to 80% of ΔA_{max} on a PEDOT/SPE1/PB cell takes *ca.* 40 min to be completed), mainly due to the low ionic conductivities of these SPE's.

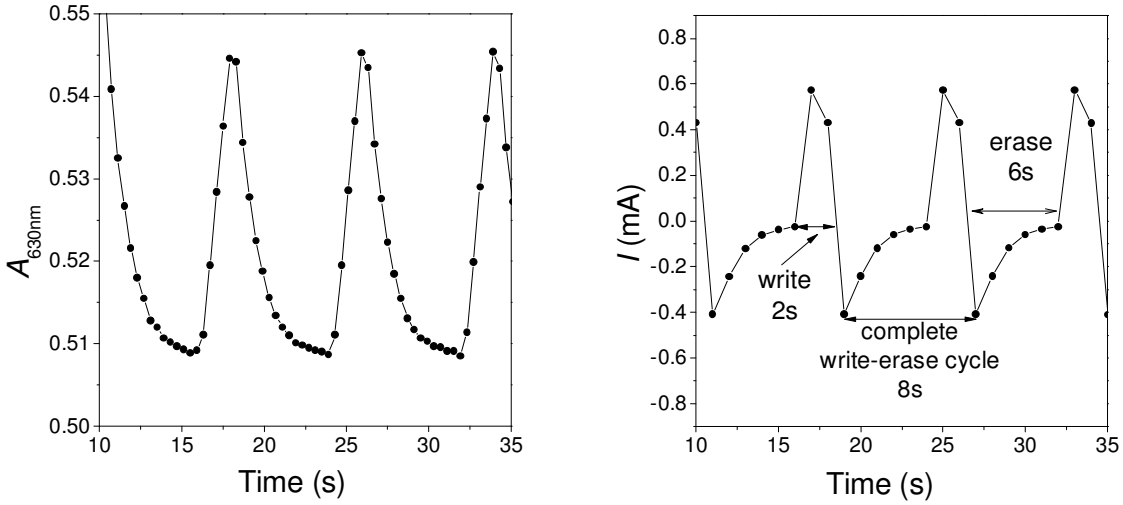

Figure 5.13 - *In situ* chronocoulometry/chronoabsorptometry data for PET/ITO/PB/SPE1/PEDOT/ITO/PET electrochromic cell during short cycling tests; chronoabsorptometry recorded at 630nm (left), chronoamperometry (right).

Spectroelectrochemical data (Table 5.8) shows maximum transmittance variations ($\Delta\%T_{630nm,0}$) between the bleached to the coloured state over a wide range of values: 8–30%. A global correlation could not be found between the $\Delta\%T_{630nm,0}$ and the SPE's characteristics (ionic conductivity and the amount of PEO in the blend). However, we can observe the effect of the amount of lithium salt in the SPE for the same polymer blend. SPE's with the higher concentrations of Li^+ ions show greater $\%\Delta T$.

Table 5.8 - Spectroelectrochemical data for the different electrochromic cells PB/SPE#/PEDOT.

Cell (#)	$A_{c,630nm}$ [a]	$A_{b,630nm}$ [b]	$\Delta A_{630nm,0}$ [c]	$\Delta\%T_{630nm,0}$ [d]
1	0.75	0.51	0.24	13
2	0.85	0.64	0.21	9
3	0.38	0.23	0.15	17
4	0.93	0.70	0.23	8
5	0.66	0.28	0.38	30
6	0.71	0.38	0.33	22

[a] A_c – coloured state.

[b] A_b – bleached state.

[c] Maximum absorbance variation – full switch before any cycling test.

[d] Respective transmittance variation of the $\Delta A_{630nm,0}$

Cycling stability tests

Cycling tests were performed on all the electrochromic cells. Due to the long time needed for full colour switch, short times (and correspondingly low ΔA) were chosen to compare the performance of each SPE in the PET/ITO/PB/SPE#/PEDOT/ITO/PET (PB/SPE#/PEDOT) electrochromic cells. Each cell was cycled (write-erase) 2500 times, choosing coloration–bleaching times that correspond to *ca.* 20% of the full colour switch; these times vary in the range 8–70 s. Table 5.9 summarizes the short cycling test conditions for each cell. At the end of the 2500 short cycles, the full switch colour data was again recorded. Fig.5.14 compares the results for the short time cycling stress induced in each electrochromic cell.

Table 5.9 - Short cycling conditions.

Cell (#) PB/SPE#/PEDOT	$\Delta A_{630nm,0}$	ΔA short cycling	Colouration time (s)	Bleaching time (s)
1	0.24	0.04	2	6
2	0.21	0.05	8	15
3	0.15	0.05	18	34
4	0.23	0.03	5	7
5	0.37	0.04	7	20
6	0.32	0.07	53	19

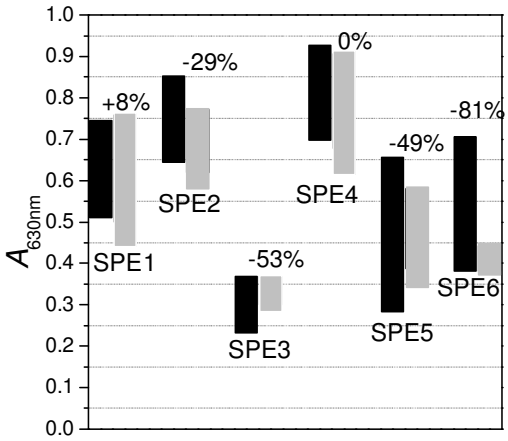

Figure 5.14 - Full switch in absorbance of the electrochromic cells before (black) and after (grey) 2500 short cycles (write-erase cycling, conditions presented in Table 5.9); the figure in each column accounts for the relative variation of full switch of absorbance at 630nm after 2500 short cycles = $(\Delta A_{2500} \times 100/\Delta A_{initial}) - 100$, see section 1.2.1 ECD parameters. The absorbance at 630nm for the coloured and bleached states for each cell is the values of the top and at the bottom of each column, respectively.

Reasonable cycle stability was found in devices based on SPE4 and SPE1 films while cells based on SPE2, SPE3, SPE5 and SPE6 show a large Δ*A* loss. The most interesting result was obtained for the device based on SPE1. After completing 2500 cycles, the full switch Δ*A* increased by 8% relative to initial values. Ho et al.[31] proposed a 4-stage behaviour for the cycling stability of PB/electrolyte/PEDOT electrochromic cells. The first stage involves film stabilization; during the second stage the optical variations remain constant throughout the cycles. A dramatic decrease in the Δ*A* is observed during the third stage, and finally in the last stage, the device gradually begins to lose performance at a moderate rate. In the case of the PB/SPE1/PEDOT assembly, a substantial increase in the total absorbance variation at 630nm was observed after 2500 cycles, corresponding to the first stage of device stabilization, indicating a very high stability to cycle testing.

The cell PB/SPE5/PEDOT was subjected to a higher stress by cycling with longer step times, forcing the device to switch between larger values of Δ*A* (*ca.* 50% of $\Delta A_{630nm,0}$). Fig. 5.15 shows the cycling conditions and absorbance changes at 630nm for the first cycles; Fig. 5.16 shows the long-term stability of the cell. Under these cycling conditions, Fig. 5.16 clearly shows an exponential decay of Δ*A* with cycling that reaches a plateau after *ca.* 100 cycles when Δ*A* has dropped by 65%. This observation is not explained by the 4-stage behaviour for the cycling stability of PB/electrolyte/PEDOT electrochromic cell proposed by Ho et al. This data confirms the low stability towards cycling already observed during the short 2500

cycle test (Fig.5.14). The coloration efficiency was also determined for 50% of full switch in absorbance. The values obtained (see Table 5.10) are comparable to those presented by other authors, ranging from 213 to 338 $C^{-1}cm^2$.[2,2 31,34,35] After completion of 180 cycles, a drop of 21% in the CE value was observed (see Table 5.10). The percentage of CE drop is not proportional to the decrease in total absorbance (65%) after cycling.

Table 5. 10 - Coloration efficiency parameters for PB/SPE5/PEDOT before and after cycling test stabilities.

Cycle	ΔA	$\Delta Q'$ (mC cm^{-2})	CE (C^{-1} cm^2)	Energy consumption ($mJcm^{-2}$) consumption
1	0.115	0.38	296	0.38
180	0.04	0.17	235	0.17

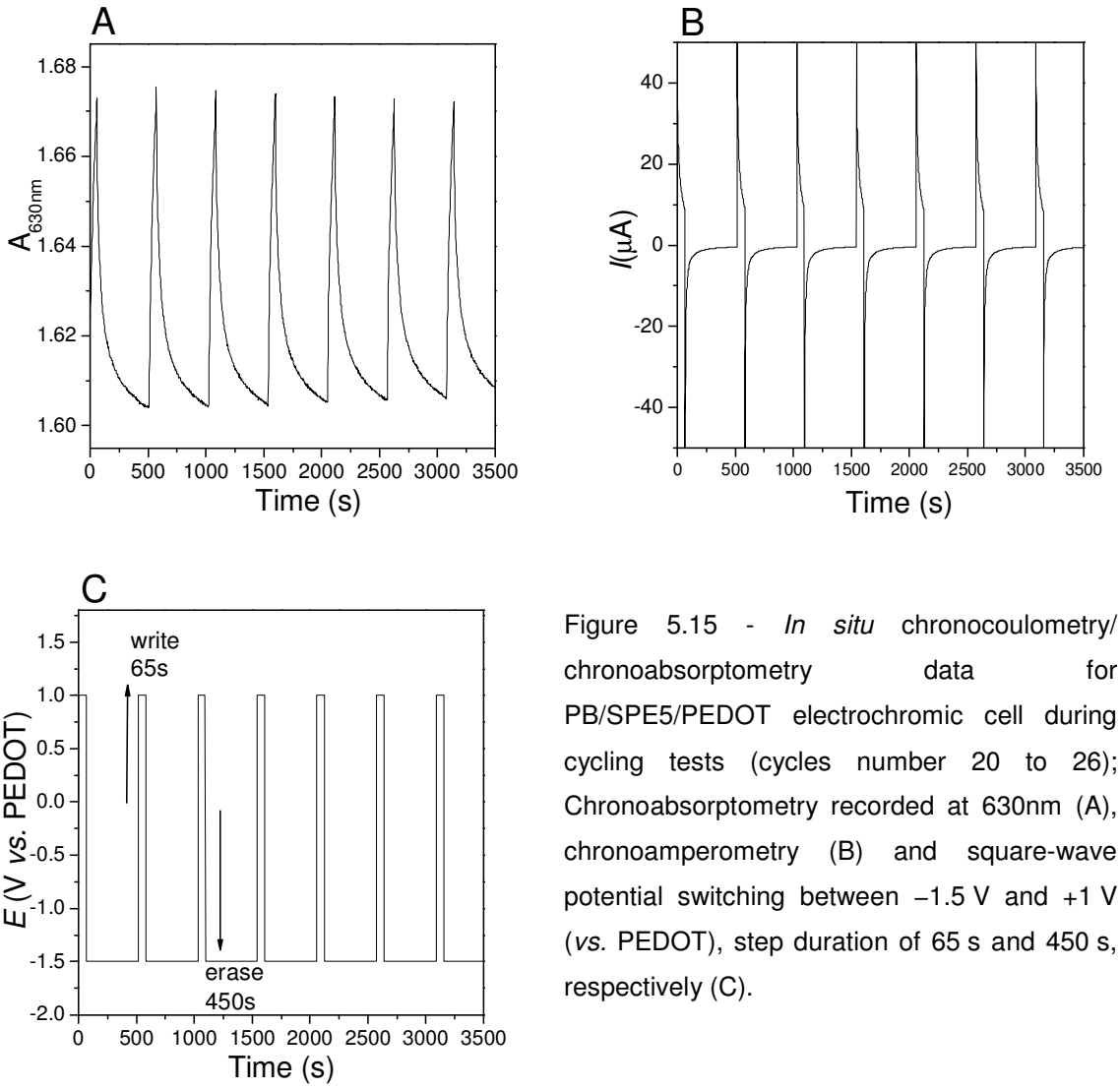

Figure 5.15 - *In situ* chronocoulometry/ chronoabsorptometry data for PB/SPE5/PEDOT electrochromic cell during cycling tests (cycles number 20 to 26); Chronoabsorptometry recorded at 630nm (A), chronoamperometry (B) and square-wave potential switching between –1.5 V and +1 V (*vs.* PEDOT), step duration of 65 s and 450 s, respectively (C).

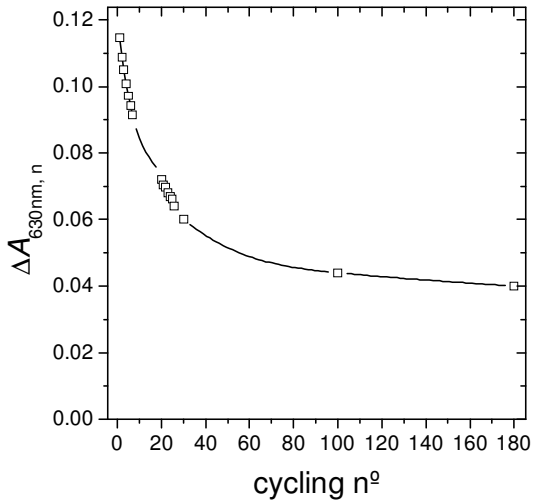

Figure 5.16 – The total ΔA at 630nm during the write-erase cycling test of the PET/ITO/PB/SPE5/PEDOT/ITO/PET.

5.4 General Conclusions

The clear and opaque gel electrolyte presented fluid characteristics appropriate to assemble electrochromic devices with coating techniques. The easy film formation properties and high adhesion to the PET-ITO modified electrodes were found to improve the performance and appearance of the devices. The fluidity of the gel allows to pour the electrolyte over the electrodes surface easily and in a short period of time a sticky gel is formed. The electrolyte film does not flow when the electrode is tilted. It shows also strong adhesion properties which helped to assemble the electrochromic device. The only drawback found working with the gel electrolyte is the necessity that edges of the device have to be perfectly sealed. When pressure is applied over the sticky gel electrolyte film it will deform and leak through unsealed edges.

The gel electrolyte electrochemical stability was adequate for ECD assembled in this study, however still far from that presented by SPE. The ionic conductivity of the gel electrolyte showed a linear increase with the concentration of lithium salt until a maximum is reached at *ca.* 4% of salt. After this point, further addition of salt did not result in an increase of the ionic conductivity and the equivalent conductivity shows a decrease. Optimum mass proportions of solvent, polymer and salt of 67:27:4 showed an ionic conductivity in the order of 10^{-2}Scm^{-1}.

Design of opaque electrolyte layers allows to use the same electrochromic material at both electrodes of the ECD – symmetric ECD. The application of identical electrochromic material and film in both electrodes has shown to improve the ECD performance. Identical electron and ion transfer kinetics in both ECD electrodes seems to reduce undesirable hysteresis through the ECD and consequently premature failure.

We devised a simple strategy to assess the influence of different ionic conductivities of the electrolyte layer on the ECD's; performed at three different levels: coloration efficiency, switching times and cycling stability.

Optical contrast and cycling stability was found to be strongly influenced by the ionic conductivity of the electrolyte layer. ECD assembled with a high conductor electrolyte layer (ECD-2) showed an improved stability in comparison to ECD assembled with a low conductor electrolyte layer (ECD-1). In addition, the optical contrast was improved. These results are related with the different salt content in both electrolytes.

ECD-1 and ECD-2 showed a linear variation of the reflectance values when switch potential is applied reaching a saturation point. ECD-1 showed approximately the same optical transition rate during the first moments of the optical transition (*ca.*200-300ms after the potential trigger). After this period both devices start to be diffusion dependent and reflectance value is constant until the end of the colouration step. It was also found ECD-1 does not spend as much charge as the ECD-2 to complete a full optical switch. Coloration

efficiency showed to be influenced by the ionic conductivity of the electrolyte. ECD-2 seems to spend more current in processes that are no contributing to optical variation. Consequently these devices present lower CE.

The electrochemical stability of solid polymer electrolytes, based on p(TMC)/PEO interpenetrating networks doped with lithium perchlorate electrolytes prepared from these blends, is considered adequate for applications in a variety of technological devices. Prototype electrochromic devices were successfully cycled between the light and dark blue shades of the bleached and coloured states, respectively, corresponding to the optical transitions for the Prussian blue and PEDOT electrochromic layers. When subjected to short cycling times, the devices show rather poor stability, with the exception of those based on SPE1 and SPE4. Cycling tests performed at larger ΔA variations for the electrochromic cell based on SPE5 show unexpected behaviour when compared to other studies in the literature, where only a decay of the ΔA values was observed.

The attempt to reduce the time needed to perform a large number of cycling tests failed. The stability observed for the SPE5 during the short cycling stability tests were completely different from the stability cycling test performed at a higher interval of applied potential. The electrochromic device showed an accelerated decrease of the optical contrast when subjected to cycling tests with longer intervals.

These results show the importance of carrying out extended cycling tests using *in situ* spectroscopic data—spectroelectrochemistry. Further studies should be carried out to determine the cause of the low cycling stabilities of SPE3, SPE5 and SPE6 and to clarify the stability behaviour during the full cycle test of cells based on SPE1, SPE2 and SPE4.

5.5 Bibliography

1. Zoski, C. G., *Handbook of electrochemistry*. Elsevier: Amsterdam, 2007.
2. Moore, W. J., Physical chemistry. 4th ed.; Longmans: London, 1966.
3. Kobayashi, N.; Miura, S.; Nishimura, M.; Goh, Y., Gel electrolyte-based flexible electrochromic devices showing subtractive primary colors. *Electrochimica Acta* 2007, *53* (4), 1643-1647.
4. Meyer, W. H., Polymer electrolytes for lithium-ion batteries. *Advanced Materials* 1998, *10* (6), 439-448.
5. Vidinha, P.; Lourenco, N. M. T.; Pinheiro, C.; Bras, A. R.; Carvalho, T.; Santos-Silva, T.; Mukhopadhyay, A.; Romao, M. J.; Parola, J.; Dionisio, M.; Cabral, J. M. S.; Afonso, C. A. M.; Barreiros, S., Ion jelly: a tailor-made conducting material for smart electrochemical devices. *Chemical Communications* 2008, (44), 5842-5844.
6. Monk, P. M. S.; Mortimer, R. J.; Rosseinsky, D. R., Electrochromism and electrochromic devices. Cambridge University Press: Cambridge, 2007.
7. Monk, P. M. S., The viologens: physicochemical properties, synthesis and applications of the salts of 4,4'-bipyridine. John Wiley and Sons: Chichester, 1998.
8. Wedler, G., Manual de química físi*ca.* 4th ed.; Wiley-VCH: Weinheim, 1997.
9. Gray, F. M., Solid polymer electrolytes. Fundamental and technological applications. Wiley-VCH: Weinheim, 1991.
10. Kuo, T. H.; Hsu, C. Y.; Lee, K. M.; Ho, K. C., All-solid-state electrochromic device based on poly(butyl viologen), Prussian Blue, and succinonitrile. *Solar Energy Materials and Solar Cells* 2009, *93* (10), 1755-1760.
11. Reiche, A.; Steurich, T.; Sandner, B.; Lobitz, P.; Fleischer, G., Ion-transport in gel electrolytes. *Electrochimica Acta* 1995, *40* (13-14), 2153-2157.
12. Song, J. Y.; Wang, Y. Y.; Wan, C. C., Review of gel-type polymer electrolytes for lithium-ion batteries. *Journal of Power Sources* 1999, *77* (2), 183-197.
13. Croce, F.; Appetecchi, G. B.; Persi, L.; Scrosati, B., Nanocomposite polymer electrolytes for lithium batteries. *Nature* 1998, *394* (6692), 456-458.
14. Gadjourova, Z.; Andreev, Y. G.; Tunstall, D. P.; Bruce, P. G., Ionic conductivity in crystalline polymer electrolytes. *Nature* 2001, *412* (6846), 520-523.
15. Arico, A. S.; Bruce, P.; Scrosati, B.; Tarascon, J. M.; Van Schalkwijk, W., Nanostructured materials for advanced energy conversion and storage devices. *Nature Materials* 2005, *4* (5), 366-377.

16. Kreuer, K. D.; Paddison, S. J.; Spohr, E.; Schuster, M., Transport in proton conductors for fuel-cell applications: Simulations, elementary reactions, and phenomenology. *Chemical Reviews* 2004, *104* (10), 4637-4678.
17. Wang, P.; Dai, *Q.*; Zakeeruddin, S. M.; Forsyth, M.; MacFarlane, D. R.; Gratzel, M., Ambient temperature plastic crystal electrolyte for efficient, all-solid-state dye-sensitized solar CeN. *Journal of the American Chemical Society* 2004, *126* (42), 13590-13591.
18. Bruce, P. G.; Vincent, C. A., Polymer electrolytes. *Journal of the Chemical Society-Faraday Transactions* 1993, *89* (17), 3187-3203.
19. Tarascon, J. M.; Armand, M., Issues and challenges facing rechargeable lithium batteries. *Nature* 2001, *414* (6861), 359-367.
20. Saunier, J.; Alloin, F.; Sanchez, J. Y., Electrochemical and spectroscopic studies of polymethacrylonitrile based electrolytes. *Electrochimica Acta* 2000, *45* (8-9), 1255-1263.
21. Watanabe, M.; Nagano, S.; Sanui, K.; Ogata, N., Ion conduction mechanism in network polymers from poly(ethylene oxide) and poly(propylene oxide) containing lithium perchlorate. *Solid State Ionics* 1986, *18-9*, 338-342.
22. Goodenough, J. B.; Kim, Y., Challenges for rechargeable Li batteries. *Chemistry of Materials* 2010, *22* (3), 587-603.
23. Wang, Y. M., Recent research progress on polymer electrolytes for dye-sensitized solar cells. *Solar Energy Materials and Solar Cells* 2009, *93* (8), 1167-1175.
24. Sekhon, S. S.; Deepa; Agnihotry, S. A., Solvent effect on gel electrolytes containing lithium salts. *Solid State Ionics* 2000, *136*, 1189-1192.
25. Sekhon, S. S., Conductivity behaviour of polymer gel electrolytes: role of polymer. *Bulletin of Materials Science* 2003, *26* (3), 321-328.
26. Tarascon, J. M.; Gozdz, A. S.; Schmutz, C.; Shokoohi, F.; Warren, P. C., Performance of Bellcore's plastic rechargeable Li-ion batteries. *Solid State Ionics* 1996, *86-8*, 49-54.
27. Panyukov, S.; Rabin, Y., Statistical physics of polymer gels. *Physics Reports-Review Section of Physics Letters* 1996, *269* (1-2), 1-131.
28. *XII International Symposium on Polymer Electrolytes* [Online]. Available: http://www.chimi*ca*.unipd.it/ispe12/ [Accessed July 2010].
29. Perrin, D. D.; Armarego, W. L. F., Purification of laboratory chemicals. Pergamon Press: New York, 1988.
30. Wright, M. R., An introduction to aqueous electrolyte solutions. Wiley: Chichester, 2007.

31. Witzke, H.; Schnatterly, S. E. 1974. *Symmetrical electrochromic cell*. United States of America patent application 384,052.
32. Lin, T. H.; Ho, K. C., A complementary electrochromic device based on polyaniline and poly(3,4-ethylenedioxythiophene). *Solar Energy Materials and Solar Cells* 2006, *90* (4), 506-520.
33. Tung, T. S.; Ho, K. C., Cycling and at-rest stabilities of a complementary electrochromic device containing poly(3,4-ethylenedioxythiophene) and Prussian Blue. *Solar Energy Materials and Solar Cells* 2006, *90* (4), 521-537.
34. Deepa, M.; Awadhia, A.; Bhandari, S.; Agrawal, S. L., Electrochromic performance of a poly(3,4-ethylenedioxythiophene) - Prussian Blue device encompassing a free standing proton electrolyte film. *Electrochimica Acta* 2008, *53* (24), 7266-7275.
35. Sindhu, S.; Rao, K. N.; Gopal, E. S. R., Comparison of performance parameters of poly(3,4-ethylenedioxythiophene) (PEDOT) based electrochromic device on glass with and without counter electrode. *Bulletin of Materials Science* 2008, *31* (1), 15-18.

Chapter 6

Paper, textile and white board ECD

6.1 Motivation

Chromogenic systems are good candidates to develop smart objects. In chapter 1, several examples of commercially available products based on chromogenic systems are described. Photochromism and thermochromism present a spontaneous response to light and temperature, respectively. The development of displays requires chromogenic systems that are controlled on command and not spontaneously.

Photochromic and thermochromic systems are dependent on ambience conditions. Considering a thermochromic product designed to interact with the body temperature, such system should have a threshold in the range of temperature between 30 to 40ºC. Depending on the ambience temperature, such system could be triggered by the action of a purposeless stimulus. Similar interferences take place between photochromic systems and light ambience factors.

Electrochromic devices present a linear behaviour at different operating range of temperature and light conditions.[1] ECD's are relatively isolated systems and are triggered by a non-ambience dependent stimulus. Electrochromism shows appropriate characteristics to be applied on the development of displays.

Commercial or almost in the market electrochromic displays are based on plastic electrodes (PET-ITO) showing monochromatic optical transitions. A great effort has been done to develop electrochromic displays with improved lifetime, contrast ratio, switch time, flexibility and colour gamut. Nevertheless, switch rates are still too low to display video and the colours presented are limited; as reported in section 1.2.1 (Commercial applications) all the commercial electrochromic displays show colour transitions between blue and uncoloured (NTera technology) or light blue (PaperDisplay technology).

Although ECD shows several advantages for programmable interactive systems, electrochromic materials require a more complex architecture when compared with the photochromic and thermochromic materials. A photochromic or thermochromic ink can be easily coated as a unique functional layer over almost any surface. In opposite to photochromic and thermochromic systems, an electrochromic system requires a minimum of five active layers to be functional (see section 1.2.1 Electrochromic devices).

Actual electrochromism technology development is focused on plastic electrodes, *e.g.* PET-ITO electrodes, and no alternatives are available. YDreams aims to produce ubiquitous electrochromic displays for mass markets like paper, textile and white boards. The strategy to reach such objective is the integration of the technology with daily life products such as paper, textiles and white boards.

Paper

The application of paper in our daily life is vast and used in packaging, printing and writable substrate, and in sanitary products. Paper is a cheap and largely available product showing interesting physical properties which makes it an attractive product for several industries; and it is recyclable. Moreover, it is as visual information vehicle that is used over two millennia. Since its invention paper industry has achieved better physical characteristics and ink reception capabilities for printing purposes. Recent technologies such as nanotechnology and bioengineering have been used to obtain paper with a better white appearance and increased resistance to traction and ink reception capabilities. However, the paper product concept remains unchanged since its origin.

Paper is actually the best and cheapest display man has ever made, it shows high contrast, easy viewing, and wide range of angle viewing, very flexible, lightweight, low-power consumption and relatively stable. Those are the main reasons why paper is so widely used. Nevertheless, industry and society are always seeking for new functionalities and this is true for paper products.

Printed paper information is immutable. Information once recorded cannot be reversibly erased or modified. The challenge is how to create a paper where the printed ink can be reversibly modified or reversibly erased.

Several Paper-like displays have been developed since more than a decade. Applications are found for intelligent cards, digital signatures, billboards, electronic labels, clocks, calculators or mobiles. Actual state-of-the-art of paper-like displays is based on electrophoretic particles from E-Ink corp. and electrochromism from NTera and ACREO. All these products, however, are based on plastic substrates (E-Ink and NTera) or plastic coated paper substrates (ACREO) and not on raw paper.

Textile for clothing

The tendency to integrate data processing systems in items of clothing has been explored since the early 80's by Steve Mann.[2] The wearable computing concept is explored by engineers, designers and artists to develop ways to worn your personal computer. A good example of a wearable computing product is the calculator watch.[3] Approaches to develop wearable computers are based on attached devices like computer processor unit, display and some other interfaces like sensors on clothes. Real embedded systems have not been developed and several examples of wearable computers show bulky LCD and LED displays directly sew into the clothes. Prototypes are not of practical use than for demonstration purposes. This approach moves itself away from a true concept of fusion between the computer and the fabric, while the interactive component continues separated of the fabric.

White Boards

The white board is an essential instrument for group communication due to its intuitive way to present or support a message. Visual communication boards are present in any office or meeting room. Several visual communication board models are available in different colours, formats and sizes; however, they all show the same basic function.

Introduction of digital technology is used to develop the so called “Smart Boards”. This new kind of white boards allows the projection of virtual information and to record the information written on the board in a digital format. Nevertheless, Smart Boards did not successfully substitute the traditional white boards. The major drawback found was its complexity. The entire system contains several units - projectors, image trackers and computer - and requires alignment and correct positioning of the projector and the board. Another kind of technological solution was explored using embedded LCD displays in the boards. This solution was also not successful due to the high cost and size limitations.

Industry is seeking for new ways to innovate and re-invent their products. Science and Technology create new opportunities through the development of smart materials and systems. Such driving forces create a synergetic effect towards ubiquitous computing concepts. As already discussed electrochromism phenomena is one of the most promising ways to add interactivity to objects; however, actual state-of-the-art electrochromic devices are far from real integration with our daily-life products.

Embedded low information content displays was the main motivation which led YDreams in collaboration with Univ. Nova de Lisboa and other Portuguese industrial partners to start three applied research and development projects; “YInvisible-Papel”, “YInvisible-Textil” and “YInvisible-Quadros”. These projects were executed in the framework of the “IDEIA” programs coordinated by the Portuguese Innovation Agency (ADI). The objective was to obtain proofs of concept of electrochromic devices based on paper, textile and white boards. The following chapter presents an overview of the results obtained in YInvisible-Papel, YInvisible-Textil and YInvisible-Quadros projects that correspond to the work developed with paper, textile and visual communication boards, respectively. The Portuguese industrial partners that participated were RENOVA (Paper industry), Filobranca (Textile industry) and Bi-Silque (Visual Communication Boards industry). The scientific groups belong to the Fac. Ciências e Tecnologia of the Univ. Nova de Lisboa, Photochemistry and Supramolecular Group (FOT group) and CENIMAT. FOT group belongs to the green chemistry network REQUIMTE associate laboratory and CENIMAT is a research centre from the material engineering department, belong to I3N associate laboratory. Finally, YDreams was the consortium leader and responsible for the electronic integration and for the interactivity concepts.

6.2 Strategy and project execution organization

The IDEIA projects YInvisible-Papel, YInvisible-Textil and YInvisible-Quadros were organized in work packages in which one of the partners was the principal leader and responsible for execution. In Fig. 6.1, the global work pipeline with the respective responsible partner is presented.

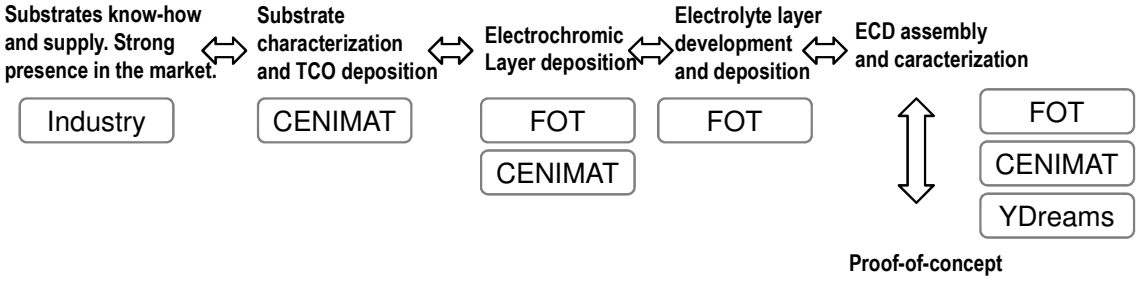

Figure 6.1 – Schematic plan of the pipeline of the applied R&D work executed during the IDEIA projects, YInvisible-Papel, YInvisible-Textil and YInvisible-Quadros.

The industrial partners were responsible to supply the rest of the team with sets of samples of the materials they use to manufacture their products. In Table 6.1, the most representative materials used during the projects are listed.

Table 6.1 – Raw materials used in each industry, RENOVA, Filobranca and Bi-Silque

Industrial Partner	Raw Materials/Products
RENOVA	Copy Paper (with different thicknesses)
	Kraft
	Tracing Paper
Filobranca	Textile (cotton)
	Textile coated with a silicon layer
Bi-Silque	Resin coated Ceramic over an Aluminium foil
	High-Pressure-Laminate (FORMICA)

The industrial partners contributed also with their large expertise on the materials used in the respective industries, paper, textile and white boards. All the partners are major players in both the national and the international markets.

The first and one of the most challenging problems to solve within the project was to modify the electrical characteristics of the substrates. All the substrates used have a high electrical resistance and are known as electrical insulators. CENIMAT group was responsible to deposit successfully a transparent conductive oxide (TCO) layer over the supplied substrates – substrate-electrode. Raw industrial materials presented non-ideal surface characteristics such as: highly porosity, roughness and thermal sensitivity.

The electrical conductive layer was successfully deposited over paper and Bi-Silque white board substrates. In contrast, the textile electrodes obtained were highly unstable. Initial electrical conductivity of the prepared electrodes was acceptable, although they lost conductivity and became resistive over a short period of time. The reason for such behaviour was not unveiled; although, a straightforward explanation could be that the high flexibility of the textile structure would easily break the conductive paths of the entire electrode surface. Other approaches were used to overcome this problem. Textiles coated with a silicon layer, usually used to print motives over the textile, were used as electrode substrate and commercially available conductive fabrics as an intrinsic conductive fabric electrode (Flectron N).

Electrodes based on white board materials from Bi-Silque were obtained based on the same strategy used with the previous materials. The CENIMAT group deposited TCO layer over two different kinds of laminated boards: ceramic laminated over an aluminium foil and FORMICA™. These materials were the less challenging due to its non-porous surface characteristics. Despite the excellent conductivities obtained with the TCO deposition over the ceramic/aluminium laminated board oxidation of the aluminium material occurs during electrochemical tests. The ceramic layer should act as an electrical barrier between the aluminium foil and the deposited TCO. However, it was found that electrical contact was established between the two materials due to structural defects created during the TCO deposition. Electrochemical tests with these electrodes lead to full oxidation and dissolution of the aluminium foil.

After the development and production of the substrate-electrodes by the CENIMAT group the following tests were performed by the FOT group: electrochromic layer deposition and electrochemical characterization, development of a convenient electrolyte and finally electrochromic device assembly and test.

In Table 6.2 the selected substrate-electrodes used in our studies are listed.

Table 6.2 – Electrode substrates used during the IDEIA projects

Industrial Partner	Electrode substrate
RENOVA	Tracing paper
Filobranca*	Textile coated with a silicon layer
Bi-Silque	High-Pressure-Laminated board

Additionally to the textile electrodes obtained from Filobranca materials intrinsically conductive fabric was used for comparative and alternative study.

During the two year project a large amount of knowledge and experience of working with raw materials was generated within the partners. Scientific and technological knowledge was successfully transferred to the industrial partners as the industrial knowledge was also successfully transferred to the scientific partners. The main work developed within the framework of my Ph.D. thesis was the development of ECD based on paper, textile and white board electrodes using the architecture shown in Fig. 6.2. As already mentioned the electrodes were fabricated by our project partner CENIMAT, and my work is downstream to it. The following subchapter will resume the results obtained concerning only the work developed in the FOT group.

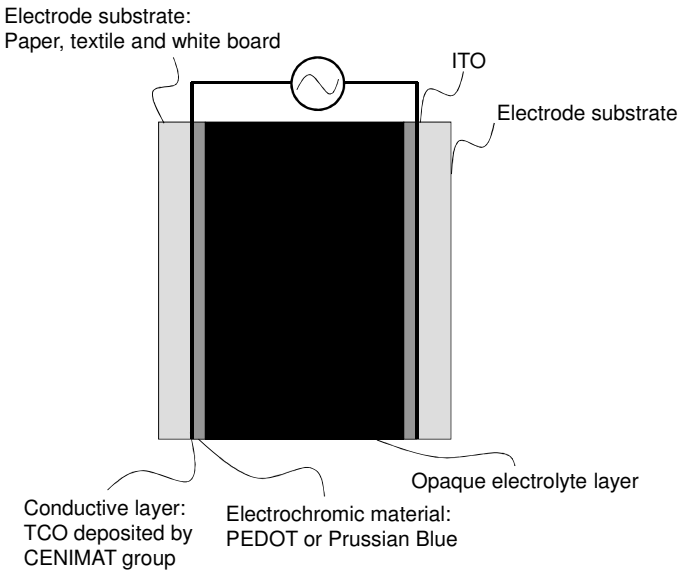

Figure 6.2 – Schematic view of the symmetric ECD model for the IDEIA projects.

6.3 Results and Discussion

All the substrate-electrodes received from CENIMAT were prepared with electrical wires to make the electrical contact with the electrochemical apparatus connectors easier (Fig.6.3).

Figure 6.3 – Substrate-electrode preparation with an electrical contact. Cupper electrical wires were connected to the TCO layer through conductive silver glue (left, textile-electrode sample). After the silver glue is dried epoxy glue is used to seal and give structure to the contact between electrical wire and the substrate-electrode (right, white board-electrode sample).

6.3.1 Electrochromic layer

Two well known electrochromic materials were explored: Prussian Blue (PB) and PEDOT:PSS (PEDOT). The substrate-electrodes tested during the entire project are listed in Table 6.2.

Prussian Blue

PB films were electrodeposited by electrochemical potentiostatic technique. In Table 6.3 the general experimental details are presented.

Table 6.3 – Prussian Blue electrodeposition experimental conditions

Electrochemical deposition method	Potentiostatic
Electrodeposition solution	$FeCl_3.6H_2O$ (5mM) and $K_3[Fe(CN)_6]$ (5mM).
Deposition time (s)	300 to 600
Voltage (V *vs.* SCE)	0.55
Reference electrode	SCE
Counter electrode	Pt
Working electrode	Substrate-electrode
Supporting electrolyte	KCl (1M) in water

In general, the PB deposition obtained over the paper-electrode, textile-electrode and FORMICA-electrode where highly heterogeneous. The PB modified paper and textile-electrodes present small areas covered by the electrochromic material, approximately less than 30% of the electrode area.
The best result was obtained with the PB modified FORMICA-electrodes, see Fig. 6.4.

Figure 6.4 – Prussian Blue film electrochemically deposited over a TCO coated white board (white board electrode). The PB films are highly heterogeneous in all the electrode-substrates tested.

The electrochromic activity of all the PB modified substrate-electrodes was tested by cyclic voltammetry (see experimental details in Table 6.4). In Fig.6.5 a picture of the electrochemical cell with the PB modified FORMICA-electrode is shown.

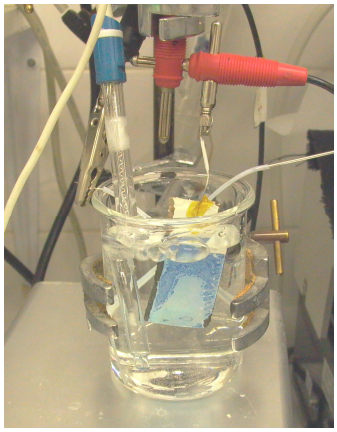

Figure 6.5 – Picture of the three electrodes electrochemical cell. Working electrode is the PB modified FORMICA-electrode, counter-electrode is a platinum wire and reference electrode is a SCE electrode.

Table 6.4 – Electrochromism test of the PB layers by cyclic voltammetry, experimental details

Electrochemical method	Cyclic voltammetry
Scan rate	10mV/s
Potential interval limits	[-0.2V; 0.6V] (*vs.* SCE)
Reference electrode	SCE
Counter electrode	Pt
Working electrode	PB modified substrate-electrode
Supporting electrolyte	KCl (1M) in water

Cyclic voltammograms of all the PB films tested did not present any significant electrochemical signal; and consequently no electrochromic behaviour could be observed for the PB modified substrate-electrodes.

PEDOT

Commercially available aqueous formulation of a mixture of poly(ethylenedioxythiophene) and poly(styrene sulfonate) (PEDOT:PSS) was used as the electrochromic layer. Several deposition techniques were explored to deposit an uniform layer of PEDOT:PSS over the paper-, textile- and FORMICA-electrodes: drip coating, blade coating, spin-coating and brush application. The PEDOT:PSS depositions were not satisfactory in terms of aesthetical aspects; however, they were used only to evaluate the possible electrochromic activity. In Fig. 6.6 PEDOT depositions over the substrate-electrodes are shown.

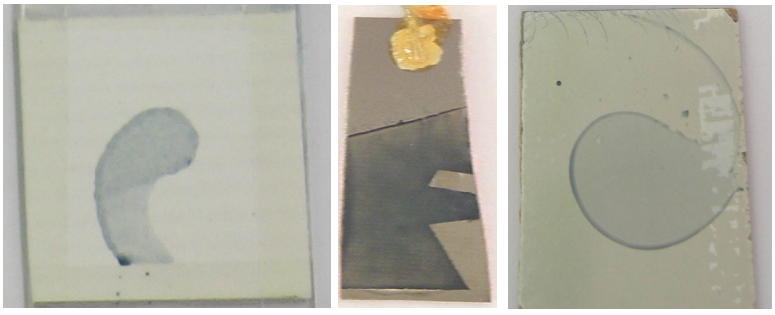

Figure 6.6 –PEDOT:PSS deposited over paper-electrode (left, by spin-coating), textile-electrode (middle, with a brush) and board-electrode (right, by spin-coating).

The PEDOT:PSS modified paper-, textile and FORMICA-electrodes showed the characteristic PEDOT:PSS optical transition between the light blue and deep blue state. Similar to PB modified electrodes electrochromism was screened using cyclic voltammetry and chronoamperometry, see Table 6.5 and 6.6 for the experimental details.

Table 6.5 - Electrochromism test of the PEDOT:PSS layers by cyclic voltammetry, experimental details

Electrochemical method	Cyclic voltammetry
Scan rate	10mV/s
Electrochemical window	[-1.5V; 1.5V] (*vs.* SCE)
Reference electrode	SCE
Counter electrode	Pt
Working electrode	PEDOT:PSS modified substrate-electrode
Supporting electrolyte	LiClO4 (0.1M) in acetonitrile

Table 6.6 - Electrochromism test of the PEDOT:PSS layers by chronoamperometry, experimental details

Electrochemical method	Chronoamperometry
Number of step potentials	2
Step potential (V *vs.* SCE)	Step 1:-1.5V and Step 2: 1.5V
Step duration (s)	10
Reference electrode	SCE
Counter electrode	Pt
Working electrode	PEDOT:PSS modified substrate-electrode
Supporting electrolyte	LiClO4 (0.1M) in acetonitrile

Contrary to the results obtained for Prussian Blue, electrochromic layers PEDOT:PSS modified substrate-electrodes present interesting electrochromic characteristics. In Fig. 6.7 the doped (oxidized state at +1.5V *vs.* SCE) and the neutral (reduced state at -1.5V *vs.* SCE) optical state of PEDOT:PSS layer deposited over paper-electrode is shown. In Figs. 6.8 and 6.9 the same behaviour is observed for PEDOT:PSS modified textile- and white board-electrode.

Figure 6.7 – Images of the optical transition of PEDOT:PSS layer deposited over the paper-electrode by electrochemical oxidation (left) and electrochemical reduction(right). See experimental details in Table 6.6.

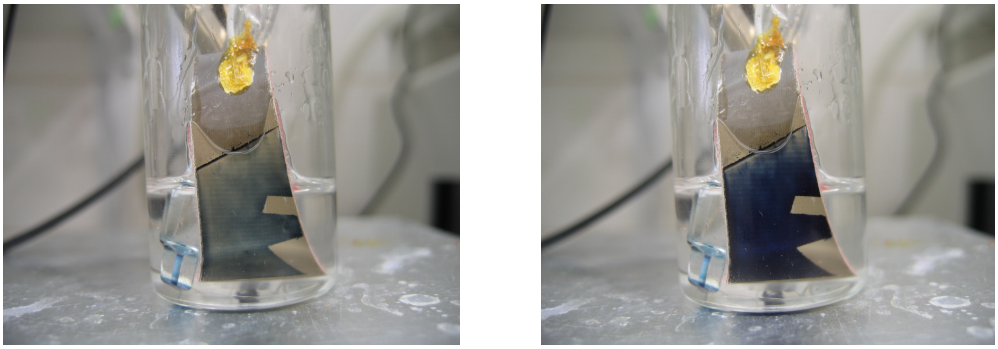

Figure 6.8 – Images of the optical transition of PEDOT:PSS layer deposited over the textile-electrode by electrochemical oxidation (left) and electrochemical reduction (right). See experimental details in Table 6.6.

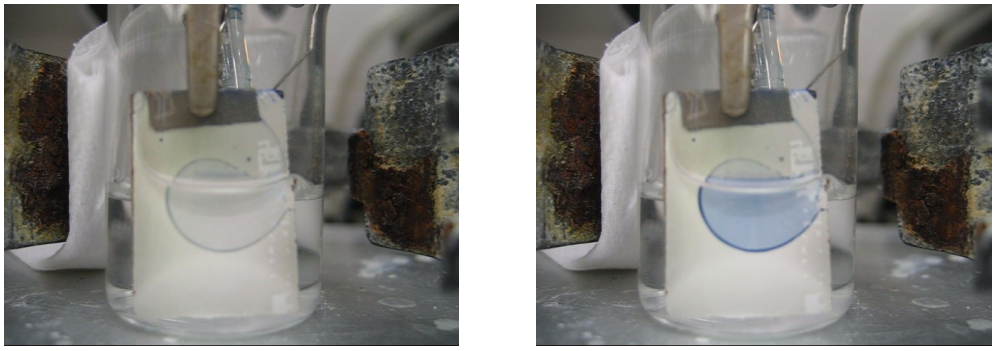

Figure 6.9 – Images of the optical transition of PEDOT:PSS layer deposited over the board-electrode by electrochemical oxidation (left) and electrochemical reduction (right). See experimental details in Table 6.6.

6.3.2 ECD Assembly with paper-, textile- and white board electrodes

The deposited PB modified substrate-electrodes did not show electrochromism when an electrical potential was applied by electrochemical methods. In contrast, the organic semiconductor PEDOT:PSS modified substrate-electrodes presented optical transition between the dark-blue and light-blue optical state.

The symmetric architecture ECD was used to produce the low information content proof-of-concept displays based on paper, textile and white board. The electrochromic material used is the PEDOT:PSS aqueous dispersion and as the electrolyte layer the opaque gel electrolyte reported in section 5.2. The requirement to have an opaque electrolyte layer to operate a symmetric ECD is discussed in section 1.2.1 (Electrochromic devices).

Paper

ECD requires that at least one of the electrodes is optically transparent. Paper, textile and white boards are opaque materials. Initially the plan to overcome this issue was to use a transparent electrode of PET-ITO as the primary electrode and the modified substrate-electrode as the counter-electrodes. This strategy was used initially to assemble all the ECD; however, later results obtained with tracing paper-electrodes ECD show that the transparency of the substrate was high enough to see the optical contrast of the PEDOT layer.

The deposition of TCO over the tracing paper produced the most stable substrate-electrodes, and exhibits a relative transparency to the visible light. Tracing paper is used to take tracing from drawings and for this reason it is chemically modified to obtain a translucent paper. These properties allow to assemble an ECD where the information is printed over the paper-electrode (primary electrode) and the PET-ITO modified electrode is used as counter-electrode. The transparency of the tracing paper was enough to see the deposited PEDOT:PSS optical transition through it.

The electrochromic cells were assembled depositing a non patterned layer of PEDOT:PSS over the counter-electrode and a patterned layer of PEDOT:PSS over the primary electrode. The electrolyte layer was drip-coated over one of the PEDOT:PSS modified electrodes and finally both electrodes were laminated (cell assembly is similar to the one reported in section 5.2.1.4).

Deposition of a patterned PEDOT:PSS layer over the PET-ITO electrodes was printed using the photolithography process with the facilities and know-how of CENIMAT team. A combination of spin-coating deposition and patterning with the photolithography process was used. In the particular case of paper based devices the paper-electrode was used as the primary electrode, the patterned PEDOT:PSS layer was printed by ink-jet. Details on the development of ink-jet printing to build ECD are given in chapter 7.

Electrochromic cells were successfully assembled using the PEDOT:PSS modified paper-electrodes as the counter-electrode (see Fig.6.10) and as the primary electrode (see Fig.6.11). The applied potentials used to operate all the devices were -1.5V and +1.5V (*vs.* the PEDOT:PSS modified substrate-electrode).

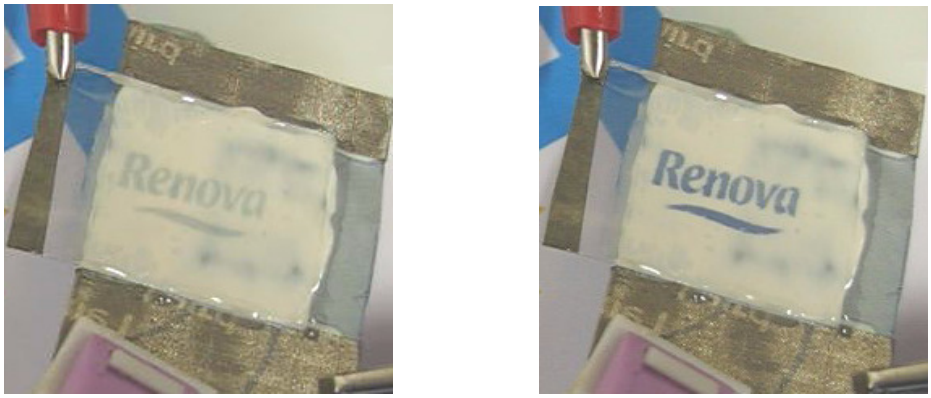

Figure 6.10 – Pictures of the bleached (left) and coloured (right) optical transition of an ECD based on PEDOT:PSS modified paper-electrode. Electrochromic device architecture: Paper-electrode/PEDOT:PSS/white opaque electrolyte/PEDOT:PSS/ITO-PET, where the primary electrode is the PET-ITO.

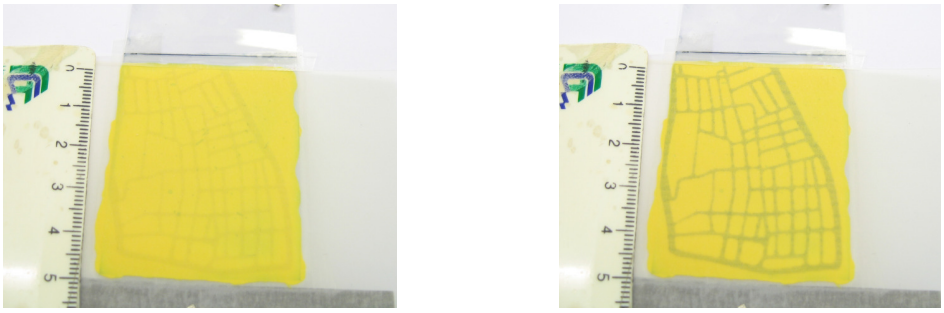

Figure 6. 11 - Pictures of the bleached (left) and coloured (right) optical transition of an ECD based on PEDOT:PSS modified paper-electrode. Electrochromic device architecture: Paper-electrode/PEDOT:PSS/yellow opaque electrolyte/PEDOT:PSS/ITO-PET, where the primary electrode is the paper-electrode.

Textile

As discussed above the textile substrate was the most challenging to obtain a electrical conductive surface by the deposition of a TCO layer. Nevertheless ECD with a textile coated with a layer of silicon were assembled. To achieve the goals of the project an alternative conductive textile was acquired to the Less EMF company. The trade name of the intrinsic conductive textile is Flectron N. The devices were assembled as described for ECD based on paper-electrodes. Electrochromic cells were successfully assembled using the PEDOT:PSS modified textile-electrodes as the counter-electrode with a silicon layer coated over the textile (see Figs.6.12) and with Flectron N textile (see Fig. 6.13). The applied potentials used to operate all the devices were -1.5V and +1.5V (*vs.* the PEDOT:PSS modified substrate-electrode).

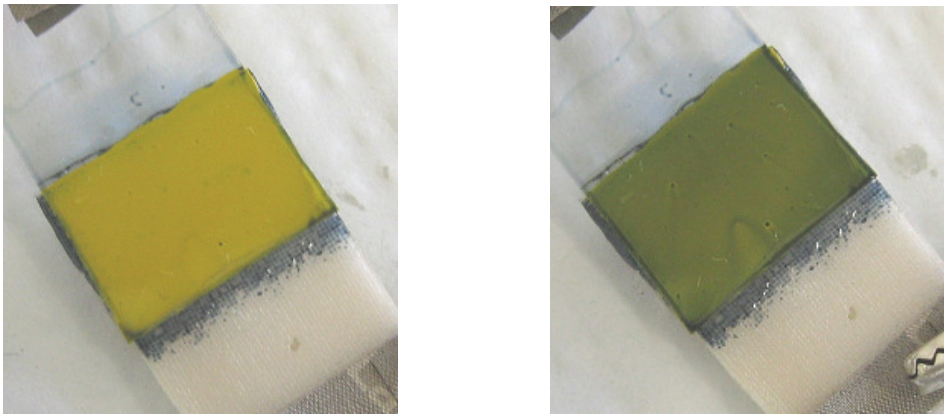

Figure 6.12 - Pictures of the bleached (left) and coloured (right) optical transition of an ECD based on PEDOT:PSS modified textile silicon coated-electrode. Electrochromic device architecture: Textile silicon coated-electrode/PEDOT:PSS/yellow opaque electrolyte/PEDOT:PSS/ITO-PET where the primary electrode is the PET-ITO.

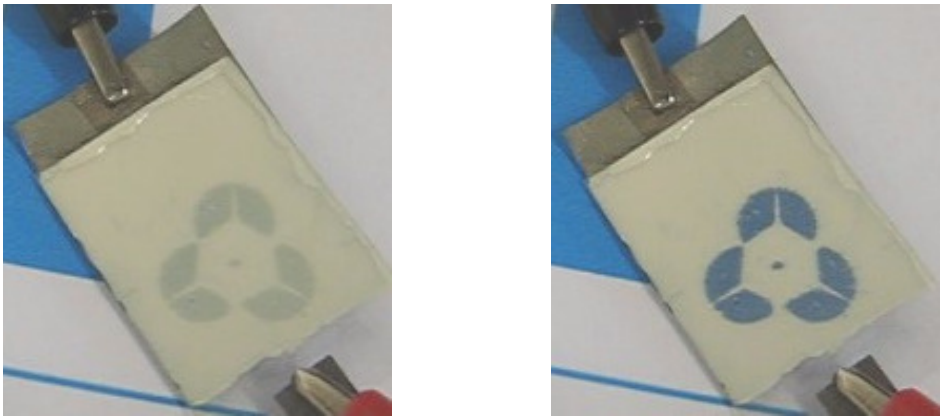

Figure 6.13 - Pictures of the bleached (left) and coloured (right) optical transition of an ECD based on PEDOT:PSS coated Flectron N conductive textile. Electrochromic device architecture: Conductive textile-electrode/PEDOT:PSS/white opaque electrolyte/PEDOT:PSS/ITO-PET, where the primary electrode is the PET-ITO.

The high electrical conductivity of the Flectron N textile improved significantly the speed of write-erase transition when compared with all the others devices (paper, textile (cotton) and white board).

White Board

The FORMICA™ based electrodes were preferred to build the white boards ECD instead of the ceramic laminated over an aluminium foil. The physical defects created during TCO deposition over the ceramic layer creates short-circuit between the TCO layer and the aluminium foil (see section 6.3.1). All the white board ECD were assembled using the PEDOT:PSS modified

white board (FORMICA)-electrodes as the counter-electrode (see Fig.6.14). The applied potentials used to operate all the devices were -1.5V and +1.5V (*vs.* the PEDOT:PSS modified substrate-electrode).

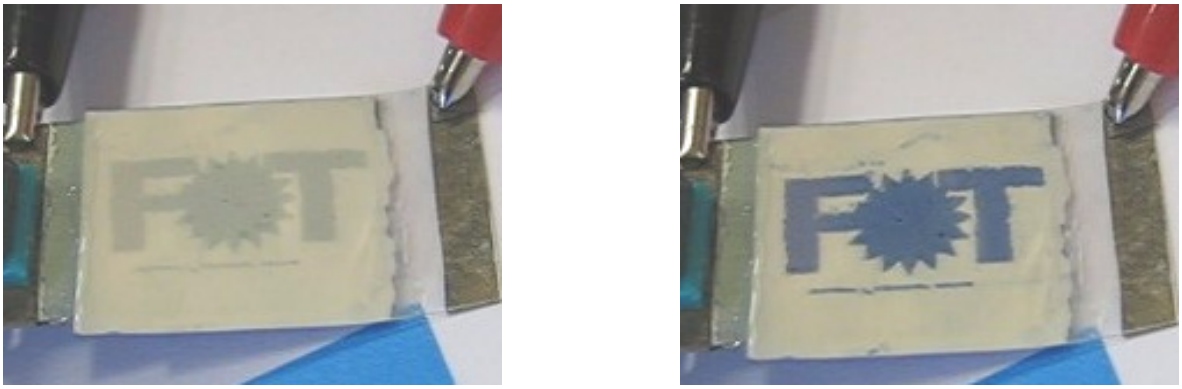

Figure 6.14 – Pictures of the bleached (left) and coloured (right) optical transition of an ECD based on PEDOT:PSS modified white board-electrode. Electrochromic device architecture: White board-electrode/PEDOT:PSS/white opaque electrolyte/PEDOT:PSS/ITO-PET.

6.3.3 ECD characterization

The ECD based on paper-, textile- as well as white board-electrodes were characterized by spectroelectrochemistry. Stability of the devices was studied by cycling tests between the coloured and bleached state (write-erase). During this characterization the paper based ECD were assembled using the paper-electrode as the primary electrode (see an example in Fig. 6.11).

A square-wave potential function was applied to the ECD between -1.5V and +1.5V (potentials are reported versus the PEDOT:PSS modified substrate-electrodes). The time required to complete a write-erase process for each ECD is different being the faster the ECD using Flectron N and all the other devices present the same switch time. In Table 6.7 the experimental details of the cycling tests and the total reflectance variation ($\Delta\%R_{630nm,0}$) for each device are shown.

Table 6.7 – Performance of the ECD based on Paper, textile and white board

ECD	Coloration Time (s)	Bleaching Time (s)	$\Delta\%R_{630nm,0}$
Flectron N	3	3	66
Textile silicon coated	10	10	70
White board	10	10	30
Paper	10	10	16

The optical contrast found across all the devices was satisfactory, the highest value being found for the textile-ECD and the smallest for paper-ECD (see Table 6.7). The high optical contrast obtained with the textile based devices can be explained by the capacity of the porous textile substrate to absorb larger quantities of electrochromic material. In this case, the primary electrode will not be limited by the counter-electrode electroactive material. On the other hand, the low $\Delta\%R_{630nm,0}$ found for paper-ECD is related with the low transmittance of the tracing paper and dispersion of light by diffuse reflectance. Despite the relative transparency of the paper-electrode, it is not comparable with the transparent PET-ITO.

The stability towards cycling was found to be substrate dependent. The less stable systems are those based in textile and the most stable one was the electrochromic device based on paper (see Table 6.8).

The textile coated with a silicon layer was used to overcome the instability of the TCO layer deposited over raw fabric; however the resulting textile-electrodes were not so robust than those based on paper and FORMI*CA*. The lower stability of the textile ECD was already predicted considering the textile-electrode electrical behaviour. The electrochromic devices assembled with the white board-electrodes show a moderate degradation after one thousand cycles. In contrast cycling results of the electrochromic devices based on paper-electrodes did not show any degradation after five thousand cycles. The devices showed an increase of the total reflectance of 38% when compared with the initial values.

Table 6.8 – Write-erase cycling test results for the ECD based on paper, textile and white board.

ECD	$\Delta\%R_{630nm,0}$	$\Delta\%R_{630nm,n}$	n	Colouration loss (see Eq.1.4)
Flectron N	66	37	2000	-44%
Textile silicon coated	70	55	825	-21
White board	30	29	1000	-3%
Paper	16	22	5000	+38%

Since the ECD based on paper-electrodes showed a surprising stability towards cycling, deepest analysis of the results were carried on. In Fig. 6.15 the evolution of the optical transition between coloured and bleached states (in percentage of reflectance) along the cycling test is plotted. The initial reflectance variation increases during the first one thousand cycles until it reaches a value of approximately 23%. During the next 3500 cycles the device seems to stabilize and then degradation starts to occur; a variation of -1.5% compared with the maximum value obtained during the first 1000 cycles is observed.

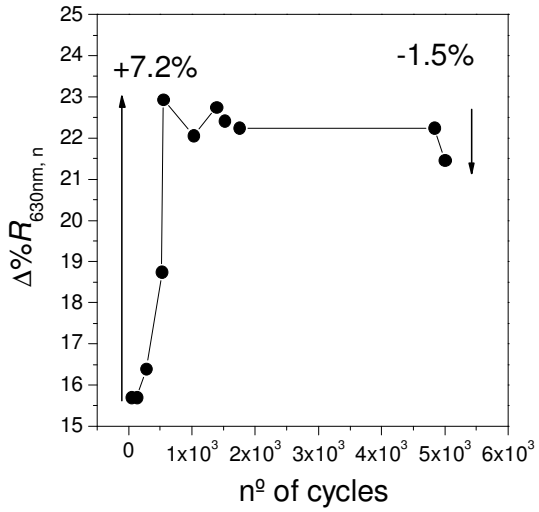

Figure 6.15 – Variation of the total optical contrast of a paper-ECD during write-erase cycling test.

Complete analysis of spectroelectrochemical data for first cycle of the paper-ECD is presented in Table 6.9.

Table 6.9 - Collected data from spectroelectrochemical experiments for paper-ECD, befor the write-erase cycles

Optical transition	Time (s)	%full switch	$\Delta\%R_{630nm,0}$	$\Delta Q'$ (Ccm^{-2})	CE ($C^{-1}cm^2$)	CR	%R
Bleaching	0	0	0	0	0	-	39.7
	4	90.0	13.6	1.5E-04	9.1E+04	-	53.3
	6	95.2	14.4	1.8E-04	8.1E+04	-	54.1
	8.4	99.2	15.0	2.0E-04	7.4E+04	-	54.7
	8.8	100.1	15.1	2.1E-04	7.3E+04	-	54.8
Colouration	0	0	0	0	0	1.9	54.0
	7.6	90.3	12.9	2.2E-04	5.9E+04	2.4	41.1
	8.8	95.2	13.6	2.4E-04	5.8E+04	2.5	40.4
	9.6	98.7	14.1	2.5E-04	5.7E+04	2.5	39.9
	10	100.0	14.3	2.5E-04	5.7E+04	2.5	39.7

The CE obtained for both colouration and bleaching process is comparable with results obtained for the symmetric electrochromic device based exclusively on PEDOT:PSS modified PET-ITO electrodes (ECD-1 and ECD-2) reported in section 5.2.2, Tables 5.4 and 5.4. As already explained the contrast ratio of the paper ECD is smaller than the devices

using PET-ITO as the primary electrode. The switch time for 90% of full switch is also longer when compared with ECD using PEDOT:PSS modified PET-ITO electrodes.

6.4 Conclusions

Low information content displays were successfully obtained using electrochromic devices based on paper-, textile- and white board-electrodes. The most challenging substrate was the raw fabric where the deposited TCO layers were highly unstable. An alternative silicon coated fabric was used as a surface treatment of the raw fabric and commercially available conductive fabrics were studied as well. The silicon coated textile improved the TCO layer stability, however, the resulting ECD demonstrated low cycling stability.

The lifetime of the ECD products will be dependent on their stability towards the number of optical cycles (write-erase). The cycling stability found for all the devices are satisfactory considering they are only proof of concept; however a real application for interactive white boards must be largely improved.

The performance obtained with the paper and textile ECD met the requirements of application in disposable products. Possible applications can be envisaged for advertisement, e.g. an interactive t-shirt for an event that only needs to last one day or a post-it with a blinking advertisement.

The switch time determined for all the substrate-electrode based ECD was longer than that observed for other ECD reported in the literature and also in chapter 5. This behaviour was expected due to the nature of the electrodes substrates and consequently the electrical properties of the conductive layer. All the ECD's reported in literature are based on non-porous electrodes, which present a more adequate surface to deposit a TCO layer. The intrinsically conductive fabric ECD present the shortest switching times. The Flectron N fabric is composed by threads covered by metallic particles showing electrical properties similar to a metallic electrode.

The transparency of the tracing paper-electrode was found to be suitable to use it as the viewing electrode in the ECD. The final architecture adopted is an inversion of the original one, proposed at the beginning of the projects (see Fig. 6.2). The tracing paper presents enough transparency to transmit the optical switch of the electrochromic PEDOT:PSS layer deposited on the opposite face. The paper-electrode structure seems to contribute to the improved cycling stability of the ECD, attained a relative degradation of 1.5% of the total reflectance optical transition.

The incorporation of a plastic layer to assemble the ECD does not meet real integration of technology and the object like: sheet of paper, a piece of clothing and white board. However, each product was differently affected by the integration of a plastic electrode as one of the constituent layer. The textile ECD is the most affected by the introduction of a plastic layer of *ca.* 125µm. Although the PET used is flexible it does not emulate the tactile and flexibility of the common fabric. For the paper ECD the application of the tracing paper allows to

assemble an electrochromic visualization unit underneath the piece of paper. However the primary electrode is the paper, the counter electrode is made of plastic. The white boards are usually coated with a plastic layer that gives the shiny aspect and allows to use the dry erasable ink; the ECD assembled with the transparent plastic electrode did not modify the visual aspect or the general surface properties of the final white board.

In Fig. 6.16 pictures of the paper-ECD proof-of-concept presented as one of the results achieved for the IDEIA project Yinvisible-Papel. The pictures show a map of Lisbon downtown. When the tourist touches the adequate flat button, the streets of the most popular neighbourhoods of Lisbon will be highlighted from the rest of the map information.

Figure 6.16 – Pictures of the proof-of-concept paper-ECD. This device shows an electrochromic map of the Lisbon downtown. The buttons on the bottom of the map will highlight a specific area of interest. The colour contrast is obtained by the electrochemical control of the coloured and bleached states of the PEDOT layer deposited over PET-ITO. The counter electrode is PEDOT coated paper-electrode. The opaque gels electrolytes used were pink (Alfama) and yellow (Bairro Alto). To power the device small flat batteries were integrated in the map.

6.5 Bibliography

1. Kobayashi, N.; Nishimura, M., Electrochromic imaging with polymer electrolyte having high-temperature-dependent conductivity. *Solar Energy Materials and Solar Cells* 2006, *90* (4), 538-545.
2. Mann, S., Wearable computing: A first step toward personal imaging. *Computer* 1997, *30* (2), 25-31.
3. *Modern living: going digital* [Online]. New York: Time, Inc. 1975 Available: http://www.time.com/time/magazine/article/0,9171,879586,00.html [Accessed July 2010].

Chapter 7

Feasibility study for an electrochromic display built by ink-jet

7.1 Introduction

In the framework of applied research, it is not enough to produce laboratory scale technology. The processes involved to produce the entire device must be adapted to an industrial scale. In chapter 6 three proofs of concept electrochromic devices were described using laboratory scale techniques. During the development of the electrochromic devices one of the major challenges found was how to pattern the electrochromic layer. Patterning is of fundamental importance, it allows to transform a display with a simple blinking square in text or pictogram information. In Fig. 7.1, an example of a non-patterned and patterned ECD is presented.

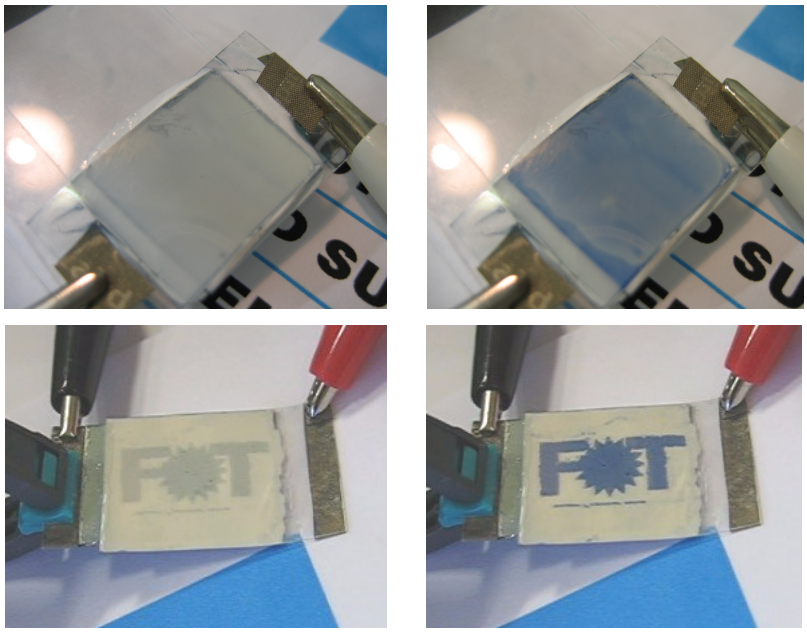

Figure 7.1 – ECD with a non-patterned electrochromic layer (up) and a patterned electrochromic layer as the primary electrode. Pictures show the bleached and coloured states for both devices at the left and right side, respectively.

In the previous chapter, the photolithography process was used to pattern the PEDOT:PSS layer over the electrodes. Photolithography is used in a wide range of applications such as screen-printing and microelectronics fabrication. The pattern can be printed with a precision of hundred of nanometres[1], however, the technique is time consuming and expensive. A low information content display does not require such a higher printing resolution. On the other hand, we are interested to print over a wide range of substrates like paper and textile where the photolithography process has no application. The photolithography process requires the deposition of uniform layers of polymer liquid solutions, porous substrates such as paper, textile will absorb most of the fluid, and the process will not result in a continuous film.

The ink-jet deposition technique was identified as an adequate process to build electrochromic devices. Ink-jet allows to deposit controlled amounts of a liquid solution (ink) as a coating or as a pattern over almost any kind of substrates with any kind of shapes. Recently ink-jet was also applied to print three-dimensional objects. In the present chapter, an overview of the results reached in a one-week workshop carried in collaboration with the ink-jet technology integrator Xennia Technology Ltd. is presented. The objective of the project was to demonstrate the feasibility of using the ink-jet technology for the industrial production of symmetric PEDOT:PSS based electrochromic displays.

7.1.1 Ink-jet technique

Ink-jet printing is a non-contact technique where the ink is jetted as small drops with volumes in the range of the picoliter. The ink-jet printing offers particular advantages over other deposition methods: precise patterning capability; reduction in waste products; high speed and low cost fabrication; room temperature deposition; and printing onto large areas and flexible substrates.

An ink-jet prints material by expelling small droplets of liquid ink from an orifice (nozzle) as it is moved in the two (2D) or three (3D) dimensions of the substrate. The pattern of droplets left behind on the substrate constitutes the printed output.[2] As illustrated in Fig. 7.2 ink-jet technologies can be classified as continuous ink jet and “Drop-on-Demand” (DoD) ink-jet, regarding how the landing position of the droplets is controlled and how the droplets are formed.

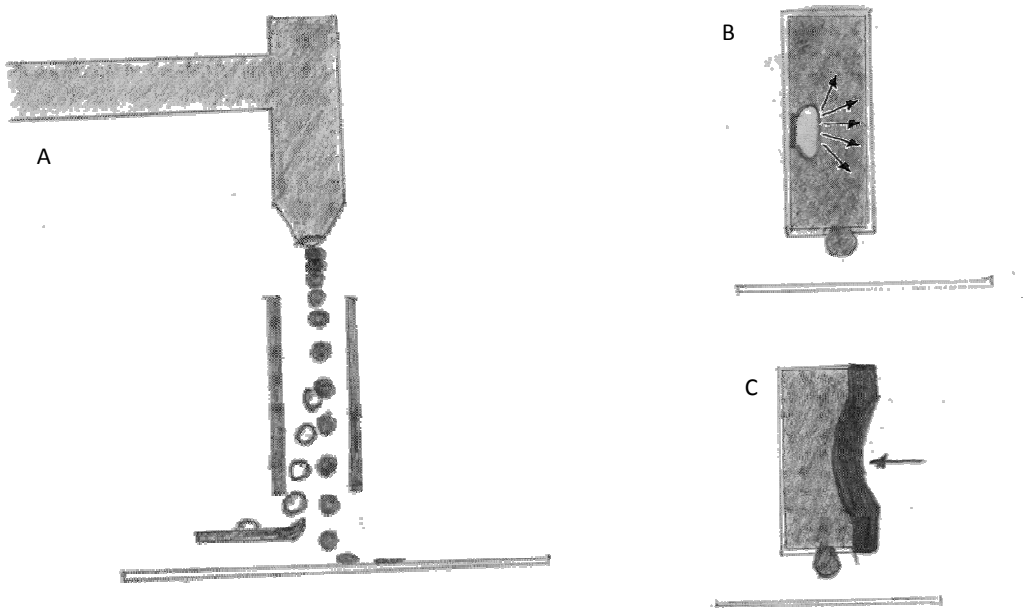

Figure 7.2 – Schematic view of different ink-jet print-head technologies. Continuous mode technology (A), the drops are deflected by the electric field created between the two plate electrodes at the exit of the nozzle. The deflection of the drops allows to control the position where the ink land. The deflected drops (open circle) are collected back to the ink chamber. The non-deflected drops (full circle) land over the printing substrate. DoD ink-jet technology (B and C). Thermal print-head (B) ejects drops by the rapid vaporization of the ink at the surface of an electrode inside the ink chamber. Piezoelectric print-head in bend-mode (C) expulses a jet of ink by the application of pressure in the ink chamber by the stimulus of the piezoelectric ceramic plate.

The continuous ink jet technology generates a constant stream of small ink droplets which are charged according to the image and controlled electronically. The charged droplets are deflected by a subsequent electric field, while the uncharged ones flow onto the paper. With continuous ink-jet only a small part of the ink jetted is deposited over the substrate in accordance with the print information. The large part is fed back into the system.[3] A primary advantage of continuous systems is the high number of drops per unit time available per nozzle.

The drop formation in continuous ink-jet printers is based on the instability of liquid jets described by Lord Rayleigh in 1878.[4] The drop formation from a jet stream is a very complex mechanism and almost impossible to obtain a reliable prediction of the phenomenon. A uniform size and spacing drop formation is obtained applying a periodic perturbation at an appropriate frequency, typically by means of a vibrating piezoelectric transducer attached to the chamber.[5] Depending on the technology, the continuous flow of the drops can reach the frequency of 1’000’000 per second (1MHz). This type of system is generally referred as "continuous" because drops are continuously produced and their trajectories are varied by the amount of charge applied.[6]

In contrast to continuous ink-jet systems the so called DoD ink-jet technology, only jets ink where the digital images require, accordingly to the image pattern. Ink is ejected from the nozzle by applying a pulse of pressure to the fluid ink inside the chamber in the supply tube, upstream of that nozzle.[7] Two main technologies are used to create the pulse pressure thermal ink-jet and piezoelectric ink-jet printing.

Thermal ink-jet generates the drops by heating and localizes vaporization of the ink solvent in a jet chamber. With piezoelectric ink-jet the ink drop is formed and catapulted out of the nozzle by mechanically deforming the jet chamber, an action resulting from an electronic signal and the piezoelectric properties of the chamber wall.[3]

The thermal ink-jet technology uses a resistive metallic layer in the walls of the ink channel leading to each nozzle. When a pulse of electrical current is applied to the resistive metallic layer, temperature raises until the ink near the metallic layer will boil. The current flows for a short period of approximately one microsecond and its amplitude is so that a thin layer of ink explosively boils.[7] This creates a four stage drop formation; bubble nucleation, drop ejection, bubble collapsing and nozzle refill.[8] The nucleation occurs when the temperature of the resistive layer rises up to *ca.* 300ºC and the ink starts to evaporate at the surface of the electrode. The ink forms a vapour bubble and expands about one thousand times in volume. A pressure pulse is created inside the chamber and a drop of ink is ejected through the nozzle towards the substrate. After several microseconds, the temperature drops and the vapour bubble collapses. Finally, the nozzle is refilled by the action of the capillary forces of the ink meniscus. At this point the cycle can be repeated for more than 5'000 times per second (5kHz).[3,7]

In DoD systems, each droplet takes ballistic trajectory to the substrate on command by a pressure impulse, accordingly to the digital image information. Another physical phenomenon used in ink-jet to create a pressure impulse within the ink chamber is the piezoelectric effect. When an electrical voltage is applied across a piezoelectric material, it suffers a mechanical stress, resulting in a deformation of the material. Two configurations are commonly used: piezoelectric rods which elongate under applied fields (push-mode) or bimorphs which bend (bend-mode). In a push-mode design, the piezoelectric actuator is on the rear wall of the nozzle in the form of rods, as the rods expand it pushes against the ink to eject the droplets. In a typical bend-mode design, a flat plate of piezo-ceramic material forms one wall of the ink chamber forming an array of laminar electromechanical transducers used to eject the ink droplets.[4,5] In theory, piezodrivers can directly contact and push against the ink. However, in practical implementation, a thin diaphragm between the piezodrivers and the ink is incorporated to prevent undesirable interactions.

In contrast to thermal ink-jet and push-mode piezoelectric technology, bend-mode piezoelectric ink-jet technology requires a sequence of electrical signals (see Fig. 7.3) in order to control the drop formation.

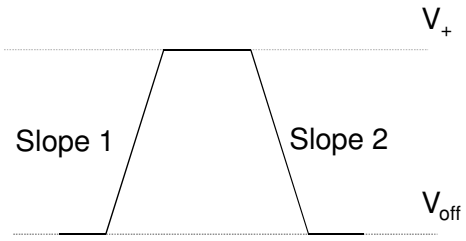

Figure 7.3 – Piezoelectric print-head waveform

In the case of a bend-mode design, the full sequence involves five steps. First, a positive-going voltage (slope 1) is applied to expand the chamber walls and draw fluid into the chamber from the reservoir. The potential is then kept constant at a fixed positive voltage (V^+) to allow the pressure wave to propagate through the ink. Next, a negative-going (slope 2) voltage to compress the chamber wall and squeeze fluid out of the nozzle is applied. Again, the negative potential is kept constant to dampen resonances in the chamber and ink reservoir. Finally, the voltage is kept until a defined resting voltage (V_{off}). After this point, the cycle can restart to form a second drop and the maximum firing frequency is *ca.* 20'000 drops per second (20kHz).

To jet uniform and reproducible drops of ink, it is essential to tune the electric signal waveform of the print-head technology finely. Ideally, the parameters should be adjusted to produce a stable mono-disperse stream (single drop-per-trigger) which exhibits: no satellite drops (an undesirable tiny drop that is formed from the principal drop); the smallest droplet size; maximum droplet velocity; minimum deviation from a straight-line trajectory; and, minimum velocity deviations from drop-to-drop. In addition, the parameters should produce a robust process such as that variations in the inks, the jetting devices, or reservoir fluid level have minimal affects on jetting.

The print head characteristics and electrical signal modulation are not the only factors affecting the droplet formation. Ink rheology is of extreme importance to achieve a reliable ink-jet process. Actually, both print head waveform modulation and ink physical characteristics will influence each other, and optimization will always depend on this two components.

The rheology of the ink as it flows through the nozzle will control the drop formation mechanism, specially the ink viscosity and surface tension.[9] The viscosity will resist the necking motion of the liquid filament, if all the kinetic energy created by the pressure pulse is

viscously dissipated, no droplet is ejected. For a given pressure wave at the nozzle, the lower the viscosity the greater is the velocity and the amount of fluid propelled forwards, contributing to the long tail formation behind the drop.[10] The surface tension is responsible for the spherical shape of the liquid drop emerging the nozzle. The wetting behaviour of the ink formulation with the nozzle material is another parameter that must be addressed. An undesired spray is formed when too much ink is wetting the nozzle outlet face, during the jetting process.[11]

Recommended values for the different rheological ink parameters are given in Table 7.1. These values can be useful to predict the printability of a fluid, however, due to the large number of variables usually the final tune of the print-head waveform and ink parameters are found by trial-and-error.

Table 7.1 – General ink-jet ink parameters

Ink Properties	Recommended values
Viscosity (cP)	8 – 12
Surface Tension (dyn/cm)	>32
Max. Size (μm)	1
Conductivity (μS)	No
Salt Level Chlorides (ppm)	<100

YDreams interest in ink-jet technology to manufacture low information content displays for low cost applications is based on several advantages presented by the technique. Ink-jet printing technology shows good print quality (state of the art ink-jet print heads will allow minimum feature sizes lower than $20nm^2$ and cost ratios when compared with processes such as photolithography. In particular, DoD piezoelectric technology presents a wide range of ink materials application and several advantages such as additive process (reducing waste and processing steps), wide range of substrate composition and morphology. It has also a more controlled drop production than thermal one, higher drop production rates and long head life.

Besides the several potentialities presented by ink-jet technology that contributed to YDreams decision to invest on such technology, another relevant characteristic is the data driven capability. In contrast to the major printing techniques like screen printing, flexography, offset and gravure, the ink-jet printing process does not require a physical image carrying medium (see section 1.3 Industrial Printing Techniques). The printing pattern can be modified at any time without interruption of the printing process. Such capability

allows to think in a viable production strategy based on mass production rhythm and simultaneously with a product customization design.

7.2 Strategy and project execution organization

Based on the expertise accumulated during the IDEIA projects (chapter 6), the symmetric ECD devices architecture was selected as the model objective for this project (see Fig.7.4). The starting materials were the electrochromic PEDOT:PSS aqueous dispersion and the gel electrolyte described in chapter 5.

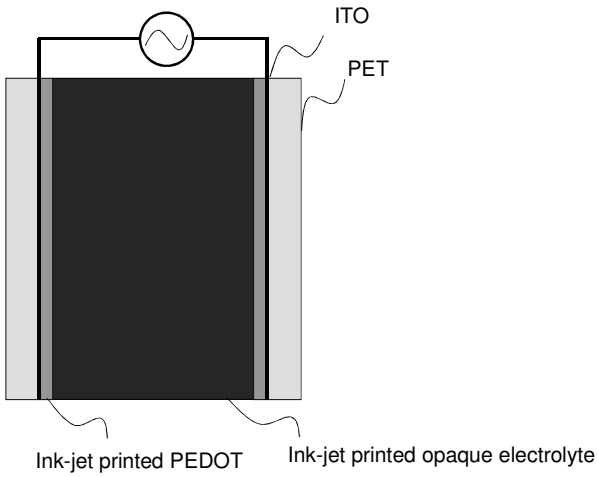

Figure 7.4 – ECD proposed to assemble with the ink-jet printing technique

Based on the architecture and the materials revealed to Xennia Technology team the project consisted of three separate phases:

-The assessment of the two PEDOT:PSS and gel electrolyte materials for ink-jet applications

-The formulation of jettable fluids containing each of these materials or equivalent alternatives to achieve reasonable jetting performance

-The production of ink-jet printed electrochromic cell display samples and the demonstration of their functionality onto PET-ITO electrode

7.3 Results and Discussion

7.3.1 Printing the Electrochromic Layer

The 1.3 wt % dispersion in H_2O of PEDOT:PSS purchased from Aldrich exhibits high viscosity but the dispersion was found to be easily diluted with water, allowing us to reduce the viscosity to achieve a printable fluid formulation. As a dispersion in water, the surface tension did not match the requirements for ink-jet printing so addition of small amounts of surfactants was required. It was also anticipated that introducing a water-soluble humectant would improve the reliability and jettability of the ink. Such humectants could be glycerol, diethylene glycol or ethylene glycol. This addition of humectants to the 1.3 wt % dispersion in H_2O of PEDOT:PSS is known in literature to increase the conductivity of the thin film polymers.[12,13]

Formulation of PEDOT:PSS as a 1.3 wt % dispersion in H_2O

The 1.3 wt % dispersion in H_2O of PEDOT:PSS, purchased from Aldrich, was diluted down with water to achieve a viscosity of 13 cP. Moreover, glycerol was added to the formulation to act as a humectant and Surfynol 465 as a non-ionic surfactant. Table 7.2 shows the exact formulation of the printable PEDOT:PSS formulation (PEDOT-F) with the physical characteristics of the ink.

Table 7.2 - Formulation of PEDOT-F and respective characteristics

Material	PEDOT-F
PEDOT:PSS 1.3 wt % dispersion in H_2O %(w/w)	52.9
Surfynol 465 %(w/w)	0.6
Water %(w/w)	26.7
Glycerol %(w/w)	19.8
Viscosity (cP)	13
Surface Tension (dyn/cm)	42
pH	2.79

The PEDOT-F was jetted using the XenJet 4000 (Xennia Technology proprietary) fitted with a Xaar 760 GS8 print head. The temperature of the print head was maintained at 30 ºC. The waveform used to carry out the jetting trials was similar to that shown in Fig. 7.3. The print resolution onto the different substrate (PET-ITO or paper) was 360 x 360 dpi. It was found that this particular formulation gives reasonably good jetting properties.

In Fig. 7.5 the stroboscopic images from the nozzle exit, the jetting reliability for the PEDOT at 100% duty cycle with the 40pl drop volume is detailed in Table 7.3. We have

determined that the jetting reliability of PEDOT formulation is good up to 3 kHz firing frequency. The ink formulation can further be fine tuned to achieve improvements in the reliability at greater firing frequencies.

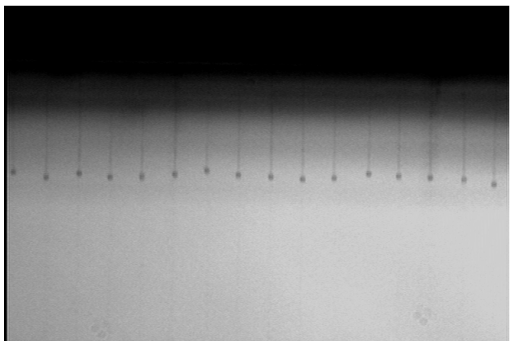

Figure 7.5 - Representative OpticaTM images captured during PEDOT reliability studies

Table 7.3 – PEDOT-F jetting reliability monitored for 100 printing nozzles

Frequency	1kHz				2kHz				3kHz			
V_{off}	0	-1	-2	-3	0	-1	-2	-3	0	-1	-2	-3
Time (min)	Number of missing nozzle											
0	0	0	0	0	0	0	0	0	0	0	0	0
1	0	0	0	0	0	1	0	1	5	5	6	1
2	2	1	1	0	3	1	1	1	5	6	1	1
3	2	1	1	0	5	6	2	2	9	6	1	1
4	3	1	1	0	12	6	2	2	9	6	3	1
5	3	1	2	1	19	6	3	2	-	12	3	1

7.3.2 Printing the Electrolyte Layer

The gel electrolyte reported in the chapter 5 is unsuitable for ink-jet printing. The initial assessment consists of dissolving the polymer into acetonitrile at about 40 wt %. The fluid obtained was found to exhibit high viscosity and high viscoelasticity properties which would prevent formation of the droplets to be ejected from the print head.

At this point, two alternative strategies were devised and implemented which involved either sourcing a lower molecular weight polyethylene oxide polymers (PEO-2) or using a UV-curing technology.

UV-curing technology consists of polymerization of reactive monomers by the action of UV-light. This technology has the advantage of being environmentally friendly as UV-formulation contains low or no Volatile Organic Compounds. Acrylate monomers are usually used as reactive diluents. Physical properties such as flexibility, shrinkage, hardness and solvent resistance of the resulting printed film could be fine tuned by a careful choice of

those monomers to the end applications. UV-formulations will also contain photoinitiators, additives such as surfactants/dispersants and pigments particles. The idea of using the UV-technology is to be able to jet a reliably fluid containing acrylate monomers and to obtain after the exposition to UV-light a polymer with relatively high molecular weight that will have a similar structure as the polymer in the PEO-2 gel electrolyte.

In order to operate a symmetric electrochromic device the electrolyte the light scattering titanium dioxide (TiO_2) nanoparticles were incorporated in the electrolyte ink. For ink-jet printing applications, chemically stable suspension with evenly nanoparticles distributed throughout the ink is critical. Two different dispersions of TiO_2 were used in this project, the first in water (TiO_2-W) and the other one in dipropyleneglycol diacrylate (TiO_2-DPGDA).

Formulation of the electrolyte layer derived from the Poly(ethylene glycol)-block-poly(propylene glycol) (PEO-2)

Formulations were attempted using the two different grades of PEO-2 purchased from Aldrich. A solution of 20% of the 5,800 Da PEO-2 reaches a viscosity of 2.1cP while a solution of 20% of the 14,600 Da PEO-2 polymer reaches a viscosity of 5.32cP. The two grades of PEO-2 were easily dissolved in acetonitrile as well as the $LiClO_4$ salt.

A few starting formulations were prepared by mixing the three different materials, PEO-2 polymer, TiO_2-W and $LiClO_4$ salt in a solvent composed of acetonitrile/ethyl lactate (1:1, v/v). It was found that it was not possible to obtain a TiO_2-W stable suspension when the three materials were present in a single formulation. Formulation trials were carried out using different quantities of each of the components, using some other polymers such as polyvinylacetate or polyvinylpyrrolidinone and using different solvents but this did not lead to a successful solution. Since all the three materials did not lead to a stable suspension it was decided to separate them and create two electrolyte layers consisting in two separate ink formulations prepared in acetonitrile/ethyl lactate (1:1, v/v). One layer contains the $LiClO_4$ salt and the PEO-2 polymer (clear layer) the other one contains the TiO_2-W and salt (opaque layer). It was thought that this idea was best implemented if the TiO_2 layer was sandwiched between the two clear layers electrolyte, as described in Fig. 7.6.

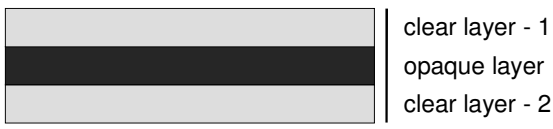

Figure 7.6 – Electrolyte consisting in three stacked layers. Clear layer contains polymer, solvent and salt and the white opaque layer contains solvent, salt and TiO_2 nanoparticles. Polymer and TiO_2 suspended particles are not present in the same ink to avoid particle sedimentation (see text).

As this idea involved some alterations of the original architecture, electrochromic cell samples were first created by using a pipette to deposit the different layers to demonstrate the functionality of this new layout. It was found that the drying time of each of the layers was important to have a correctly sealed cell, but even so the two transparent conducting layers were able to slide from each other. The gel electrolyte used in previous chapters act as a sealant; however, the fluid created with low molecular weight PEO-2 polymers did not present this effect.

To overcome this lack of strong adhesion forces between the two transparent conducting layers, experiments were carried on with the incorporation of small quantities of UV-monomers and photoinitiators. The printed electrolyte layers obtained after UV curing did not present the desired sealant effect. The ECD assembled with the two layer electrolyte did not present the desired structural characteristics.

Table 7.4- Formulation of the clear and opaque electrolyte ink

Material	Clear electrolyte %(w/w)	Opaque electrolyte %(w/w)
Ethyl lactate	22	
PEO-PPO Mw5600	5	
PEO-PPO Mw14600	5	
LiClO4	3.5	4
Tego Glide 432	0.5	
Acetonitrile	33	
DPGDA	26	
Irgacure 819	5	
TiO2-W		48
Surfynol 465		0.6
Water		15.4
Glycerol		36

The components were carefully chosen for material compatibility issues in the formulation (Table 7.4). The surfactant used was polyether siloxane copolymer especially designed for UV-curing formulations and exhibits excellent substrate wetting. The opaque electrolyte layer contains a dispersion of TiO_2-W with glycerol acting as humectants and thickeners and a water-soluble surfactant, the same used in the PEDOT-F.

The formulations obtained were jetted using the XenJet 4000 fitted with a Xaar 760 GS8 print head. The temperature of the print head was maintained at 35ºC. The waveform used to

carry out the jetting trials was similar to the presented in Fig. 7.3. It was found that both formulations give reasonably good jetting properties, however, these formulations were not used to build printed ECD.

Formulation of the UV-curing electrolyte ink

The key element in the development of the electrolyte layer derived from UV-curing technology was the screening phase for compatible solvents that could dissolve the $LiClO_4$ salt and maintain the stability of the TiO_2-DPGDA. Ethyl Acetate was found to meet that requirement. In addition 2-methyl-1,4-pentanediol was incorporated to act as a humectant. Table 7.5 exemplifies the formulation of the UV-curable electrolyte layer and shows its physical properties.

Table 7. 5- Formulation of UV-curing electrolyte layer

Material	UV-curing electrolyte ink
Ethyl acetate %(w/w)	27.5
TiO_2-DPGDA %(w/w)	25
Tego Glide 432 %(w/w)	0.5
Irgacure 819 %(w/w)	5
2-methyl-1,4-pentanediol %(w/w)	10
DPGDA %(w/w)	25
$LiClO_4$ %(w/w)	7
Viscosity	9
Surface Tension	27
Filtration (1μm)	yes

7.3.3 Demonstration of the ink-jet printed electrochromic cells

At the end of the project two strategies were available to create an ink-jet printed electrolyte layer, the one constituted by three layers (see Fig. 7.6) and the UV-curing electrolyte. Both resulted to work as ion conductor and devices were able to present reasonable electrochromism. However, the ECD assembled with the clear and opaque electrolytes layers did not present enough structural stability and the prototypes created were not useful even for demonstration purposes. In the following section only the results of the printed ECD using UV-curing electrolyte ink are presented.

ECD based on UV-curable electrolyte

The electrochromic cell was printed according to the original architecture as shown in Figure 7.4, using piezoelectric ink-jet technology. The formulation PEDOT-F was, first, ink-jet printed at 360x360 dpi using the 8pl drop onto both PET-ITO electrodes (primary and counter-electrode). In the primary electrode a patterned layer of PEDOT was created, while in the counter electrode a plain square covering all the active area was printed. Several passes were carried out to deposit more PEDOT for a larger optical contrast between the bleached and coloured states. The UV-curing electrolyte formulation was then ink-jet printed onto the primary electrode deposited at 360x180 dpi using the 40pl. Finally, the assembly of the ECD is obtained by lamination of both electrodes (see Fig. 7.7).

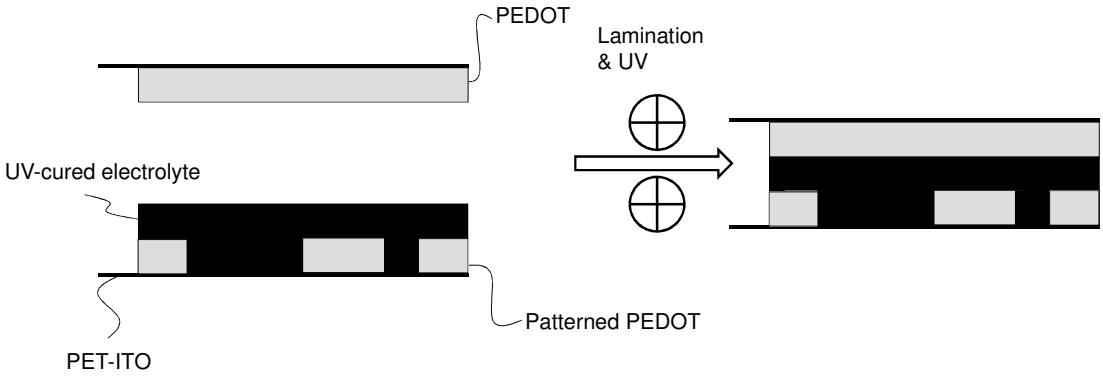

Figure 7.7 – Schematic view of the process to assemble an ECD using ink-jet and lamination techniques.

In Fig. 7.8 pictures one example of the ink-jet printed ECD at Xennia are shown.

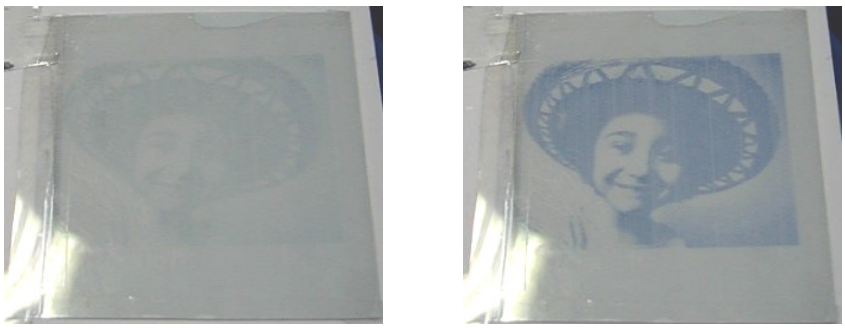

Figure 7.8 - Ink-jet printed ECD (7 x 7 cm) showing the coloured state (left) and bleached state (right)

7.4 Conclusion

This feasibility project demonstrates the viability of using ink-jet technology for the industrial production of the electrochromic displays according to the ECD architecture proposed. Ink-jet formulation of PEDOT:PSS as a 1.3 wt % dispersion in H_2O (PEDOT:PSS) was created and proved to achieve a good printing performance.

The physical characteristics of the gel electrolyte previously developed in IDEIA projects showed to be inappropriate for the ink-jet technique. Two alternatives were explored to obtain a printable electrolyte formulation. The first approach was based on a diluted solution of low weight PEO-PPO copolymer; although the resulting formulation was ink-jettable, the resulting printed layers did not succeed to seal the electrodes. The UV-curing electrolyte formulation was explored as a second alternative, and was crucial to the success of the project.

Studies that relate ink-jet printability of polymer-containing inks to their physical properties are rare.[10] Polymer printed with the ink-jet technique was used to build organic electronics components and circuits, including the PEDOT:PSS dispersions.[14] One of the most interesting applications of polymer ink-jet printing is the manufacture of polymer light-emitting diodes displays.[15] Shubert Ulrich *et al* reviewed the most relevant published studies on the rheological characteristics of polymer ink formulation and the ink-jet printability.[10] They observe that a small amount of the polymer influences the drop formation from the jet stream created in ink-jet. The increase of the polymer weight printed shifts the drop formation mechanism from single isolated drops, with dome satellites formation, to a “bead-on-a-string” structure (see Fig.7.9).

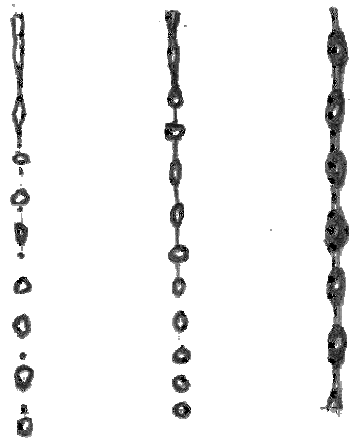

Figure 7.9 – Schematic representation of the influence of the polymer weight on the ink drop formation. From the left to the right the weight of the polymer dissolved in the ink-jet ink increases. For low molecular weight polymers the drop are easily detached from the ink stream and small drops (satellites) are formed. When the polymer weight is high the drops do not succeed to detach from the ink stream and a “bead-on-a-string” is observed. The drawings are inspired from the pictures published in ref.10.

UV-curable ink-jet formulation is a clever method to avoid polymer printing issues. The UV-curable ink is a molecular based solution with a Newtonian behaviour that allows the perfect control of the drop formation mechanism and at the same time the printed layer can be UV polymerized. The alternative UV-curable ink-jet formulation electrolyte allows to generate the electrolyte *in situ*. The electrolyte ink resulted in relatively good printing performance. A similar polymer network was thus created compared with the PEO-PPO gel electrolyte. This formulation allowed the production of ECD samples. Their functionality was proved and matched the requirements for electrochromic display applications.

7.5 Bibliography

1. *The application of photographic technology* [Online]. Available: http://www.nikon.com/products/precision/society/story0203/index.htm [Accessed July 2010 2010].
2. Fuller, S.; Wilhelm, E.; Jacobson, J., Ink-jet printed nanoparticle microelectromechanical systems. *Journal of Microelectromechanical Systems* 2002, 54-60.
3. Kipphan, H., *Handbook of print media: technologies and production methods*. Springer: Heidelberg, 2001.
4. Le, H., Progress and trends in ink-jet printing technology. *Journal of Imaging Science and Technology* 1998, 49-62.
5. *Computer peripherals - ink-jet printers* [Online]. Lintech organisation. Available: http://www.lintech.org/comp-per/15INK.pdf [Accessed July 2010].
6. Microfab. *Continuous mode ink-Jet technology - 1* [Online]. Available: http://www.microfab.com/equipment/technotes/technote99-01/id2.htm [Accessed July 2010].
7. Hanson, E. *How an ink jet printer works* [Online]. The Society for Imaging Science and Technology. Available: http://www.imaging.org/ist/resources/tutorials/inkjet_printer.cfm [Accessed July 2010].
8. Willis, Ink-jet Academy. In *Theory of ink-jet technology*, IMI Europe: Lisbon, 2008.
9. Tuladhar, T.; Mackley, M., Filament stretching rheometry and break-up behaviour of low viscosity polymer solutions and inkjet fluids. *Journal of Non-Newtonian Fluid Mechanics* 2008, 97-108.
10. de Gans, B.; Duineveld, P.; Schubert, U., Inkjet printing of polymers: State of the art and future developments. *Advanced Materials* 2004, 203-213.
11. de Gans, B.; Kazancioglu, E.; Meyer, W.; Schubert, U., Ink-jet printing polymers and polymer libraries using micropipettes. *Macromolecular Rapid Communications* 2004, 292-296.
12. Lee, M. W.; Lee, M. Y.; Choi, J. C.; Park, J. S.; Song, C. K., Fine patterning of glycerol-doped PEDOT:PSS on hydrophobic PVP dielectric with ink jet for source and drain electrode of OTFTs. *Organic Electronics* 2010, *11* (5), 854-859.
13. Ouyang, B.; Chi, C.; Chen, F.; Xi, Q.; Yang, Y., High-conductivity poly (3,4-ethylenedioxythiophene): poly(styrene sulfonate) film and its application in polymer optoelectronic devices. *Advanced Functional Materials* 2005, 203-208.

14. Nilsson, D.; Kugler, T.; Svensson, P. O.; Berggren, M., An all-organic sensor-transistor based on a novel electrochemical transducer concept printed electrochemical sensors on paper. *Sensors and Actuators B-Chemical* 2002, *86* (2-3), 193-197.
15. van der Vaart, N. C.; Lifka, H.; Budzelaar, F. P. M.; Rubingh, J.; Hoppenbrouwers, J. J. L.; Dijksman, J. F.; Verbeek, R.; van Woudenberg, R.; Vossen, F. J.; Hiddink, M. G. H.; Rosink, J.; Bernards, T. N. M.; Giraldo, A.; Young, N. D.; Fish, D. A.; Childs, M. J.; Steer, W. A.; Lee, D.; George, D. S., Towards large-area full-color active-matrix printed polymer OLED television. *Journal of the Society for Information Display* 2005, *13* (1), 9-16.

Chapter 8

List of Publications

8.1 List of publications

The results detailed in the present thesis have been published in several international scientific journals. In addition to the papers that resulted directly from the present work, during my Ph.D. the experience acquired with the chromogenic systems gave me the opportunity to contribute scientifically in the publication of other papers and patents. The list of publications and patents is organized chronologically and the correspondence with the respective chapter is given.

1. Branco, A.; Pinheiro, C.; Fonseca, J.; Tedim, J.; Carneiro, A.; Parola, A. J.; Freire, C.; Pina, F., Solid-state electrochromic cells based on [M(salen)]-derived electroactive polymer films. *Electrochemica land Solid-State Letters* 2010**,** *13* (9), J114-J118. (Indirect contribution of the present thesis).
2. Barbosa, P. C.; Rodrigues, L. C.; Silva, M. M.; Smith, M. J.; Parola, A. J.; Pina, F.; Pinheiro, C., Solid-state electrochromic devices using pTMC/PEO blends as polymer electrolytes. *Electrochimica Acta* 2010**,** *55* (4), 1495-1502. (Chapter 5).
3. Pinheiro, C.; Parola, A.; Pina, F.; Laia, C., Electrochromism of Crystal Violet Lactone in the presence of Fe(III)/Fe(II) redox pair. *Electrochimica Acta* 2009, 5593-5597. (Chapter 3).
4. Pinheiro, C.; Parola, A.; Laia, C.; Camara, A.; Pina, F., Multiresponsive chromogenic systems operated by light and electrical inputs. *New Journal of Chemistry* 2009, 2144-2147. (Chapter 3).
5. Co-inventor in Portuguese Utility Patent 103852 “MÉTODO DE CROMISMO” <METHOD OF CHROMISM>.
6. Co-inventor in Portuguese Utility Patent 105152 “MÉTODO DE CROMISMO” <METHOD OF CHROMISM>.
7. Co-inventor in the Provisory Portuguese Utility Patent 104696 “VISUALIZADOR TÁCTIL ELETROCRÓMICO” <TOUCH-SCREEN ELECTROCHROMIC DEVICES>.
8. Pinheiro, C.; Parola, A.; Pina, F.; Fonseca, J.; Freire, C., Electrocolorimetry of electrochromic materials on flexible ITO electrodes. *Solar Energy Materials and Solar Cells* 2008, 980-985. (Chapter 4).
9. Vidinha, P.; Lourenco, N. M. T.; Pinheiro, C.; Bras, A. R.; Carvalho, T.; Santos-Silva, T.; Mukhopadhyay, A.; Romao, M. J.; Parola, J.; Dionisio, M.; Cabral, J. M. S.; Afonso, C. A. M.; Barreiros, S., Ion jelly: a tailor-made conducting material for smart electrochemical devices. *Chemical Communications* 2008**,** (44), 5842-5844. (Indirect contribution of the present thesis).

10. Jimenez, A.; Pinheiro, C.; Parola, A.; Maestri, M.; Pina, F., The chemistry of 6-hydroxyflavylium: zwitterionic base and p-quinoidal chalcones. A multiswitchable system operated by proton, electron and photon inputs. *Photochemical & Photobiological Sciences* 2007, 372-380. (Chapter 2)